Ionosphere and Prof.S.P.Gupta
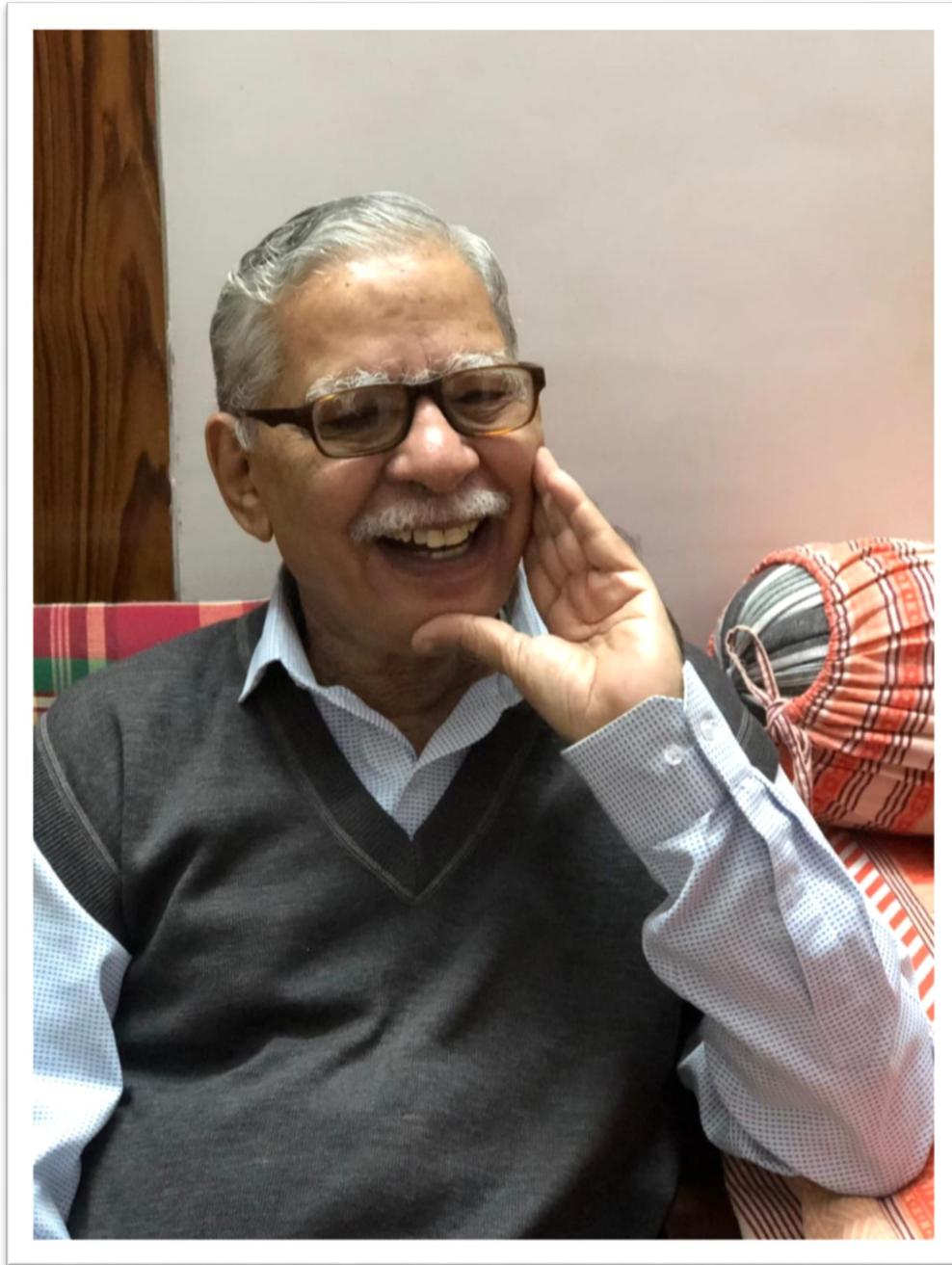
Commemorating Prof.S.P.Gupta's contributions to Space Science and Atmospheric Science
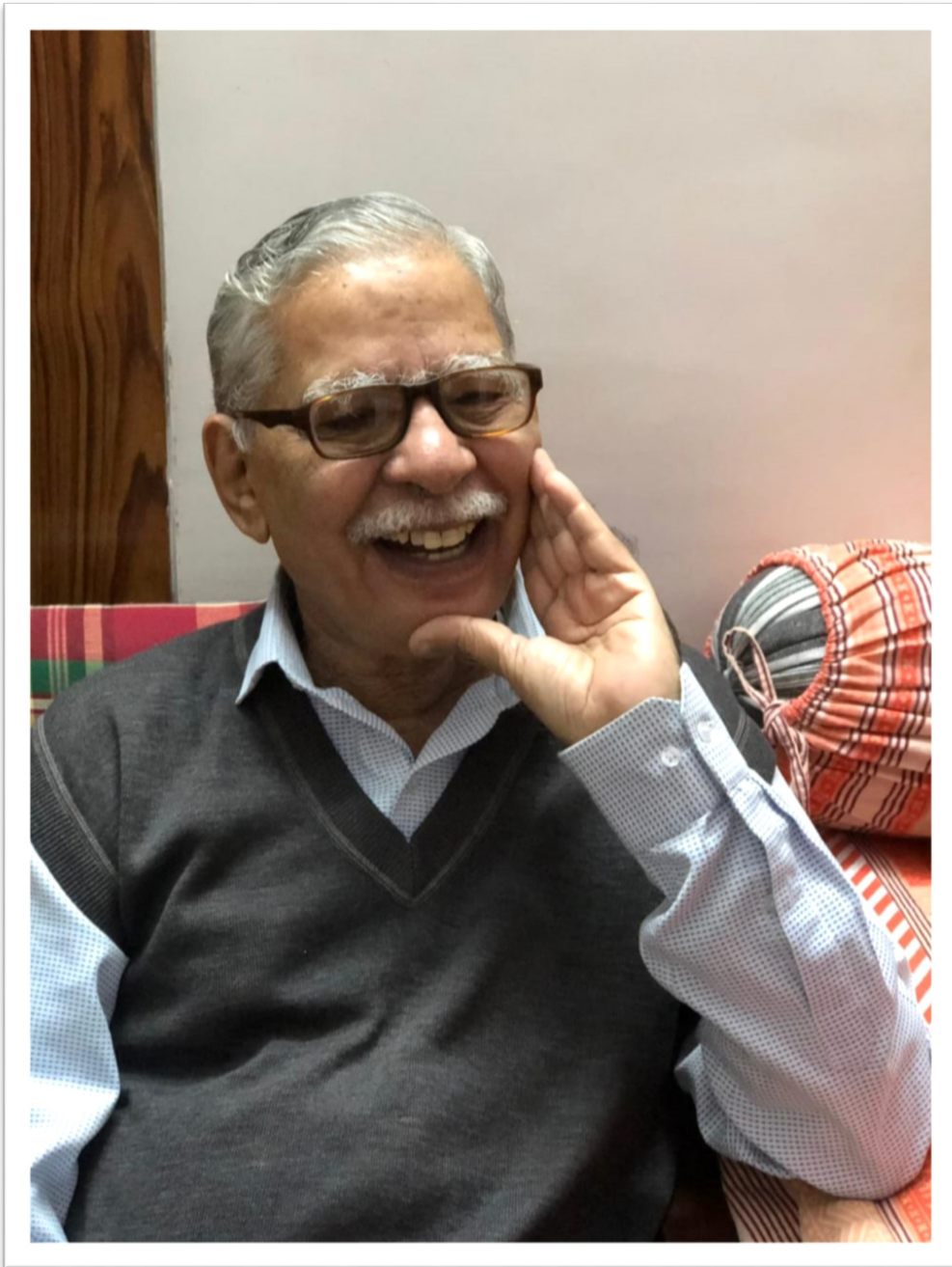

Prof.S.P.Gupta

(1941–2021)

Contents

Prof.S.P.Gupta

(1941—2021)

Former-Professor at Physical Research Laboratory (PRL), India

COSPAR Associate, Humbolt fellow (1975-1977), Max Planck fellow 1990

Biography

Prof.S.P. Gupta joined PRL in 1963 as a research student for his Ph.D. degree. He was involved in the design, development and fabrication of high frequency Langmuir probes. These were flown from the Thumba Equatorial Rocket Launching Station (TERLS), Trivandrum to measure in-situ the electron density, fluctuations in electron density (irregularities) and the electron temperature. The results led to the identification, for the first time, of the two types of plasma density irregularities associated with the cross-field and two stream instabilities. The spectral indices of the in-situ fluctuations in the scale size range from a meter to few hundreds of meters were also obtained for the first time. His PhD advisors were Prof. Sarabhai and Prof Satya Prakash. Based on this work he was awarded Ph.D. degree in 1971 from Gujarat University. His thesis was titled "The study of the lower ionosphere at low latitude."

From 1971 to 1975, Prof. Gupta actively participated in several international rocket campaigns from Thumba in collaboration with different countries like France, Germany, UK and Russia. About 25 instrumented rockets were flown from Thumba out of which 15 carried Langmuir probe. Two rocket launches were carried out during the counter-electrojet events and provided the first in-situ measurements under such geophysical conditions. The measurements in night and morning hours showed that the two-stream instability is operative even during night and morning hours.

In May 1975, Prof. Gupta was awarded Humboldt fellowship for a period of two years to work with Prof. K. Rawer at Freiburg, Germany to investigate instability processes in Laboratory Plasma. On return he continued participation in several rocket campaigns like Ursids meteor shower (1978), solar eclipse (February 1980) and spread-F (1982). In the solar eclipse campaign, near simultaneous Langmuir probe measurements were made from Thumba and SHAR and electron loss rate were derived. The spread-F campaign from SHAR involved multi-instrumented payloads from RH-560 rockets resulting in several new findings.

Prof. Gupta concentrated more in middle atmosphere program from 1984 that led to the development of a new Relaxation Probe that was flown from balloons launched from Hyderabad to measure electrical conductivity and electric field in troposphere and stratosphere. Solar cycle effect on conductivity was observed. Measurements carried under IMAP during a decade (1984-1994) have provided new results. He was the working group chairman of the Electrodynamics of the Indian Middle Atmosphere Programme (IMAP).

Prof. Gupta was also awarded Max Planck Fellowship in 1990 to work with Prof. W.I. Axford at Max Planck Institute of Aeronomy at Lindau/Harz, Germany for six months. He had organised several workshops and symposia in COSPAR assemblies during 1996-2000 and edited three volumes of Advances in Space Research. He was also a member of the Task Team on International Reference Ionosphere. He had participated in the solar eclipse campaign on 15 Jan. 2010 at Thumba. The results obtained from this campaign were compared with 16 Feb. 1980 solar eclipse campaign.

Prof. Gupta had authored seventy papers in major scientific journals.

He had also contributed immensely to several balloon-borne experiments dedicated to under-standing the mobility of positive ions in the near-Earth region. These experiments were conducted from the National Balloon Facility in Hyderabad.

Prof. Gupta was a Humboldt Fellow and was also actively involved in COSPAR activities. He had organized several scientific symposia in COSPAR assemblies in Scientific Commission C., namely electrodynamics of low and sub auroral latitude, (1996) Birmingham, UK. Middle atmosphere and lower thermosphere (1998) Nagoya, Japan. He was co-scientific organizer in COSPAR assemblies in Warsaw, Poland (2000), Houston, USA (2002) and Paris, France (2004) in scientific symposia on middle atmospheric electrodynamics and chaired several sessions. At the 39th COSPAR assembly in July 2012 in Mysore, India, he presented results on long term measurements of electrical parameters in middle atmosphere using rockets and balloons over the Indian zone.

Reference: COSPAR's Information Bulletin *Space Research Today*, (SRT)

Dec 2021, pg 7-9

Obituary written by his colleagues at PRL

Dr. Vikram Sarabhai: Revered teacher and guide, Vikram Patrika

(Magazine in Hindi) special issue 2019, Sarabhai birth centenary

special, pg 20-22

UCAR Center for Science Education

Obituary

Prof.S.P. Gupta

(1941 - 2021)

Prof. S. P. Gupta had a distinguished career in PRL for over three decades, wherein he was actively involved in more than 40 rocket experiments that were carried out from Thumba and SHAR.

Along with his supervisor, Prof. Gupta had perfected the technique of high frequency Langmuir Probe payload. He was the first to discover the presence of sub-meter class scale sizes in plasma irregularities in the ionosphere based on this technique. This high frequency Langmuir Probe is the only in-situ technique in the world that can yield unambiguous information on plasma waves over a wide range of scale sizes! This ability has produced numerous theses and new results of international repute

He had also contributed immensely to several balloon-borne experiments dedicated to understanding the mobility of positive ions in the near-earth region. These experiments were conducted from the National Balloon Facility in Hyderabad.

Prof. Gupta had uncanny abilities to decipher geophysical information from raw databases. He had contributed significantly in solving the mystery of the disappearance of a particular type of plasma waves over Thumba by finding out its association with the slow movement of dip-equator, and thereby connecting the geo-dynamics to the behaviour of spaceplasma activities.

Prof. Gupta was a Humboldt Fellow and was also actively involved in COSPAR activities.

Prof. Gupta had superannuated close to two decades ago from PRL, however, his passion and participation for all that is PRL, has been immense and wholehearted. He had a

genuine curiosity in sciences of all fields. He used to actively participate in almost all the colloquiums, and Area Seminars of several fields, held in PRL, both before and after his superannuation. He used to keep himself updated with ground-breaking research results published in reputed journals like Nature/Science till recently. He falls into the class of a rare breed of scientists who used to pay money from his pocket to attend both international and national conferences or meet fellow international scientists (like Prof Rawer) even after superannuation. Such was his passion and dedication!

Prof. Gupta was bestowed with a great memory and could recollect verbatim the conversations that he had had with several high-profile visitors to PRL or those whom he visited including Nobel Laureates. He had a great sense of humour and, in an informal setting, discussion with him on any topic was full of fun and filled with interesting anecdotes of his interactions with fellow scientists.

Prof. Sarabhai was his official guide and one could see that on all the days he came to PRL, he used to bow his head in reverence to Prof. Sarabhai's statue at the main gate before moving in further.

Prof. Gupta was a scientist with childlike curiosity and had a deep sense of desire and passion for PRL and all its activities. With his demise, PRL has lost an illustrious alumnus who had direct association with Prof. Sarabhai.
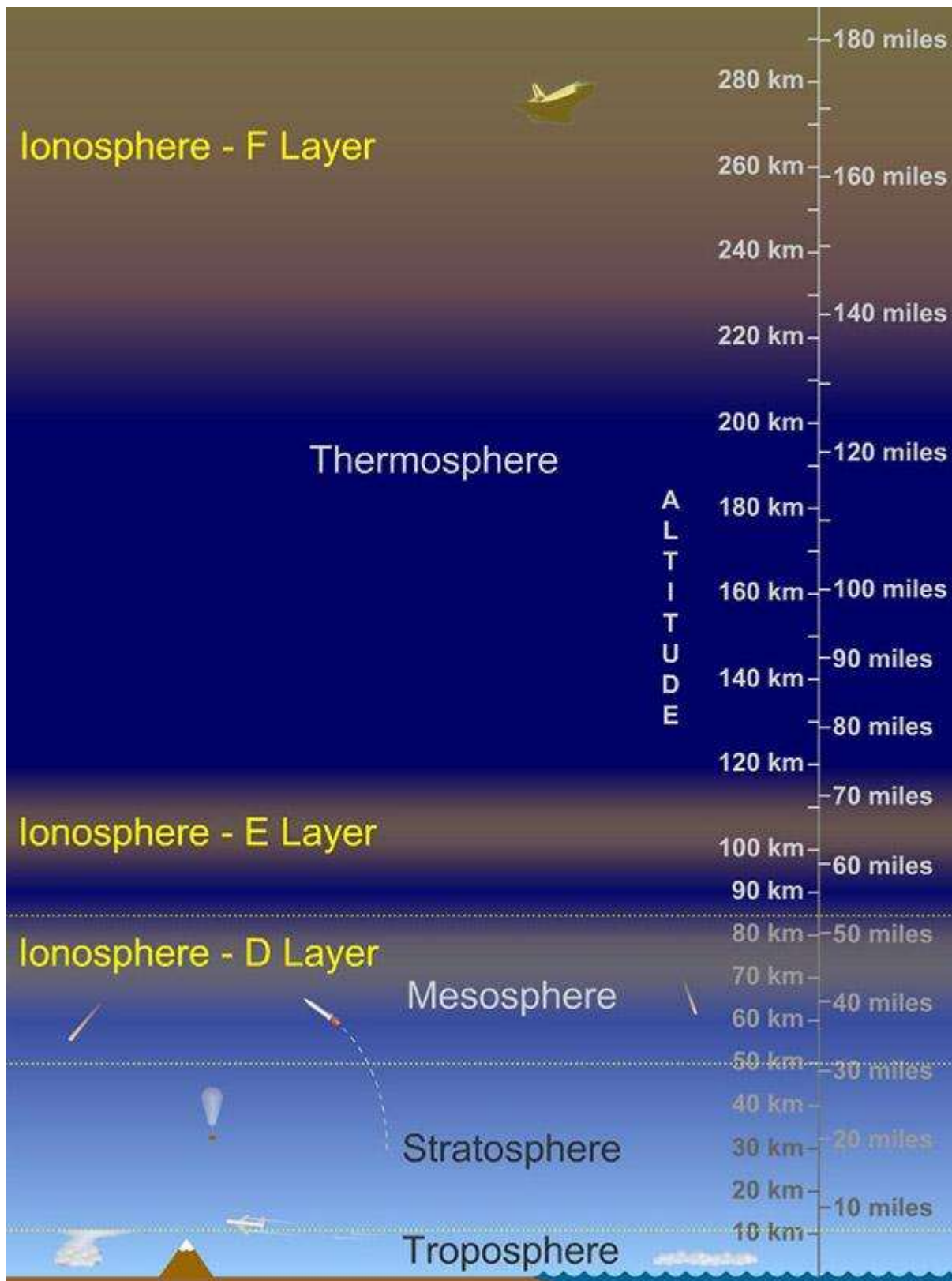
Layers of the Earth's Atmosphere

Image Credit: UCAR Center for Science Education

Collected Works

Bibliography of Prof. S.P.Gupta's publications in scientific journals

Publication in scientific journals (2001-2021)

70 Altitude of Two-Stream Irregularities in Equatorial E Region Using Sounding Rocket Experiments From Thumba
   Pandey, K., Gupta, S.P.
   Journal of Geophysical Research: Space Physics, 2020, 125(4), e2019JA027195

69 On the Occurrence of Afternoon Counter Electrojet Over Indian Longitudes During June Solstice in Solar Minimum
   Pandey, K., Sekar, R., Anandarao, B.G., Gupta, S.P., Chakrabarty, D.
   Journal of Geophysical Research: Space Physics, 2018, 123(3), pp. 2204–2214

68 Comparison of quiet time vertical plasma drifts with global empirical models over the   Indian sector: Some insights
    Pandey, K., Sekar, R., Gupta, S.P., Chakrabarty, D., Anandarao, B.G.
   Journal of Atmospheric and Solar-Terrestrial Physics, 2017, 157-158, pp. 42–54

67 Estimation of nighttime dip-equatorial E-region current density using measurements and models
   Pandey, K., Sekar, R., Anandarao, B.G., Gupta, S.P., Chakrabarty, D.
  Journal of Atmospheric and Solar-Terrestrial Physics, 2016, 146, pp. 160–170

66 Electrical conductivity of the stratosphere over Hyderabad,India: Results from balloon borne measurements
   Gupta, S.P., Thampi, S.V.
  Indian Journal of Radio and Space Physics, 2015, 44(3), pp. 132–137

65 On the altitude of initiation of the gradient drift waves at different longitude sectors in the vicinity of the dip equator
   Sekar, R., Gupta, S.P., Chakrabarty, D.
  Journal of Atmospheric and Solar-Terrestrial Physics, 2014, 121(PA), pp. 59–62

64 Characteristics of E-region background ionosphere and plasma waves measured over the dip equator during total solar eclipse campaign
   Sekar, R., Gupta, S.P., Chakrabarty, D.
   Journal of Atmospheric and Solar-Terrestrial Physics, 2014, 114, pp. 58–65

63 Absence of streaming plasma waves around noontime over Thumba in recent times: Is it related to the movement of the dip equator?
  Sekar, R., Gupta, S.P., Acharya, Y.B., Tiwari, D., Choudhary, R.K.
 Journal of Atmospheric and Solar-Terrestrial Physics, 2013, 103, pp. 8–15

62 Advances in Space Research: Preface
  Gupta, S.P.
  Advances in Space Research, 2005, 35(8 SPEC. ISS.), pp. 1433

61 Latitude gradients in the natural variance in stratospheric conductivity - Implications for studies of long-term changes
  Bering III, E.A., Benbrook, J.R., Holzworth, R.H., Byrne, G.J., Gupta, S.P.
  Advances in Space Research, 2005, 35(8 SPEC. ISS.), pp. 1385–1397

60 High-resolution mesospheric layer structures from MST radar backscatter echoes over low latitude
  Chakravarty, S.C., Datta, J., Kamala, S., Gupta, S.P.
Journal of Atmospheric and Solar-Terrestrial Physics, 2004, 66(10), pp. 859–866

59 Solar activity and atmospheric tide effect on the polar conductivity and the vertical electric field in the stratosphere at low latitude
  Gupta, S.P.
  Advances in Space Research, 2004, 34(8), pp. 1798–1800

58 In situ measurements of sub-meter plasma waves over low-latitude ionosphere during Leonid-99 meteor storm
  Gupta, S.P., Sekar, R., Acharya, Y.B.
  Annales Geophysicae, 2004, 22(6), pp. 2033–2036

57 A new plasma wave over low latitude ionosphere during Leonid meteor storm
  Gupta, S.P., Sekar, R., Acharya, Y.B.
  Current Science, 2003, 84(10), pp. 1340–1342

56 Long term changes in the electrical conductivity of the stratosphere
  Bering III, E.A, Benbrook, J.R., Byrne, G.J., Holzworth, R., Gupta, S.P.
  Advances in Space Research, 2003, 32(9), pp. 1725–1735

55 Advances in Space Research: Preface
  The Scientific Symposium 2.6
  Lightning middle atmosphere interaction
  S.P Gupta
  2002 COSPAR, Adv. Space Res. Vol. 30, No. 11, p. 2583, 2002

54 Semidiurnal variations of stratospheric conductivity at balloon float altitude
  Gupta, S.P.
  Advances in Space Research, 2002, 30(11), pp. 2631–2635

Refer Collected works of Prof S.P.Gupta 2001

Publication in scientific journals (1968-2001):

53 In-situ measurements of equatorial ionospheric parameters during Leonids 99 meteor shower
  Gupta,S.P, Das.S.R, Acharya.Y.B, Sekar R, Sridharan R, Pukhunkov A.A
  J Atmos. Solar Terr.Physics

52 Solar cycle variation of stratospheric conductivity over low latitude
  Gupta, S.P.
  Advances in Space Research, 2000, 26(8), pp. 1225–1229

51 Two stream instability in E region over magnetic equator during morning hours
  Gupta, S.P.
  Advances in Space Research, 2000, 26(8), pp. 1257–1261

50 Features of lower ionosphere during day and night over magnetic equator
   Gupta,S.P.
   Advances in Space Research, 2000, 25(1), pp. 53–63

49 Diurnal and seasonal variation of D-region electron density at low latitude
   Gupta, S.P.
   Advances in Space Research, 1998, 21(6), pp. 875–881

48 Electron density measurements in the Indian equatorial region during daytime conditions
   Thiemann, H., Rohde, V., Piel, A., Gupta, S.P.
   Advances in Space Research, 1998, 21(6), pp. 883–886

47 Features of E region irregularities at the magnetic equator and in its vicinity
   Gupta, S.P.
   Advances in Space Research, 1997, 20(11), pp. 2195–2198

46 Middle atmospheric electrodynamics at low lattitude over India
   Chakravarty, S.C., Gupta, S.P., Chandrasekaran, S.
   Advances in Space Research, 1997, 20(11), pp. 2181–2189

45 Thin layers of ionization observed by rocketborne probes in equatorial E region
   Gupta, S.P.
   Advances in Space Research, 1997, 19(1), pp. 169–173

44 Role of vertical electric field and neutral winds in the formation of blanketing type of sporadic-E layer over Thumba
   Gupta, S.P, Chandra H.
   Memoirs Geophysical Society of India, 24, pp.401-408(1992)

43 Meteoric ions as tracers for gravity waves over the magnetic equator
   Gupta, S.P.
   Advances in Space Research, 1992, 12(10), pp. 141–144

42 Electrical conductivity and electric field measurements in the stratosphere by balloon- borne probes from Hyderabad
   Gupta.S.P, Acharya.Y.B, Narayan.A.
   Indian J.of Radio and Space Phys., 1991, 20, pp. 295-298

41 A technique for measurement of electrical potential of a balloon-borne gondola
   Narayan, A., Acharya, Y.B., Gupta, S.P.
   Review of Scientific Instruments, 1990, 61(12), pp. 3866–3870

40 Rocket-borne electron-density measurements up to 300 km by day over India
   Gupta, S.P., Thiemann, H.
   Advances in Space Research, 1990, 10(8), pp. 39–40

39 Ionisation layers over the magnetic equator during meteor shower days
   Gupta, S.P.
   Advances in Space Research, 1990, 10(10), pp. 105–108

38 In-situ measurements of plasma parameters in the equatorial ionosphere by the resonance cone technique
   Thiemann, H., Piel, A., Gupta, S.P.
   Advances in Space Research, 1988, 8(8), pp. 147–150

37 Expansion of plasma in the wake region of moving rockets-evidence of enhanced electron temperature
   Gupta, S.P.
   Advances in Space Research, 1988, 8(1), pp. 225–228

36 Latitudinal variation in the ionospheric parameters: a Soviet-Indian experiment by simultaneous launchings
   Danilov, A.D., Pokhunkov, A.A., Varfolomeev, V.A., Gupta, S.P., Das, S.R.
   Journal of Atmospheric and Terrestrial Physics, 1988, 50(3), pp. 175–179

35 Ion-conductivity measurements by a balloon-borne probe in the low latitude stratosphere
   Narayan, A., Gupta, S.P.
   Advances in Space Research, 1987, 7(10), pp. 359–362

34 In situ measurements of winds, electric fields and electron densities at the onset of equatorial spread-F
   Raghavarao, R., Gupta, S.P., Sekar, R., Babu, V.V., Sudhakar, V.
   Journal of Atmospheric and Terrestrial Physics, 1987, 49(5), pp. 485–492

33 Balloon-borne measurements of ion conductivity over low latitude stratosphere
   Gupta, S.P., Narayan, A.
   Planetary and Space Science, 1987, 35(4), pp. 439–443

32 Electron density profiles in the equatorial F-region during evening hours
   Gupta, S.P.
   Advances in Space Research, 1987, 7(6), pp. 69–71

31 Formation of sporadic E layers at low magnetic latitudes
   Gupta, S.P.
   Planetary and Space Science, 1986, 34(11), pp. 1081–1085

30 Structure of the equatorial lower ionosphere from the Thumba Langmuir probe   experiments
   Subbaraya, B.H., Prakash, S., Gupta, S.P.
   Advances in Space Research, 1985, 5(7), pp. 35–38

29 Meteorological effects observed in the D-region of the equatorial ionosphere
   Gupta, S.P., Narayan, A.
   Advances in Space Research, 1984, 4(4), pp. 167–169

28 Role of neutral winds in generating irregularities in equatorial F-region
   Gupta, S.P.
   Advances in Space Research, 1982, 2(10), pp. 143–146

27 Importance of electric field measurement over low latitudes at stratospheric heights by balloons
   Gupta, S.P.
   Advances in Space Research, 1983, 3(6), pp. 115–116

26 Mesospheric ionisation over dip equator at sunrise
   Gupta, S.P.
   Advances in Space Research, 1982, 2(10), pp. 217–219

25 The resonance cone technique for exciting electron acoustic waves in equatorial ionosphere
   Gupta, S.P.
   Advances in Space Research, 1982, 2(7), pp. 87–88

24 On variation of lambda and alpha effect in the mesosphere during the solar eclipse
   Gupta,S.P. ,Chakravarty,D.K.
   Proc. Indian Acad.Sci. , Earth Suppl., 1982, 48A, p518

23 Plasma sheets, plasma currents and electric field double layers in the equatorial ionosphere
   Gupta, S.P.
   Advances in Space Research, 1981, 1(1), pp. 201–203

22 On the formation of a sharp layer of metallic constituents at sunrise in the lower thermosphere
   Shirke, J.S., Sridharan, R., Gupta, S.P.,Semenov, V.K., Verfolomeev, V.A.
   Proceedings of the Indian Academy of Sciences - Earth and Planetary Sciences, 1981, 90(2), pp. 141–146

21 A review of the electron density irregularities in the equatorial D and E regions.
   Prakash, S., Gupta, S.P., Subbaraya, B.H., Pandey, R
   Adv. Space Explorer, 1980, .8, pp3–16

20. In situ measurements of equatorial E region plasma parameters during spread F conditions
   Gupta, S.P.
   COSPAR Colloquia Series, 1980, 20(C), pp. 127–130

19 Plasma irregularities and soft energy electron fluxes in the equatorial E-region
   Gupta, S.P.
   Space Research XIX, 1979, 19. p.275

18 Experimental evidence of ion plasma oscillations in the apogee region of the Nike-Apache rocket
   Gupta, S.P., Prakash, S.
   Planetary and Space Science, 1979, 27(2), pp. 145–150

17 Electric fields in the E-region during counter electrojet.
   Prakash, S., Gupta, S.P., Subbaraya, B.H., Pandey, R.,
   Space Res. 1979, 19, 279–282.

16 Special characteristics of cross field and two stream instability as revealed by rocketborne studies
   Gupta, S.P., Subbaraya, B.H, Prakash Satya
   J.Geophys.1977, 43, pp 681-686

15 Electron temperature in equatorial E-region during day and night
   Gupta, S.P, Subbaraya, B.H, Prakash Satya
   Space Res, 1977, XVII, Pergamon Press, Oxford, pp.399-402

14 Preliminary report on Common Wealth collaborative rocket programme from Thumba
   Rees.D., Bhavsar.P.B, Desai J N, Gupta S.P, Farmer A. D.
   Space Res.1976, XVI, pp.407-412

13 Ionization irregularities in the E-region during counter electrojet
   Prakash Satya, Gupta.S.P. , Sinha H.S.S. and Rao T.R.
   Space Res., 1976, XVI, Akademic-Verlag Berlin, pp.401-405

12 Measurement of electron temperatures in the lower ionosphere by detecting the space potential on the langmuir probe characteristic
   Subbaraya, B.H., Prakash, S., Gupta, S.P., Sinha, H.S.S.
   Planetary and Space Science, 1974, 22(1), pp. 180–181

11 Some features of the equatorial D-region as revealed from the Langmuir probe experiment
   Subbaraya,B.H.,Prakash Satya and Gupta,S.P.
   Space Research, XIV, 1974, pp.259-265

10. Rocket Measurements of Ionization Irregularities in the equatorial Ionosphere at Thumba and Identification of Plasma Instabilities
   Satya Prakash,B.H.Subbaraya and S.P.Gupta
   Indian Journal of Radio and Space Physics, Vol 1, March 1972, pp 72-80

9 Night-time E-region at Thumba.
   Subbaraya,B.H,Prakash.Satya, Gupta.S.P.
   Indian J. of Pure and Applied Phys, 1971, 9, pp.626-630

8 Experimental evidence for cross field instability in the equatorial
   Prakash.Satya, Gupta.S.P,, Subbaraya,B.H,
   Space Research, XI, 1971, pp.1139-1145, Akademic-Verlag, Berlin

7 Investigation of the daytime lower ionosphere over the equator using Langmuir probe and plasma noise probe
   Prakash, S., Subbaraya, B.H., Gupta, S.P.
   Journal of Atmospheric and Terrestrial Physics, 1971, 33(2), pp. 129–135

6 Electrostatic plasma instabilities in the equatorial electrojet.
   Prakash, S., Gupta, S.P., Subbaraya, B.H., Jain, C.L.,
   1971b. , Nature 233 (38), 56–58 http://dx.doi.org/10.1038/physci233056a0.

5 Crossfield instability and ionisation irregularities in equatorial E region,
   Prakash, S., S.P. Gupta and B.H. Subbaraya,
   Nature Physical Sci., (1971a), 230-16, pp 170-171.

4 A study of the irregularities in the night time equatorial E-region using a Langmuir probe and plasma noise probe
   Prakash, S., Gupta, S.P., Subbaraya, B.H.
   Planetary and Space Science, 1970, 18(9), pp. 1307–1318

3 A study of the lower ionosphere over the geomagnetic equator Thumba using a Langmuir probe and plasma noise probe.
   Prakash, S, Gupta S.P, Subbaraya B.H.
   Space Research IX, 1969, pp. 237-244

2 Irregularities in the Equatorial E Region Over Thumba
   Prakash, S., Gupta, S.P., Subbaraya, B.H.
   Radio Science, 1969, 4(9), pp. 791–796

1 A study of the equatorial E-region during evening twilight using a Langmuir probe
   Prakash, S., Subbaraya, B.H., Gupta, S.P.
   Journal of Atmospheric and Terrestrial Physics, 1968, 30(6), pp. 1193–1202

Reports:

Balloonborne experiments for middle atmospheric conductivity campaign,
ISRO-IMAP S.R. 39, 1992.
Gupta, S.P., S.C. Chakravarty and S. Chandrasekaran (Editor)

DEOS: Dynamics of the equatorial ionosphere over SHAR: Indo-German low-latitude rocket project
Thiemann, H., Mayer, G., Piel A, Steigies C. , Olsen, N,. Primdahl, F, Sridharan, R., Gupta
S.P, Rangarajan, G. K.Rao, D.R.K., Rao, P.B.
European Space Agency, (Special Publication) ESA SP, 1997, (397), pp. 349–354

Electron Densities in the Equatorial Lower Ionosphere from the Langmuir Probe Experiments
Conducted at Thumba
During 1966–1978
Subbaraya, B.H., Prakash, S., Gupta, S.P.
1983, ISRO Scientific Report, ISRO-PRL-SR-15-83.

PhD Thesis, 1970:

The Study of the Lower Ionosphere at Low Latitude
S.P.Gupta

Altitude of Two-Stream Irregularities in Equatorial *E* Region Using Sounding Rocket Experiments From Thumba

Kuldeep Pandey[1] iD and **S. P. Gupta[1]**

[1]Physical Research Laboratory, Ahmedabad, India

Abstract Amplitudes of two-stream irregularities and equatorial electrojet (EEJ) current are known to peak around the same altitude. Sounding rocket-borne magnetometer experiments have consistently shown that the EEJ current density maximizes around 105-km altitude whereas the theoretical models predict the EEJ peak around 100 km. One of the propositions to bridge this difference in the altitude has been based on the inclusion of small-scale turbulence (wavelength of <100 m) with the large-scale dynamics (kilometer size). This proposition is examined based on in situ measurements of E region electron density and plasma irregularities (two-stream and gradient-drift irregularities) obtained at different times of the day and night. These measurements were obtained based on sounding rocket flight experiments conducted from Thumba Equatorial Rocket Launching Station (8.54° N, 76.86° E), a facility in the vicinity of the dip equator. Whenever two-stream irregularities are present, the minimum electrojet current density is estimated based on the threshold velocity required for generation of these plasma irregularities. This method provides estimates of nighttime E region current also, which is difficult to measure. It is found that amplitudes of both two-stream irregularities and the estimated EEJ current peak around 105-km altitude irrespective of the presence or absence of the gradient-drift irregularities at the base of electrojet (95- to 100-km altitude).

1. Introduction

In the equatorial *E* region, a strong eastward current flows during daytime that is known as equatorial electrojet (EEJ). General characteristics of EEJ have been studied based on a large number of experiments conducted using ground-based magnetometers (e.g., Rastogi & Iyer, 1976), sounding rocket-borne magnetometers (e.g., Sampath & Sastry, 1979b; Sastry, 1970), magnetometers onboard satellites (e.g., Jadhav et al., 2002; Lühr et al., 2004), and very high frequency radar (e.g., Vikramkumar et al., 1987). Excellent reviews on this topic are available in literature (Forbes, 1981; Raghavarao & Anandarao, 1987; Yamazaki & Maute, 2017). On some occasions, the direction of electrojet current reverses to westward that is popularly known as counter electrojet. Variations in the horizontal component of magnetic field produced by EEJ are used to obtain the ionospheric zonal electric field (Anderson et al., 2004; Pandey et al., 2017), which plays an important role in different ionospheric processes.

Sounding rocket-borne magnetometer experiments conducted from both Indian (Sastry, 1970; Sampath & Sastry, 1979b) and Peruvian (Davis et al., 1967; Pfaff et al., 1997) sectors have consistently shown that the EEJ current peaks around 105-km altitude. However, theoretical models (Anandarao, 1976; Richmond, 1973; Sugiura & Poros, 1969) predict the peak of EEJ current to be around 100 km. This is because the Cowling conductivity, which is responsible for the electrojet current and used in these models, maximizes around 100 km (Kelley, 2009). Many propositions (Gagnepain et al., 1977; Kelley & Ilma, 2013; Ronchi et al., 1990; Stening, 1985) were made to resolve this difference in altitude of EEJ peak between observations and theoretical models. Gagnepain et al. (1977) noticed that, if the value of the electron collision frequency is taken as four times the laboratory data, then the computed EEJ peak shifts to around 105-km altitude. Based on the two-fluid, nonlocal theory of the gradient-drift instability, Ronchi et al. (1990) showed that the effects of including the small-scale (scale-size of <100 m) turbulence on the large-scale (kilometer scale) dynamics are to increase the effective electron collision frequency by a factor of 4, which was the same as suggested by Gagnepain et al. (1977).

The electrojet region is known (Farley, 2009; Fejer & Kelley, 1980) to host mainly two types of plasma irregularities: Type I or two-stream irregularity and Type II or gradient-drift irregularity. Two-stream irregularities are generated when electrons stream with speed more than the ion acoustic velocity of the medium (Farley, 1963). These irregularities appear in the altitude range 100–110 km (Prakash et al., 1971b) with scale sizes 1–15 m (Balsley & Farley, 1971; Prakash et al., 1969). The gradient-drift irregularities are produced when the electron density gradient is parallel to the vertical electric field (Prakash et al., 1971a, 1972; Reid, 1968). These irregularities can be generated almost throughout the *E* region (Prakash et al., 1971a) and have scale sizes longer than 3 m (Farley, 1963). As the gradient-drift irregularities at smaller scale sizes are weaker and difficult to obtain directly from telemetry charts, the amplitude of 30- to 300-m scale size irregularities is taken as representative of the amplitude of these plasma irregularities (Prakash et al., 1970). Both two-stream and gradient-drift irregularities have been studied comprehensibly using ground-based radars (Balsley & Farley, 1971; Bowles et al., 1960; Cohen & Bowles, 1967; Hysell et al., 2007; Krishna Murthy et al., 1998; Lu et al., 2008; Reddy et al., 1987) and sounding rocket-borne Langmuir probes (Gupta, 2000; Pfaff et al., 1997; Prakash & Muralikrishna, 1976; Prakash et al., 1971a, 1971b).

High-resolution measurements of two-stream and gradient-drift irregularities were carried out using sounding rocket-borne Langmuir probe experiments conducted over several decades from Thumba Equatorial Rocket Launching Station (TERLS). Based on those experiments, percentage amplitudes of plasma irregularities with scale sizes 1–15 and 30–300 m at different times of the day (Gupta, 2000; Prakash et al., 1971b) and night (Gupta, 1986, 1997) were reported in literature. The percentage amplitude of 1- to 15-m irregularities was obtained based on a filter and amplifier onboard rocket flight. On the other hand, the amplitudes of irregularities at larger scale sizes (30–300 m) were obtained directly from the telemetry chart of electron density. It is to be noted that the amplitudes of 15- to 30-m irregularities were not reported in earlier literature because of the difficulties involved in identifying the changes at this scale size directly from the telemetry charts. The earlier studies primarily focused on the presence or absence of two-stream irregularities (1- to 15-m size irregularities) and their spectral characteristics. However, no special attention has been given to investigate the change, if any, in the altitude of two-stream irregularities in the presence or absence of gradient-drift irregularities at the base of electrojet (95–100 km). This is probably due to the fact that, on almost all the occasions, the gradient-drift irregularities are present below 100-km altitude (Gupta & Prakash, 1979; Prakash et al., 1971a, 1980; Sekar et al., 2014).

In the present investigation, the dip-equatorial *E* region current densities are estimated corresponding to the time of rocket flights in which two-stream irregularities are present. This method provides estimates of nighttime dip-equatorial *E* region current density, which is difficult to measure (Sastry, 1970; Shuman, 1970). In addition, altitudes of the peak amplitude of the two-stream irregularities and the estimated EEJ current density are investigated for the cases in which gradient-drift irregularities are either present or absent at the base of electrojet (95–100 km). Results obtain are used to examine the proposition made by Ronchi et al. (1990) that the interaction of small-scale turbulence (wavelength of <100 m) with large-scale dynamics (kilometer size) can shift the altitude of peak EEJ to 105 km from 100-km altitude in theoretical models.

2. Data Set and Methodology

In situ measurements of altitude profiles of *E* region electron density and irregularities were obtained using sounding rocket flight experiments conducted from TERLS (8.54° N, 76.86° E). These experiments were carried out at different times of the day and night over several decades (Gupta, 2000; Prakash et al., 1970; Sekar et al., 2014; Subbaraya et al., 1983). In the present investigation, the experiments conducted from 1960 to 1990 are considered because during this period, the dip angle over TERLS was less than 1.5°. Among these, only those experiments are used in which two-stream irregularities were detected. Further, these experiments are categorized in two groups. The first group includes the rocket flights in which gradient-drift irregularities are present at the base of EEJ (95- to 100-km altitude). The second group consists of those rocket flights that did not detect the presence of gradient-drift irregularities at the base of EEJ.

As a representative for the first category, in which gradient-drift irregularities are present in the range of 95–100 km, the measurements from rocket flight experiments conducted at 1040 IST on 28 January 1971 are used. For the second category, in which gradient-drift irregularities are absent between 95- and 100-km altitude, three rocket flight experiments are identified. These include one daytime flight conducted at 1532 IST on 17 August 1972 and two nighttime flights conducted at 0559 IST on 09 February 1975 and 2204

IST on 15 March 1975. Here, IST refers to Indian Standard Time (IST = UT + 5.5 hr). Altitude profiles of electron density and amplitudes of two-stream irregularities obtained using the experiments carried out on 28 January 1971 (Prakash et al., 1980), 17 August 1972 (Prakash et al., 1976, 1979), 09 February 1975 (Gupta, 1986), and 15 March 1975 (Gupta, 1997) are reproduced from literature. In addition, the telemetry records of all the four rocket flights are analyzed to obtain the amplitude of gradient-drift irregularities at scale sizes 30–300 m. The records of spectrum analysis of both the daytime flights are also used to provide the amplitude of plasma irregularity with different scale sizes between 1 and 15 m. The records of spectrum analysis for nighttime flights are not available. These spectrum records along with the direction of background electric field and gradient in electron density are used to establish whether the 1- to 15-m scale size irregularities have contribution from gradient-drift irregularities. As stated in section 1, the amplitude of 1- to 15-m scale size irregularities is obtained using an onboard filter and amplifier, whereas the amplitudes of 30- to 300-m irregularities are obtained directly from the telemetry records. Therefore, in case of 1- to 15-m irregularities, even the smaller amplitudes (larger than 0.5%) are taken as geophysical, whereas, for 30- to 300-m size irregularities, the amplitudes below 3–4% are not considered significant.

Ground-based magnetograms of dip-equatorial station Trivandrum (TRD, 8.48° N, 76.95° E) and Alibag (ABG, 18.64° N, 72.87° E) are used to obtain the magnetic field produced by EEJ current (Rastogi & Iyer, 1976). These magnetograms are obtained from World Data Centre for Geomagnetism—Indian Institute of Geomagnetism, Mumbai, for 28 January 1971 and digitalized from Prakash et al. (1976) for 17 August 1972. The polarity of magnetic field produced by EEJ is used to infer the direction of the zonal electric field. The positive and negative values are taken as indicative of eastward and westward electric fields, respectively. Subsequently, this information is used to infer the direction of the vertical electric field (Pandey et al., 2017).

As stated in section 1, two-stream irregularities are generated when electrons stream with speed more than the ion acoustic velocity of the medium. Therefore, whenever two-stream irregularities are present, the zonal velocity ($\mathbf{V}_d$) of electrons must be

$$\mathbf{V}_d > \mathbf{V}_i(1 + \psi), \tag{1}$$

where $\mathbf{V}_i$ is the ion thermal velocity and ψ is given as follows:

$$\psi = \frac{\nu_i \nu_e}{\Omega_i \Omega_e}. \tag{2}$$

Here ν and Ω represent collision and gyrofrequencies with subscripts i and e representing ions and electrons, respectively. Around 105-km altitude, the values of ψ and $\mathbf{V}_i$ are about 0.1 and 330 m/s, respectively (Sekar et al., 2013). This corresponds to $\mathbf{V}_d$ more than 360 m/s. Therefore, whenever two-stream irregularities are present, the threshold EEJ current density ($\mathbf{J}$) is determined as follows:

$$\mathbf{J} = N_e \cdot \mathbf{e} \cdot \mathbf{V}_d, \tag{3}$$

where N_e and $\mathbf{e}$ are electron density and electronic charge, respectively.

3. Results

A typical example of *E* region plasma measurements when two-stream irregularities are observed in the presence of gradient-drift irregularities at the base of EEJ (below 100 km) is shown in Figure 1. These profiles are based on sounding rocket flight experiment conducted at 1040 IST on 28 January 1971. Altitude profile of electron density is depicted with black color solid line in Figure 1a. In addition, percentage amplitudes of two-stream (scale size of 1–15 m) and gradient-drift (scale size of 30–300 m) irregularities are depicted with red color solid line and blue color dots, respectively. It can be noticed that the amplitude of two-stream irregularities peaks around 105-km altitude. Gradient-drift irregularities are present below 100-km altitude, wherein the electron density gradient is upward (positive). The temporal variation of magnetic field produced by EEJ current on this day is depicted in Figure 1b with black color. The black arrow marked in this figure demarcates the time of rocket flight experiment. It can be seen that, at the time of rocket flight experiment the normal EEJ is present with a strength of about 45 nT. This indicates that the zonal electric field is eastward and the corresponding vertical electric field would be upward. Therefore, the presence of gradient-drift irregularities below 100-km altitude (wherein the electron density gradient is upward) is consistent with the generation mechanism of these plasma irregularities.
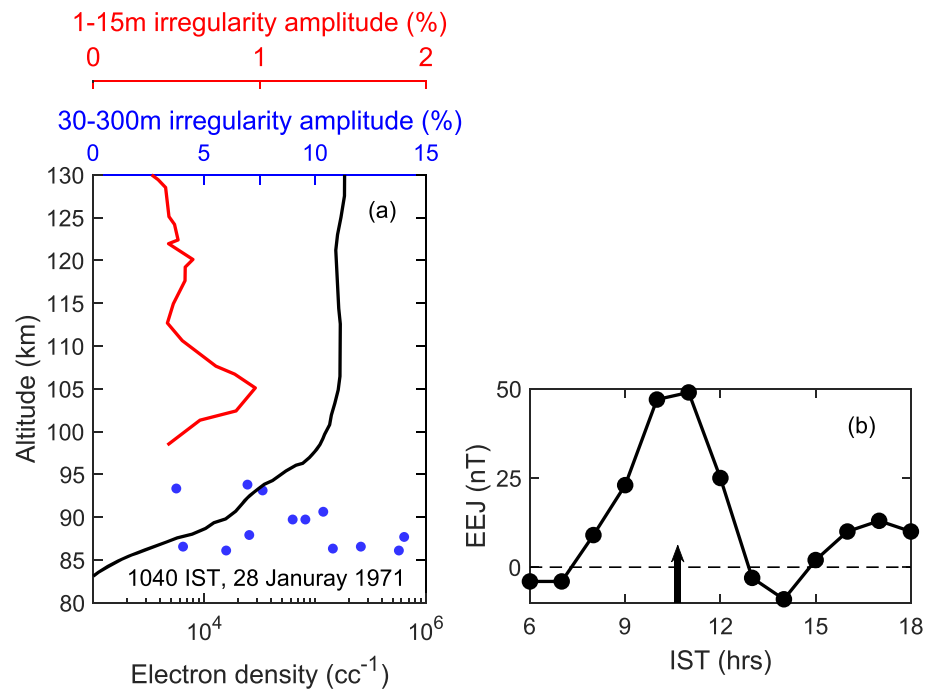
Figure 1. (a) Altitude profiles of *E* region electron density (black) along with 1- to 15-m (red) and 30- to 300-m (blue) scale size irregularities obtained based on sounding rocket flight experiment conducted at 1040 IST on 28 January 1971 and (b) temporal variation of equatorial electrojet (EEJ) strength obtained using ground-based magnetograms. The black arrow indicates the time of rocket flight experiment.

The 1- to 15-m plasma irregularities can have possible contributions from both two-stream and gradient-drift irregularities, as both two-stream and gradient-drift mechanisms can generate 3- to 15-m irregularities. Therefore, spectrum analysis of plasma irregularities with different scale sizes between 1 and 15 m is also looked into. The records of such spectrum analysis for the rocket flight conducted on 28 January 1971 are depicted in Figure 2. The results of spectrum analysis around 94-, 97-, and 105-km altitudes are depicted in left, middle, and right panels of the figure. In each panel, the scale size of plasma irregularities is in decreasing order from top to bottom channels. The scale sizes of plasma irregularities depicted at the top and bottom are about 10–15 and 1–2 m, respectively. It can be seen that the 10- to 15-m scale size irregularities are present at all these altitudes, though in varying strengths. However, the 1- to 2- and 2- to 3-m scale size irregularities are absent at 94 and 97 km and present around 105-km altitude. Therefore, at the time of
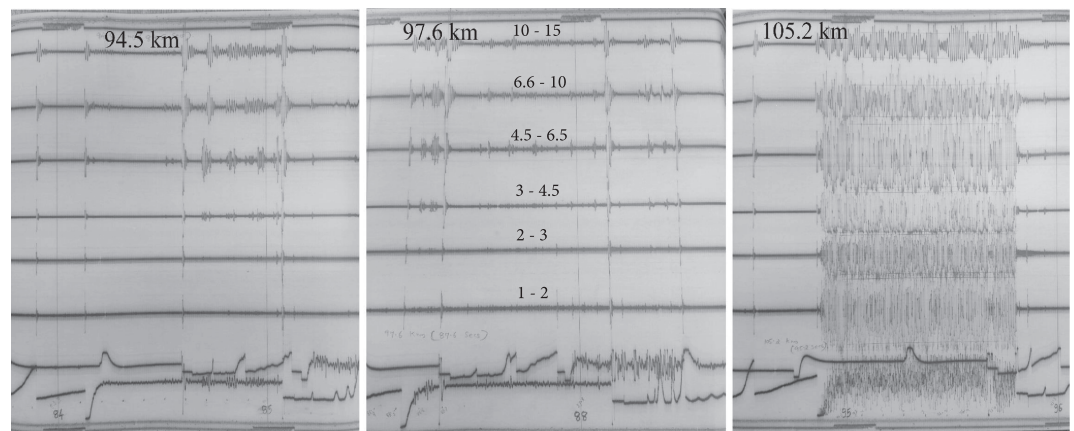

Figure 2. Plasma irregularities with different scale sizes between 1 and 15 m obtained based on the rocket flight experiment conducted at 1040 IST on 28 January 1971. The scale sizes of the plasma irregularities are in decreasing order from top to bottom. Scale sizes of irregularities (in meters) are written in the middle panel.
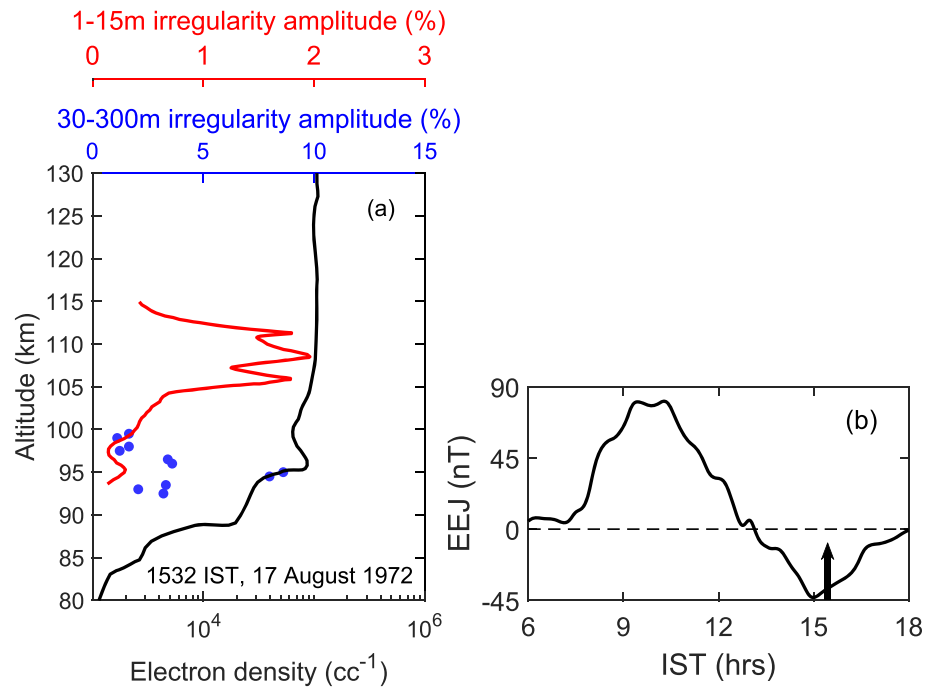
Figure 3. Same as Figure 1 but for sounding rocket experiment conducted at 1532 IST on 17 August 1972.

this rocket flight experiment, the gradient-drift irregularities are present throughout 94- to 105-km altitude range, and the amplitude of two-stream irregularities peaks around 105-km altitude.

The E region plasma measurements obtained using sounding rocket experiment conducted at 1532 IST on 17 August 1972 are depicted in Figure 3a. The altitude profile of electron density is depicted with black color solid line. The percentage amplitudes of 1- to 15- and 30- to 300-m scale size irregularities are depicted with red color solid line and blue color dots, respectively. It can be seen that the amplitude of two-stream (1–15 m) irregularities maximizes around 109 km with additional peaks around 106 and 111 km. The 30- to 300-m scale size irregularities are very weak below 100-km altitude except between 94 and 95 km. It is to be noted that the gradient in electron density is upward except in the altitude range 96–99 km. Therefore, the presence of these irregularities around 94–95 km is not due to gradient-drift mechanism. Figure 3b depicts the temporal variation of the magnetic field produced by EEJ current on this day. The black arrow marks the time at which the rocket flight experiment was conducted. It is to be noted that the counter electrojet condition is prevalent at the time of rocket flight. This indicates that, at this time, the zonal and vertical electric fields are westward and downward, respectively. This is consistent with the absence or very weak presence of gradient-drift irregularities during this flight.

Spectrum analysis of plasma irregularities with different scale sizes between 1 and 15 m, obtained for the sounding rocket experiment conducted on 17 August 1972, is depicted in Figure 4. The results obtained from this analysis around 93-, 96-, and 107-km altitudes are depicted in left, middle, and right panels of the figure. It is to be noted that, in this case, the number of frequency channels used for the spectrum analysis is more than those used in the case of the other daytime flight (28 January 1971). In each panel, the scale size of plasma irregularities is in decreasing order from top to bottom channels. The plasma irregularities in the top and bottom channels correspond to scale sizes of about 12–15 and 1–2 m, respectively. It can be seen that irregularities at all the scale sizes are absent at both 93- and 96-km altitudes. Around 107-km altitude, the 1- to 2- and 2- to 3-m scale size irregularities are present, but 8- to 12- and 12- to 15-m irregularities are absent. Therefore, during this rocket flight, the gradient-drift irregularities are absent below 100 km, and two-stream irregularities peak around 109 km with secondary peaks around 106- and 111-km altitudes.

Figures 5a and 5b depict the E region measurements reported based on sounding rocket experiments conducted at 0559 IST on 09 February 1975 and at 2204 IST on 15 March 1975, respectively. In each figure, the electron density profile is depicted with black color sold line along with the amplitudes of 1- to 15- and 30-
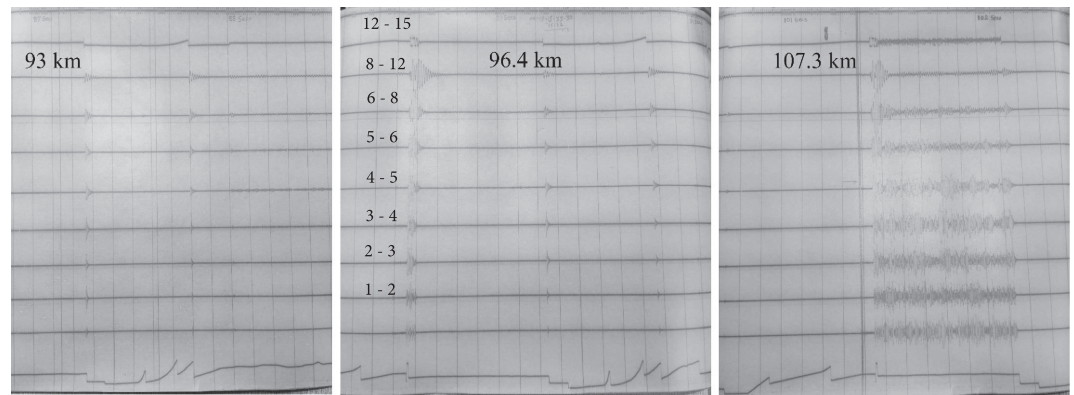
Figure 4. Same as Figure 2 but based on sounding rocket experiment conducted at 1532 IST on 17 August 1972. Note that the number of spectrum channels is more in this case.

to 300-m irregularities shown with red color solid line and blue color dots, respectively. It can be noticed from Figure 5a that the electron density gradient is negligible in the altitude range 90–98 km. Further, the amplitude of gradient-drift irregularities is also very small in this altitude range. In Figure 5b, the electron density gradient is upward between ~95- and 100-km altitude range wherein the amplitude of gradient-drift irregularities is very small. It is to be noted that the amplitudes of two-stream irregularities in both cases peak around 105-km altitude, though the amplitudes of gradient-drift irregularities at the base (95–100 km) are either very small or these irregularities are absent.

The minimum EEJ current densities at times of all the four rocket flights are estimated based on equation (3). The estimates are obtained for range of altitudes wherein two-stream irregularities are present. This is done by using V_d value of 360 m/s and Ne at that particular altitude. The estimated zonal current density and the altitude of its peak value for each rocket flight are listed in Table 1. The zonal current densities are estimated to be about 9.6 $\mu A/m^2$ around noon, -5.7 $\mu A/m^2$ during afternoon counter electrojet event, -0.6 $\mu A/m^2$ in
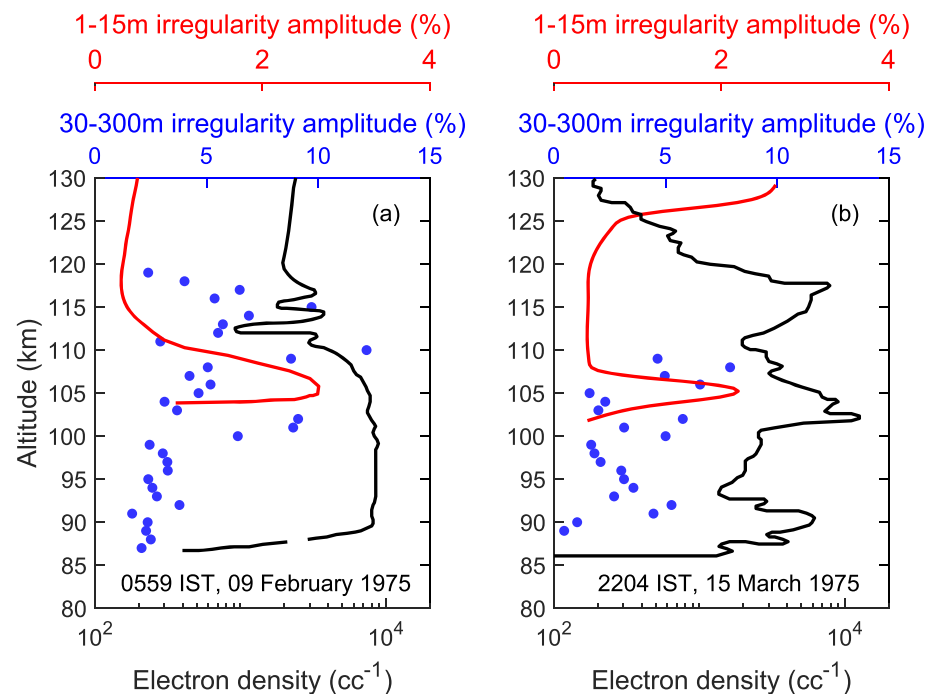

Figure 5. Altitude profiles of E region electron density (black) along with 1- to 15-m (red) and 30- to 300-m (blue) scale size irregularities obtained based on sounding rocket flight experiments conducted at (a) 0559 IST on 09 February 1975 and (b) 2204 IST on 15 March 1975.

Table 1
Estimates of Threshold Zonal Current Density and Altitude of its Peak Amplitude at the Times of Four Sounding Rocket Flight Experiments

Time (IST) and date	Zonal current density $\mathbf{J}$ (μA/m^2)	Altitude of peak $\mathbf{J}$ (km)
1040 on 28 January 1971	9.58	106
1532 on 17 August 1972	−5.67	108
0559 on 09 February 1975	−0.56	106
2204 on 15 March 1975	−0.44	104

predawn hours, and −0.4 μA/m^2 in premidnight. It is to be noted that in all the four cases under consideration, the altitude of EEJ peak and amplitude of two-stream irregularities are found to be around 105 km or above. Implications of these results are discussed in section 4.

4. Discussion

Two-stream irregularities at 3-m scale size have been studied using ground-based radars (Hysell et al., 2007; Krishna Murthy & Ravindran, 1994; Krishna Murthy et al., 1998; Lühr et al., 2004; Ravindran & Krishna Murthy, 1997). As the two-stream irregularities are generated only after a threshold electric field is reached, observations of these irregularities during counter eletrojet are sparse. Despite long history of radar-based observations of two-stream irregularities, the presence of these plasma irregularities during the counter electrojet conditions was noticed on only a few occasions (Crochet et al., 1979; Somayajulu et al., 1994; Woodman & Chau, 2002). Therefore, the sounding rocket flight-based observation of two-stream irregularities during the counter electrojet conditions at 1532 IST on 17 August 1972 is an important experiment. This counter electrojet event occurred during the afternoon hours in June solstice under solar minimum conditions that has been shown (Pandey et al., 2018) to be the time for the most frequent occurrence of counter electrojet events over the Indian sector. The advantage of this rocket flight experiment is that the simultaneous observations of electron density are available along with the plasma irregularities in different scale sizes.

In radar-based experiments, the Doppler echoes of two-stream irregularities are received from 100 to 110 km. However, these studies cannot precisely determine the altitude of the peak amplitude of these irregularities. The low-power radars cannot detect the presence of two-stream irregularities during nighttime due to small electron density values. Though the high-power radars can detect the presence or absence of two-stream irregularities at nighttime also, the altitude of the peak amplitude of such irregularities cannot be determined. Sounding rocket-borne Langmuir probe experiments are crucial to study the *E* region irregularities during nighttime and for better determination of altitude of the peak amplitude of two-stream irregularities. Therefore, the sounding rocket flight-based high-resolution measurements of *E* region electron density profiles and structures are used in the present investigation. These rocket flight experiments were conducted during 1971–1975 when the dip angle over TERLS was between −1.1° to −1.0°. Therefore, the presence of two-stream irregularities at the times of these rocket flights is consistent with the observation made by Sekar et al. (2013) that the two-stream irregularities are generated over Thumba when the dip angle is less than 1.5°.

The results obtained from four rocket flight experiments conducted at different times of day and nighttime are depicted in Figures 1–5. Two of these rocket flight experiments were conducted in the daytime, and the other two at night. Among the daytime flights, one (28 January 1971) was conducted under normal electrojet conditions, whereas at the time of other flight (17 August 1972) counter electrojet conditions were prevalent. The other two rocket flights were conducted in predawn (09 February 1975) and premidnight (15 March 1975) hours. As stated in section 3, the gradient-drift irregularities are present below 100 km for the flight conducted on 28 January 1971 under normal electrojet, whereas, for the flight conducted under counter electrojet condition (17 August 1972) the 30- to 300-m scale size irregularities are absent below 100 km except for the altitude range 94–95 km. At the times of both predawn and premidnight experiments, these irregularities are either absent below 100-km altitude or present with weak strength. Further, it is to be noted that in all these four rocket flights, the peak amplitude of two-stream irregularities is around 105-km altitude or above (see Figures 1, 3, and 5).

The minimum strength of electrojet current densities on all four rocket flight experiments is estimated (see Table 1) based on threshold velocity required for the generation of two-stream irregularities. The EEJ current density is found to be about 9.6 μA/m^2 around noon hours. This value is in the range of typical daytime EEJ current density of about 8–14 μA/m^2 measured based on sounding rocket flight experiments (Sastry, 1970; Sampath & Sastry, 1979a, 1979b). The strength of counter electrojet current density is estimated to be about −5.7 μA/m^2. The current densities are estimated to be about −0.4 μA/m^2 in premidnight hours and about −0.6 μA/m^2 in predawn hours. It is to be noted that it is difficult to measure (Davis et al., 1967; Sastry, 1970; Shuman, 1970) or estimate (Pandey et al., 2016; Stening & Winch, 1987) the nighttime E region current. It is important to note that, in all the four cases, the electrojet current maximizes around 105 km or above (see Table 1).

It is found that the peak amplitude of two-stream irregularities and electrojet current remains around 105 km or above, irrespective of the presence or absence of gradient-drift irregularities at the base of EEJ (95–100 km). Therefore, the presence or absence of 30- to 300-m scale size irregularities at the base of electrojet has no significant effect on the altitude of peak EEJ current, and it peaks around ∼105 km or above in all four cases (see Table 1). It shows that the interaction of the small-scale (wavelength of <100 m) turbulence on large-scale (kilometer size) dynamics would not result in significant shift in the altitude of peak EEJ current.

5. Summary

Sounding rocket flight-based high-resolution measurements of E region electron density and plasma irregularities are used to estimate the threshold EEJ current density at both daytime and nighttime whenever the two-stream irregularities are present. Based on this investigation, the following points have emerged.

1. The minimum magnitudes of current densities are estimated to be about 9.6 μA/m^2 around noontime, about 5.7 μA/m^2 during a counter electrojet event in afternoon hours, 0.4 μA/m^2 in premidnight, and 0.6 μA/m^2 in predawn hours.
2. The presence or absence of gradient-drift irregularities at the base of EEJ (95–100 km) does not change the altitude (∼105 km) of peak amplitude of two-stream irregularities.
3. The presence or absence of 30- to 300-m scale size irregularities does not change the altitude of peak EEJ current. It peaks around ∼105 km or above. It shows that the interaction of small-scale (wavelength of <100 m) turbulence on large-scale (kilometer size) dynamics would not result in significant shift in the altitude of peak EEJ current.

References

Anandarao, B. G. (1976). Effects of gravity wave winds and wind shears on equatorial electrojet. *Geophysical Research Letters*, *3*(9), 545–548. https://doi.org/10.1029/GL003i009p00545

Anderson, D., Anghel, A., Chau, J., & Veliz, O. (2004). Daytime vertical E×B drift velocities inferred from ground-based magnetometer observations at low latitudes. *Space Weather*, *2*, S11001. https://doi.org/10.1029/2004SW000095

Balsley, B. B., & Farley, D. T. (1971). Radar studies of the equatorial electrojet at three frequencies. *Journal of Geophysical Research*, *76*(34), 8341–8351. https://doi.org/10.1029/JA076i034p08341

Bowles, K. L., Cohen, R., Ochs, R. G., & Balsley, B. B. (1960). Radio echoes from field-aligned ionization above the magnetic equator and their resemblance to auroral echoes. *Journal of Geophysical Research*, *65*(6), 1853–1855. https://doi.org/10.1029/JZ065i006p01853

Cohen, R., & Bowles, K. L. (1967). Secondary irregularities in the equatorial electrojet. *Journal of Geophysical Research*, *72*(3), 885–894. https://doi.org/10.1029/JZ072i003p00885

Crochet, M., Hanuise, C., & Broche, P. (1979). Hf radar studies of two-stream instability during an equatorial counter-electrojet. *Journal of Geophysical Research*, *84*(A9), 5223–5233. https://doi.org/10.1029/JA084iA09p05223

Davis, T. N., Burrows, K., & Stolarik, J. D. (1967). A latitude survey of the equatorial electrojet with rocket-borne magnetometers. *Journal of Geophysical Research*, *72*(7), 1845–1861. https://doi.org/10.1029/JZ072i007p01845

Farley, D. T. (1963). A plasma instability resulting in field-aligned irregularities in the ionosphere. *Journal of Geophysical Research*, *68*(22), 6083–6097. https://doi.org/10.1029/JZ068i022p06083

Farley, D. T. (2009). The equatorial E-region and its plasma instabilities: A tutorial. *Annales Geophysicae*, *27*(4), 1509–1520. https://doi.org/10.5194/angeo-27-1509-2009

Fejer, B. G., & Kelley, M. C. (1980). Ionospheric irregularities. *Reviews of Geophysics*, *18*(2), 401–454. https://doi.org/10.1029/RG018i002p00401

Forbes, J. M. (1981). The equatorial electrojet. *Reviews of Geophysics*, *19*(3), 469–504. https://doi.org/10.1029/RG019i003p00469

Gagnepain, J., Crochet, M., & Richmond, A. (1977). Comparison of equatorial electrojet models. *Journal of Atmospheric and Terrestrial Physics*, *39*(9), 1119–1124. https://doi.org/10.1016/0021-9169(77)90020-4

Gupta, S. P. (1986). Formation of sporadic E layers at low magnetic latitudes. *Planetary and Space Science*, *34*(11), 1081–1085. https://doi.org/10.1016/0032-0633(86)90019-X

Gupta, S. P. (1997). Features of E region irregularities at the magnetic equator and in its vicinity. *Advances in Space Research*, *20*(11), 2195–2198. https://doi.org/10.1016/S0273-1177(97)00670-4

Gupta, S. P. (2000). Two stream instability in E region over magnetic equator during morning hours. *Advances in Space Research*, *26*(8), 1257–1261. https://doi.org/10.1016/S0273-1177(99)01212-0

Gupta, S. P., & Prakash, S. (1979). Experimental evidence of ion plasma oscillations in the apogee region of the Nike-Apache rocket. *Planetary and Space Science*, *27*(2), 145–150. https://doi.org/10.1016/0032-0633(79)90044-8

Hysell, D. L., Drexler, J., Shume, E. B., Chau, J. L., Scipion, D. E., Vlasov, M., et al. (2007). Combined radar observations of equatorial electrojet irregularities at Jicamarca. *Annales Geophysicae*, *25*(2), 457–473. https://doi.org/10.5194/angeo-25-457-2007

Jadhav, G., Rajaram, M., & Rajaram, R. (2002). A detailed study of equatorial electrojet phenomenon using Ø rsted satellite observations. *Journal of Geophysical Research*, *107*(A8), 1175. https://doi.org/10.1029/2001JA000183

Kelley, M. C. (2009). *The Earth's Ionosphere: Plasma Physics and Electrodynamics* (2nd ed.). Academic Press.

Kelley, M. C., & Ilma, R. R. (2013). On the development of nonlinear waves in the equatorial electrojet. *Journal of Atmospheric and Solar-Terrestrial Physics*, *103*, 3–7. https://doi.org/10.1016/j.jastp.2012.12.009

Krishna Murthy, B. V., & Ravindran, S. (1994). Effect of small-scale plasma turbulence on altitude profiles of electron drift velocity in the equatorial electrojet: An experimental study. *Journal of Geophysical Research*, *99*(A10), 19,549–19,554.

Krishna Murthy, B. V., Ravindran, S., Viswanathan, K. S., Subbarao, K. S. V., Patra, A. K., & Rao, P. B. (1998). Small-scale (∼3 m) E region irregularities at and off the magnetic equator. *Journal of Geophysical Research*, *103*(A9), 20,761–20,773. https://doi.org/10.1029/98JA00928

Lu, F., Farley, D. T., & Swartz, W. E. (2008). Spread in aspect angles of equatorial E region irregularities. *Journal of Geophysical Research*, *113*, A11309. https://doi.org/10.1029/2008JA013018

Lühr, H., Maus, S., & Rother, M. (2004). Noon-time equatorial electrojet: Its spatial features as determined by the CHAMP satellite. *Journal of Geophysical Research*, *109*, A01306. https://doi.org/10.1029/2002JA009656

Pandey, K., Sekar, R., Anandarao, B. G., Gupta, S. P., & Chakrabarty, D. (2016). Estimation of nighttime dip-equatorial E-region current density using measurements and models. *Journal of Atmospheric and Solar-Terrestrial Physics*, *146*, 160–170. https://doi.org/10.1016/j.jastp.2016.06.002

Pandey, K., Sekar, R., Anandarao, B. G., Gupta, S. P., & Chakrabarty, D. (2018). On the occurrence of afternoon counter electrojet over Indian longitudes during June solstice in solar minimum. *Journal of Geophysical Research: Space Physics*, *123*, 2204–2214. https://doi.org/10.1002/2017JA024725

Pandey, K., Sekar, R., Gupta, S. P., Chakrabarty, D., & Anandarao, B. G. (2017). Comparison of quiet time vertical plasma drifts with global empirical models over the Indian sector: Some insights. *Journal of Atmospheric and Solar-Terrestrial Physics*, *157*, 42–54. https://doi.org/10.1016/j.jastp.2017.03.012

Pfaff, R. F., Sobral, J. H. A., Abdu, M. A., Swartz, W. E., LaBelle, J. W., Larsen, M. F., et al. (1997). The Guará Campaign: A series of rocket-radar investigations of the Earth's upper atmosphere at the magnetic equator. *Geophysical Research Letters*, *24*(13), 1663–1666. https://doi.org/10.1029/97GL01534

Prakash, S., Gupta, S. P., Sinha, H. S. S., & Rao, T. R. (1976). Ionization irregularities in the E region during counter electrojet. *Space Research*, *XVI*, 401–405.

Prakash, S., Gupta, S. P., & Subbaraya, B. H. (1969). Irregularities in the equatorial E region over Thumba. *Radio Science*, *4*(9), 791–796. https://doi.org/10.1029/RS004i009p00791

Prakash, S., Gupta, S. P., & Subbaraya, B. H. (1970). A study of the irregularities in the night time equatorial E-region using a Langmuir probe and plasma noise probe. *Planetary and Space Science*, *18*(9), 1307–1318. https://doi.org/10.1016/0032-0633(70)90141-8

Prakash, S., Gupta, S. P., & Subbaraya, B. H. (1971a). Cross field instability and ionization irregularities in the equatorial E region. *Nature Physical Science*, *230*, 170–171. https://doi.org/10.1038/physci230170a0

Prakash, S., Gupta, S. P., Subbaraya, B. H., & Jain, C. L. (1971b). Electrostatic plasma instabilities in the equatorial electrojet. *Nature Physical Science*, *233*(38), 56–58. https://doi.org/10.1038/physci233056a0

Prakash, S., Gupta, S. P., Subbaraya, B. H., & Pandey, R. (1979). Electric fields in the E region during the counter electrojet. *Space Research*, *XIX*, 279–282.

Prakash, S., Gupta, S., Subbaraya, B., & Pandey, R. (1980). A review of the electron density irregularities in the equatorial D & E. *Advances in Space Research*, 3–16. https://doi.org/10.1016/B978-0-08-024439-6.50006-5

Prakash, S., & Muralikrishna, P. (1976). The nature of electric field in E-region close to morning and evening reversals. *Geophysical Research Letters*, *3*(8), 445–447. https://doi.org/10.1029/GL003i008p00445

Prakash, S., Subbaraya, B. H., & Gupta, S. P. (1972). Rocket measurements of ionization irregularities in the equatorial ionosphere at Thumba & identification of plasma instabilities. *Indian Journal of Radio & Space Physics (IJRSP)*, *01*(1), 72–80.

Raghavarao, R., & Anandarao, B. G. (1987). Equatorial electrojet and the counter-electrojet. *Indian Journal of Radio & Space Physics*, *16*, 54–75.

Rastogi, R. G., & Iyer, K. N. (1976). Quiet day variation of geomagnetic H-field at low latitudes. *Journal of Geomagnetism and Geoelectricity*, *28*(6), 461–479. https://doi.org/10.5636/jgg.28.461

Ravindran, S., & Krishna Murthy, B. V. (1997). Occurrence of type I plasma waves in the equatorial electrojet during morning and evening hours. *Journal of Geophysical Research*, *102*(A5), 9761–9765. https://doi.org/10.1029/96JA03742

Reddy, C. A., Vikramkumar, B. T., & Viswanathan, K. S. (1987). Electric fields and currents in the equatorial electrojet deduced from VHF radar observations—I. A method of estimating electric fields. *Journal of Atmospheric and Terrestrial Physics*, *49*(2), 183–191. https://doi.org/10.1016/0021-9169(87)90053-5

Reid, G. C. (1968). The formation of small-scale irregularities in the ionosphere. *Journal of Geophysical Research*, *73*(5), 1627–1640. https://doi.org/10.1029/JA073i005p01627

Richmond, A. D. (1973). Equatorial electrojet—I. Development of a model including winds and instabilities. *Journal of Atmospheric and Terrestrial Physics*, *35*(6), 1083–1103. https://doi.org/10.1016/0021-9169(73)90007-X

Ronchi, C., Sudan, R. N., & Similon, P. L. (1990). Effect of short-scale turbulence on kilometer wavelength irregularities in the equatorial electrojet. *Journal of Geophysical Research*, *95*(A1), 189–200. https://doi.org/10.1029/JA095iA01p00189

Sampath, S., & Sastry, T. S. G. (1979a). Results from in situ measurements of ionospheric currents in the equatorial region-I. *Journal of Geomagnetism and Geoelectricity*, *31*(3), 373–379. https://doi.org/10.5636/jgg.31.373

Sampath, S., & Sastry, T. S. G. (1979b). AC electric fields associated with the plasma instabilities in the equatorial electrojet-III. *Journal of Geomagnetism and Geoelectricity*, *31*(3), 391–400. https://doi.org/10.5636/jgg.31.391

Sastry, T. S. G. (1970). Diurnal changes in the parameters of the equatorial electrojet as observed by rocket-borne magnetometers. *Space Research*, *X*, 778–785.

Sekar, R., Gupta, S. P., Acharya, Y. B., Chakrabarty, D., Pallamraju, D., Pathan, B. M., et al. (2013). Absence of streaming plasma waves around noontime over Thumba in recent times: Is it related to the movement of the dip equator? *Journal of Atmospheric and Solar-Terrestrial Physics*, *103*, 8–15. https://doi.org/10.1016/j.jastp.2013.02.005

Sekar, R., Gupta, S. P., & Chakrabarty, D. (2014). On the altitude of initiation of the gradient drift waves at different longitude sectors in the vicinity of the dip equator. *Journal of Atmospheric and Solar-Terrestrial Physics*, *121*, 59–62. https://doi.org/10.1016/j.jastp.2014.10.004

Shuman, B. M. (1970). Rocket measurement of the equatorial electrojet. *Journal of Geophysical Research*, *75*(19), 3889–3901. https://doi.org/10.1029/JA075i019p03889

Somayajulu, V. V., Selvamurugan, R., Devasia, C. V., & Cherian, L. (1994). VHF backscatter radar observations of type I waves during a counter electrojet event. *Geophysical Research Letters*, *21*(18), 2047–2050. https://doi.org/10.1029/94GL01590

Stening, R. J. (1985). Modeling the equatorial electrojet. *Journal of Geophysical Research*, *90*(A2), 1705–1719. https://doi.org/10.1029/JA090iA02p01705

Stening, R. J., & Winch, D. E. (1987). Night-time geomagnetic variations at low latitudes. *Planetary and Space Science*, *35*(12), 1523–1539. https://doi.org/10.1016/0032-0633(87)90078-X

Subbaraya, B. H., Prakash, S., & Gupta, S. P. (1983). Electron densities in the equatorial lower ionosphere from the Langmuir probe experiments conducted at Thumba during 1966–1978. *Scientific Report*, 31-42. ISRO-PRL-SR-15-83.

Sugiura, M., & Poros, D. J. (1969). An improved model equatorial electrojet with a meridional current system. *Journal of Geophysical Research*, *74*(16), 4025–4034. https://doi.org/10.1029/JA074i016p04025

Vikramkumar, B., Rao, P. B., Viswanathan, K. S., & Reddy, C. A. (1987). Electric fields and currents in the equatorial electrojet deduced from VHF radar observations III. Comparison of observed H values with those estimated from measured electric fields. *Journal of Atmospheric and Terrestrial Physics*, *49*(2), 201–207. https://doi.org/10.1016/0021-9169(87)90055-9

Woodman, R. F., & Chau, J. L. (2002). First Jicamarca radar observations of two-stream E region irregularities under daytime counter equatorial electrojet conditions. *Journal of Geophysical Research*, *107*(A12), 18-1-18-8. https://doi.org/10.1029/2002JA009362

Yamazaki, Y., & Maute, A. (2017). Sq and EEJ—A review on the daily variation of the geomagnetic field caused by ionospheric dynamo currents. *Space Science Reviews*, *206*(1), 299–405. https://doi.org/10.1007/s11214-016-0282-z

On the Occurrence of Afternoon Counter Electrojet Over Indian Longitudes During June Solstice in Solar Minimum

Kuldeep Pandey[1,2] [ID], R. Sekar[1] [ID], B. G. Anandarao[1], S. P. Gupta[1], and D. Chakrabarty[1] [ID]

[1]Physical Research Laboratory, Ahmedabad, India, [2]Department of Physics, Indian Institute of Technology Gandhinagar, Gandhinagar, India

Abstract Studies made earlier using ground-based observations of geomagnetic field over the Indian longitudes revealed that the occurrence of equatorial counter electrojet (CEJ) events in afternoon hours is more frequent during June solstice (May-June-July-August) in solar minimum than in other periods. In general, the June solstice solar minimum CEJ events occur between 1500 local time (LT) and 1800 LT with peak strength of about −10 nT at around 1600 LT. In order to understand the frequent occurrence of these CEJ events, an investigation is carried out using an equatorial electrojet model (Anandarao, 1976, https://doi.org/10.1029/GL003i009p00545) and the empirical vertical drift model by Fejer et al. (2008, https://doi.org/10.1029/2007JA012801). The strength, duration, peak value, and the occurrence time of CEJ obtained using electrojet model match remarkably well with the corresponding observation of average geomagnetic field variations. The occurrence of CEJ is found to be due to solar quiet (Sq) electric field in the westward direction which is manifested as downward drift in Fejer et al. (2008, https://doi.org/10.1029/2007JA012801) model output during 1500–1800 LT. Further, the occurrence of afternoon reversal of Sq electric field in this season is shown to be consistent with earlier studies from Indian sector. Therefore, this investigation provides explicit evidence for the role of westward Sq electric field on the generation of afternoon CEJ during June solstice in solar minimum periods over the Indian sector indicating the global nature of these CEJ events.

1. Introduction

A strong eastward current is driven in the *E* region over the magnetic dip equator owing to the orthogonal orientation of the solar quiet (Sq) electric field and the horizontal component of geomagnetic field. This current flows within $\pm3°$ dip latitude at around 105 km and is well known as equatorial electrojet (EEJ). In order to characterize the EEJ, a large number of studies were extensively conducted using ground-based (Egedal, 1947; Rastogi & Patil, 1986; Venkatesh et al., 2015), rocket-borne (Davis et al., 1967; Sastry, 1970), and satellite-based magnetometers (Cain & Sweeney, 1973; Jadhav et al., 2002; Lühr et al., 2004; Onwumechili & Agu, 1981). Modeling efforts were also made to simulate different characteristics of EEJ (Anandarao, 1976; Forbes & Lindzen, 1976; Richmond, 1973; Stening, 1985; Sugiura & Poros, 1969). Excellent reviews on this topic are available in the literature (Forbes, 1981; Raghavarao & Anandarao, 1987; Reddy, 1989; Stening, 1992; Yamazaki & Maute, 2017). The electrojet region is also known to host different types of plasma irregularities as recorded comprehensively by earlier workers (Fejer & Kelley, 1980; Gupta, 2000; Kelley, 2009; Prakash et al., 1971). Further, the geomagnetic field variations due to electrojet current can be taken as a proxy for electric field variations (Rastogi & Patel, 1975) on a time scale shorter than the time scale associated with ionospheric conductivity variation. These electric fields during magnetically quiet times are referred to as solar quiet (Sq) electric field generated essentially by a dynamo action driven by tidal winds and hence associated with global current system. The dip equatorial vertical plasma drifts driven by Sq electric fields are measured directly using radar (e.g., Fejer, 1981; Woodman, 1970), Barium vapor cloud (e.g., Haerendel et al., 1967), and ion drift meter (e.g., Hanson & Heelis, 1975) techniques. A few methodologies were described in the literature (e.g., Anderson et al., 2004; Pandey et al., 2017) to derive the zonal Sq electric field from geomagnetic field observations.

In general, as mentioned earlier, the EEJ is eastward during daytime. On many occasions, however, the flow was observed to be westward during the afternoon periods (Gouin & Mayaud, 1967). This is generally

referred to as the equatorial counter electrojet (CEJ). A number of studies (Bhargava & Sastri, 1979; Patil et al., 1990; Vichare & Rajaram, 2011; Rabiu et al., 2017) reported the occurrence of CEJ events around the globe, and their characteristics were established. Patil et al. (1990) showed that the afternoon CEJ events over the Indian sector occurred on a total of 110 days during the months of May-June-July-August (henceforth referred to as June solstice) in 1964–1965 which fall under solar minimum period. This gets credence from the work of Rastogi et al. (2014) wherein 40 years of ground-based geomagnetic field observations over Indian sector also brought out the maximum occurrence of afternoon CEJ during June solstice in low sunspot years.

Many mechanisms were proposed to explain the occurrence of CEJ events. Gouin and Mayaud (1967) suggested a possible scenario wherein there exist two counter streaming current systems at two different altitudes, and depending on their relative strengths, the EEJ or CEJ can be generated. However, the experimental support for this hypothesis in the form of a vertical profile of current density is not available in the literature. The effects of lunar phase variation on the occurrence of CEJ are extensively studied (Hutton & Oyinloye, 1970; Rastogi, 1974; Stening, 1989a). However, occurrence of afternoon CEJ on 25 days in a month of July during solar minimum over the Indian sector (see Rastogi et al., 2014, for details) cannot be accounted for by the lunar phase variation. Raghavarao and Anandarao (1980) showed that large vertical winds ($\sim$20 ms^{-1}) of gravity wave origin can generate CEJ. However, sustenance of such winds on daily basis lasting for $\sim$3 h could be difficult (Stening, 1992). Further, the effects of zonal wind and its vertical shears were shown to be mostly ineffective in altering the zonal current over the dip equator (Anandarao & Raghavarao, 1987; Richmond, 1973). It is also known that the polarity of the Sq electric field can be altered (e.g., Chau et al., 2009; Fejer et al., 2010) by the winds associated with the significant rise in temperature (known as sudden stratospheric warming or SSW) in the polar stratosphere in the winter hemisphere (Schoeberl, 1978) owing to disruption of polar vortex of westerly winds. This can lead to occurrence of CEJ during SSW events (Sridharan et al., 2009). However, the effects of SSW are pronounced in local winter (Schoeberl, 1978), and hence, frequent occurrence of CEJ in June solstice is not likely to be of SSW origin. Therefore, these mechanisms cannot successfully account for the characteristics of CEJ events in June solstice over the Indian sector. Though space weather events like disturbance dynamo (Blanc & Richmond, 1980), overshielding (Kobea et al., 2000), and substorm (Kikuchi et al., 2003) also produce CEJ, however, the present study is focused on the occurrence of CEJ during geomagnetically quiet conditions. The abnormal depressions in horizontal magnetic field over the dip equatorial stations, similar to the magnetic field signatures of CEJ events, were correlated with f_oF2 variation by Onwumechili and Akasofu (1972). Although those observations were in another season (December solstice) and may have a common driver, these authors did not explicitly discuss the possible role of Sq electric field. In addition, these authors (Onwumechili & Akasofu, 1972) did not remove off-equatorial magnetic field in their work, which was shown in later years (Rastogi, 1975) to be essential to ascertain CEJ events. In another investigation, the possibility of CEJ being part of global current system was discussed by Gurubaran (2002). However, in the investigation of Gurubaran (2002), the alteration of Sq electric fields was not explicitly discussed.

Taking into account of the facts that the Sq electric field pattern changes with season and the occurrence of CEJ events maximizes over the Indian sector during June solstice in solar minimum years, an investigation is carried out to establish the connection between polarity change in diurnal variation of Sq electric field and the occurrence of these CEJ events. This is done by computing the E region current densities and the corresponding horizontal magnetic field induced at ground using electrojet model by Anandarao (1976) (methodology described in section 2) providing inputs (described in section 2.1) corresponding to June Solstice in solar minimum years. Details of magnetic field observations used to compare with the magnetic field computed from model results are described in section 3. The results obtained are presented in section 4 and discussed in detail in section 5.

2. Methodology

A first principle model to compute the E region current densities was developed by Anandarao (1976) by solving generalized Ohm's law, current conservation equation along with curl-free electric field condition. These equations were reduced to a differential equation involving a current function and its derivatives in spherical polar coordinate system. This differential equation was solved numerically to compute the components of electric fields to obtain the zonal current density (J_ϕ) using the following equation.

$$J_\phi = \sigma_H \left(E_r \cos I - E_\theta \sin I \right) + \sigma_P E_\phi \tag{1}$$
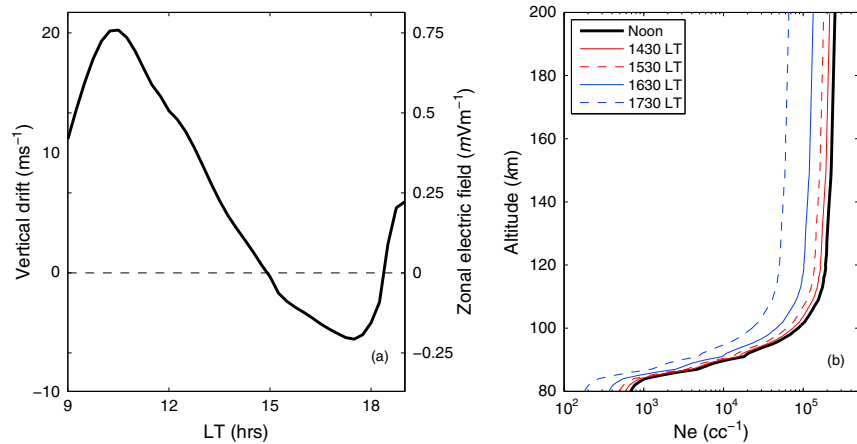
Figure 1. Inputs to the electrojet model (a) Vertical drifts (left Y axis) over 60°E longitude from Fejer et al. (2008) and the corresponding zonal electric field (right Y axis). (b) Altitude profiles of electron density (Ne) at different local times. The solid bold line represents the averaged electron density profile based on the measurements conducted from Trivandrum during 1000–1400 local time (LT) under low ($\langle F10.7 \rangle \leq 120$ sfu) solar activity periods. The other profiles are generated based on the solar zenith angle (χ) variation (see text for details).

where $\sigma_H, \sigma_P, E_r, E_\theta, E_\phi$, and I are conductivities in Hall and Pedersen directions; electric fields in radial, meridional, and zonal directions; and dip angle, respectively. The details of the model can be obtained from the earlier works of Anandarao and Raghavarao (1987) and Raghavarao and Anandarao (1987). In the present work, the average values of zonal current densities between 0930 local time (LT) and 1730 LT during June solstice in solar minimum years over the Indian sector are computed based on equation (1).

A method to evaluate the horizontal component of magnetic field induced (H_{ind}) at ground by this current system is described by Anandarao (1977) based on Biot-Savart's law.

$$H_{ind} = \frac{\mu_0 C}{2\pi r} \left[\frac{(r/a)\sin\theta - 1}{(r/a)^2 + 1 - 2(r/a)\sin\theta} \right], \tag{2}$$

where C represents the line current obtained by integrating the current density J_ϕ over the radial distance r and the magnetic colatitude θ in a geocentric coordinate system ($C = \int_r \int_\theta J_\phi \, dr \, d\theta$). The symbol "a" denotes the radius of Earth. Using the above equation, the average horizontal component of the induced magnetic field is computed for LT between 0930 and 1730 h during June solstice in solar minimum period over the Indian sector.

2.1. Inputs to the Electrojet Model

The inputs to the electrojet model are zonal Sq electric field, altitude profiles of E region electron density, neutral atmospheric density, and temperature, in addition to the three-dimensional geomagnetic field. The neutral atmospheric density and temperature are obtained from Naval Research Laboratory Mass Spectrometer Incoherent Scatter Extension-00 (NRLMSISE-00; Picone et al., 2002) model, and the geomagnetic field is taken from International Geomagnetic Reference Field-12th generation (IGRF-12; Thébault et al., 2015) model.

The systematic ground-based measurements of Sq electric field over India covering all local times and seasons are not available because of the absence of incoherent scatter radar in this sector. Based on in situ measurements of vertical drifts obtained using ion drift meters onboard AE-E and ROCSAT-1 satellites, Scherliess and Fejer (1999) and Fejer et al. (2008), respectively, developed global empirical models of vertical drifts. Recently, based on the scattered data that were available, Pandey et al. (2017) showed that the vertical drifts reported by Fejer et al. (2008) model corresponding to 60°E longitude (with ±15° longitude and ±5° dip latitude bin) represent the vertical drifts over the Indian sector fairly well at different local times of the day barring early morning hours. Therefore, the Sq electric fields at different local times are obtained based on climatological vertical drifts of Fejer et al. (2008) model. Figure 1a depicts these vertical drifts during June solstice in low solar flux conditions ($F10.7 \approx 130$ sfu). This is based on Figure 7 of Fejer et al. (2008) empirical model corresponding to 60°E longitude sector. The input zonal Sq electric field is then obtained by taking the cross product of vertical drift with and Earth's horizontal magnetic field (~37,400 nT) over Trivandrum (TRD).
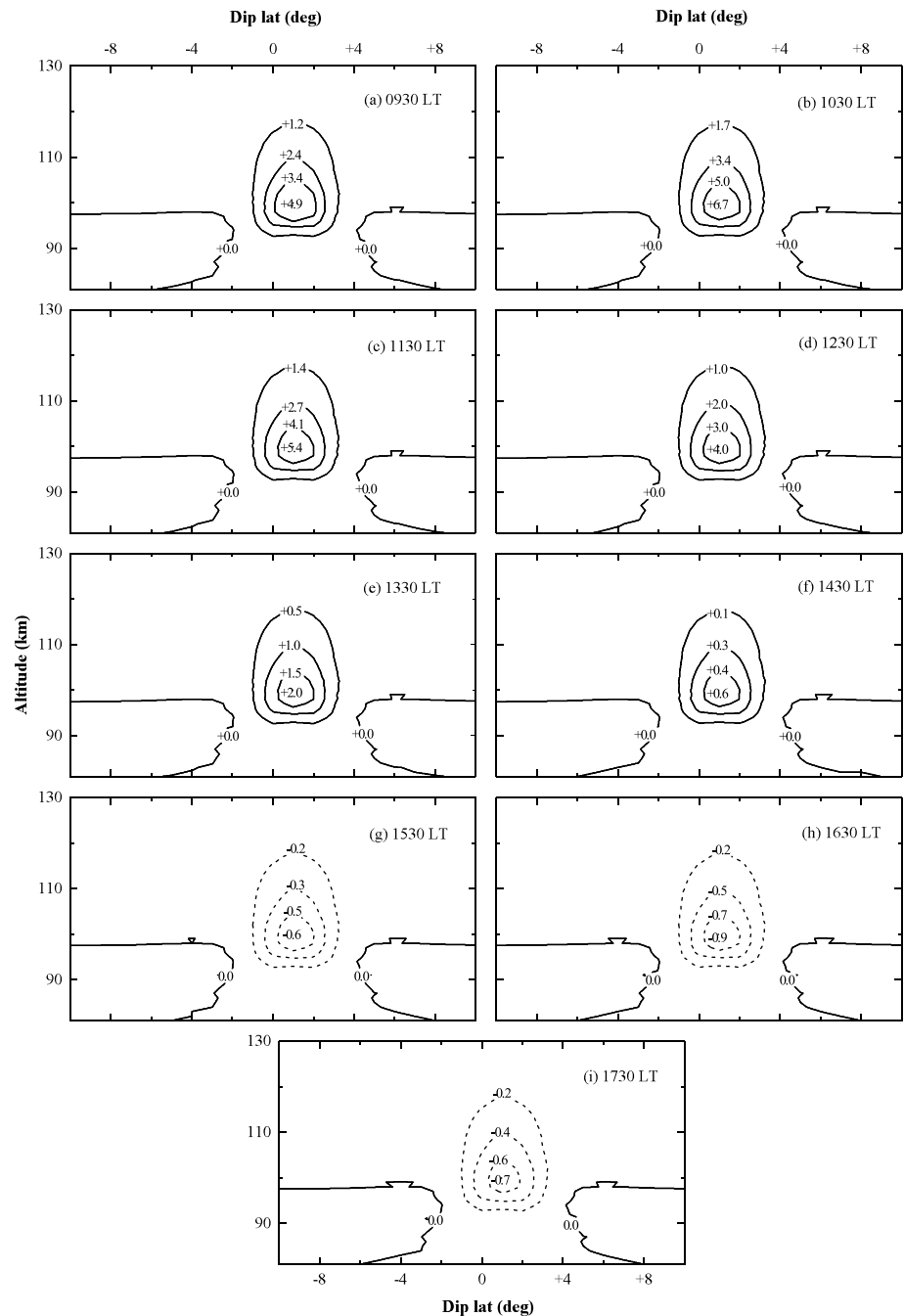
Figure 2. The contours of isocurrent densities (in μAm^{-2}) in the zonal direction, obtained from electrojet model in altitude dip latitude plane corresponding to inputs at different local times. Note that the solid and dashed whorls represent the positive (eastward) and negative (westward) values of current density, respectively. The current density values are shown on each contour with the maximum value marked at the center. LT = local time.

The input of E region electron densities to the model is based on the in situ measurements (Gupta, 2000; Subbaraya et al., 1983) that have been obtained using high-frequency Langmuir probe (Prakash & Subbaraya, 1967) onboard rocket experiments, conducted over TRD at different local times between 1968 and 1982. It is noticed that electron density profiles over the electrojet altitudes (90–110 km) do not reveal significant temporal variation during 1000–1400 LT for a given solar epoch. Therefore, electron density profiles measured between this time interval under low solar epoch (⟨F10.7⟩ ≤ 120 sfu, where ⟨F10.7⟩ stands for annually averaged F10.7) are averaged and used as representative profile at noon (shown in Figure 1b). Since in situ
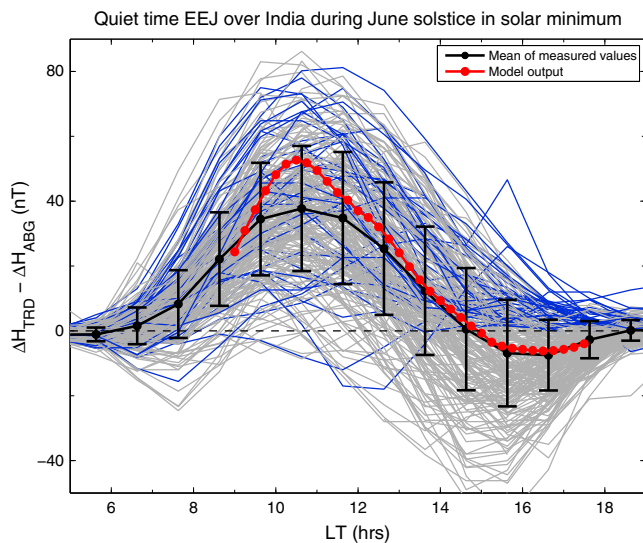
Figure 3. The hourly variations of equatorial electrojet (EEJ) strength deduced using magnetometer data corresponding to individual geomagnetic quiet days with normal (blue) and afternoon counter (gray) electrojet during June solstice in solar minimum years of solar cycle 22. It consists of 235 quiet days of observations whose mean values are depicted by black curve. The 1σ variation for each point is also indicated with vertical bars. The red curve corresponds to the magnetic field strength computed using EEJ model. LT = local time.

electron density profiles are not available at all local times, the empirical relationship between the electron density and solar zenith angle (χ) through $\cos^{1.31/2}(\chi)$ (IRI-90, Bilitza, 1990) is used along with the measured averaged noontime density profile to generate electron density profiles during 0930–1730 LT (see Figure 1b).

3. Details of Ground-Based Magnetic Field Observations Used for Comparison With Model Results

In order to compare the computed magnetic field (based on equation (2)) with the observations of electrojet strength, the ground-based magnetic field observations over India are utilized. The observations of horizontal component of geomagnetic field (H) from an equatorial (eq) and off-equatorial (off-eq) stations are conventionally used to extract the strength of EEJ (Rastogi & Patel, 1975). This is done by computing $\Delta H_{eq} - \Delta H_{off\text{-}eq}$ where ΔH is obtained by subtracting average values of H at nighttime from instantaneous H values. The geomagnetic field observations from an equatorial station TRD (8.5°N, 76.9°E, dip latitude 1°S) and off-equatorial station Alibag (ABG, 18.6°N, 72.9°E, dip latitude 10°N) are utilized to compute the strength of electrojet. The hourly variations of geomagnetic fields on quiet days ($Kp \leq 3$ and $DST \geq -20$, with similar conditions on previous day to avoid the effects of disturbance dynamo), are obtained from World Data Center Kyoto (http://wdc.kugi.kyoto-u.ac.jp/). For the present study, the differential horizontal geomagnetic field variations on 235 quiet days covering 6 years during June solstice months in solar minimum periods ($\langle F10.7 \rangle \leq 120$ sfu) are considered. These 235 days are spread over ascending (1985–1987) and descending (1993–1995) phases of solar cycle 22.

4. Results

The model-generated contours of isocurrent densities along the zonal direction in altitude dip latitude plane are depicted in Figure 2 at various local times. The strength of zonal current density (J_ϕ in units of μAm^{-2}) is also shown on each contour with the maximum value marked at the center. Based on the sensitivity studies carried out with various model inputs, the uncertainty in current density was found to be less than 18% (Pandey et al., 2016). The contours of current density plotted with solid and dashed lines correspond to the positive (eastward) and negative (westward) values of current density, respectively. It is to be noted that eastward electrojet peaks around 1030 LT. The flow of current becomes westward between 1430 LT and 1530 LT, and it remains so till 1730 LT. The peak of westward current density in general is found to be ~ -1 μAm^{-2} between 1530 LT and 1630 LT.

The horizontal components of magnetic field induced at ground by the electrojet currents are computed based on equation (2). The computation is carried out for every 15 min interval from 0930 LT and 1730 LT. Figure 3 depicts the computed variations of magnetic field (red curve with dots). The observed hourly variations of $\Delta H_{TRD} - \Delta H_{ABG}$ for 235 quiet days during June solstice in solar minimum periods are also shown in the figure as the blue and gray curves corresponding to normal EEJ and afternoon CEJ days, respectively. Out of these 235 quiet days of observations, CEJ occurred during 1500–1800 LT on 194 days. In order to generate a quiet time average variation of $\Delta H_{TRD} - \Delta H_{ABG}$, all the 235 quiet days (including both normal EEJ and afternoon CEJ days) are considered. This average curve is depicted in black with dots indicating hourly intervals. In addition, the 1σ variation for each point is indicated with vertical bars.

It is evident from Figure 3 that the model computed and mean of observed magnetic fields match well (within 1σ variation) between 0930 LT and 1730 LT. The peak magnetic field values corresponding to eastward electrojet occur $\sim$1030 LT in both computed and observed values. On an average, CEJ events occur between 1500 LT and 1800 LT with peak (~ -10 nT) occurring around 1600 LT. In spite of using averaged inputs from different sets of data (see section 2), remarkable similarities are observed between the computed and mean observed values of magnetic field during CEJ hours ($\sim$1500–1730 LT). The time of commencement and the duration of CEJ obtained from the model computations closely follow the respective observations.

Further, the strength of peak CEJ and its time of occurrence obtained from model computations are almost the same as those from observations. The implications of these results are discussed in the following section.

5. Discussion

From Figures 1a and 2 it is clear that the reversal in electrojet takes place when the Sq electric field becomes westward. It is to be noted that the peak of the current density (see Figure 2) and the magnetic fields (see Figure 3) corresponding to normal electrojet are found to be at the same time (~1030 LT) when the zonal Sq electric field from empirical model (Fejer et al., 2008) maximizes (see Figure 1a). Incidentally, the local time corresponding to the monthly mean of Sq focii over the Indian sector during June solstice in solar minimum period was found to be around 1030 LT (Vichare et al., 2017). However, in afternoon hours, local time corresponding to the peak of CEJ current (~1630 LT) does not coincide with the time when westward Sq electric field maximizes (~1730 LT). This is due to considerable amount of decrease in electron density with χ variation after 1630 LT (see Figure 1b) that results in reduction of CEJ strength after ~1630 LT. Hence, the time of peak westward current is determined from the optimum values of zonal Sq electric field and electron density.

The average characteristics of CEJ events (strength, duration, peak value, and its time of occurrence) reported by earlier studies (Patil et al., 1990; Rastogi et al., 2014) pertain to different solar cycles and are similar to the observations presented in Figure 3. Further, the results obtained in the present work using electrojet model have exceptional similarities with these observations. However, on some occasions, the amplitude of CEJ is observed to be substantially larger than 1σ compared to averaged CEJ strength and commencement of some of CEJ events is at earlier local times (<1500 LT). These aspects are discussed later. It is clear from Figure 2 that depending on the polarity of the zonal Sq electric field being eastward or westward, the EEJ or CEJ appears. Thus, it is important to know the polarity of the zonal Sq electric field in afternoon hours. Fejer et al. (2008) model, employed in the present investigation, reveals westward Sq electric field during 1500–1800 LT in June solstice in solar minimum over Indian longitude. Considering the smaller values of westward Sq electric field after ~1500 LT and the uncertainties (less than 10% particularly during daytime) associated with the Fejer et al. (2008) model, additional clues for the westward Sq electric fields during afternoon hours in this season over the Indian region are gleaned from the earlier works and discussed in the ensuing subsection.

5.1. Earlier Observations That Indirectly Support Westward Sq Electric Field During Afternoon Hours

Various earlier measurements that indicate the westward Sq electric field in afternoon hours over the Indian sector during June solstice in solar minimum periods are described in the ensuing paragraphs.

The vertical Doppler drifts from the radar echoes due to the presence of plasma irregularities at 150 km region act as a proxy to zonal Sq electric field (Chau & Woodman, 2004; Kudeki & Fawcett, 1993). These measurements have been extensively used over the Peruvian sector (Hui & Fejer, 2015). Over the Indian sector, such measurements of the vertical drifts over Gadanki (13.5°N, 79.2°E, dip latitude 6.5°N) are reported by Pavan Chaitanya et al. (2014) and Patra et al. (2014). Patra et al. (2014) reported the vertical drifts for 4 days during July–August 2009 that indicate downward trend at ~1500 LT. As the radar observational time was limited to ~1500 LT, the westward Sq electric field could not be ascertained on most of the cases beyond this local time. However, on one occasion, simultaneous measurements of vertical drifts using in situ measurements by Communication/Navigation Outage Forecast System (C/NOFS) satellite and 150 km echo revealed westward electric field at ~1400 LT. On this CEJ day, continuous operation of radar revealed westward electric field till the end of the observation (~1530 LT). Some of the earlier reversals seen in Figure 3 can be accounted by westward electric field similar to this measurement. Further, Pavan Chaitanya et al. (2014) reported observations of 150 km echoes during 5 months in 2009 for a few consecutive days in each month. It is noticed from their observations that, on an average, the vertical drifts are close to 0 or negative ~1500 LT in June and July months and show decreasing trend around this time. Note that the decreasing trend in afternoon hours in months other than June solstice (e.g., December month) was not observed by both Pavan Chaitanya et al. (2014) and Patra et al. (2014). Thus, these case studies give credence to the presence of westward Sq electric fields in afternoon hours during June solstice in solar minimum period.

The polarity of Sq electric field can also be inferred from the measurements of E region electron density profiles and structures in them (Pandey et al., 2017). Recently, Pandey et al. (2017) have shown that the polarity of zonal Sq electric field and the limiting values of the drift deduced from such measurements match well with the empirical model of vertical drift (Fejer et al., 2008). Based on a rocket flight experiment conducted

at 1554 LT on 17 August 1972 from TRD, Prakash et al. (1976) reported that the streaming waves were present on a CEJ day around 105–110 km and amplitudes of irregularities at altitudes below 100 km were found to be of the order of nongeophysical noise level (~0.5%) and thus considered by them as absence of irregularities. However, over the Indian region, the gradient drift waves are in general observed above 87 km in positive gradient region (Sekar et al., 2014), where electrojet current is negligible due to low value of R (ratio of Hall to Pedersen conductivities) (Pandey et al., 2016). Thus, the absence of gradient drift waves in the positive gradient region at very low altitudes (~90 km) indicates toward the westward Sq electric field on that day. Further, the presence of streaming waves above 105 km altitude indicates that the downward drift corresponding to zonal Sq electric field was more than the limiting value of 12 ms^{-1} (Pandey et al., 2017). Thus, the Sq electric field can be westward and with large amplitude on some occasions during afternoon in June solstice under solar minimum periods. This can account for large deviations (more than 1σ) in the amplitude of CEJ as observed on some occasions compared to the averaged CEJ strength depicted in Figure 3. Thus, the above set of observations provides another evidence for the presence of westward Sq electric field during daytime on a CEJ day.

The strength of Sq electric field can also be gauged from the morphology of the latitudinal location of the peak of ionization. The latitudinal distribution of ionization in low-latitude F region is controlled by plasma fountain effect. The equatorial plasma fountain is due to eastward Sq electric field pumping up the plasma from equatorial region vertically upward, which subsequently diffuses along the geomagnetic field with the modulation due to meridional wind to form a crest region over low latitudes (Hanson & Moffett, 1966). However, the location of the crest region of equatorial plasma fountain depends on the strength of zonal electric field (Anderson, 1973). The stronger eastward electric field shifts the crest of plasma fountain further away from the dip equator. Several works reported strong correlation between integrated EEJ strength and the development of plasma fountain (Aggarwal et al., 2012; Raghavarao et al., 1978; Rama Rao et al., 2006; Rush & Richmond, 1973). This correlation was also observed in total electron content (TEC) variations reported by earlier workers (e.g., Iyer et al., 1976), though seasonal dependence of TEC under different solar epochs is sparse (Rama Rao et al., 2006; Yadav et al., 2013). In one such work by Rama Rao et al. (2006), the monthly mean values of TEC at different latitudes over India are reported. The crest location of TEC during 2004, which is in the descending phase of solar cycle 23 ($\langle F10.7\rangle \leq 110$ sfu), is found to be at ~12°N dip latitude. It can be noticed from Figure 7 of their work that the TEC values peaked for a short interval of time around noon and fall off sharply afterward during June–July compared to other months. The noontime peak in TEC indicates that zonal Sq electric field peaks around 1000–1030 LT as it takes about 2 h (Sanatani, 1966) to diffuse to the location of 12°N dip latitude. In addition, sharp decrease in TEC after noon indicates sharp decrease in zonal electric field. Further, the location of peak TEC was shown not to exceed beyond 6°N dip latitude during afternoon hours in June solstice, indicating that the zonal Sq electric field was relatively weak. Thus, the morphological variations of TEC over India indicate the decreasing trend of Sq electric field in the afternoon hours during June solstice in solar minimum periods. Since the latitudinal extent of EEJ is limited ($\pm 3°$), the correlation between EEJ and plasma fountain obtained by these workers indicates the common role of Sq electric field in controlling both the phenomena.

An indirect inference of earlier (afternoon) reversal of Sq electric field can be obtained from the magnetic field observations at the focii of Sq current system. Based on geomagnetic field observations using chain of magnetometers during low solar activity ($\langle F10.7\rangle < 90$ sfu) years 2006–2010, Vichare et al. (2017) reported that the local time corresponding to monthly mean of focii of Sq current system over the Indian sector during June solstice occurs earlier (~1030 LT) compared to other seasons. Interestingly, the time of maximum eastward electric field corresponding to vertical drifts over Indian sector reported by Fejer et al. (2008) model is also earlier (~1030 LT) in June solstice compared to other seasons. These observations are consistent with morphological variations of TEC observations discussed earlier. As the maximum of Sq current is observed earlier, it is expected that the descending phase of diurnal tide starts early during this season. Under these conditions, the contributions from components other than diurnal tides can govern the Sq current system and hence the zonal electric field depending upon the relative magnitudes and phases of diurnal and higher-order tidal components. These aspects can result in small or opposite polarity of zonal Sq electric field in afternoon hours during June solstice compared to other seasons.

A chain of magnetic field observations can also provide a clue to the polarity of the Sq electric field. Based on the principal component analysis of geomagnetic field variations measured using a chain of magnetometers over Indian region during June–July 1995, Gurubaran (2002) reported that the second harmonic plays

a crucial role in the occurrence of CEJ in afternoon hours. The author (Gurubaran, 2002) also showed that on days of afternoon CEJ, a clockwise current system (located ~20 dip latitude in afternoon hours) owing to higher harmonics is superposed on the normal counterclockwise Sq current vortex (located ~30 dip latitude at noon) due to primary component. The author wondered whether CEJ is a part of global current system. Bhattacharyya and Okpala (2015) applied a similar analysis to quiet time geomagnetic field variations between 1999 and 2012 and reported that second and third harmonics contribute to the occurrence of CEJ events. In recent investigation, Bhardwaj and Subba Rao (2017) showed that the higher harmonics are associated with clockwise current system in afternoon. Therefore, the studies by Bhattacharyya and Okpala (2015) can also be taken to produce clockwise current cell in the afternoon. Thus, the results obtained from these systematic magnetic field variations measured using a chain of magnetometers over Indian region indicate toward formation of a counterclockwise current cell in morning and clockwise current cell during afternoon hours on CEJ days in addition to normal counterclockwise current cell. This can be taken as a support for eastward Sq electric field in morning hours and westward Sq electric field during afternoon hours at least during the periods of June solstice in solar minimum.

5.2. Possible Reason for Westward Sq Electric Field in Afternoon Hours

Section 5.1 provides alternate evidences for westward Sq electric field around 1500–1800 LT during June solstice in solar minimum periods that are consistent with the results of Fejer et al. (2008) for the Indian sector. Possible reason for this westward Sq electric field is discussed below.

Simultaneous long-term (1993-2011) observations of mesospheric winds by medium frequency (MF) radar at Tirunelveli (8.7°N, 77.8°E), a station close to the dip equator over India, and the strength of EEJ using geomagnetic field observations revealed that the second principal component acts as proxy for the occurrence of CEJ with enhanced tidal activities during solar minimum year when the occurrence of CEJ is more (Gurubaran et al., 2016). However, the role of relative strengths of diurnal and semidiurnal tides particularly during June solstice in solar minimum periods for the generation of CEJ is not clear from this work. Month-to-month variations of tidal amplitudes of mesospheric winds over TRD obtained using a meteor radar from June 2004 to May 2005 (descending phase of solar cycle 23, $\langle F10.7 \rangle \leq 110$ sfu) are reported by Deepa et al. (2006). It is observed from Figures 9 to 14 of their work that the semidiurnal amplitudes are found to be larger than corresponding diurnal amplitude in meridional direction in the altitude region 94–98 km during the June solstice months. The phase difference between meridional diurnal and semidiurnal tides was found to be around 12 h in the altitude region 94–98 km in this solstice barring the month of June. Possible role of semidiurnal tides on equatorial quiet time vertical ion drifts measured by C/NOFS satellite was indicated by Stoneback et al. (2011) based on measurements over the Indian sector during deep solar minimum period (2008–2010) of solar cycle 23. Further, when semidiurnal tide is effective and contributes to the generation of afternoon CEJ, it is expected to cause eastward electric field influence around midnight hours. This aspect is confirmed by the premidnight ascent of *F* layer and upward ion drift observed by C/NOFS over the Indian sector during June solstice in deep solar minimum years 2008–2009 (Chakrabarty et al., 2014). These aspects are in support of role played by the semidiurnal tides during June solstice.

In theoretical studies (Forbes & Lindzen, 1976; Hanuise et al., 1983; Marriott et al., 1979) with assumptions of concentric geomagnetic and geographic equator and reduced amplitude of diurnal components, the features of CEJ are modeled by combination of symmetric semidiurnal tides. The observational support for the second assumption was provided by Sridharan et al. (2002) wherein a reduction in the diurnal tidal component and/or enhancement in semidiurnal amplitude was reported on afternoon CEJ days during June–July months in 1995 observed over Tirunelveli using MF radar and chain of magnetometers simultaneously. On the other hand, Stening (1989b) reproduced many features of CEJ by introducing antisymmetric semidiurnal tidal components. Numerical simulation of simultaneous Sq current and CEJ using different combinations of semidiurnal and diurnal tidal components is beyond the scope of this manuscript. However, based on earlier simulation works discussed above and the observational support on tidal winds from recent times, it appears that the semidiurnal tides play a crucial role in altering Sq electric field, which is shown by the present investigation to be essential to cause CEJ during June solstice in solar minimum periods over the Indian region.

Finally, the present investigation brings out the important consequence of the westward Sq electric fields that were obtained by Fejer et al. (2008) empirical model over Indian longitudes during June solstice in solar minimum in the generation of CEJ. Though the process appears to be obvious, the present work reproduces

all the observed CEJ characteristics remarkably well. Further, if the Sq electric field is responsible for the generation of CEJ, the requirement (Stening, 1977) of a separate return current becomes superfluous. Therefore, the present investigation suggests that these CEJ events are part of a global current system. As the present work is not exhaustive covering all the seasons and solar epochs, the other suggested mechanisms discussed in section 1 are not precluded.

6. Summary

An investigation was carried out using an EEJ model and the inputs based on measurements and empirical model of vertical drift to understand frequent occurrence of CEJ events in afternoon hours over the Indian sector during June solstice in solar minimum period. The occurrence of CEJ is shown to be due to the westward Sq electric field between 1500 LT and 1800 LT. The empirical model-based westward Sq electric field is substantiated by various earlier observations from India. The magnetic field derived from the electrojet model is compared with the corresponding magnetic observations from India. The comparison revealed that the strength, duration, peak value, and the occurrence time of CEJ computed by the model match well with the observation, suggesting the explicit role of westward Sq electric field in the generation of these CEJ events. Therefore, the present investigation suggests that afternoon CEJ events over the Indian sector during June solstice in solar minimum periods are part of the global current system.

References

Aggarwal, M., Joshi, H. P., Iyer, K. N., Kwak, Y. S., Lee, J. J., Chandra, H., & Cho, K. S. (2012). Day-to-day variability of equatorial anomaly in GPS-TEC during low solar activity period. *Advances in Space Research*, *49*(12), 1709–1720. https://doi.org/10.1016/j.asr.2012.03.005

Anandarao, B. G. (1976). Effects of gravity wave winds and wind shears on equatorial electrojet. *Geophysical Research Letters*, *3*(9), 545–548. https://doi.org/10.1029/GL003i009p00545

Anandarao, B. G. (1977). Studies on the dynamics of the equatorial ionosphere (PhD thesis). Gujarat University.

Anandarao, B. G., & Raghavarao, R. (1987). Structural changes in the currents and fields of the equatorial electrojet due to zonal and meridional winds. *Journal of Geophysical Research*, *92*(A3), 2514–2526. https://doi.org/10.1029/JA092iA03p02514

Anderson, D., Anghel, A., Chau, J., & Veliz, O. (2004). Daytime vertical E × B drift velocities inferred from ground-based magnetometer observations at low latitudes. *Space Weather*, *2*, S11001. https://doi.org/10.1029/2004SW000095

Anderson, D. N. (1973). A theoretical study of the ionospheric F region equatorial anomaly—I. Theory. *Planetary and Space Science*, *21*(3), 409–419. https://doi.org/10.1016/0032-0633(73)90040-8

Bhardwaj, S. K., & Subba Rao, P. B. V. (2017). The afternoon counter-electrojet current system along the 75°E meridian during the IEEY. *Earth, Planets and Space*, *69*(1), 91. https://doi.org/10.1186/s40623-017-0675-6

Bhargava, B. N., & Sastri, N. S. (1979). Some characteristics of the occurrence of the afternoon counter-electrojet events in the India region. *Journal of Geomagnetism and Geoelectricity*, *31*(2), 97–101. https://doi.org/10.5636/jgg.31.97

Bhattacharyya, A., & Okpala, K. C. (2015). Principal components of quiet time temporal variability of equatorial and low-latitude geomagnetic fields. *Journal of Geophysical Research: Space Physics*, *120*, 8799–8809. https://doi.org/10.1002/2015JA021673

Bilitza, D. (Ed.) (1990). *International Reference Ionosphere 1990, NSSDC/WDC-A-R&S 90-22*. Greenbelt, MD: National Space Science Data Center.

Blanc, M., & Richmond, A. D. (1980). The ionospheric disturbance dynamo. *Journal of Geophysical Research*, *85*(A4), 1669–1686. https://doi.org/10.1029/JA085iA04p01669

Cain, J. C., & Sweeney, R. E. (1973). The POGO data. *Journal of Atmospheric and Terrestrial Physics*, *35*(6), 1231–1247. https://doi.org/10.1016/0021-9169(73)90021-4

Chakrabarty, D., Fejer, B. G., Gurubaran, S., Pant, T. K., Abdu, M. A., & Sekar, R. (2014). On the pre-midnight ascent of F-layer in the June solstice during the deep solar minimum in 2008 over the Indian sector. *Journal of Atmospheric and Solar-Terrestrial Physics*, *121*, 177–187. https://doi.org/10.1016/j.jastp.2014.01.002

Chau, J. L., & Woodman, R. F. (2004). Daytime vertical and zonal velocities from 150-km echoes: Their relevance to F-region dynamics. *Geophysical Research Letters*, *31*, L17801. https://doi.org/10.1029/2004GL020800

Chau, J. L., Fejer, B. G., & Goncharenko, L. P. (2009). Quiet variability of equatorial E × B drifts during a sudden stratospheric warming event. *Geophysical Research Letters*, *36*, L05101. https://doi.org/10.1029/2008GL036785

Davis, T. N., Burrows, K., & Stolarik, J. D. (1967). A latitude survey of the equatorial electrojet with rocket-borne magnetometers. *Journal of Geophysical Research*, *72*(7), 1845–1861. https://doi.org/10.1029/JZ072i007p01845

Deepa, V., Ramkumar, G., Antonita, M., Kumar, K. K., & Sasi, M. N. (2006). Vertical propagation characteristics and seasonal variability of tidal wind oscillations in the MLT region over Trivandrum (8.5°N, 77°E): First results from SKiYMET meteor radar. *Annales Geophysicae*, *24*, 2877–2889.

Egedal, J. (1947). The magnetic diurnal variation of the horizontal force near the magnetic equator. *Terrestrial Magnetism and Atmospheric Electricity*, *52*(4), 449–451. https://doi.org/10.1029/TE052i004p00449

Fejer, B. G. (1981). The equatorial ionospheric electric fields. A review. *Journal of Atmospheric and Terrestrial Physics*, *43*(5), 377–386.

Fejer, B. G., & Kelley, M. C. (1980). Ionospheric irregularities. *Reviews of Geophysics*, *18*(2), 401–454. https://doi.org/10.1029/RG018i002p00401

Fejer, B. G., Jensen, J. W., & Su, S. Y. (2008). Quiet time equatorial F region vertical plasma drift model derived from ROCSAT-1 observations. *Journal of Geophysical Research*, *113*, A05304. https://doi.org/10.1029/2007JA012801

Fejer, B. G., Olson, M. E., Chau, J. L., Stolle, C., Lühr, H., Goncharenko, L. P., et al. (2010). Lunar-dependent equatorial ionospheric electrodynamic effects during sudden stratospheric warmings. *Journal of Geophysical Research*, *115*, A00G03. https://doi.org/10.1029/2010JA015273

Forbes, J. M. (1981). The equatorial electrojet. *Reviews of Geophysics*, *19*(3), 469–504. https://doi.org/10.1029/RG019i003p00469

Forbes, J. M., & Lindzen, R. S. (1976). Atmospheric solar tides and their electrodynamic effects—II. The equatorial electrojet. *Journal of Atmospheric and Terrestrial Physics*, *38*(9), 911–920. https://doi.org/10.1016/0021-9169(76)90074-X

Gouin, P., & Mayaud, P. N. (1967). A propos de l'existence possible d'un "contre electrojet" aux latitudes magnetiques equatoriales. *Annales Geophysicae*, *23*, 41–47.

Gupta, S. P. (2000). Two stream instability in E region over magnetic equator during morning hours. *Advances in Space Research*, *26*(8), 1257–1261. https://doi.org/10.1016/S0273-1177(99)01212-0

Gurubaran, S. (2002). The equatorial counter electrojet: Part of a worldwide current system? *Geophysical Research Letters*, *29*(9), 1337. https://doi.org/10.1029/2001GL014519

Gurubaran, S., Sathishkumar, S., & Veenadhari, B. (2016). On the role of atmospheric tides in the quiet-time variabilities of equatorial electrojet. *Journal of Indian Geophysical Union*, *Special Volume-2*, 87–98.

Haerendel, G., Lüst, R., & Rieger, E. (1967). Motion of artificial ion clouds in the upper atmosphere. *Planetary and Space Science*, *15*(1), 1–18. https://doi.org/10.1016/0032-0633(67)90062-1

Hanson, W. B., & Heelis, R. A. (1975). Techniques for measuring bulk gas-motions from satellites. *Space Science Instrumentation*, *1*, 493–524.

Hanson, W. B., & Moffett, R. J. (1966). Ionization transport effects in the equatorial F region. *Journal of Geophysical Research*, *71*(23), 5559–5572. https://doi.org/10.1029/JZ071i023p05559

Hanuise, C., Mazaudier, C., Vila, P., Blanc, M., & Crochet, M. (1983). Global dynamo simulation of ionospheric currents and their connection with the equatorial electrojet and counter electrojet: A case study. *Journal of Geophysical Research*, *88*(A1), 253–270. https://doi.org/10.1029/JA088iA01p00253

Hui, D., & Fejer, B. G. (2015). Daytime plasma drifts in the equatorial lower ionosphere. *Journal of Geophysical Research: Space Physics*, *120*, 9738–9747. https://doi.org/10.1002/2015JA021838

Hutton, R., & Oyinloye, J. O. (1970). The counter-electrojet in Nigeria. *Annales Geophysicae*, *26*, 921–926.

Iyer, K. N., Deshpande, M. R., & Rastogi, R. G. (1976). The equatorial anomaly in ionospheric total electron content and the equatorial electrojet current strength. *Proceedings of the Indian Academy of Sciences - Section A*, *84*(4), 129–138. https://doi.org/10.1007/BF03046803

Jadhav, G., Rajaram, M., & Rajaram, R. (2002). A detailed study of equatorial electrojet phenomenon using Ørsted satellite observations. *Journal of Geophysical Research*, *107*(A8), 1175. https://doi.org/10.1029/2001JA000183

Kelley, M. C. (2009). *The Earth's ionosphere: Electrodynamics and plasma physics*. Burlington, MA: Academic Press.

Kikuchi, T., Hashimoto, K. K., Kitamura, T. I., Tachihara, H., & Fejer, B. (2003). Equatorial counterelectrojets during substorms. *Journal of Geophysical Research*, *108*(A11), 1406. https://doi.org/10.1029/2003JA009915

Kobea, A. T., Richmond, A. D., Emery, B. A., Peymirat, C., Lühr, H., Moretto, T., et al. (2000). Electrodynamic coupling of high and low latitudes: Observations on May 27, 1993. *Journal of Geophysical Research*, *105*(A10), 22,979–22,989. https://doi.org/10.1029/2000JA000058

Kudeki, E., & Fawcett, C. D. (1993). High resolution observations of 150 km echoes at Jicamarca. *Geophysical Research Letters*, *20*(18), 1987–1990. https://doi.org/10.1029/93GL01256

Lühr, H., Maus, S., & Rother, M. (2004). Noon-time equatorial electrojet: Its spatial features as determined by the CHAMP satellite. *Journal of Geophysical Research*, *109*, A01306. https://doi.org/10.1029/2002JA009656

Marriott, R. T., Richmond, A. D., & Venkateswaran, S. V. (1979). The quiet-time equatorial electrojet and counter-electrojet. *Journal of Geomagnetism and Geoelectricity*, *31*(3), 311–340. https://doi.org/10.5636/jgg.31.311

Onwumechili, A., & Akasofu, S. I. (1972). On the abnormal depression of Sq(H) under the equatorial electrojet in the afternoon. *Journal of Geomagnetism and Geoelectricity*, *24*(2), 161–173. https://doi.org/10.5636/jgg.24.161

Onwumechili, C. A., & Agu, C. E. (1981). Longitudinal variation of equatorial electrojet parameters derived from POGO satellite observations. *Planetary and Space Science*, *29*(6), 627–634. https://doi.org/10.1016/0032-0633(81)90111-2

Pandey, K., Sekar, R., Anandarao, B. G., Gupta, S. P., & Chakrabarty, D. (2016). Estimation of nighttime dip-equatorial E-region current density using measurements and models. *Journal of Atmospheric and Solar-Terrestrial Physics*, *146*, 160–170. https://doi.org/10.1016/j.jastp.2016.06.002

Pandey, K., Sekar, R., Gupta, S. P., Chakrabarty, D., & Anandarao, B. G. (2017). Comparison of quiet time vertical plasma drifts with global empirical models over the Indian sector: Some insights. *Journal of Atmospheric and Solar-Terrestrial Physics*, *157*, 42–54. https://doi.org/10.1016/j.jastp.2017.03.012

Patil, A. R., Rao, D. R. K., & Rastogi, R. G. (1990). Equatorial electrojet strengths in the Indian and American sectors. Part I. During low solar activity. *Journal of Geomagnetism and Geoelectricity*, *42*(7), 801–811.

Patra, A. K., Chaitanya, P. P., Otsuka, Y., Yokoyama, T., Yamamoto, M., Stoneback, R. A., & Heelis, R. A. (2014). Vertical E × B drifts from radar and C/NOFS observations in the Indian and Indonesian sectors: Consistency of observations and model. *Journal of Geophysical Research: Space Physics*, *119*, 3777–3788. https://doi.org/10.1002/2013JA019732

Pavan Chaitanya, P., Patra, A. K., & Rao, S. V. B. (2014). Quiet time short-period and day-to-day variations in E × B drift studied using 150 km radar echoes from Gadanki. *Journal of Geophysical Research: Space Physics*, *119*, 3053–3065. https://doi.org/10.1002/2013JA019668

Picone, J. M., Hedin, A. E., Drob, D. P., & Aikin, A. C. (2002). NRLMSISE-00 empirical model of the atmosphere: Statistical comparisons and scientific issues. *Journal of Geophysical Research*, *107*(A12), 1468. https://doi.org/10.1029/2002JA009430

Prakash, S., Gupta, S. P., Sinha, H. S. S., & Rao, T. R. (1976). Ionization irregularities in the E region during counter electrojet. *Space Research XVI*, *26*, 401–405.

Prakash, S., Gupta, S. P., Subbaraya, B. H., & Jain, C. L. (1971). Electrostatic plasma instabilities in the equatorial electrojet. *Nature*, *233*(38), 56–58. https://doi.org/10.1038/physci233056a0

Prakash, S., & Subbaraya, B. H. (1967). Langmuir probe for the measurement of electron density and electron temperature in the ionosphere. *Review of Scientific Instruments*, *38*(8), 1132–1136. https://doi.org/10.1063/1.1721035

Rabiu, A. B., Folarin, O. O., Uozumi, T., Abdul Hamid, N. S., & Yoshikawa, A. (2017). Longitudinal variation of equatorial electrojet and the occurrence of its counter electrojet. *Annales Geophysicae*, *35*(3), 535–545.

Raghavarao, R., & Anandarao, B. G. (1980). Vertical winds as a plausible cause for equatorial counter electrojet. *Geophysical Research Letters*, *7*(5), 357–360. https://doi.org/10.1029/GL007i005p00357

Raghavarao, R., & Anandarao, B. G. (1987). Equatorial electrojet and the counter-electrojet. *Indian Journal of Radio and Space Physics*, *16*, 54–75.

Raghavarao, R., Sharma, P., & Sivaraman, M. R. (1978). Correlation of ionization anomaly with the intensity of the electrojet. In *Space Research XVIII* (pp. 277–280). Oxford: Pergamon Press Ltd.

Rama Rao, P. V. S., Gopi Krishna, S., Niranjan, K., & Prasad, D. S. V. V. D. (2006). Temporal and spatial variations in TEC using simultaneous measurements from the Indian GPS network of receivers during the low solar activity period of 2004–2005. *Annales Geophysicae*, *24*(12), 3279–3292.

Rastogi, R. G. (1974). Lunar effects in the counter electrojet near the magnetic equator. *Journal of Atmospheric and Terrestrial Physics*, *36*(1), 167–170. https://doi.org/10.1016/0021-9169(74)90074-9

Rastogi, R. G. (1975). On the criterion of geomagnetic field at the time of disappearance of equatorial Esq layer. *Indian Journal of Radio & Space Physics*, *4*, 1–5.

Rastogi, R. G., Chandra, H., Janardhan, P., & Rahul, S. (2014). Equatorial and mid-latitude ionospheric currents over the Indian region based on 40 years of data at Trivandrum and Alibag. *Indian Journal of Radio & Space Physics*, *43*, 274–283.

Rastogi, R. G., & Patel, V. L. (1975). Effect of interplanetary magnetic field on ionosphere over the magnetic equator. *Proceedings of the Indian Academy Of Science*, *82*(A), 121–141.

Rastogi, R. G., & Patil, A. (1986). Complex structure of equatorial electrojet current. *Current Science*, *55*(9), 433–436.

Reddy, C. A. (1989). The equatorial electrojet. *Pure and Applied Geophysics*, *131*(3), 485–508. https://doi.org/10.1007/BF00876841

Richmond, A. D. (1973). Equatorial electrojet—I. Development of a model including winds and instabilities. *Journal of Atmospheric and Terrestrial Physics*, *35*(6), 1083–1103. https://doi.org/10.1016/0021-9169(73) 90007-X

Rush, C. M., & Richmond, A. D. (1973). The relationship between the structure of the equatorial anomaly and the strength of the equatorial electrojet. *Journal of Atmospheric and Terrestrial Physics*, *35*(6), 1171–1180. https://doi.org/10.1016/0021-9169(73)90013-5

Sanatani, S. (1966). Electron density distribution in the ionosphere (PhD thesis). Gujarat University.

Sastry, T. S. G. (1970). Diurnal changes in the parameters of the equatorial electrojet as observed by rocket-borne magnetometers. *Space Research*, *X*, 778–785.

Scherliess, L., & Fejer, B. G. (1999). Radar and satellite global equatorial *F* region vertical drift model. *Journal of Geophysical Research*, *104*(A4), 6829–6842. https://doi.org/10.1029/1999JA900025

Schoeberl, M. R. (1978). Stratospheric warmings: Observations and theory. *Reviews of Geophysics*, *16*, 521–538. https://doi.org/10.1029/RG016i004p00521

Sekar, R., Gupta, S. P., & Chakrabarty, D. (2014). On the altitude of initiation of the gradient drift waves at different longitude sectors in the vicinity of the dip equator. *Journal of Atmospheric and Solar-Terrestrial Physics*, *121*, 59–62. https://doi.org/10.1016/j.jastp.2014.10.004

Sridharan, S., Gurubaran, S., & Rajaram, R. (2002). Structural changes in the tidal components in mesospheric winds as observed by the MF radar during afternoon counter electrojet events. *Journal of Atmospheric and Solar-Terrestrial Physics*, *64*(12), 1455–1463. https://doi.org/10.1016/S1364-6826(02)00109-8

Sridharan, S., Sathishkumar, S., & Gurubaran, S. (2009). Variabilities of mesospheric tides and equatorial electrojet strength during major stratospheric warming events. *Annales Geophysicae*, *27*(11), 4125–4130. https://doi.org/10.5194/angeo-27-4125-2009

Stening, R. J. (1977). Magnetic variations at other latitudes during reverse equatorial electrojet. *Journal of Atmospheric and Terrestrial Physics*, *39*(9), 1071–1077. https://doi.org/10.1016/0021-9169(77)90015-0

Stening, R. J. (1985). Modeling the equatorial electrojet. *Journal of Geophysical Research*, *90*(A2), 1705–1719. https://doi.org/10.1029/JA090iA02p01705

Stening, R. J. (1989a). A diurnal modulation of the lunar tide in the upper atmosphere. *Geophysical Research Letters*, *16*(4), 307–310. https://doi.org/10.1029/GL016i004p00307

Stening, R. J. (1989b). A calculation of ionospheric currents due to semidiurnal antisymmetric tides. *Journal of Geophysical Research*, *94*(A2), 1525–1531. https://doi.org/10.1029/JA094iA02p01525

Stening, R. J. (1992). The enigma of the counter equatorial electrojet and lunar tidal influences in the equatorial region. *Advances in Space Research*, *12*(6), 23–32.

Stoneback, R. A., Heelis, R. A., Burrell, A. G., Coley, W. R., Fejer, B. G., & Pacheco, E. (2011). Observations of quiet time vertical ion drift in the equatorial ionosphere during the solar minimum period of 2009. *Journal of Geophysical Research*, *116*, A12327. https://doi.org/10.1029/2011JA016712

Subbaraya, B. H., Prakash, S., & Gupta, S. P. (1983). Electron densities in the equatorial lower ionosphere from the Langmuir probe experiments conducted at Thumba during 1966–1978 (Scientific Report). ISRO-PRL-SR-15-83.

Sugiura, M., & Poros, D. J. (1969). An improved model equatorial electrojet with a meridional current system. *Journal of Geophysical Research*, *74*(16), 4025–4034. https://doi.org/10.1029/JA074i016p04025

Thébault, E., Finlay, C. C., Beggan, C. D., Alken, P., Aubert, J., Barrois, O., et al. (2015). International Geomagnetic Reference Field: The 12th generation. *Earth, Planets and Space*, *67*(1), 1–19. https://doi.org/10.1186/s40623-015-0228-9

Venkatesh, K., Fagundes, P. R., Prasad, D. S. V. V. D., Denardini, C. M., de Abreu, A. J., de Jesus, R., & Gende, M. (2015). Day-to-day variability of equatorial electrojet and its role on the day-to-day characteristics of the equatorial ionization anomaly over the Indian and Brazilian sectors. *Journal of Geophysical Research: Space Physics*, *120*, 9117–9131. https://doi.org/10.1002/2015JA021307

Vichare, G., & Rajaram, R. (2011). Global features of quiet time counter electrojet observed by Ørsted. *Journal of Geophysical Research*, *116*, A04306. https://doi.org/10.1029/2009JA015244

Vichare, G., Rawat, R., Jadhav, M., & Sinha, A. K. (2017). Seasonal variation of the Sq focus position during 2006–2010. *Advances in Space Research*, *59*(2), 542–556. https://doi.org/10.1016/j.asr.2016.10.009

Yadav, S., Dabas, R. S., Rupesh, M. D., Upadhayaya, A. K., & Gwal, A. K. (2013). Temporal and spatial variation of equatorial ionization anomaly by using multistation ionosonde data for the 19th solar cycle over the Indian region. *Advances in Space Research*, *51*(7), 1253–1265. https://doi.org/10.1016/j.asr.2012.11.009

Yamazaki, Y., & Maute, A. (2017). Sq and EEJ—A review on the daily variation of the geomagnetic field caused by ionospheric dynamo currents. *Space Science Reviews*, *206*(1), 299–405. https://doi.org/10.1007/s11214-016-0282-z

Woodman, R. F. (1970). Vertical drift velocities and east-west electric fields at the magnetic equator. *Journal of Geophysical Research*, *75*(31), 6249–6259. https://doi.org/10.1029/JA075i031p06249
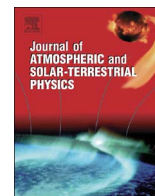
Comparison of quiet time vertical plasma drifts with global empirical models over the Indian sector: Some insights

Kuldeep Pandey[a,b], R. Sekar[a,*], S.P. Gupta[a], D. Chakrabarty[a], B.G. Anandarao[a]

[a] Physical Research Laboratory, Navrangpura, Ahmedabad 380009, India
[b] Indian Institute of Technology-Gandhinagar, Ahmedabad 382424, India

ABSTRACT

The threshold vertical plasma drifts and their polarities are inferred from E-region irregularities reported earlier using different experiments conducted from India during geomagnetically quiet time. In addition, the hourly variations of magnetometer data sets are used in conjunction with an equatorial electrojet model (Anandarao, 1976) to deduce the vertical drifts around noon time (10:00–140:00 LT). These results are then compared with the vertical drifts presented by empirical models (Scherliess and Fejer, 1999; Fejer et al., 2008a) corresponding to the $60°E$ longitude sector. In general, the vertical drifts presented by empirical models are consistent with those inferred from snapshot measurements of E-region irregularities at different local times of the day except around sunrise hours. Further, the vertical drifts presented by Fejer et al. (2008a) model match fairly well with seasonally averaged vertical drifts deduced (within 1σ variation) using magnetometer data. A time difference is noticed between occurrence of pre-reversal enhancement in vertical drifts over India reported earlier using different techniques and Scherliess and Fejer (1999) model. Probable reason for the time difference is discussed. The occurrence characteristic of afternoon equatorial counter electrojet in June solstice during low solar epoch is consistent with the drifts obtained from empirical models. The seasonally averaged vertical drifts during nighttime reported earlier using ionosonde/HF radar experiments are not consistent with the presence of streaming plasma waves on a few occasions. Further, nocturnal vertical drifts are systematically under-estimated and probable reason for this is discussed.

1. Introduction

It is well known that the solar quiet (Sq) time electric field (E) is generated in the E-region of ionosphere by dynamo action. Sq electric fields over low latitude regions are mapped to the dip-equatorial F-region where they cause electrodynamic drifts of the plasma, $\mathbf{V} = \frac{\mathbf{E} \times \mathbf{B}}{B^2}$, B being the strength of the geomagnetic field. Therefore, the E-region zonal electric field (E_x) is treated as driving agency for the vertical drift (V_z) in the F-region. The vertical drifts are known (Fejer, 1981) to be upward during daytime and downward in nocturnal hours under geomagnetically quiet periods. The diurnal variations of vertical drifts in different seasons over the Peruvian sector had been presented (e.g., Woodman, 1970) in the past using highly accurate (better than $2\,\mathrm{ms}^{-1}$) measurements of V_z obtained with Incoherent Scatter Radar (ISR) at Jicamarca.

The low latitude ionosphere is characterized by several large scale plasma processes, like equatorial electrojet, plasma irregularities (streaming and gradient drift waves) associated with it, plasma fountain, plasma bubbles, etc. The generation and evolution of all

these processes depend on the strength and/or polarity of Sq electric field. Hence, in order to address the low latitude ionospheric processes in a comprehensive manner, it is important to know the variations in Sq electric field in different seasons and solar cycles. In absence of ISR over the Indian sector, the vertical drifts or zonal electric fields had been traditionally deduced (refer Section 2) based on ionosonde, phase path sounder, HF Doppler radar and magnetometer measurements. Considering the fact that each of these techniques come with its own limitations and uncertainties (discussed later), it is important to evaluate the consistency of the vertical drifts derived from different techniques with those obtained from global empirical models already available. This will help not only to understand the merits and demerits of individual techniques in a better way but also to evaluate the applicability of global models of vertical drifts to accurately capture the ionospheric processes over the Indian sector.

As already stated, each technique used to derive the vertical drift comes with its own limitation(s). For example, in an ionosonde experiment the recorded movement of ionospheric F-layer along the vertical direction can be due to production by photo-ionization and/or

loss by chemical recombination and/or by electrodynamic processes. The presence of all the three processes during daytime makes it difficult to compute the vertical drifts from the recorded layer movements. But, during nighttime, when plasma production is negligible in absence of solar ionizing radiation, the vertical drifts are deduced from the temporal movement of F-layer (apparent drift) after correcting for the layer movement due to chemical loss. Further, for layer movements above 300 km altitude the difference between electrodynamic and apparent vertical drifts arising due to recombination processes is shown (Bittencourt and Abdu, 1981; Krishna Murthy et al., 1990) to be negligible.

The measurements of V_z during twilight time and their nocturnal variations have been reported earlier (refer Section 2) using several experiments conducted from Trivandrum (TRD, 8.5°N, 76.9°E). In addition, the threshold value and polarity of vertical drift can be deduced from the presence/absence of E-region irregularities (streaming and gradient drift waves) reported earlier (refer Section 2) at different local times of the day using sounding rocket flight and VHF radar experiments over TRD.

A number of works reported in the past provided snap-shot as well as seasonally averaged vertical drifts. In the present work, an attempt is made to consolidate the measurements of vertical drifts made by a few techniques from the Indian dip-equatorial stations and compare them with the drifts presented by global empirical models of Scherliess and Fejer (1999) and Fejer et al. (2008a) (henceforth Scherliess-99 and Fejer-08), to investigate their consistencies over the Indian sector. Further, considering the fact that in empirical models the vertical drifts have been averaged over at least ±5° dip-latitude, the vertical drifts presented earlier using ionosonde and HF radar techniques over Kodaikanal (KDK, 10.3°N, 77.5°E), whose dip-latitude is less than 1.5°, are also used for this comparison. In addition, the vertical drifts around noon hours are deduced using seasonally averaged hourly variation of magnetometer data in conjunction with an equatorial electrojet model (Anandarao, 1976) and used for this comparison.

2. Details of the dataset

In the present investigation, the average F-region vertical drifts measured during nighttime from ionosonde (Sastri, 1984; Subbarao and Krishna Murthy, 1994; Krishna Murthy and Hari, 1996; Madhav Haridas et al., 2015), phase path sounder (Ramesh and Sastri, 1995; Sastri, 1996) and HF Doppler radar (Nair et al., 1993) experiments are used. Further, the electric fields deduced from E-region irregularities during day and night are also utilized. As the equatorial vertical drifts are sensitive to geomagnetic conditions (Fejer et al., 2008b), the present work pertains to only the quiet time conditions with Ap < 30 and/or Kp ≤ 3. The available observational data sets span over five decades (1957–2008) involving solar flux variations during several solar cycles. The solar flux levels of $F_{10.7} < 130$ *sfu* and $F_{10.7} > 160$ *sfu* are respectively considered to represent the low and high solar epochs similar to those considered by the empirical models.

The observations with different time axes are converted into a single time format corresponding to the local time (*LT*) at TRD (longitude 76.9°E). The observations are classified into three seasons, namely, December solstice (November–December–January–February), equinox (March-April, September-October) and June solstice (May–June–July–August) similar to the seasonal classifications followed in Scherliess-99 and Fejer-08.

The ionosonde observations of F layer movement reported by Subbarao and Krishna Murthy (1994) are converted into vertical plasma drift after correcting for chemical recombination effects based on their work. Further, apparent drifts reported by Sastri (1984) using ionosonde observations over KDK during 1957–1959 can be treated as electrodynamic drifts since the layer heights are well above 300 km during solar maximum.

The vertical drifts have been reported using phase path sounder

over KDK (Ramesh and Sastri, 1995; Sastri, 1996) and Doppler radar over TRD (Nair et al., 1993) operated at 4 MHz and 5.5 MHz respectively. As the altitudes of reflecting layers, corresponding to these high operative frequencies, were considered to be well above 300 km during pre-midnight hours, no explicit corrections for the recombination losses were made in those results.

The presence of streaming and gradient drift waves was reported using back scatter radars operated from TRD in HF (18 MHz) (Tiwari et al., 2003) and VHF (54.95 MHz) (Prakash and Muralikrishna, 1976) frequencies. The limiting values of plasma drifts using threshold condition of streaming waves (refer Section 3) and their polarities from Doppler shift are deduced. The plasma drifts deduced from the E-region structures (e.g., Reddy et al., 1987; Viswanathan et al., 1987) are not considered in the present work, as the calibration factors to convert them to ambient plasma drifts are not available.

The in-situ measurements (e.g., Prakash et al., 1971; Gupta, 2000) of electron density profiles and structures in them had been obtained using high frequency Langmuir probes (Prakash and Subbaraya, 1967; Subbaraya et al., 1983, 1985) on board rocket flight experiments. Those were conducted over TRD at different local times of the day covering different seasons under high and low solar epochs. The generation processes of electron density structures depend on the ambient electric fields. As mentioned earlier, the limiting plasma drifts are deduced from the presence of streaming waves. In addition, the observed gradient in the altitude profile of electron densities and the presence/absence of gradient drift waves are used to deduce the polarity of vertical electric field from which the direction of zonal electric field is inferred, as these two components are related over the dip-equator.

The vertical drifts deduced from the observations of E-region structures, mentioned above, under high and low solar epochs are summarized in Tables 1 and 2 respectively. The Tables provide limiting values of vertical drift for the presence of streaming waves ($> + 12$ ms^{-1} during daytime, $< - 12$ ms^{-1} during nighttime) while the inverse conditions are taken for their absence. Further, for the time interval when streaming waves have been detected on some days and found absent on some other days the vertical drift are indicated with $\sim \pm 12$ ms^{-1}. The observations of streaming waves spanned from 1967 to 1999 when the dip angle over TRD was between $-0.9°$ and $+1.2°$ (IGRF-12, Thébault, 2015). Hence, the existence of streaming waves is consistent with the conclusion of Sekar et al. (2013).

Barium vapour cloud release experiments provide in-situ measurements of plasma drifts associated with ambient electric field. The vertical drifts around twilight time measured with these experiments over TRD (e.g., Anandarao et al., 1977) and Sriharikota (SHK, 13.7°N, 80.2°E, a station close to the dip-equator) (e.g., Sekar, 1990) are used in the present work.

In the present work, a methodology (see Appendix) is adopted to derive the quiet time vertical drifts during 10:00–14:00 *LT* using magnetometer datasets. The parameter $\Delta H_{equator} - \Delta H_{off-equator}$ (where H is the horizontal component of geomagnetic field and ΔH is calculated by subtracting nighttime base value from the instantaneous H values), derived using ground based magnetometer data, is conventionally (Rastogi and Patel, 1975) used as a proxy for the strength of equatorial electrojet. Assuming that the variations in ionospheric conductivities are not significant during 10:00–14:00 *LT*, variations in $\Delta H_{equator} - \Delta H_{off-equator}$ during this period can be treated as variations in the zonal electric fields.

Finally, the empirical models Scherliess-99 and Fejer-08 provide the dip-equatorial vertical plasma drifts at different local times and seasons during geomagnetically quiet periods. In order to compare with the vertical drifts derived based on measurements by different techniques mentioned earlier, the model drifts corresponding to 60°E longitude which is closest to Indian-dip equator are reproduced from Figure 8 of Scherliess-99 and Figure 7 of Fejer-08.

3. Results

Fig. 1 depicts the diurnal variations of vertical drift (black colored solid curves) presented by Scherliess-99 model for high solar epoch. Subplots 1(a), 1(b) and 1(c) show the vertical drifts in December solstice (November–December–January–February), equinox (March–April, September–October) and June solstice (May–June–July–August) respectively.

In subplot 1(a), the blue and green colored (solid, dash and dash-dot) curves portray the average nocturnal variations of V_z obtained using ionosonde/radar experiments from TRD and KDK respectively. The blue colored dash curve represents V_z computed using the average nocturnal variations of $h'F$ presented by Subbarao and Krishna Murthy (1994); and blue colored dash-dot curve portrays the average V_z variation during nighttime presented by Madhav Haridas et al. (2015). The green colored dashed and solid curves depict the average vertical drifts during dusk-midnight hours presented by Sastri (1984) and Ramesh and Sastri (1995) respectively. The 1σ variation in vertical drift at prereversal enhancement (PRE) time, as provided by Ramesh and Sastri (1995), is reproduced with green colored solid vertical bar on the top right corner of subplot 1(a) as well as in subplots 1(b-c). It must be noted that 1σ variation will be provided subsequently in this work wherever it is available in the literature under consideration here.

The twilight time in-situ measurements of vertical drifts reported by Anandarao et al. (1977) and Sekar (1990) are shown with magenta colored dots at the particular LT of the experiments. The average nocturnal variation of vertical drifts corresponding to the zonal electric fields presented by Krishna Murthy and Hari (1996) is shown with the dark magenta colored solid curve. In addition, average variation of vertical drift around noon hours deduced from magnetometer records is portrayed with the maroon colored solid curve. The standard deviation (σ) of these deduced vertical drifts, estimated based on the variations in $\Delta H_{TRD} - \Delta H_{ABG}$ (see Appendix), is shown as vertical bars on the curve.

The vertical arrows (at the bottom of subplot) are drawn at the particular LT corresponding to the sounding rocket experiments, listed in Tables 1 and 2, in which the streaming waves have been observed. Similarly, the solid horizontal lines (at the bottom of subplot) are drawn for the particular time interval during which the streaming waves have been observed using VHF radar experiments, listed in Tables 1 and 2. The presence or absence of streaming waves is respectively portrayed with teal or red colors. It is to be noted that teal and red colored horizontal lines are simultaneously used for certain durations when presence of streaming waves were detected on some days and found absent on some other days.

In subplots 1(b) and 1(c) the same notations which have been used in subplot 1(a) are followed to present the vertical drifts corresponding to equinox and June solstice respectively. An additional green colored dotted curve in subplot 1(c) depicts the vertical drift presented by Sastri (1996). The 1σ variation in vertical drifts at PRE time, as provided by Sastri (1996), is reproduced with green colored dotted vertical bar on top right corner in subplot 1(c).

Fig. 2 depicts the diurnal variations of vertical drift (black solid curves) presented by Scherliess-99 model corresponding to different seasons under low solar epoch. The values of V_z obtained using experiments conducted from TRD, KDK, SHK and magnetometer records are overlaid in respective subplots with same notations as in Fig. 1. Note that, if the ionosonde/radar derived average nocturnal vertical drifts are not available from the same works that are used to construct Fig. 1, the respective color codes and pattern of the curves are not utilized in Fig. 2 to maintain uniformity and avoid ambiguity. The additional blue colored solid curves in Fig. 2 portray the average nocturnal V_z variations presented by Nair et al. (1993). The nighttime averaged 1σ variation in vertical drifts, as provided by Nair et al. (1993), is reproduced with blue colored solid vertical bars in respective subplots of Fig. 2.

Figs. 3 and 4 depict the diurnal variations of vertical drifts (black curves) presented by Fejer-08 model corresponding to different seasons under high and low solar epochs respectively. The vertical drifts obtained using experiments conducted over TRD, KDK, SHK and magnetometer records under high and low solar epochs are overlaid in Figs. 3 and 4 with same notations and color codes as in Figs. 1 and 2 respectively.

The gray colored horizontally shaded region in each subplot marks the range of vertical drift values in which presence of streaming waves can be expected. The reasoning for this demarcation is as follows. The generation of streaming waves is known (Farley, 2009) to get triggered whenever magnitude of zonal drift (V_x) of electrons exceeds the ion-acoustic speed of the medium, which is about $370\ \mathrm{ms}^{-1}$ at ~105 km altitude over the Indian sector. The plasma drifts along the zonal (V_x) and vertical (V_z) directions are known (Anandarao et al., 1977; Sekar et al., 2013) to be connected, over the dip-equator, by a relation $V_x = RV_z$, where R is equal to the ratio of Hall to Pedersen conductivities. Recently, R is shown (Pandey et al., 2016) to remain nearly same, irrespective of local time of the day and solar epoch, with it's value about 30 at ~105 km altitude. Hence, whenever the streaming waves are present the magnitude of vertical drift must be greater than $12\ \mathrm{ms}^{-1}$. The above inference of limiting plasma drift of $\sim \pm 12\ \mathrm{ms}^{-1}$ gets the support from the occurrence of streaming waves on some days and absence on some other days (see subplots 1b, 2a-2c, 3b, 4a-4c). It is expected that the vertical drifts would lie within or outside this gray colored shaded region whenever the streaming waves are present (teal colored vertical arrows/horizontal lines) or absent (red colored vertical arrows/horizontal lines) respectively.

As stated earlier, Tables 1 and 2 summarize the results from sounding rocket flights (e.g. Prakash et al., 1969, 1970, 1974; Prakash and Pal, 1985; Gupta and Prakash, 1979; Gupta, 1986, 1997) and VHF/HF radar (e.g. Sastri et al., 1991; Ravindran and Krishna Murthy, 1997a, 1997b; Krishna Murthy et al., 1998) experiments. The necessary vertical drift for the observed presence ($> + 12\ \mathrm{ms}^{-1}$ or $< - 12\ \mathrm{ms}^{-1}$), absence ($\leq +12\ \mathrm{ms}^{-1}$ or $\geq -12\ \mathrm{ms}^{-1}$) or some days present and some days absent ($\sim \pm 12\ \mathrm{ms}^{-1}$) of streaming waves is also provided in the respective entries of Tables 1 and 2. In addition, the vertical drifts obtained from Scherliess-99 and Fejer-08 models at respective LT, season and solar epoch corresponding to the rocket flights are also given in Tables 1 and 2. Further, the vertical drifts obtained from both the empirical models corresponding to the starting time of the respective VHF radar experiments are also provided in Tables. Note that, if the magnitude of vertical drift obtained from empirical model deviates from the criterion of deduced $|V_z|$ given above, the value is highlighted with red color. Further, if direction of this vertical drift differs from that deduced from observation, the cell is highlighted with gray color. This notation is not followed for cases wherein deduced $|V_z| \sim 12\ \mathrm{ms}^{-1}$.

On comparing the vertical drifts given in Tables 1 and 2 it is observed that in general, vertical drifts presented by both the empirical models are consistent with the criterion for presence or absence of streaming waves, though some deviations are also observed. The amplitudes of vertical drifts obtained from Scherliess-99 and Fejer-08 models are found to deviate from the deduced threshold values of $|V_z|$ on six and five occasions respectively (see the red colored entries in Tables 1 and 2). The deviations in V_z with respect to Fejer-08 model drifts are within the uncertainly limits of measurements (about 10%) for Fejer-08 model, barring two durations 13:38−14:38 LT in December solstice under high solar epoch and 09:23−10:23 LT in June solstice under low solar epoch. However, in case of Scherliess-99 model, except an occasion during 14:08−14:38 LT in equinox under high solar epoch, all the deviations in V_z are beyond the uncertainty limits of measurements (relative precision of about $2\ \mathrm{ms}^{-1}$). Even in the cases when streaming waves are present on some days and absent on some other days (implying amplitude of vertical drifts closer to $12\ \mathrm{ms}^{-1}$), the Fejer-08

Table 1
Comparison of vertical plasma drifts in high solar epoch deduced from experimental observations (rocket/radar) with global empirical model (Scherliess-99 and Fejer-08) drifts. Positive and negative values indicate upward and downward drift respectively. The red colored entries denote the instances when the magnitudes of the model drifts are different from the threshold drifts deduced from E-region irregularity observations whereas the gray boxes identify the instances when the polarity of the model drifts are not in accordance with the inferred polarities.

Season	Experiment	Date	Time/ Duration	Vertical drift (ms^{-1})			Literature
				Deduced	Scherliess- 99	Fejer- 08	
December solstice	Rocket	21-12-1978	02:08	< -12	-21.2	-24.4	Gupta (2000)
		21-12-1978	05:53	< -12	-09.5	-15.8	Gupta (2000)
		12-02-1981	10:35	$> +12$	$+17.4$	$+24.0$	Prakash and Pal (1985)
		02-02-1968	18:34	$> +12$	$+26.8$	$+30.5$	Prakash et al. (1969); Gupta and Prakash (1979)
	Radar	03-02-1999	07:08–09:38	$\leq +12$	$+03.3$	$+05.4$	Tiwari et al. (2003)
		03-02-1999	10:08–13:08	$> +12$	$+16.3$	$+23.2$	Tiwari et al. (2003)
		03-02-1999	13:38–14:38	$\leq +12$	$+14.3$	$+17.1$	Tiwari et al. (2003)
Equinox	Rocket	28-04-1980	05:58	$> +12$	-18.3	-23.1	Gupta (2000)
		12-03-1967	18:35	$> +12$	$+32.9$	$+41.5$	Gupta (2001)
	Radar	19-03-1991	04:43–05:13	< -12	-24.8	-41.5	Ravindran and Krishna Murthy (1997a)
		15-03-1991	06:18–06:38	≥ -12	-06.5	-13.0	Ravindran and Krishna Murthy (1997a)
		15-03-1991	07:48–08:13	$\leq +12$	$+07.2$	$+02.7$	Ravindran and Krishna Murthy (1997a)
		20-03-1979, 15-03-1991, 17-03-1991	07:53–09:08	$\sim +12$	$+12.3$	$+08.0$	Viswanathan et al. (1987); Ravindran and Krishna Murthy (1997a)
		20-03-1979, 21-03-1979, 21-09-1979	10:08–13:38	$> +12$	$+23.8$	$+27.0$	Viswanathan et al. (1987); Ravindran and Krishna Murthy (1997b)
		20-03-1979, 21-03-1979	13:38–14:08	$\sim +12$	$+15.3$	$+12.0$	Viswanathan et al. (1987)
		21-03-1979	14:08–14:38	$\leq +12$	$+12.8$	$+12.0$	Viswanathan et al. (1987)
		15-03-1979, 21-03-1979	14:38–16:48	$\sim +12$	$+10.8$	$+11.4$	Viswanathan et al. (1987); Ravindran and Krishna Murthy (1997a)
		15-03-1979, 16-03-1979, 21-03-1979	16:48–17:38	$\leq +12$	$+07.7$	$+10.2$	Viswanathan et al. (1987); Ravindran and Krishna Murthy (1997a)
		15-03-1979, 16-03-1979	17:38–18:23	$> +12$	$+15.6$	$+21.5$	Ravindran and Krishna Murthy (1997a)
June solstice	Rocket	13-08-1982	07:02	$\leq +12$	$+01.6$	-02.9	Gupta (2001)
		12-08-1982	07:18	$\leq +12$	$+05.1$	-02.0	Gupta (2001)
		29-08-1968	13:53	$\leq +12$	$+06.5$	$+08.7$	Gupta (2001)
		29-08-1968	22:38	< -12	-16.6	-16.2	Prakash et al. (1970); Gupta and Prakash (1979)

model drifts seem to be more consistent with deduced vertical drifts than Scherliess-99 model drifts. This is clearly visible during 08:00–10:00 *LT* and 13:00–16:00 *LT*. Hence, Fejer-08 model is found to represent the vertical drifts over the Indian sector better compared to Scherliess-99 model. However, it is observed that both the empirical models fail to capture the polarity of vertical drift during early morning hours (around 06:00 *LT*), see gray colored cells in Tables 1 and 2, though in June solstice the Scherliess-99 model seems to predict better compared to Fejer-08 model. The probable reasons for deviations in amplitude and polarity of the vertical drifts presented by empirical models from the deduced V_z on a few occasions are discussed in Section 4.

Around noon hours (10:00–14:00 *LT*), the average variations of vertical drifts deduced from magnetometer records match (within 1σ variation) with the corresponding variations presented by both Scherliess-99 and Fejer-08 models in equinox and June solstice under high solar epoch, see maroon and black colored solid curves in Figs. 1 and 3. However, the vertical drift deduced in these seasons during low solar epoch match (within 1σ variation) with the corresponding variations presented by Fejer-08 model better compared to Scherliess-99 model, see Figs. 2 and 4. In December solstice (when 1σ variations are largest) the deduced values of V_z match (within 1σ variation) with the corresponding variations presented by both the empirical models irrespective of solar epoch. In general, the average values of deduced V_z match fairly well with both the empirical models during high solar epoch while these values match well with Fejer-08 model during low solar epoch. This is probably due to better long-itudinal resolution used in Fejer-08 model (refer Section 4). Further, the values of V_z deduced from magnetometer data are observed to capture the presence or absence of streaming waves. Interestingly, the deduced vertical drifts are ~12 m s^{-1} during the time intervals wherein streaming waves were detected on some days and found absent on some other days.

During nighttime, the average values of V_z obtained using ionosonde/radar experiments are not sufficient for the generation of streaming waves in low solar epoch (see Figs. 2 and 4) on a few occasions. In high solar epoch, the pre-midnight vertical drifts in both the solstices are (in general) sufficient for the presence of streaming waves (see subplots 1a, 3a and 1c, 3c), though during post-midnight hours the vertical drifts are sufficient for the presence of streaming waves on some occasions only (see subplots 3a and 3c). However, during equinox in high solar epoch some of the average vertical drifts are sufficient to capture the presence of streaming waves. Further, it is observed that the ionosonde/radar deduced vertical drifts are always smaller than those presented by empirical models in different seasons (e.g., see subplots 3a, 3b and 3c) and solar flux levels (e.g., see subplots 3a and 4a). In general, the differences are about 10 ms^{-1} or greater with the maximum deviation occurring in equinoctial months (e.g., notice the difference in V_z of middle panel compared to top or bottom panel in any figure). It is to be noted that considering typical height resolution of 3 km (Patra et al., 2005) and the temporal resolution of 15 min in ionosonde experiments (Sastri, 1984; Krishna Murthy and Hari, 1996; Madhav Haridas et al., 2015), the typical uncertainty in vertical drift is ~5 ms^{-1}. The uncertainty in the vertical drifts deduced using HF phase path sounder or Doppler radars is less than 1 ms^{-1} (Prabhakaran Nayar and Sreehari, 2004). Therefore, the observed differences between the measured vertical drifts (derived using ionosonde/Phase path sounder/Doppler radar) and the model drifts are larger than the typical uncertainties of the measurements involved. The probable reasons for significant difference are discussed in Section 4. In addition, it is observed that during nighttime Scherliess-99 model values of V_z are smaller compared to Fejer-08 model. The probable reasons for this are also discussed in Section 4.

During PRE hours, the peak amplitude of V_z is known to vary day-to-day (Balan et al., 1992) and also dependent on the solar flux level

Table 2
Same as Table (1) but corresponds to low solar epoch.

Season	Experiment	Date	Time/ Duration	Vertical drift (ms^{-1})			Literature
				Deduced	Scherliess-99	Fejer-08	
December solstice	Rocket	09-02-1975	05:37	< −12	−13.1	−18.8	Gupta (1986)
		28-01-1971	10:18	> +12	+18.2	+18.9	Prakash et al. (1971)
		19-02-1975	10:43	> +12	+18.4	+19.1	Gupta (1997)
		28-01-1971	10:48	> +12	+18.4	+19.3	Prakash et al. (1971)
	Radar	18-01-1974	05:38–06:08	< −12	−13.0	−24.6	Prakash and Muralikrishna (1976)
		18-01-1974, 23-11-1983	06:58–08:08	≤ +12	+03.7	+03.6	Prakash and Muralikrishna (1976); Viswanathan et al. (1987)
		23-11-1983, 25-11-1983, 05-01-1993	08:08–10:08	~ +12	+10.4	+10.9	Viswanathan et al. (1987); Ravindran and Krishna Murthy (1997b)
		23-11-1983, 25-11-1983, 26-11-1983, 05-01-1993	10:08–12:38	> +12	+17.9	+18.5	Viswanathan et al. (1987); Ravindran and Krishna Murthy (1997b)

Table 2 *(continued)*

		Date	Time				Reference
December solstice	Radar	23-11-1983 to 26-11-1983, 05-01-1993	12:38–15:38	∼ +12	+15.6	+14.7	Viswanathan et al. (1987); Ravindran and Krishna Murthy (1997b)
		23-11-1983, 26-11-1983	15:38–17:23	≤ +12	+06.5	+04.8	Viswanathan et al. (1987)
		06-12-1973	19:38–20:38	≤ +12	−03.6	−01.3	Prakash and Muralikrishna (1976)
Equinox	Rocket	03-03-1973	11:58	> +12	+21.2	+19.5	Gupta (2001)
		07-04-1972	12:08	> +12	+20.6	+17.9	Gupta and Prakash (1979)
		13-10-1972	12:38	≤ +12	+18.6	+13.6	Gupta (2001)
		15-03-1975	21:42	< −12	−16.9	−27.5	Gupta (1997)
	Radar	06-09-1994	03:53–05:38	< −12	−13.7	−30.0	Krishna Murthy et al. (1998)
		10-03-1972, 05-09-1994	06:38–08:38	≤ +12	−08.9	−06.0	Prakash et al. (1974); Krishna Murthy et al. (1998)
		10-03-1972, 12-10-1983	08:38–09:38	∼ +12	+16.5	+15.9	Prakash et al. (1974); Sastri et al. (1991)
		10-03-1972, 12-10-1983, 05-09-1994	09:38–13:08	> +12	+20.8	+26.7	Prakash et al. (1974); Viswanathan et al. (1987); Krishna Murthy et al. (1998)
		10-10-1983, 12-10-1983, 05-09-1994	13:08–14:38	∼ +12	+16.6	+09.7	Viswanathan et al. (1987); Krishna Murthy et al. (1998)
Equinox	Radar	10-03-1972, 11-10-1983, 12-10-1983, 05-09-1994	14:38–17:53	≤ +12	+10.4	+06.3	Prakash et al. (1974); Viswanathan et al. (1987); Krishna Murthy et al. (1998)
June solstice	Rocket	12-08-1972	07:23	≤ +12	+02.8	−04.9	Gupta and Prakash (1979)
	Radar	20-06-1983, 24-06-1983	07:53–08:53	≤ +12	+09.6	−01.1	Viswanathan et al. (1987)
		21-06-1983, 24-06-1983	08:53–09:23	∼ +12	+20.0	+09.6	Viswanathan et al. (1987)
		23-06-1983, 24-06-1983	09:23–10:23	≤ +12	+23.1	+14.8	Viswanathan et al. (1987)
		20-06-1983 to 23-06-1983	11:23–13:23	∼ +12	+21.4	+16.3	Viswanathan et al. (1987)
		20-06-1983, 23-06-1983	13:23–13:53	≤ +12	+07.5	+06.8	Viswanathan et al. (1987)

(Ramesh and Sastri, 1995; Sastri, 1996). However, the time of PRE over the Indian sector have been shown (Namboothiri et al., 1989; Nair et al., 1993) to be same within a solar epoch and hence the occurrence times of PRE are compared. Incidentally, it is found that the vertical drifts presented using ionosonde/radar experiments maximize around the time of Barium vapour cloud experiments (the solid blue, green and magenta colored curves in subplots 3(a), 3(b) and 4(a) peak around the time of magenta colored solid circles). It is also to be noted that the
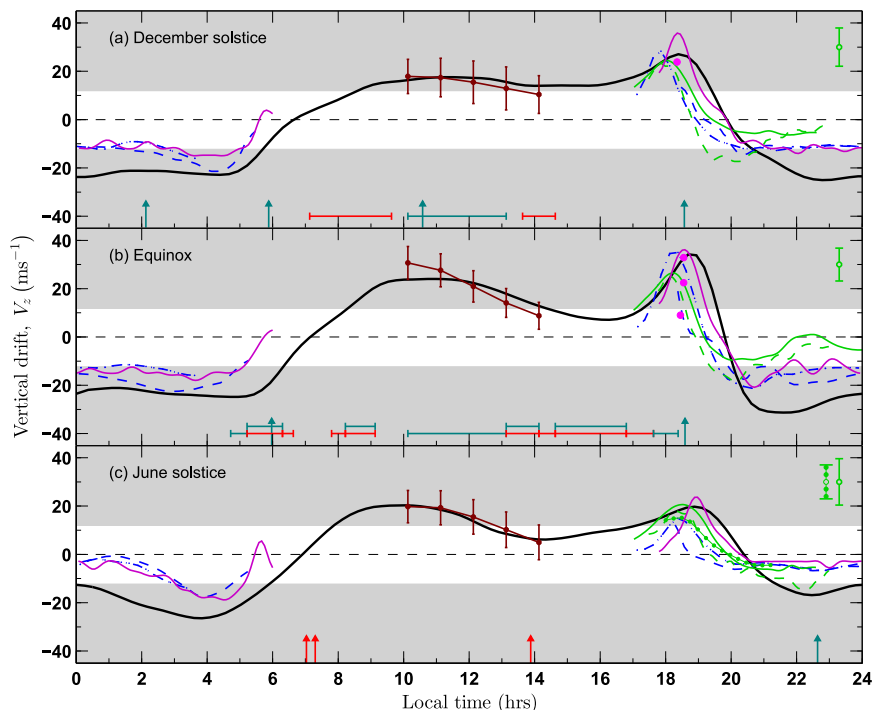
Fig. 1. Vertical drift variations during high solar epoch over the Indian sector provided by Scherliess and Fejer (1999) model (black) and experiments conducted from TRD and KDK (blue, dark magenta and green colored curves respectively) along with the 1σ variation in them (wherever available) with the same notation shown on the top right corner. Vertical drifts measured using vapour release experiments are shown with magenta colored dots and those deduced from magnetometer records is shown with maroon colored curves. The presence or absence of streaming waves observed using sounding rocket flights (vertical arrows) and VHF Doppler radars (horizontal lines) are portrayed with teal or red colors respectively. The durations when streaming waves were detected on some days and found absent on some other days are depicted with simultaneous horizontal lines in teal and red colors. (See text for more details). (For interpretation of the references to color in this figure legend, the reader is referred to the web version of this article.)

time of PRE observed in V_z presented by Scherliess-99 model is later in *LT* compared to these times (e.g., see Fig. 1). A probable reason for this difference in time is discussed in Section 4.

4. Discussion

As mentioned in Section 3, Fejer-08 model is found to be more consistent with the reported presence or absence of streaming waves than Scherliess-99 model. Further, the vertical drift provided by Fejer-08 model also seem to represent the measured drifts better during low
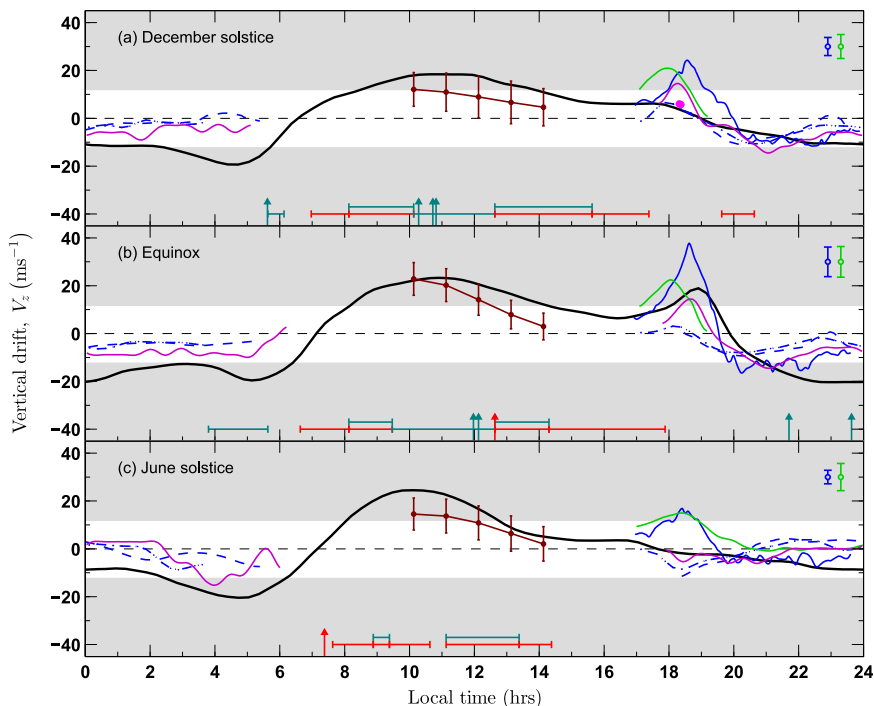
Fig. 2. Same as Fig. 1 but corresponds to low solar epoch. (For interpretation of the references to color in this figure, the reader is referred to the web version of this article.)
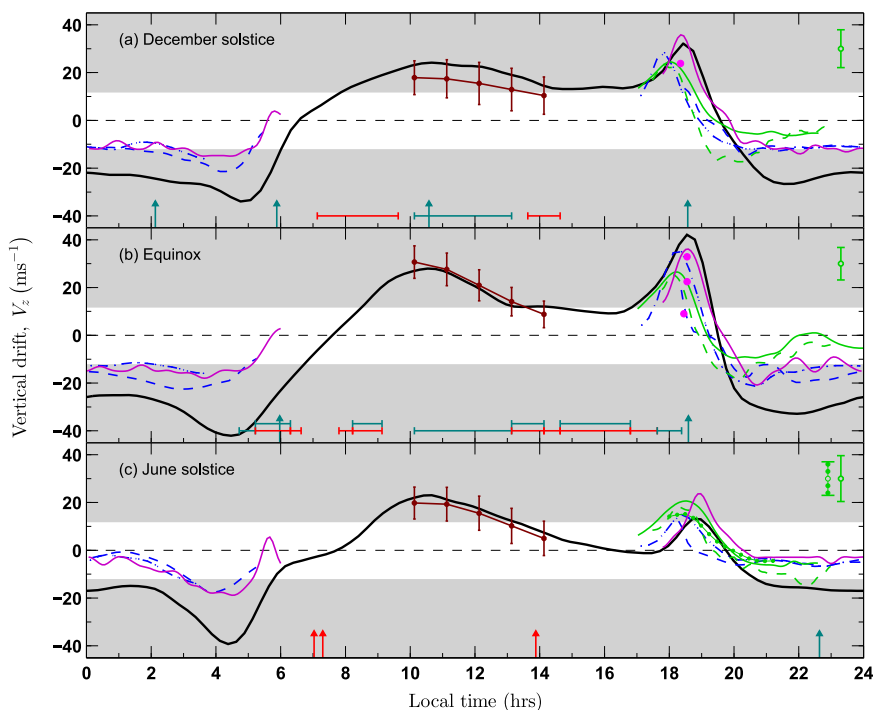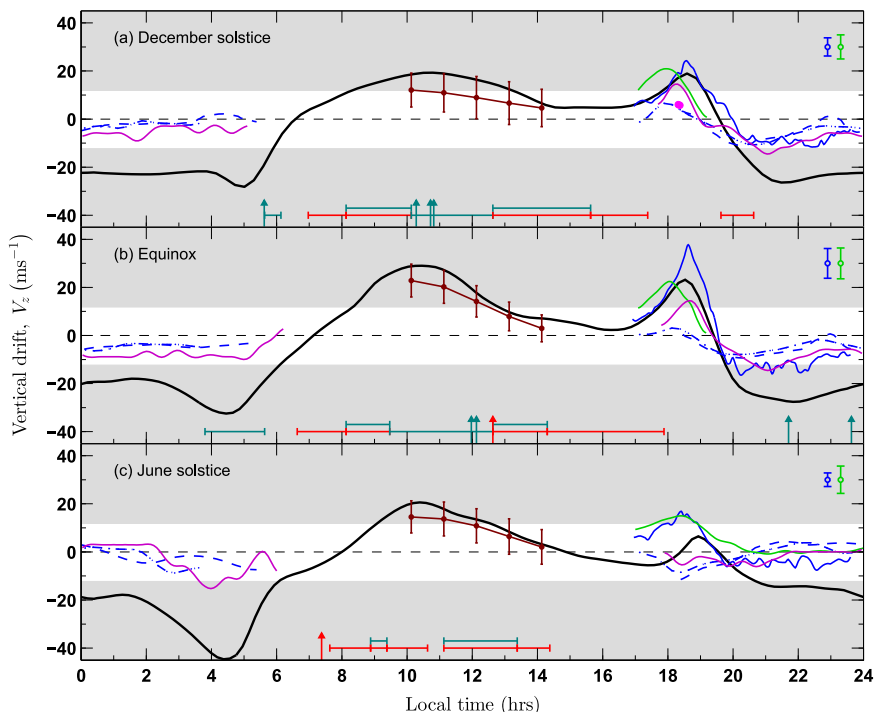
Fig. 3. Same as Fig. 1 but comparison is with the Fejer et al. (2008a) model drifts. (For interpretation of the references to color in this figure, the reader is referred to the web version of this article.)

solar epoch as far as the PRE and daytime deduced drifts are concerned. To investigate the probable reasons for Fejer-08 model being more consistent than Scherliess-99 model, the data sets and methodology used to develop these empirical models are looked into.

It is to be noted that empirical models were developed based on the in-situ observations of plasma drifts at the altitude of satellite. The

techniques employed to measure the plasma drifts are entirely different from the experimental techniques adopted to get these observations over the Indian sector. In Scherliess-99 model, the input for vertical drifts were obtained from Ion Drift Meter (IDM, on board AE-E satellite) measurements over ± 7.5° dip-latitude ranges around the globe during 1977–1979 and Jicamarca ISR measurements from 1968

Fig. 4. Same as Fig. 2 but comparison is with the Fejer et al. (2008a) model drifts. (For interpretation of the references to color in this figure, the reader is referred to the web version of this article.)

to 1992. On the other hand, in Fejer-08 model the input for vertical drifts were obtained from Ionospheric Plasma and Electrodynamics Probe Instrument (IPEI, on board ROCSAT-1 satellite) measured vertical drifts over $\pm 5°$ dip-latitude ranges around the globe from 1999 to 2004. These vertical drifts were binned over $60°$ and $30°$ longitudes in Scherliess-99 and Fejer-08 models respectively. Further, different methodologies were adopted to develop both the empirical models. In Scherliess-99 model, the V_z values around the globe were constrained with different statistical weights to make electric field curl-free ($\oint \mathbf{E} \cdot d\mathbf{l} = 0$). However, in Fejer-08 model, the vertical drifts were not constrained to satisfy for irrotational electric field, though, this condition was used to estimate the accuracy of this model. As mentioned in Scherliess and Fejer (1999), satellite measurements of V_z during nighttime (that have more uncertainty compared to daytime) were given less statistical weight compared to daytime measurements and whenever the highly accurate daytime vertical drifts were available from Jicamarca ISR, those data sets were given even higher statistical weight (about 75%). Under this scenario, the V_z values provided by Scherliess-99 model over the Indian sector, which is nearly at antipodal point of the Peruvian sector, could become uncertain.

The occurrence of afternoon equatorial counter electrojet (CEJ) had been shown (Rastogi et al., 2014) to be highest during June solstice under low solar epoch. Interestingly, the Fejer-08 model drift values reveal downward drifts in the afternoon hours which is consistent with the observations of Rastogi et al. (2014). The presence of downward drift in June solstice during solar minimum years also gets credence from the works of Gurubaran (2002) and Bhattacharyya and Okpala (2015). It was shown that equatorial CEJ under similar conditions was due to additional contribution from global current system that gets superimposed on the Sq current system. Further, the small afternoon upward drifts in this season given by Scherliess-99 model are also favorable for the generation of CEJ with a little help from additional external agency. Therefore, both the models support the morphological feature of occurrence of CEJ during this season. As far as the high solar epoch is concerned, negligible vertical plasma drift obtained from Fejer-08 model in the afternoon hours during the June solstice is consistent with the occurrence characteristic of partial CEJ at this local time reported by Rastogi et al. (2014). This feature is not efficiently captured by Scherliess-99 model. In view of these outcomes, in the forthcoming discussion on vertical drifts during different times of the day, barring evening hours, V_z presented by experimental observations are compared with Fejer-08 model only. During PRE time a discussion based on both the models is presented.

4.1. Vertical drifts in morning hours

The vertical drifts presented using ionosonde/radar experiments are insufficient for the generation of streaming waves observed around 06:00 *LT*. Their presence is supported by Fejer-08 model, although the polarity of vertical drifts presented by this model is not consistent with the respective observation on a few occasions during 06:00–08:00 *LT*, as mentioned in Section 3. To investigate the probable reasons for this inconsistency with the empirical model, the diurnal variations of V_z over the dip-equatorial longitudes presented in Fig. 4 of Fejer-08 become important. It is observed from their work that, though the vertical drifts are small during 06:00–08:00 *LT* around the Indian sector, they show variation in polarity with longitude even for a particular *LT*. Therefore, the longitudinal averaging of V_z used in Fejer-08 model (given above) could result in loss of polarity information. Therefore, it is rather difficult to bring out the clear picture of V_z during morning hours.

4.2. Vertical drifts during daytime

In general, the daytime vertical drifts presented by Fejer-08 model and those deduced using magnetometer data sets around noon hours (10:00–14:00 *LT*) match within 1σ variation. In general, the magnetometer deduced V_z capture the presence or absence of streaming waves, suggesting that the magnetometer data can be effectively used to gauge the vertical drift/zonal electric field variations from 10:00 *LT* to 14:00 *LT*.

4.3. Vertical drifts in evening hours

It is noticed that the time of occurrence of PRE, as predicted by Scherliess-99 model, is slightly later than the corresponding times observed by most of the ionosonde/HF radar experiments during high solar epoch. In this regard, Fejer-08 model is closer with Indian observations. This may be partly due to the better longitudinal resolution of the Fejer-08 model in comparison with the Scherliess-99 model. More importantly, the Indian stations are east of $60°E$ longitude and the model drifts have been presented corresponding to $60°E$ with finite longitudinal averaging. As the local sunset will occur over the Indian sector earlier than that over $60°E$, the model drifts can occur at a later time than what Indian observations suggest. During low solar epoch, the PRE feature itself is more conspicuous in Fejer-08 model (particularly during solstices) than in Scherliess-99 model and the Indian observations are reasonably consistent with the Fejer-08 model outputs in all the seasons except in June solstice as far as the time of occurrence of PRE is concerned.

It is interesting to note here that in June solstice under low solar epoch, PRE was found to be present (e.g., Ramesh and Sastri, 1995) on some occasions, absent (e.g., Scherliess-99) on other occasions and reverse PRE (e.g., Subbarao and Krishna Murthy, 1994; Chakrabarty et al., 2014) was also observed. Therefore, the occurrence of PRE in June solstice under low solar epoch is ambiguous. The suppression of PRE in June solstice under low solar epoch was also reported over Peruvian (Scherliess and Fejer, 1999) and African (Oyekola, 2006) sectors. Further, the occurrence of reverse PRE is also noticed in the vertical drifts over African sector that was presented in Fig. 1(a) of Oyekola et al. (2007) corresponding to June solstice in low solar epoch. In general, the occurrence of reverse PRE is found in June solstice when solar flux level is low. The modeling studies of reverse PRE are not found, though simulation results for suppressed PRE are available (Fesen et al., 2000; Millward et al., 2001). The observed variability on the occurrence of PRE during June solstice in low solar epoch needs to be investigated in detail to arrive at a bigger picture. There are differences, of course, between the magnitude of V_z during PRE time given by Indian observations and the model values on some occasions. It is known that the peak values of V_z during PRE hours depend on solar flux level (Fejer et al., 1996; Sastri, 1996; Madhav Haridas et al., 2015) and change on a day-to-day basis (Woodman, 1970; Balan et al., 1992). In absence of significant recombination effect (as the layer height is generally more than 300 km) during PRE time and unlikely occurrence of equatorial spread-F before PRE, ionosonde/HF radar measurements can be used to infer V_z on a day-to-day basis.

4.4. Vertical drifts during nighttime

The vertical drifts presented by Fejer-08 model capture the observed presence/absence of streaming waves during nighttime. However, the vertical drifts presented using ionosonde/HF radar experiments are not sufficient, on most of the occasions, to capture the observed presence of streaming waves and differ from vertical drifts presented by Fejer-08 model by $10\,\text{ms}^{-1}$ or more in general. The

sources of these deviations could be improper correction of βH, gradients in vertical drifts, instrumental bias and/or inaccurate determination of height of plasma layer, etc. To delineate the probable causes of these large differences the contributions that can arise from these factors are looked into.

As the vertical drifts (used in the present work) are, in general, obtained only for the duration when altitude of plasma layers remains above 300 *km*, the contribution due to chemical recombination would be negligible (Bittencourt and Abdu, 1981). Even otherwise, it is shown (Kakad et al., 2012; Subbarao and Krishna Murthy, 1994) that contribution due to recombination process can be about $2 \, \mathrm{ms^{-1}}$ or $4 \, \mathrm{ms^{-1}}$ corresponding to the movement of plasma layer above or below 300 km respectively.

The altitude variation of vertical drifts over the Indian sector around PRE hours have been reported earlier (Raghavarao et al., 1987; Sastri et al., 1995; Prabhakaran Nayar and Sreehari, 2004). However, the altitude gradient in vertical drifts during nighttime over the Indian sector are not known. Therefore, a typical (Pingree and Fejer, 1987) altitude gradient in the vertical drift over the dip-equatorial station (Jicamarca) is taken as a representative value. The altitude averaged gradient in nocturnal V_z was shown by Pingree and Fejer (1987) to be around $0.005 \, \mathrm{ms^{-1} \, km^{-1}}$ (averaged nighttime value). As the altitudes probed by the ionosonde/radar experiments (bottom side of F-layer, i.e. around 300 km) and the ROCSAT-1 satellite (used in Fejer-08 model) are separated by about 300 km, V_z values could differ by about $2 \, \mathrm{ms^{-1}}$. Further, if the altitude gradient in vertical drifts are assumed to follow the opposite pattern above and below F-layer peak as observed by Fejer et al. (2014) and simulated by models (Klimenko et al., 2012; Qian et al., 2015), the difference in V_z would be even less than $2 \, \mathrm{ms^{-1}}$.

Finally, the accuracy of vertical drifts deduced using ionosonde/radar experiments depends (to the first order) on how accurately the altitude of plasma layer is determined. This is particularly difficult during equatorial spread-F (ESF) events. Therefore, to investigate a possible relationship, if any, between the percentage occurrence of ESF (Subbarao and Krishna Murthy, 1994) over TRD and difference between V_z, obtained using ionosonde/radars experiments and Fejer-08 model, the two parameters are looked together. In general, the differences in V_z are found to follow the percentage of occurrence of ESF. For e.g., under high solar epoch, the occurrence of ESF was higher (Subbarao and Krishna Murthy, 1994) during pre-midnight than post mid-night hours in all the seasons; and the corresponding differences in vertical drifts are observed to follow the similar pattern (see Fig. 3). Under low solar epoch, the ESF occurrence in June solstice was higher (Subbarao and Krishna Murthy, 1994) during post-midnight than pre-midnight hours; and corresponding differences in vertical drifts are observed to follow this pattern (see subplot 4b). Further, under high solar epoch the occurrence of ESF during pre-midnight hours was maximum in equinox; and the differences in vertical drifts are also maximum during pre-midnight hours in equinox (see subplot 3b). Under low solar epoch, the occurrence of ESF during post-midnight was maximum in June solstice; and the difference in vertical drifts during post-midnight is also maximum in June solstice (see subplot 4c).

From the above discussion, it appears that the seasonal V_z presented using ionosonde/radar experiments might have suffered from an uncertainty arising out of the inaccurate determination of ionospheric height parameter in the presence of ESF events. It is important to note that the plasma irregularities associated with ESF move upward and thus can result in systematic underestimation of the downward drifts, which is seen in Figs. 1–4. Therefore, presence of ESF is probably the most important reason for the underestimation of ionosonde/HF radar derived vertical drifts. Further, with appropriate (without ESF traces) choice of ionograms and proper correction for

recombination loss, the ionosonde/HF radar experiments can be used to deduce the vertical drifts during nighttime. Another interesting feature in vertical drifts during June solstice under low solar epoch was reported by Chakrabarty et al. (2014). They had shown that the vertical drifts increase and become upward during midnight hours, which is not observed in vertical drifts presented by the empirical models but confirmed by C/NOFS observations.

5. Summary

The vertical plasma drifts obtained or deduced with several techniques over the Indian sector are compared with those presented by the global empirical models (Scherliess and Fejer, 1999; Fejer et al., 2008a). The salient points that have emerged from this study are as follows:

1. In general, the vertical drifts presented by Fejer et al. (2008a) model represent vertical drifts over the Indian sector better than Scherliess and Fejer (1999) model and other average nocturnal vertical drifts deduced using ionosonde/radar experiments.
2. The empirical models fail to capture the direction of vertical drifts in morning hours (around 06:00 *LT*). This is probably due to longitudinal averaging that results in loss of polarity information.
3. The vertical drifts (corresponding to zonal electric fields) deduced around noon hours (10:00–14:00 *LT*) from magnetometer records match with vertical drifts presented by Fejer et al. (2008a) model and capture the presence/absence of streaming waves in general.
4. For distinctive drift features like PRE, the time difference between occurrence of PRE reported by the empirical models and the ground-based observations is found on some occasions and this can be due to the different longitudinal averaging schemes used in the models.
5. The seasonally averaged nocturnal vertical drifts deduced using ionosonde/HF radar experiments are not sufficient, on most of the occasions, to capture the observed presence of streaming waves. The deviations of vertical drifts obtained using ionosonde/HF radar experiments from the Fejer et al. (2008a) model drift values closely follow the percentage occurrence of ESF indicating inaccuracy in the determination of vertical drifts based on ionospheric height variations in the presence of ESF.
6. Both the empirical models Scherliess and Fejer (1999) and Fejer et al. (2008a) support the occurrence characteristic of afternoon equatorial CEJ in June solstice under low solar epoch.

Appendix A

A model was developed by Anandarao (1976) to obtain the ionospheric current density and details of the model can be obtained from the earlier works of Anandarao and Raghavarao (1987) and Raghavarao and Anandarao (1987). The inputs required to the model are altitude profiles of electron density (N_e), neutral density, temperature and dip-equatorial zonal electric field. In addition, a methodology to obtain the horizontal component (H) of magnetic field induced at ground by the electrojet current along zonal direction was described by Anandarao (1977) using,

$$H_{induced} = \frac{\mu_0 C}{2\pi r} \frac{(r/a)\sin\theta - 1}{(r/a)^2 + 1 - 2(r/a)\sin\theta} \tag{1}$$

where C is line current obtained from zonal current density (J_ϕ or J_x), $C = \int_r \int_\theta J_x dr d\theta$. Here r and θ denote the distance and magnetic co-latitude of the line current respectively and a denotes the Earth's radius. Note that J_x values, integrated in the altitude and dip-latitude ranges of 80 to 130 km and $-5°$ to $+5°$ respectively, are used to derive $H_{induced}$. The $H_{induced}$ is taken as the representative of the H component of magnetic field induced at ground due to the equatorial electrojet.

In present work, the problem is reversed in pursuit of zonal electric field from the magnetometer observations. This is done by computing J_x with varying zonal electric field input to the electrojet model till the derived $H_{induced}$ value becomes equal to the observed $\Delta H_{equator} - \Delta H_{off-equator}$. Further, it is noticed that the N_e profiles, measured using sounding rocket flight experiments (Subbaraya et al., 1983; Gupta, 2001), over the equatorial electrojet region (90–110 km) did not reveal any significant temporal variation during 10:00–14:00 LT irrespective of solar epoch, though the absolute values of N_e are larger (about 40%) during solar maximum. Hence, the average N_e profile corresponding to the particular solar epoch and typical profiles of neutral parameters, as their effects on J_x are negligible (Pandey et al., 2016), are used in the electrojet model (Anandarao, 1976) to evaluate $H_{induced}$ for different zonal electric field values. The sensitivity studies (Pandey et al., 2016) were carried out by varying different parameters. This suggests ~5% uncertainty in the estimated zonal electric field.

The hourly magnetometer measurements from a dip-equatorial station Trivandrum (TRD, 8.5°N, 76.9°E, dip-lat. 1°S) and an off-equatorial station Alibag (ABG, 18.6°N, 72.9°E, dip-lat. 10°N) during 1985–1995 are used to obtain $\Delta H_{equator} - \Delta H_{off-equator}$ on geomagnetically quiet days (Kp ≤ 3 and Dst ≥ −20, on the selected day and also on the previous day). The observed values of $\Delta H_{TRD} - \Delta H_{ABG}$ on individual quiet days (gray) and their seasonally averaged (red) values along with 1σ variation during high (left panel) and low (right panel) solar epochs are depicted in Fig. 5. Based on these seasonally averaged values of $\Delta H_{TRD} - \Delta H_{ABG}$, the vertical drifts corresponding to zonal electric fields are obtained during 10:00–14:00 LT.
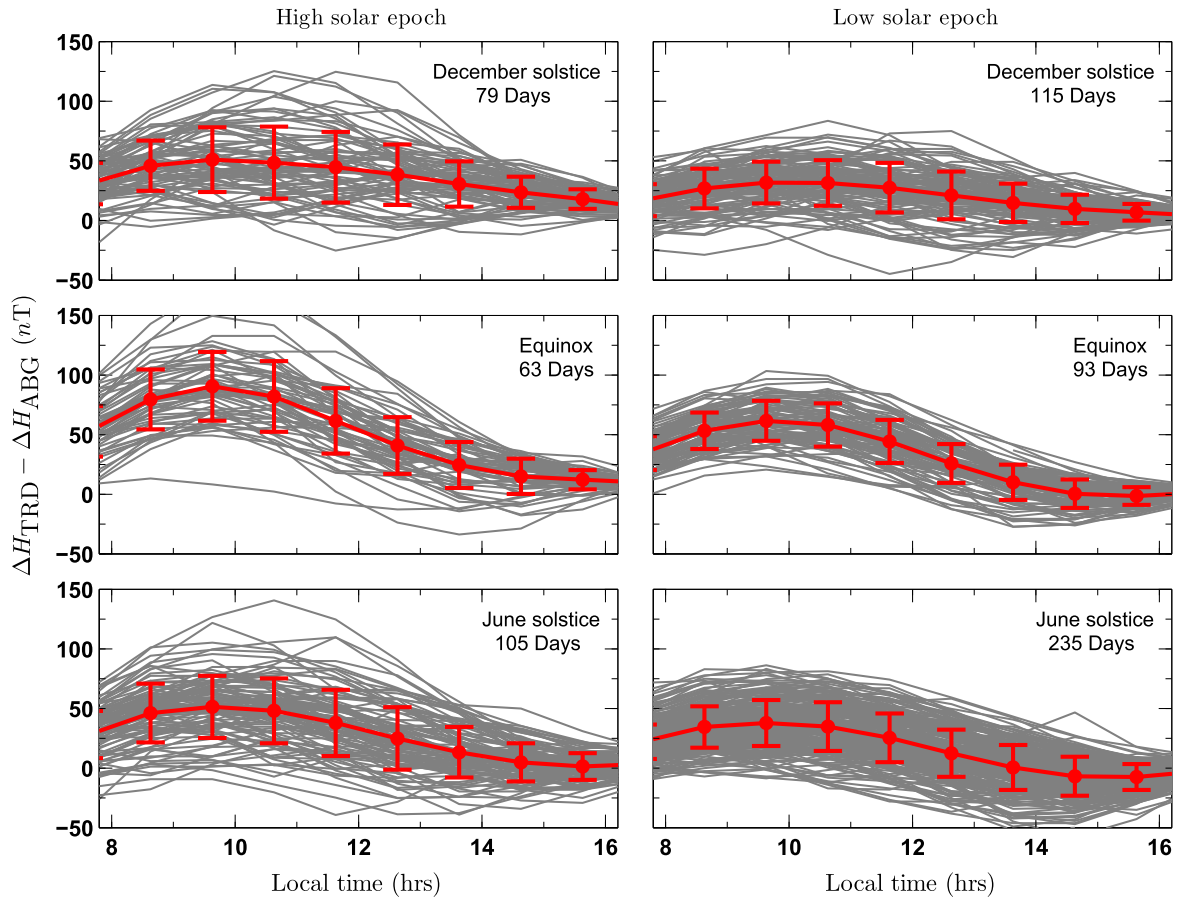

Fig. 5. Hourly variations of individual quiet days (gray colored lines) and seasonally averaged (red colored line) $\Delta H_{TRD} - \Delta H_{ABG}$ values along with 1σ variation during high (left panel) and low (right panel) solar epochs. The upper, middle and lower subplots represent variations in December solstice, equinox and June solstice respectively. The number of days used for seasonal average are also mentioned in each subplot. (The hourly values of magnetic field measurements are obtained from the World Data Center for Geomagnetism, Kyoto).

References

Anandarao, B.G., 1977. Studies on the Dynamics of the Equatorial Ionosphere. (Ph.D. thesis), Gujarat University.

Anandarao, B.G., 1976. Effects of gravity wave winds and wind shears on equatorial electrojet. Geophys. Res. Lett. 3 (9), 545–548, ⟨http://dx.doi.org/10.1029/GL003i009p00545⟩.

Anandarao, B.G., Raghavarao, R., 1987. Structural changes in the currents and fields of the equatorial electrojet due to zonal and meridional winds. J. Geophys. Res. 92 (A3), 2514–2526, ⟨http://dx.doi.org/10.1029/JA092iA03p02514⟩.

Anandarao, B.G., Desai, J.N., Giles, M., Martelli, G., Raghavarao, R., Rothwell, P., 1977. Electric field in the equatorial ionosphere. J. Atmos. Terr. Phys. 39, 927–931.

Balan, N., Jayachandran, B., Balachandran, R.Nair., Namboothiri, S.P., Bailey, G.J., Rao, P.B., 1992. HF Doppler observations of vector plasma drifts in the evening F-region at the magnetic equator. J. Atmos. Terr. Phys. 54 (1112), 1545–1554, ⟨http://dx.doi.org/10.1016/0021-9169(92)90162-E⟩..

Bhattacharyya, A., Okpala, K.C., 2015. Principal components of quiet time temporal variability of equatorial and low-latitude geomagnetic fields. J. Geophys. Res. 120 (10), 8799–8809, ⟨http://dx.doi.org/10.1002/2015JA021673⟩.

Bittencourt, J.A., Abdu, M.A., 1981. A theoretical comparison between apparent and real vertical ionization drift velocities in the equatorial F region. J. Geophys. Res. 86 (A4), 2451–2454, ⟨http://dx.doi.org/10.1029/JA086iA04p02451⟩.

Chakrabarty, D., Fejer, B.G., Gurubaran, S., Pant, T.K., Abdu, M.A., Sekar, R., 2014. On the pre-midnight ascent of F-layer in the June solstice during the deep solar minimum in 2008 over the Indian sector. J. Atmos. Sol. Terr. Phys. 121 (Part B), 177–187, ⟨http://dx.doi.org/10.1016/j.jastp.2014.01.002⟩.

Farley, D.T., 2009. The equatorial E-region and its plasma instabilities: a tutorial. Ann. Geophys. 27 (4), 1509–1520, ⟨http://dx.doi.org/10.5194/angeo-27-1509-2009⟩.

Fejer, B.G., 1981. The equatorial ionospheric electric fields. A Rev. J. Atmos. Terr. Phys. 43 (5), 377–386, ⟨http://www.sciencedirect.com/science/article/pii/002191698190101X⟩.

Fejer, B.G., Jensen, J.W., Su, S.Y., 2008a. Quiet time equatorial F region vertical plasma drift model derived from ROCSAT-1 observations. J. Geophys. Res. 113 (A5), 304, ⟨http://dx.doi.org/10.1029/2007JA012801⟩.

Fejer, B.G., Jensen, J.W., Su, S.Y., 2008b. Seasonal and longitudinal dependence of equatorial disturbance vertical plasma drifts. Geophys. Res. Lett. 35 (20), L20106, ⟨http://dx.doi.org/10.1029/2008GL035584⟩.

Fejer, B.G., Hui, D., Chau, J.L., Kudeki, E., 2014. Altitudinal dependence of evening equatorial F region vertical plasma drifts. J. Geophys. Res.: Space Physics 119 (7), 5877–5890, ⟨http://dx.doi.org/10.1002/2014JA019949⟩.

Fejer, B.G., de Paula, E.R., Scherliess, L., 1996. Incoherent scatter radar, ionosonde, and satellite measurements of equatorial F region vertical plasma drifts in the evening sector. Geophys. Res. Lett. 23 (14), 1733–1736, ⟨http://dx.doi.org/10.1029/96GL01847⟩.

Fesen, C.G., Crowley, G., Roble, R.G., Richmond, A.D., Fejer, B.G., 2000. Simulation of the pre-reversal enhancement in the low latitude vertical ion drifts. Geophys. Res. Lett. 27 (13), 1851–1854, ⟨http://dx.doi.org/10.1029/2000GL000061⟩.

Gupta, S.P., Prakash, S., 1979. Experimental evidence of ion plasma oscillations in the apogee region of the Nike-Apache rocket. Planet. Space Sci. 27 (2), 145–150, ⟨http://dx.doi.org/10.1016/0032-6633(79)90044-8⟩..

Gupta, S.P., 1986. Formation of sporadic E layers at low magnetic latitudes. Planet. Space Sci. 34 (11), 1081–1085, ⟨http://dx.doi.org/10.1016/0032-6633(86)90019-X⟩..

Gupta, S.P., 1997. Features of E region irregularities at the magnetic equator and in its vicinity. Adv. Space Res. 20 (11), 2195–2198, ⟨http://dx.doi.org/10.1016/S0273-1177(97)00670-4⟩..

Gupta, S.P., 2000. Two stream instability in E region over magnetic equator during morning hours. Adv. Space Res. 26 (8), 1257–1261, ⟨http://dx.doi.org/10.1016/S0273-1177(99)01212-0⟩.

Gupta, S.P., 2001. Collected Works. Physical Research Laboratory, India.

Gurubaran, S., 2002. The equatorial counter electrojet: part of a world-wide current system? Geophys. Res. Lett. 29 (9), 51-1–51-4, ⟨http://dx.doi.org/10.1029/2001GL014519⟩.

Kakad, B., Tiwari, D., Pant, T.K., 2012. Study of post sunset vertical plasma drift at equatorial F-region using long-term (1990–2003) ionosonde measurements in Indian longitude. J. Atmos. Sol. Terr. Phys. 80, 239–246, ⟨http://dx.doi.org/10.1016/j.jastp.2012.02.004⟩.

Klimenko, M.V., Klimenko, V.V., Karpachev, A.T., 2012. Formation mechanism of additional layers above regular F2 layer in the near-equatorial ionosphere during quiet period. J. Atmos. Sol. Terr. Phys. 9091, 179–185 http://dx.doi.org/10.1016/j.jastp.2012.02.011.

Krishna Murthy, B.V., Hari, S.S., 1996. Electric fields in the low latitude F-region. Adv. Space Res. 18 (6), 93–98 http://dx.doi.org/10.1016/0273-1177(95)00906-X.

Krishna Murthy, B.V., Hari, S.S., Somayajulu, V.V., 1990. Nighttime equatorial thermospheric meridional winds from ionospheric h′F data. J. Geophys. Res.: Space Phys. 95 (A4), 4307–4310 http://dx.doi.org/10.1029/JA095iA04p04307.

Krishna Murthy, B.V., Ravindran, S., Viswanathan, K.S., Subbarao, K.S.V., Patra, A.K., Rao, P.B., 1998. Small-scale (~3 m) E region irregularities at and off the magnetic equator. J. Geophys. Res. 103 (A9), 20761–20773 http://dx.doi.org/10.1029/98JA00928.

Madhav Haridas, M.K., Manju, G., Pant, T.K., 2015. On the solar activity variations of nocturnal F region vertical drifts covering two solar cycles in the Indian longitude sector. J. Geophys. Res. 120 (2), 1445–1451 http://dx.doi.org/10.1002/2014JA020561.

Millward, G.H., Mller-Wodarg, I.C.F., Aylward, A.D., Fuller-Rowell, T.J., Richmond, A.D., Moffett, R.J., 2001. An investigation into the influence of tidal forcing on F

region equatorial vertical ion drift using a global ionosphere-thermosphere model with coupled electrodynamics. J. Geophys. Res. 106 (A11), 24733–24744 http://dx.doi.org/10.1029/2000JA000342.

Nair, R.B., Jayachandran, B., Rao, P.B., Balan, N., 1993. Seasonal, solar and magnetic activity effects on evening F region vertical plasma drifts. Indian J. Radio Space Phys. 22, 89–93.

Namboothiri, S.P., Balan, N., Rao, P.B., 1989. Vertical plasma drifts in the F region at the magnetic equator. J. Geophys. Res.: Space Phys. 94 (A9), 12055–12060 http://dx.doi.org/10.1029/JA094iA09p12055.

Oyekola, O.S., 2006. Comparison between nighttime ionosonde, incoherent scatter radar, AE-E satellite, and HF Doppler observations of F region vertical electrodynamic plasma drifts in the vicinity of the magnetic equator. J. Geophys. Res. 111 (A11) http://dx.doi.org/10.1029/2006JA011844.

Oyekola, O.S., Ojo, A., Akinrimisi, J., dePaula, E.R., 2007. Seasonal and solar cycle variability in F-region vertical plasma drifts over Ouagadougou. J. Geophys. Res. 112 (A12)http://dx.doi.org/10.1029/2007JA012560.

Pandey, K., Sekar, R., Anandarao, B.G., Gupta, S.P., Chakrabarty, D., 2016. Estimation of nighttime dip-equatorial E-region current density using measurements and models. J. Atmos. Sol. Terr. Phys. 146, 160–170 http://dx.doi.org/10.1016/j.jastp.2016.06.002.

Patra, A.K., Sripathi, S., Rao, P.B., Subbarao, K.S.V., 2005. Simultaneous VHF radar backscatter and ionosonde observations of low-latitude E region. Ann. Geophys. 23 (3), 773–779, ⟨http://www.ann-geophys.net/23/773/2005/⟩.

Pingree, J.E., Fejer, B.G., 1987. On the height variation of the equatorial F region vertical plasma drifts. J. Geophys. Res. 92 (A5), 4763–4766 http://dx.doi.org/10.1029/JA092iA05p04763.

Prabhakaran Nayar, S.R., Sreehari, C.V., 2004. Investigation of height gradient in vertical plasma drift at equatorial ionosphere using multifrequency HF Doppler radar. J. Geophys. Res. 109 (A12)http://dx.doi.org/10.1029/2004JA010641.

Prakash, S., Subbaraya, B.H., 1967. Langmuir probe for the measurement of electron density and electron temperature in the ionosphere. Rev. Sci. Instrum. 38 (8), 1132–1136 http://dx.doi.org/10.1063/1.1721035.

Prakash, S., Muralikrishna, P., 1976. The nature of electric field in E-Region close to morning and evening reversals. Geophys. Res. Lett. 3 (8), 445–447 http://dx.doi.org/10.1029/GL003i008p00445.

Prakash, S., Pal, S., 1985. Electric fields and electron density irregularities in the equatorial electrojet. J. Atmos. Terr. Phys. 47 (8), 853–866, ⟨http://www.sciencedirect.com/science/article/pii/0021916985900601⟩.

Prakash, S., Gupta, S.P., Subbaraya, B.H., 1969. Irregularities in the equatorial E region over thumba. Radio Sci. 4 (9), 791–796 http://dx.doi.org/10.1029/RS004i009p00791.

Prakash, S., Gupta, S.P., Subbaraya, B.H., 1970. A study of the irregularities in the night time equatorial E-region using a Langmuir probe and plasma noise probe. Planet. Space Sci. 18 (9), 1307–1318 http://dx.doi.org/10.1016/0032-6633(70)90141-8.

Prakash, S., Gupta, S.P., Subbaraya, B.H., Jain, C.L., 1971. Electrostatic plasma instabilities in the equatorial electrojet. Nature 233 (38), 56–58 http://dx.doi.org/10.1038/physci233056a0.

Prakash, S., Jain, C.L., Balsley, B.B., Greenwald, R.A., 1974. Evidence of two types of electron density irregularities in the electrojet over Thumba, India. J. Geophys. Res. 79 (28), 4334–4336 http://dx.doi.org/10.1029/JA079i028p04334.

Qian, C., Lei, J., Wang, W., 2015. A simulation study on the impact of altitudinal dependent vertical plasma drift on the equatorial ionosphere in the evening. J. Geophys. Res. 120 (4), 2918–2925 http://dx.doi.org/10.1002/2014JA020626.

Raghavarao, R., Anandarao, B.G., 1987. Equatorial electrojet and the counter-electrojet. Indian J. Radio Space Phys. 16, 54–75 http://dx.doi.org/10.1016/0021-9169(87)90042-0.

Raghavarao, R., Gupta, S.P., Sekar, R., Narayanan, R., Desai, J.N., Sridharan, R., Babu, V.V., Sudhakar, V., 1987. In situ measurements of winds, electric fields and electron densities at the onset of equatorial spread-F. J. Atmos. Terr. Phys. 49 (5), 485–492 http://dx.doi.org/10.1016/0021-9169(87)90042-0.

Ramesh, K.B., Sastri, J.H., 1995. Solar cycle and seasonal variations in F-region vertical drifts over Kodaikanal. India Ann. Geophys. 13 (6), 633–640 http://dx.doi.org/10.1007/s00585-995-0633-7.

Rastogi, R.G., Patel, V.L., 1975. Effect of interplanetary magnetic field on ionosphere over the magnetic equator. Proc. Indian Acad. Sci. 82 (A), 121–141.

Rastogi, R.G., Chandra, H., Janardhan, P., Rahul, S., 2014. Equatorial and mid-latitude ionospheric currents over the Indian region based on 40 years of data at Trivandrum and Alibag. Indian J. Radio Space Phys. 43, 274–283.

Ravindran, S., Krishna Murthy, B.V., 1997a. Occurrence of type I plasma waves in the equatorial electrojet during morning and evening hours. J. Geophys. Res. 102 (A5), 9761–9765 http://dx.doi.org/10.1029/96JA03742.

Ravindran, S., Krishna Murthy, B.V., 1997b. Up-down asymmetry of type I plasma waves in the equatorial electrojet region. Ann. Geophys. 15 (6), 774–778. http://dx.doi.org/10.1007/s00585-997-0774-y.

Reddy, C.A., Vikramkumar, B.T., Viswanathan, K.S., 1987. Electric fields and currents in the equatorial electrojet deduced from VHF radar observations-I. A method of estimating electric fields. J. Atmos. Terr. Phys. 49 (2), 183–191, ⟨http://www.sciencedirect.com/science/article/pii/0021916987900535⟩.

Sastri, J.H., 1984. Duration of equatorial spread-F. Ann. Geophys. 2, 353–358.

Sastri, J.H., 1996. Longitudinal dependence of equatorial F region vertical plasma drifts in the dusk sector. J. Geophys. Res. 101 (A2), 2445–2452.

Sastri, J.H., Varma, V.K.M., Prabhakaran Nayar, S.R., 1995. Height gradient of F region vertical drift in the evening equatorial ionosphere. Geophys. Res. Lett. 22 (19), 2645–2648 http://dx.doi.org/10.1029/95GL02668.

Sastri, J.H., Ramesh, K.B., Somayajulu, V.V., Rao, J.V.S.V., 1991. Origin of short-period (30–300 s) Doppler frequency fluctuations of lower F region reflections in the
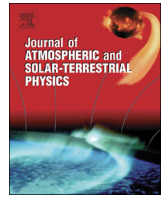
equatorial electrojet region. Radio Sci. 26 (6), 1403–1413 http://dx.doi.org/10.1029/91RS02021.

Scherliess, L., Fejer, B.G., 1999. Radar and satellite global equatorial F region vertical drift model. J. Geophys. Res. 104 (A4), 6829–6842 http://dx.doi.org/10.1029/1999JA900025.

Sekar, R., Gupta, S.P., Acharya, Y.B., Chakrabarty, D., Pallamraju, D., Pathan, B.M., Tiwari, D., Choudhary, R.K., 2013. Absence of streaming plasma waves around noontime over Thumba in recent times: is it related to the movement of the dip equator? J. Atmos. Sol.-Terr. Phys. 103, 8–15 http://dx.doi.org/10.1016/j.jastp.2013.02.005.

Sekar, R., 1990. Plasma Instabilities and the Dynamics of the Equatorial F-region. (Ph.D. thesis), Gujarat University.

Subbarao, K.S.V., Krishna Murthy, B.V., 1994. Seasonal variations of equatorial spread-F. Ann. Geophys. 12 (1), 33–39.

Subbaraya, B.H., Prakash, S., Gupta, S.P., 1985. Structure of the equatorial lower ionosphere from the Thumba Langmuir probe experiments. Adv. Space Res. 5 (7), 35–38 http://dx.doi.org/10.1016/0273-1177(85)90352-7.

Subbaraya, B.H., Prakash, S., Gupta, S.P., 1983. Electron densities in the equatorial lower ionosphere from the Langmuir probe experiments conducted at Thumba during 1966–1978. Scientific Report, ISRO−PRL−SR−15−83.

Thébault, E., et al., 2015. International geomagnetic reference field: he 12th generation. Earth, Planets Space 67 (1), 1–19 http://dx.doi.org/10.1186/s40623-015-0228-9.

Tiwari, D., Patra, A.K., Viswanathan, K.S., Jyoti, N., Devasia, C.V., Subbarao, K.S.V., Sridharan, R., 2003. Simultaneous radar observations of the electrojet plasma irregularities at 18 and 54.95 MHz over Trivandrum, India. J. Geophys. Res. 108 (A10). http://dx.doi.org/10.1029/2002JA009698.

Viswanathan, K.S., Vikramkumar, B.T., Reddy, C.A., 1987. Electric fields and currents in the equatorial electrojet deduced from VHF radar observations-II. Characteristics of electric fields on quiet and disturbed days. J. Atmos. Terr. Phys. 49 (2), 193−200, ⟨http://www.sciencedirect.com/science/article/pii/0021916987900547⟩.

Woodman, R.F., 1970. Vertical drift velocities and east-west electric fields at the magnetic equator. J. Geophys. Res. 75 (31), 6249–6259 http://dx.doi.org/10.1029/JA075i031p06249.

Estimation of nighttime dip-equatorial E-region current density using measurements and models

CrossMark

Kuldeep Pandey [a,b], R. Sekar [a,*], B.G. Anandarao [a], S.P. Gupta [a], D. Chakrabarty [a]

[a] Physical Research Laboratory, Navrangpura, Ahmedabad 380009, India
[b] Indian Institute of Technology-Gandhinagar, Ahmedabad 382424, India

ABSTRACT

The existence of the possible ionospheric current during nighttime over low-equatorial latitudes is one of the unresolved issues in ionospheric physics and geomagnetism. A detailed investigation is carried out to estimate the same over Indian longitudes using in situ measurements from Thumba (8.5°N, 76.9°E), empirical plasma drift model (Fejer et al., 2008) and equatorial electrojet model developed by Anandarao (1976). This investigation reveals that the nighttime E-region current densities vary from ∼0.3 to ∼ 0.7 A/km^2 during pre-midnight to early morning hours on geomagnetically quiet conditions. The nighttime current densities over the dip equator are estimated using three different methods (discussed in methodology section) and are found to be consistent with one another within the uncertainty limits. Altitude structures in the E-region current densities are also noticed which are shown to be associated with altitudinal structures in the electron densities. The horizontal component of the magnetic field induced by these nighttime ionospheric currents is estimated to vary between ∼2 and ∼6 nT during geomagnetically quiet periods. This investigation confirms the existence of nighttime ionospheric current and opens up a possibility of estimating base line value for geomagnetic field fluctuations as observed by ground-based magnetometer.

© 2016 Elsevier Ltd. All rights reserved.

1. Introduction

It is well known that an intense current, commonly referred to as equatorial electrojet, flows in a narrow altitudinal band (peak around 105 km) over the dip equatorial regions. The strengths and variations of these currents during daytime had been derived in detail using rocket borne magnetometer measurements over Indian (e.g. Sastry, 1970; Sampath and Sastry, 1979 and references cited therein), Peruvian (e.g. Davis et al., 1967; Shuman, 1970) and Brazilian (e.g. Pfaff et al., 1997 and references cited therein) longitudes. Systematic observations of the electrojet current strengths during daytime were obtained by ground-based magnetometers (e.g. Rastogi and Iyer, 1976). Satellite borne measurements of these current densities during daytime (Jadhav et al., 2002; Lühr et al., 2004, etc.) are also available. However, the existence (or the lack of it) of the possible ionospheric current during nighttime and its characteristics over low-equatorial latitudes are not well understood. This is because of the fact that during nighttime, the ionospheric E-region plasma density goes down drastically. As a consequence, the midnight values of Sq current are generally taken as

the base line for the overhead equivalent ionospheric current system. However, based on theoretical calculations, Takeda and Araki (1985) concluded that the ionospheric Sq currents flow westward in the nighttime during high solar activity period and their contribution to the geomagnetic Sq field is about 1/10 of the maximum Sq variation. On the other hand, the nocturnal currents are shown to be weak during low solar activity period and below the detection limit. In addition, Campbell (1973) and Mayaud (1976) found that the geomagnetic variations during nighttime are not negligible on many occasions. Campbell (1979) suggested that the ground geomagnetic variations during nighttime may be present even during apparently quiet conditions. Matsushita and Maeda (1965) used the daily mean as the base level to be representative of the zero Sq current and showed the presence of significant nighttime ionospheric current. On the other hand, if the nighttime Sq level is taken as the base value, as in Matsushita (1968), it would imply zero ionospheric current during nighttime. Therefore, determination of the base geomagnetic level is important to determine the nighttime E-region current over low-equatorial latitudes. Based on only a single rocket flight Davis et al. (1967) inferred small westward current in E-region (corresponding to magnetic variation of about 6 nT on the rocket borne magnetometer) during midnight hours around 100 km altitude over the Peruvian dip equatorial sector. This inference was derived

* Corresponding author.
    E-mail address: rsekar@prl.res.in (R. Sekar).

using the data obtained from the ascent and descent phases of the rocket flight. After a few days, under similar geomagnetic conditions, Shuman (1970) did not detect any significant current over the same place and around the same local time during the descent phase of the rocket, although the resolution of the magnetic measurements was slightly higher (5 nT). It is to be noted here that the magnetometer measurements are not expected to alter significantly depending on the ascent and descent phases of the rocket as current integrated over large area is measured. Thus, considering that rocket wake does not modify the magnetometer measurements, the results of Shuman (1970) are in contradiction with the results of Davis et al. (1967). Over the Indian dip equatorial sector (Thumba), Sastry (1970) measured about 9.4 A/km^2 peak current density during daytime but concluded the absence of such current (with uncertainty of 4 nT of magnetic measurements) during pre-midnight hours on the same day. Onwumechili (1992a) compiled the available in situ measurements of ionospheric current density over the globe and the nighttime current over the dip equatorial region was suggested to be absent.

The above observations pose an uncertainty on the magnitude of the current that can be expected to flow through the equatorial E-region during nighttime. Further, as suggested by Haerendel and Eccles (1992) and Eccles (2015), the generation of pre-reversal enhancement (PRE) of the equatorial F-region zonal electric field will depend crucially on the closure of the F-region dynamo current through the E-region in the low and equatorial latitudes. Therefore, determination of nighttime E-region current is essential to understand the underlying processes that couples E and F regions over low-equatorial latitudes during nighttime. There was an attempt by Stening and Winch (1987) to estimate the nighttime ionospheric current using the in situ measurements of electron density, obtained over Thumba (Prakash et al., 1970), and with a fixed zonal Sq electric field of −0.3 mV/m. They concluded that a finite ionospheric current flows during nighttime. Further, Rastogi et al. (1996) reported that the nocturnal variation of horizontal geomagnetic field over Huancayo showed remarkable similarity with corresponding variation of ionospheric electric field determined by Doppler radar. This indicates a finite nighttime ionospheric current which can be inferred by ground-based magnetometer. However, it is difficult to separate ionospheric and magnetospheric components from these magnetometer measurements in spite of the resolution being 0.1 nT in the present digital magnetometer systems as their effects are comparable on ground during nighttime. It is not clear whether the ground-based magnetometer measurements during nighttime, even during magnetically quiet times, are free from the contributions from magnetosphere. During geomagnetically disturbed period, many authors (e.g. Matsushita, 1971; Onwumechili and Ezema, 1977; Chakrabarty et al., 2005) had indicated the non-ionospheric (magnetospheric) origin of the currents responsible for the magnetic fluctuations observed at the ground. Therefore, a comprehensive understanding on the magnitude of the nighttime E-region current and its variation with time is missing till date although the nighttime horizontal component of the magnetic field measured by the magnetometers is being used as base or reference value for determining the daytime electric fields (Rastogi and Patil, 1986). These variations in the reference value during magnetically disturbed period make matter worse as far as the determination of the daytime electric fields is concerned. Given the above background, it is imperative that knowledge about the changes in nocturnal ionospheric current during geomagnetically quiet time is essential to comprehensively understand the equatorial electrodynamics. In this context, the present investigation is important as it provides estimation of the equatorial E-region current at a few local nighttimes by different methods using experimental data and modeling investigations.

2. Details of observations and other inputs

In the present investigation, electron densities and plasma wave information obtained from six rocket flights containing Langmuir probe system with high frequency response (Prakash and Subbaraya, 1967; Subbaraya et al., 1983, 1985) conducted over Thumba, during 1967–1975, are utilized as inputs. In addition, in situ measurements of zonal current density (Sastry, 1970; Sampath and Sastry, 1979) using magnetometer on board two rocket flights over Thumba are used. Throughout this work, time corresponds to local time (LT) which for Thumba (76.9°E) is about 22 min behind the Indian Standard Time, IST (time corresponding to 82.5°E). It is important to note here that simultaneous measurements of electron and current densities obtained on 29 August, 1968 at 1354 LT (Subbaraya et al., 1972) and 3 March, 1973 at 1159 LT (Sampath and Sastry, 1979) are used to calculate the R values ($R = \sigma_H/\sigma_P$, ratio of Hall (σ_H) to Pedersen (σ_P) conductivities). These flights correspond to high (yearly averaged sunspot number in 1968 was 150) and low (yearly averaged sunspot number in 1973 was 54) solar activity periods. This R value is used to deduce the altitude profile of nighttime current densities over the dip equator. The validity of the extrapolation of R value to the nighttime is discussed in Section 3.1. Further, the observed presence of streaming waves (plasma waves generated due to the streaming of electrons in the dip equatorial E-region with velocity exceeding ion-acoustic speed) in the electron density measurements (e.g. Farley, 2009) is also used to give the physical estimate of minimum strength of nighttime current density that must be present over the altitude range wherein streaming waves were detected. The generation of streaming wave is shown (Sekar et al., 2013) to be possible over Thumba only when the dip angle (I) < 1.5°. The present investigation makes use of the electron density observations from Thumba during 1967–1975 wherein the dip angle was between −1.0° and −1.1° and thus consistent with the conclusion of Sekar et al. (2013). Further, as the objective of the present investigation is to find out the nighttime E-region current density that is a realistic representative of the nighttime base value during quiet time, the electron density profiles before 2100 LT are avoided to minimize the contributions from PRE. The other important input parameters are as follows:

(i) The altitude profiles of neutral density and temperature are taken from Jacchia-71 (Jacchia, 1971) model which is built-in electrojet model used in this investigation.
(ii) The geomagnetic field in altitude-latitude plane is adopted from International Geomagnetic Reference Field (IGRF)-11 model (Finlay et al., 2010).
(iii) The vertical drifts corresponding to quiet time Sq electric fields over the dip equator are taken from F-region vertical plasma drift model of Fejer et al. (2008).

It is to be noted here that the accuracy of the electron density measurements is 5% (Subbaraya et al., 1983), the resolution of drift measurements is 10% (Fejer et al., 2008) and the standard deviation of neutral parameters is 8% (Marcos, 1990). These numbers determine the maximum uncertainty in the estimated nighttime current values.

3. Methods to estimate nighttime current density

Three different approaches have been adopted to estimate the nighttime current density in the equatorial E-region. These are described and compared in the subsequent sections.

3.1. Method-1: based on the ratio R deduced from observations

In order to estimate the altitude profiles of nighttime current density, the altitude profiles of electron density and plasma drifts in the zonal direction are needed. A few measurements of electron density during nighttime are available in the literature (Subbaraya et al., 1983, 1985; Gupta, 1986, 1990). However, measurement of background plasma drift in the zonal direction is difficult and systematic observations are not available over Indian longitudes. Therefore, a methodology is evolved based on a few assumptions and a coordinate system in which *x*, *y* and *z* directions are along zonal (positive eastward), meridional (positive northward) and vertical (positive upward) directions respectively. The assumptions are as follows:

1. In the present investigation, the electric fields corresponding to the F-region plasma drifts are taken to represent the E-region Sq electric field (E_{Sq}) as the low latitude E-region dynamo electric fields get mapped to the equatorial F-region. This assumption can lead to an uncertainty in drift of ~2 m/s considering the altitude of satellite (around 600 km), latitude ($\pm 5°$) binning of plasma drift measurements, geometry of magnetic field and typical altitudinal gradient (Pingree and Fejer, 1987) of plasma drifts (about 0.005 m s^{-1} km^{-1}) during nighttime over another dip equatorial station Jicamarca.

2. The zonal solar quiet time $(E_{Sq})_x$ field does not vary much within the altitude region of 100–120 km.

3. The ratio R ($= \sigma_H/\sigma_P$) remains the same during day and night in all solar epochs.

Based on these assumptions, the empirical model (Fejer et al., 2008) of F-region vertical plasma drift corresponding to $(E_{Sq})_x$ over Indian longitude sector is utilized. This model is compared with vertical plasma drifts estimated using measurements by various techniques. This comparison revealed that the model values and polarities of the plasma drifts match well (within the experimental uncertainties) with the inferred drifts from individual case studies except on a few occasions. This aspect is not directly relevant for the present work and will be addressed in a separate communication. To verify the validity of third assumption, the ratio of the conductivities (R) is estimated using neutral number density and temperature from the Jacchia-71 model (Jacchia, 1971), geomagnetic field values from IGRF-11 model and measured altitude profiles of electron density. Fig. 1a depicts the altitude profiles of R during day and night times in solar maximum and minimum conditions. The ratio R is essentially independent of electron density variations. The variations of neutral density during day-night and at different solar epochs are not significant enough to affect R. It is also verified that the R value does not change much even if one uses other neutral density models (e.g. NRLMSISE-00)
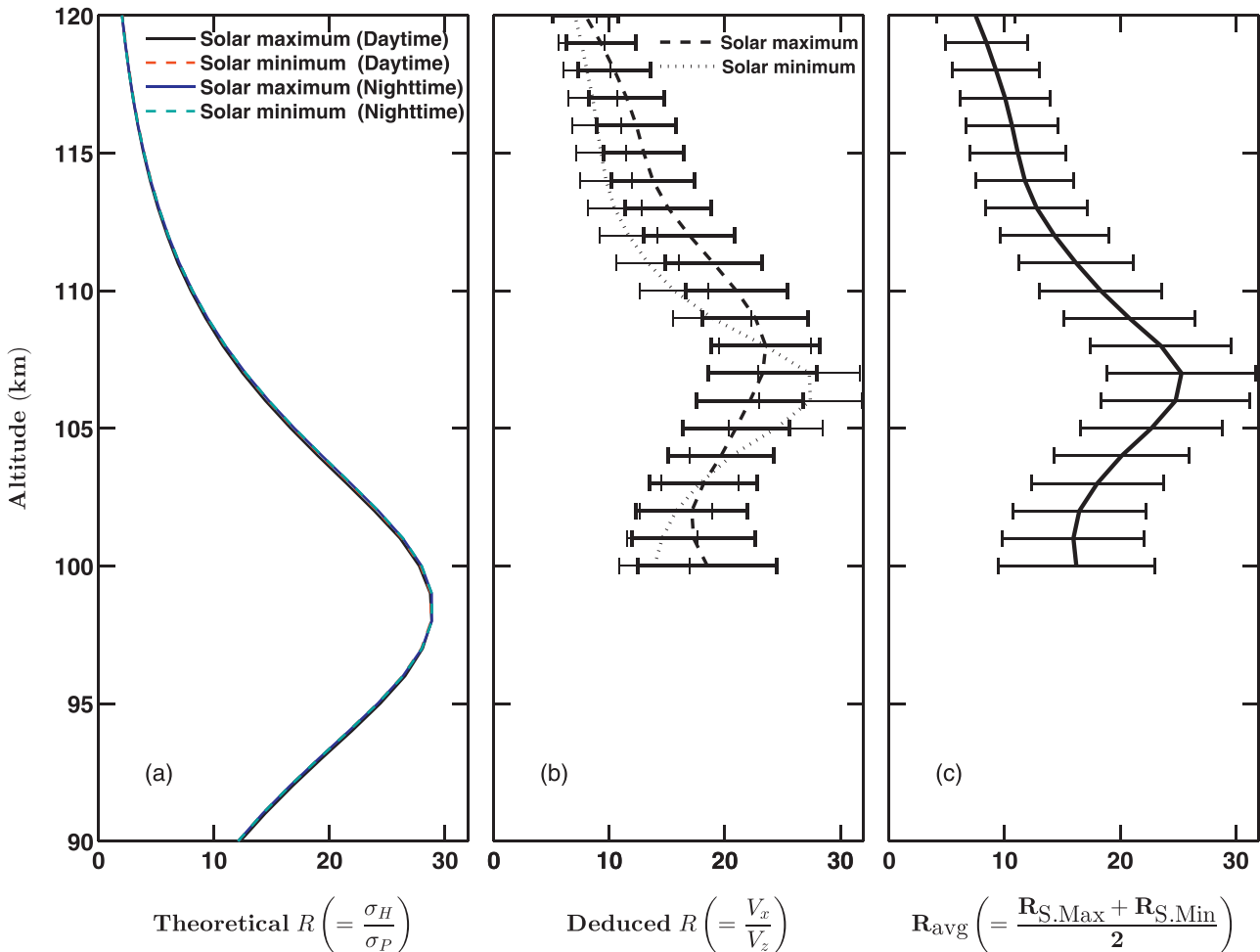

Fig. 1. (a) Altitude profiles of ratio (*R*) of the Hall to Pedersen conductivities during day and night at different solar epoch estimated using Jacchia-71 model values of neutral density and temperature along with geomagnetic fields from IGRF-11 model. (b) Deduced altitude profiles of *R* values, based on Eq. (2), using simultaneous measurements of current and electron densities during daytime at high (dotted) and low (dashed) solar activity conditions. In this estimation the plasma drift in vertical direction (corresponding to Sq electric field) at the time of measurement is obtained from the empirical model of Fejer et al. (2008). (c) The altitude profile of the average values of *R* shown in (b). (For interpretation of the references to color in this figure, the reader is referred to the web version of this paper.)

instead of Jacchia-71 model. Hence the assumption (3) is valid for the present purpose of estimation of nighttime current.

Fig. 1a reveals that the peak R value is close to 30 around 100 km. This is similar to the earlier calculation of Anandarao et al. (1977), which also reveals that these values of R are nearly same around peak E-region even if one considers the field line integrated values of conductivities. However, the peak height determined by these theoretical calculations is well known (Forbes, 1981) to be lower than the height determined from measurements by more than 5 km. This R is also shown to be equivalent to the ratio of electric fields in vertical (E_z) and zonal (E_x) directions (Anandarao et al., 1977; Sekar et al., 2013) as follows:

$$R = \frac{E_z}{E_x} = \frac{V_x}{V_z} \tag{1}$$

where V_x and V_z are the plasma drifts in zonal and vertical directions respectively. Therefore, to deduce the altitude profile of R by means of experimental observations, simultaneous measurements of electron $(N_{e,day})$ and current densities $(J_{x,day})$ are used. These values correspond to daytime in high and low solar activity periods. In addition, the vertical plasma drift (V_z) corresponding to the local time of rocket flights have been taken from Fejer et al. (2008) model:

$$R = \frac{V_x}{V_z} = \frac{1}{|\mathbf{e}|} \left(\frac{J_{x,day}}{N_{e,day}} \right) \frac{1}{V_z} \tag{2}$$

where $\mathbf{e}$ is the charge of electron. Fig. 1b depicts the altitude profiles of R and its errors in high and low solar activity periods based on Eq. (2). It is to be noted here that R values below 100 km are not shown as the current density measurements in that altitude region are below the sensitivity limit of the rocket borne magnetometer. From Fig. 1b, it is clear that the deduced R values remain the same (within the error limits) for both solar epochs. By taking clue from the theoretical calculation on the invariance of R values during day and night in all solar epochs, the average value (R_{avg}) (shown in Fig. 1c) along with measured nighttime electron density $(N_{e,night})$ and vertical plasma drift $(V_{z,night})$ from Fejer et al. (2008) model at the time of rocket flight experiment is used to estimate nighttime current density. The following expression is used to calculate the nighttime current density $(J_{x,night})$:

$$J_{x,night} = |\mathbf{e}| N_{e,night} R_{avg} V_{z,night} \tag{3}$$

The observed $N_{e,night}$ values and the empirical plasma drift model values of V_z corresponding to that local time are used.

3.2. Method-2: based on the observation of streaming waves

As mentioned earlier, the dip equatorial E-region ionosphere is characterized by the generation of streaming waves. These plasma waves are essentially generated when electrons stream through the background ions with velocity exceeding ion-acoustic speed (Farley, 2009). The electron densities measured over Thumba at different local times on several nights show (Prakash et al., 1970; Gupta, 1986) the presence of streaming plasma wave. The threshold plasma drift in the zonal direction needed to trigger the streaming waves is given (Sudan et al., 1973) by,

$$V_{x,min} = (1 + \chi)c_s \tag{4}$$

where c_s is the ion-acoustic speed (330 m/s) of the medium and χ is given by,

$$\chi = \frac{\nu_e \nu_i}{\Omega_e \Omega_i} \tag{5}$$

where ν and Ω represent neutral collision and gyro frequencies respectively and subscripts e and i are used for electron and ions

respectively. The $V_{x,min}$ values along with the corresponding electron densities are used to have the physical estimate of minimum strength of current density $(J_{x,night,min})$ that must be present over the altitude range where the presence of streaming waves was observed using the following expression:

$$J_{x,night,min} = |\mathbf{e}| N_{e,night}(1 + \chi)c_s \tag{6}$$

The observed $N_{e,night}$ values are used from those rocket flights that detected streaming waves.

3.3. Method-3: based on the equatorial electrojet model

A physics based model for equatorial electrojet was developed earlier by Anandarao (1976) and important results on the effect of winds during daytime electrojet current system (Anandarao, 1976, 1977; Anandarao and Raghavarao, 1987; Raghavarao and Anandarao, 1987, etc.) obtained using this model are available in the literatures. In the present study this model is used, without invoking the wind effects, to calculate the nighttime current density in the zonal direction with the inputs of previously mentioned electron density profiles and E-region Sq electric field values. Based on the earlier works (Richmond, 1973; Anandarao, 1976; Anandarao and Raghavarao, 1987; Raghavarao and Anandarao, 1987) during daytime, the contributions of horizontal winds and shears in them to the zonal current densities over the dip equator are not found to be significant and are well within the estimation uncertainty. In the absence of systematic measurements of vertical winds in the E-region during nighttime, the contribution of vertical wind to the current density estimates could not be determined.

In this model, the ionospheric current density $(\mathbf{J})$ is expressed in terms of Ohm's law and the current conservation equation $(\nabla \cdot \mathbf{J} = 0$ which implies $\mathbf{J} = \nabla \times \mathbf{A}$, where $\mathbf{A}$ is the vector potential) is solved along with Maxwell's equation for electrostatic condition in geocentric co-ordinate system (r, θ, ϕ) where r is the radial distance from the center of the earth, θ is the magnetic co-latitude and ϕ is the longitude. A current function ψ is defined as $\psi = -r \sin \theta A_\phi$ where A_ϕ is the component of vector potential $\mathbf{A}$ in ϕ direction. The following second order elliptic partial differential equation is derived by solving the electrodynamic equations:

$$f_1 \frac{\partial^2 \psi}{\partial r^2} + 2f_2 \frac{\partial^2 \psi}{\partial r \partial \theta} + f_3 \frac{\partial^2 \psi}{\partial \theta^2} + f_4 \frac{\partial \psi}{\partial r} + f_5 \frac{\partial \psi}{\partial \theta} + f_6 = 0 \tag{7}$$

The coefficients f_1–f_6 are functions of ionospheric conductivities and the zonal electric fields (Sugiura and Poros, 1969; Anandarao, 1977; Anandarao and Raghavarao, 1987; Raghavarao and Anandarao, 1987). Eq. (7) is numerically solved in the region encompassing 80–200 km altitude and magnetic co-latitude between 75° and 105° with the boundary conditions $\psi = 0$ at all the boundaries (i.e. $\psi_{at\ 80\ km,200\ km,-75°,105°} = 0$). In deriving Eq. (7), variations in all physical parameters along the longitudinal direction are neglected. Thus this equation is numerically solved in two dimensions along the vertical and latitudinal directions. The grid sizes of $\Delta r = 1$ km and $\Delta \theta = 0.25°$ are employed for the present investigation. Further details of this model can be found in Anandarao and Raghavarao (1987) and Raghavarao and Anandarao (1987). The inputs to the model are altitude profile of electron densities and $(E_{Sq})_x$ value at the particular time for which the model calculation is made. Further, the same electron density profile is used at all the latitudes. These inputs are taken from the in situ measurements of electron densities during nighttime (Subbaraya et al., 1983, 1985; Gupta, 1986, 1990) and the empirical model of plasma drift (Fejer et al., 2008) over the dip equator corresponding to Indian longitude. In addition to these, Jacchia-71 model of neutral density and

temperature along with IGRF-11 model of geomagnetic field are used for the evaluation of ionospheric conductivities. The equations for vertical polarization electric field (E_r) and current density in the zonal direction, without wind effects, can be written (Sugiura and Poros, 1969; Raghavarao and Anandarao, 1987) as follows:

$$E_r = \frac{\sigma_H}{\sigma_P} E_\phi \cos I + J_r\left(\frac{\cos^2 I}{\sigma_P} + \frac{\sin^2 I}{\sigma_0}\right) - J_\theta\left(\frac{1}{\sigma_0} - \frac{1}{\sigma_P}\right)\sin I \cos I \tag{8}$$

$$J_\phi = \sigma_H\left(E_r \cos I - E_\theta \sin I\right) + \sigma_P E_\phi \tag{9}$$

where σ_0 is the direct conductivity; E_r, E_θ and E_ϕ are electric fields along r, θ and ϕ directions respectively; J_r, J_θ and J_ϕ are current densities along r, θ and ϕ directions respectively. Over the dip equator, the radial (r) and azimuthal (ϕ) directions used in this section are same as vertically up (z) and zonal (x) directions used in the previous subsections. A sensitivity study of the model is performed by considering previously mentioned maximum uncertainties in the electron density, electric field, neutral density and temperature individually and the changes in peak current density over the dip equator are noted. The changes in current densities are found to be linear with changes in electron density and electric field. However, the changes with the neutral parameters yield a nonlinear response with maximum deviation less

than 3%. Combining the errors in the inputs and variations in neutral parameters, the maximum uncertainties in current density (J_x) and polarization electric field (E_z) over the dip equator are found to be less than 20% and 12% respectively.

4. Estimation of induced magnetic field

In order to estimate the magnetic field induced at ground by ionospheric current, a method described by Anandarao (1977) is adopted. In this method, the magnetic field potential (V) induced by an infinitely long line of current is defined based on Biot–Savart's law as

$$V = \frac{\mu_0 C}{2\pi} \tan^{-1}\left(\frac{\cos\theta}{(r/a) - \sin\theta}\right) \tag{10}$$

where μ_0 and C are the permeability of free space and line current (in Amperes) respectively. The line current C is obtained from current density J_x using $C = \int_r \int_\theta J_x \, dr \, d\theta$. The symbols a and r denote the earth's radius and distance of the line of current from the center of earth respectively. Further, the horizontal (northward) component of magnetic field (H) induced due to ionospheric current is given by,
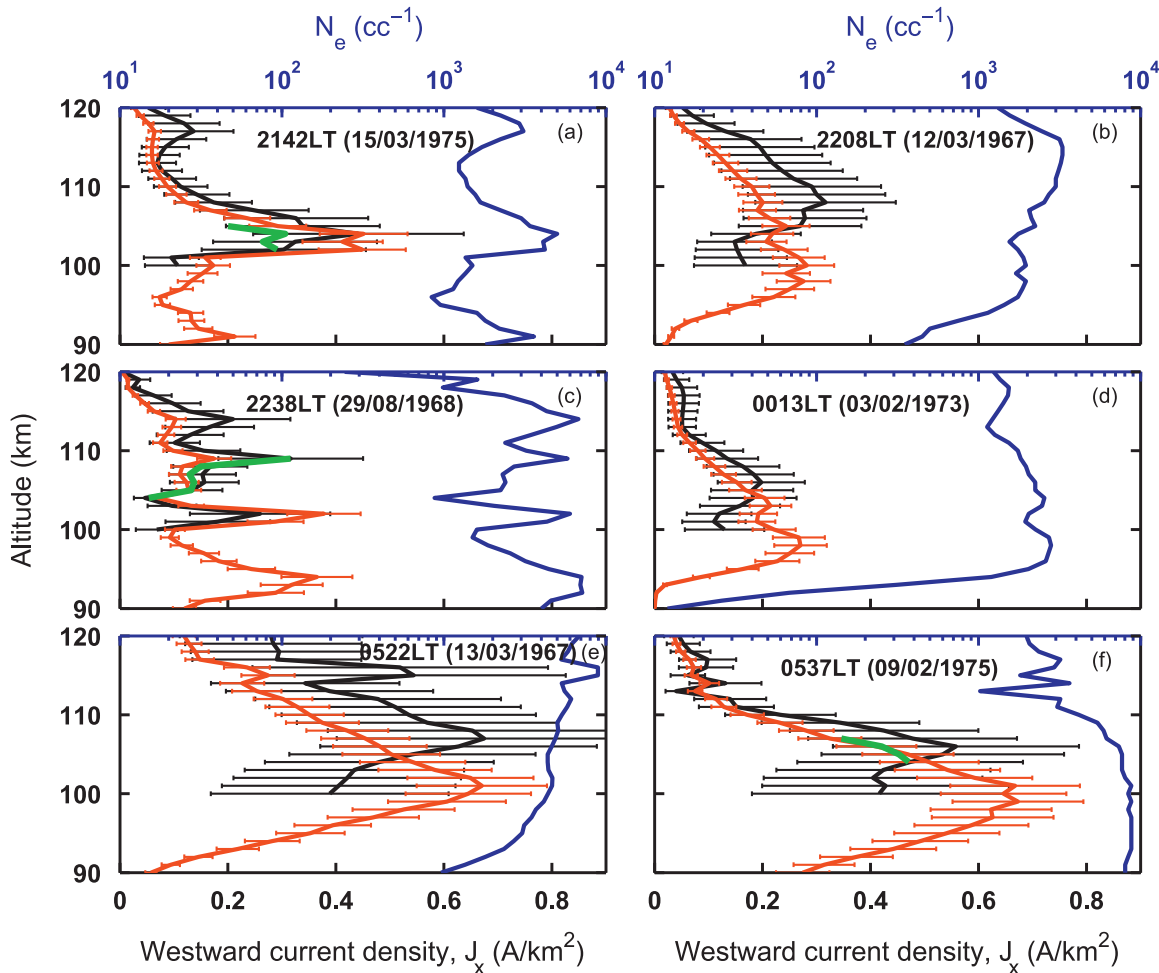
Fig. 2. Altitude profiles of estimated nighttime current densities (black) using method 1 and Eq. (3), the measured electron density profiles (blue curves) and R_{avg} values (see Fig. 1(c)). The altitude profiles of nighttime current densities over the dip equator (red colors) using the electrojet model of Anandarao (1976). The minimum current density (green) obtained using method 2 and Eq. (6) over the altitude wherein the presence of streaming waves was observed. Subplots (a–d) correspond to the profiles at various local times when the nighttime electron density measurements over Thumba during magnetically quiet conditions were available. (For interpretation of the references to color in this figure caption, the reader is referred to the web version of this paper.)

Table 1
The derived values of westward peak current density ($J_{x,max}$) using method 1, altitude (h_p) of $J_{x,max}$, measured electron density (N_e) at h_p, deduced R_{avg} at h_p and downward vertical drift (V_z) based on empirical model corresponding to the six rocket flights under consideration.

Case no.	Time and date	Altitude, h_p (km) of $J_{x,max}$	N_e (cc^{-1}) at h_p	R_{avg} at h_p	Downward V_z (m/s)	Westward $J_{x,max}$ (A/km^2)
1	2142 on 15/03/1975	104	5000	20.1	27.4	0.44
2	2208 on 12/03/1967	108	2540	23.5	33.1	0.32
3	2238 on 29/08/1968	109	5790	20.8	16.4	0.32
4	0013 on 03/02/1973	106	2240	24.8	22.2	0.20
5	0522 on 13/03/1967	107	4880	25.3	34.1	0.67
6	0537 on 09/02/1975	106	7356	24.8	19.1	0.56
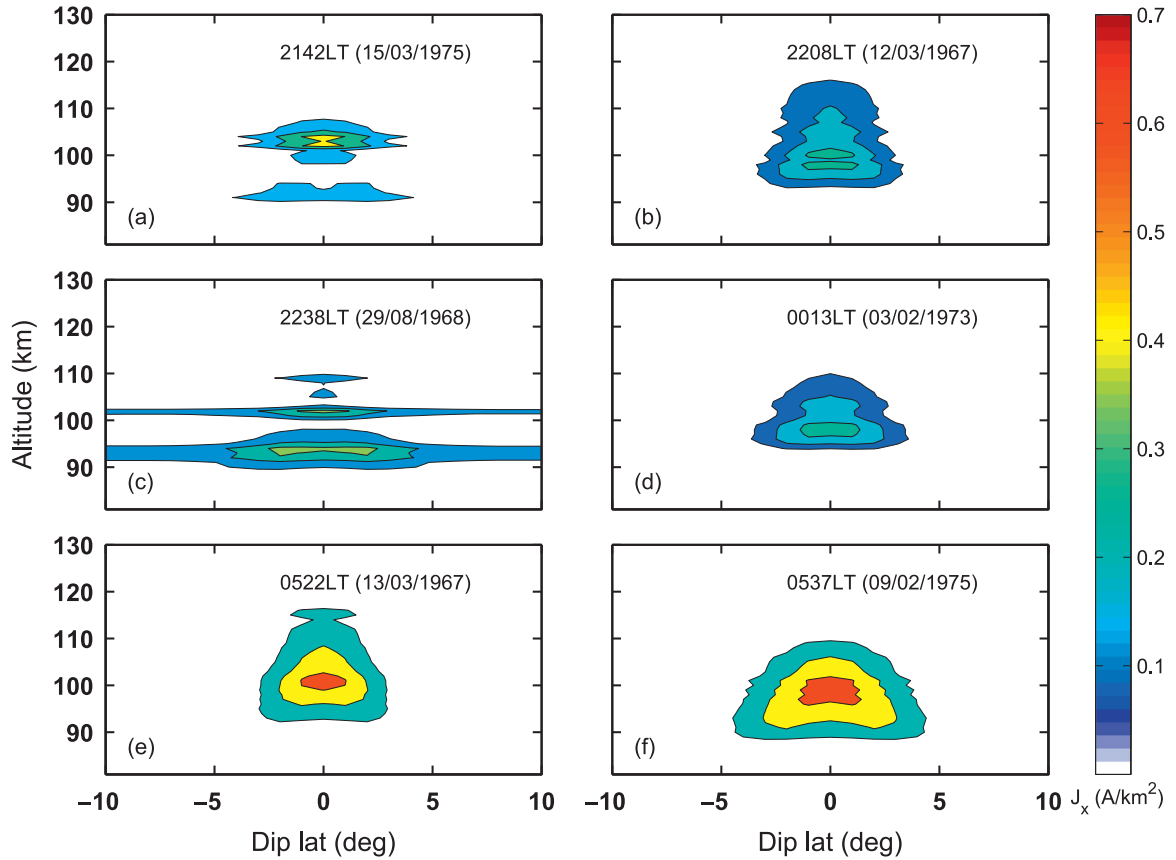
Fig. 3. Contours of iso-current density in zonal direction over magnetic latitude-altitude region obtained using electrojet model of Anandarao (1976). In this model calculation the electron densities are taken from in situ rocket measurements and zonal Sq electric field is chosen from the empirical model of plasma drift (Fejer et al., 2008) over Indian longitude. The color-bar represent strength current density (A/km^2). Current density contours in each subplot are plotted with steps of 30% of peak values over the dip equator. Subplots (a–d) correspond to iso-current contours corresponding to electron density measurement at different local times on a few nights. (For interpretation of the references to color in this figure the reader is referred to the web version of this paper.)

$$H = -\frac{1}{r}\frac{\partial V}{\partial \theta} = \frac{\mu_0 C}{2\pi r}\frac{(r/a)\sin\theta - 1}{(r/a)^2 + 1 - 2(r/a)\sin\theta} \qquad (11)$$

The numerical simulation plane is divided into $1°$(in θ) $\times$ 4 km (in r) blocks and induced H is calculated. H of each blocks are added up to get the net induced values at ground. The maximum uncertainty in H is found to be less than 20%.

5. Results and discussion

As mentioned in Section 3.1, Fig. 1 shows that R does not change significantly with respect to day and night time conditions and solar epochs. This aspect is used subsequently to derive the nighttime E-region current over the Indian sector. Fig. 2 depicts the altitude profiles of westward current densities during nighttime for geomagnetically quiet conditions estimated using the deduced R_{avg}

values (black) using Eq. (3), and electrojet model (red) using Eq. (9), over the dip equator. The corresponding electron densities measured over Thumba at different local times on a few nights are overlaid on this figure (blue). In addition, minimum current densities ($J_{x,night,min}$) estimated using Eq. (6) are also plotted in Fig. 2 (with green color) over the altitude range wherever the streaming plasma waves were observed. The nighttime current density ranges from $\sim$0.3 A/km^2 near midnight to $\sim$0.7A/km^2 during early morning hours. The electrojet model estimated current densities match well (within the uncertainty limits) with the deduced current density above altitude region of 100 km.

The present investigation of the estimation of nighttime current density is based on the in situ electron density measurements conducted at different solar epochs and seasons. Thus, it is rather difficult to bring out the local time variation of nighttime current density as the electron density (N_e) and Sq electric fields (E_{Sq}) vary with these geophysical conditions. Nevertheless, comparison of
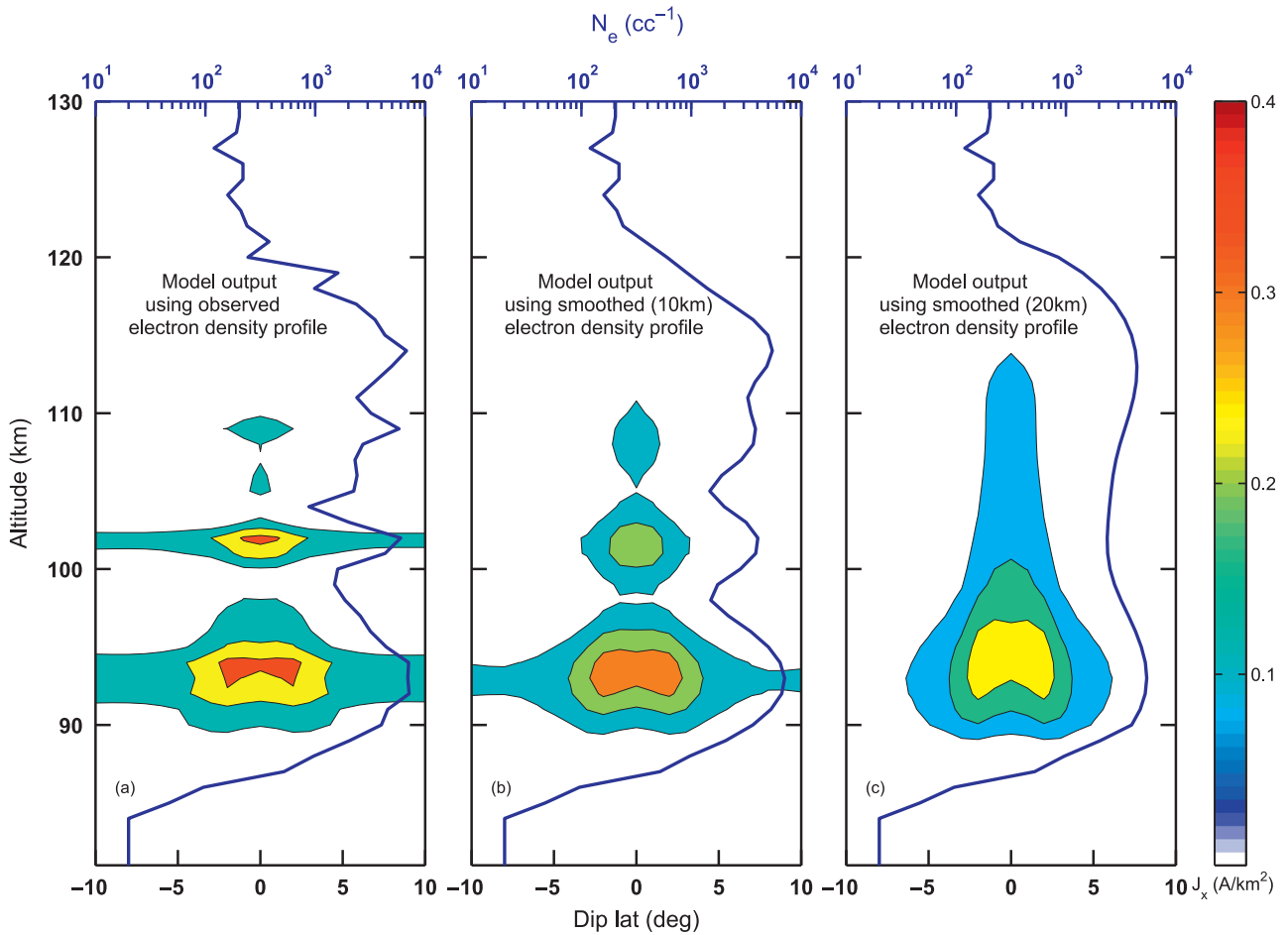
Fig. 4. (a) High resolution plots of iso-current density contours given in subplot 3(c). The input electron density profile (blue) is also overlaid. (b) and (c) Iso-current density profiles obtained after progressively smoothing the electron density profile shown in subplot (a) and using them as the input for current density calculation. The corresponding input electron density profiles are also shown in each subplot. Current density contours in each subplot are plotted with steps of 30% of the peak current values over the dip equator. *Note*: Color-bar scales are adjusted to bring out the features in current density contours. (For interpretation of the references to color in this figure caption, the reader is referred to the web version of this paper.)

these current densities in the subplots of Fig. 2 gives rise to the following points:

1. The peak altitudes (see black curves of subplots 2b, d, e and f) of the current density deduced using method 1 lie closer to the altitude of 107 km corresponding to the peak value of R whenever the altitude profiles of electron density are devoid of large structures between 100 km and 110 km. Thus, the values of R_{avg} at the altitude of peak current density remain nearly constant. Therefore, the peak values of current density ($J_{x,max}$) are found to vary, from one case to another, linearly with the variations of N_e and V_z at the peak altitude. The values given in Table 1 (obtained using method 1) are found to be consistent with this inference. For example, by comparing cases 2 and 5 in Table 1, the change in J_x is found to be almost doubled when N_e is nearly doubled without considerable change in V_z.

2. In the presence of large structures in N_e profile between 100 km and 110 km (subplots 2a and c), the current density maximizes at the altitude wherever electron densities and R_{avg} values are optimum. Thus, the peak current density need not lie around 107 km (refer cases 1 and 3 of Table 1).

3. In the absence of altitudinal structures, the altitude gradients in J_x profiles (above and/ or below $J_{x,max}$) obtained using the methods 1 and 3 are found to be larger whenever the J_x values are more (subplots 2e and f) compared to corresponding gradients whenever the J_x values are small (subplots 2b and

d). This is consistent with the work of Onwumechili (1992b) where the strength and thickness of electrojet current density based on daytime measurements over the dip-equator were shown to be inversely proportional. However, it must be noted here that multiple layers in current density (subplots 2a and c) are often observed during nighttime and determination of the thickness of the peak current layer is not unambiguous.

4. In the presence of multiple layers in current density profile whenever the electron density is structured (subplots 2a and c), the altitude of peak current density can be identified using method 2, as the streaming waves observed by rocket borne measurements usually appear in the vicinity of the peak current.

5. The peak altitudes determined by method 3 are lower than those obtained by the other methods whenever the electron densities are devoid of large structures. However, the altitude profiles of the current densities obtained from all the three methods go nearly hand-in-hand with one another whenever the altitude structures in N_e are present.

In addition to the altitudinal structure in the current densities, the electrojet model provides latitudinal extents also. As mentioned earlier the altitude profiles of electron densities and the $(E_{Sq})_x$ from plasma drift model are given as inputs to the electrojet model. Fig. 3 represents the contour plots of westward current densities over the magnetic latitude-altitude plane. The color-bar in Fig. 3 corresponds to the strength of current densities. As the
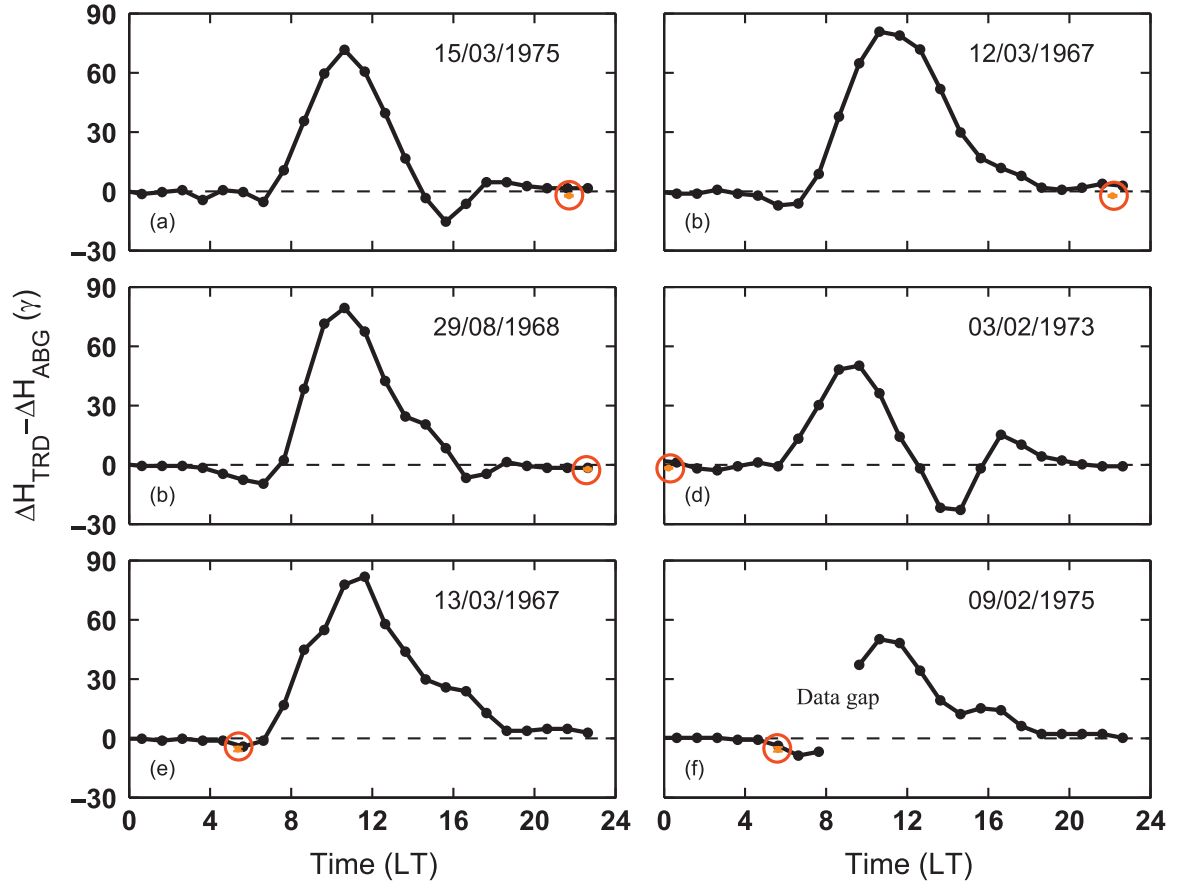
Fig. 5. Ground-based magnetometer measured hourly variation of electrojet strength over Thumba ($\Delta H_{TRD} - \Delta H_{ABG}$ in black). Orange dots correspond to the calculated horizontal component of magnetic field induced at ground by the nighttime current densities shown in Fig. 3 using Eq. (11). (For interpretation of the references to color in this figure caption, the reader is referred to the web version of this paper.)

sensitivity study revealed that maximum progressive uncertainty in the current density obtained by combining the individual uncertainties of all input parameters is less than 20%, the difference between successive contours in each subplot is kept at 30% of the corresponding peak current density values over the dip equator.

Islands of current density contours are seen in subplots 3a and c. These distinct islands are missing in subplot 3b. They are more conspicuous only when the input electron densities have altitudinal structures. As a result, the altitude of peak current densities is not well defined. However, when the input electron densities have less structures the peak current altitude is well defined and island structures (in the altitude–latitude plane) disappear (subplots 3d–f). Hence, the effect of electron density structures in nighttime electrojet current needs further attention. In order to examine this effect, the altitude structures in electron densities measured at 2238 *LT* on 29 *August*, 1968 are gradually smoothed by Savitzky–Golay method (Savitzky and Golay, 1964) in the altitude range of 90–120 km. These electron density profiles along with a single value of $(E_{Sq})_x$ are used as input to the electrojet model and the corresponding current density profiles are obtained. Fig. 4a–c depicts the resulting iso-current density contours along with the input electron density values. Without smoothing the electron density profile, the island structures and larger latitudinal extent are observed (see Fig. 4a) in current density contours. Allowing more than 10 km structures between 90 and 120 km, the gaps between the islands have reduced and the latitudinal extent of the second island around 100 km has considerably reduced (see Fig. 4b). On further smoothing of the electron density, the reduction in the latitudinal extent of current density and disappearance of island structures are noticed in Fig. 4c. Therefore, the valley and

peak in the altitude profile of electron density in region of 90–120 km appears to decide the gap between the islands and latitudinal extent of contours representing current density.

Based on the current density estimates by the electrojet model, the horizontal component (H) of the magnetic field induced at ground is calculated using Eq. (11) for all the cases depicted in Fig. 3. These calculated magnetic fields with uncertainties (marked in orange within red circles) are shown along with the hourly variations in the electrojet strength (represented by black line), derived on the basis of magnetic field measurements, in Fig. 5. It is known that strength of equatorial electrojet can be estimated based on the magnetic field measurements over a dip equatorial and an off-equatorial stations. Over the Indian sector, this can be done using magnetic measurements from Thumba and Alibag (18.6°N, 72.9°E, Dip angle 23.5°), a dip equatorial and off-equatorial stations respectively. It is known (e.g. Rastogi and Patil, 1986) that $\Delta H_{TRD} - \Delta H_{ABG}$ represents strength of equatorial electrojet where ΔH is calculated by subtracting nighttime base value from the instantaneous H value (where ΔH_{TRD} and ΔH_{ABG} represent the ΔH values over Thumba and Alibag respectively). The nighttime base value is calculated by taking average of the five hourly values starting from 2300 h to 0300 h. The H values calculated from the nighttime currents obtained from the electrojet model are found to be consistent with the magnetic measurements.

It is well known that during nighttime there is a valley in the altitude profile of the electron density centered around 125–130 km. In order to investigate the effect of this valley region on the polarization field in the vertical direction (E_z), an exercise is carried out using the electrojet model with varying depth of the valley. For this investigation, the electron density measurement obtained at 2238 *LT*
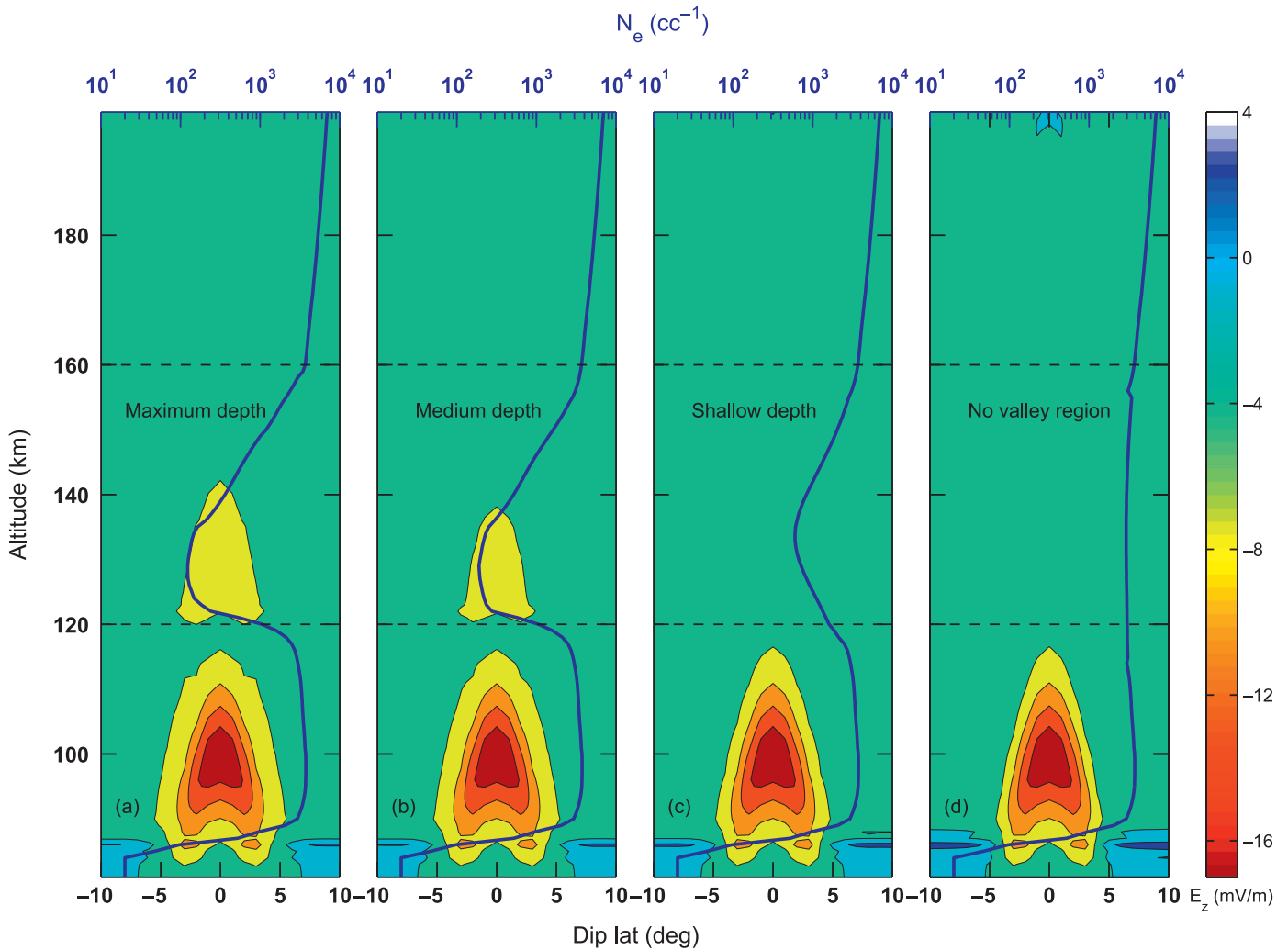
$$N_e \, (cc^{-1})$$

Fig. 6. Effects of the depth of the valley region on the polarization electric field in vertical direction (E_z in mV/m) for (a) maximum, (b) medium, (c) shallow depth and (d) no valley region. Iso-electric field contours in each subplot are plotted with steps of 20% of peak values over the dip equator. (For interpretation of the references to color in this figure, the reader is referred to the web version of this paper.)

Table 2
The values of polarization electric field in vertical direction (E_z in mV/m) obtained using electrojet model closer to the altitude of observation of streaming waves and zonal Sq electric field used in the model calculations.

Time and date	E_x (mV/m)	E_z (mV/m)
2142 on 15/03/1975	− 1.03	− 18.7
2238 on 29/08/1968	− 0.62	− 19.1
0537 on 09/02/1975	− 0.72	− 13.4

on 29 *August*, 1968 is first smoothed and then used as input to the electrojet model with varying depth of the valley region. Fig. 6 depicts the resulting contours of polarization field in the vertical direction (E_z), wherein 20% difference of the peak values are maintained by successive contours. However, there is no appreciable change in current densities around 105 km (not shown). It is found that E_z increases around 125 km when there is a deep valley while it progressively decreases as depth of the valley region reduces. Further, the minimum strength of polarization electric field in the vertical direction required for the generation of streaming waves is about 13.8 mV/m ($E_z = V_{x,min} \times B$) at 105 km. The electrojet model calculated E_z values, near the altitude region wherein the presence of streaming waves was observed during measurements (as provided in Table 2), are found to be consistent with requirement for generation of streaming waves in those altitude region barring a case

during morning hours. This is probably due to the fact that the Fejer et al. (2008) model values deviate from the measurements on a few occasions (as mentioned in Section 3.1).

This investigation suggests that the nighttime base value of the horizontal component of magnetic field during geomagnetically quiet period over the Indian dip equatorial sector is well within 6 nT if one considers pre-midnight to early morning hours. However, during magnetically disturbed periods, the horizontal magnetic field may change during midnight hours in varying degrees owing to the alteration of ionospheric electric field or modulation of the magnetospheric current systems. Under such circumstances, it is important that these aspects are taken into account before any realistic estimation is made on the nighttime E-region current over the dip equatorial region. This is beyond the scope of the present work and will be attempted in future.

6. Summary

The salient points that emerged from the present investigation are as follows:

1. The nighttime current density deduced using method 1 and the available electron density measurements as well as with an

electrojet model reveals E-region current in the range of ~ 0.3–0.7 A/km^2 during pre-midnight to early morning hours on geomagnetically quiet days.

2. The nocturnal E-region current density strength seems to decrease from the post-sunset hours to the midnight hours and then increase during early morning hours.

3. Altitude structures are seen in the nighttime E-region current density and are shown to be associated with the altitude structures in the electron density.

4. The trough and crest in the altitude structures of the electron density seem to decide the latitudinal extent and altitudinal stratification of the nighttime E-region current density.

5. The dip equatorial polarization electric field in the vertical direction obtained from the electrojet model is shown to be sufficient to drive the observed streaming waves during nighttime in a limited altitude region around 105 km baring a case during early morning hours. The current density estimated using the streaming wave criterion is found to be well within the estimated currents.

6. The ground magnetometer observed magnetic field variations during quiet time are well within 6 nT and match fairly well with the calculated induced magnetic field deduced from the current density (obtained from electrojet model).

7. The well-known dip equatorial nighttime E-region valley in the electron density around 130 km is shown to increase the polarization electric field in the vertical direction near this altitude depending upon the depth of the valley.

Acknowledgments

References

Anandarao, B.G., 1976. Effects of gravity wave winds and wind shears on equatorial electrojet. Geophys. Res. Lett. 3 (9), 545–548. http://dx.doi.org/10.1029/GL003i009p00545.

Anandarao, B.G., 1977. Studies on the dynamics of the equatorial ionosphere (Ph.D. thesis), Gujarat University.

Anandarao, B.G., Desai, J.N., Giles, M., Martelli, G., Raghavarao, R., Rothwell, P., 1977. Electric field in the equatorial ionosphere. J. Atmos. Terr. Phys. 39, 927–931.

Anandarao, B.G., Raghavarao, R., 1987. Structural changes in the currents and fields of the equatorial electrojet due to zonal and meridional winds. J. Geophys. Res. 92 (A3), 2514–2526. http://dx.doi.org/10.1029/JA092iA03p02514.

Campbell, W.H., 1973. The field levels near midnight at low and equatorial geomagnetic stations. J. Atmos. Terr. Phys. 35, 1127–1146. http://dx.doi.org/10.1016/0021-9169(73)90010-X.

Campbell, W.H., 1979. Occurrence of AE and Dst geomagnetic index levels and the selection of the quietest days in a year. J. Geophys. Res. 84 (A3), 875–881. http://dx.doi.org/10.1029/JA084iA03p00875.

Chakrabarty, D., Sekar, R., Narayanan, R., Devasia, C.V., Pathan, B.M., 2005. Evidence for the interplanetary electric field effect on the OI 630.0 nm airglow over low latitude. J. Geophys. Res. 110 (A11), 301. http://dx.doi.org/10.1029/2005JA011221.

Davis, T.N., Burrows, K., Stolarik, J.D., 1967. A latitude survey of the equatorial electrojet with rocket-borne magnetometers. J. Geophys. Res. 72 (7), 1845–1861. http://dx.doi.org/10.1029/JZ072i007p01845.

Eccles St., J.V., Maurice, J.P., Schunk, R.W., 2015. Mechanisms underlying the pre-reversal enhancement of the vertical plasma drift in the low-latitude

ionosphere. J. Geophys. Res. 120 (6), 4950–4970. http://dx.doi.org/10.1002/2014JA020664.

Farley, D.T., 2009. The equatorial E-region and its plasma instabilities: a tutorial. Ann. Geophys. 27 (4), 1509–1520. http://dx.doi.org/10.5194/angeo-27-1509-2009.

Fejer, B.G., Jensen, J.W., Su, S.Y., 2008. Quiet time equatorial F region vertical plasma drift model derived from ROCSAT-1 observations. J. Geophys. Res. 113 (A5), 304. http://dx.doi.org/10.1029/2007JA012801.

Finlay, C.C., et al., 2010. International geomagnetic reference field: the eleventh generation. Geophys. J. Int. 183 (3), 1216–1230. http://dx.doi.org/10.1111/j.1365-246X.2010.04804.x.

Forbes, J.M., 1981. The equatorial electrojet. Rev. Geophys. 19 (3), 469–504. http://dx.doi.org/10.1029/RG019i003p00469.

Gupta, S.P., 1986. Formation of sporadic E layers at low magnetic latitudes. Planet. Space Sci. 34 (11), 1081–1085.

Gupta, S.P., 1990. Ionisation layers over the magnetic equator during meteor shower days. Adv. Space Res. 10 (10), 105–108. http://dx.doi.org/10.1016/0273-1177(90)90016-S.

Haerendel, G., Eccles, J.V., 1992. The role of the equatorial electrojet in the evening ionosphere. J. Geophys. Res. 97 (A2), 1181–1192. http://dx.doi.org/10.1029/91JA02227.

Jacchia, L.G., 1971. Revised Static Models of the Thermosphere and Exosphere with Empirical Temperature Profiles, Smithsonian Astrophysical Observatory (SAO) Special Report 332.

Jadhav, G., Rajaram, M., Rajaram, R., 2002. A detailed study of equatorial electrojet phenomenon using Ørsted satellite observations. J. Geophys. Res. 107 (A8), 1175. http://dx.doi.org/10.1029/2001JA000183.

Lühr, H., Maus, S., Rother, M., 2004. Noon-time equatorial electrojet: its spatial features as determined by the CHAMP satellite. J. Geophys. Res. 109 (A1), 306. http://dx.doi.org/10.1029/2002JA009656.

Marcos, F.A., 1990. Accuracy of atmospheric drag models at low satellite altitudes. Adv. Space Res. 10 (3), 417–422. http://dx.doi.org/10.1016/0273-1177(90)90381-9.

Matsushita, S., 1968. Sq and L current systems in the ionosphere. Geophys. J. R. Astron. Soc. 15 (1–2), 109–125.

Matsushita, S., 1971. Interactions between the ionosphere and the magnetosphere for Sq and L variations. Radio Sci. 6 (2), 279–294. http://dx.doi.org/10.1029/RS006i002p00279.

Matsushita, S., Maeda, H., 1965. On the geomagnetic solar quiet daily variation field during the IGY. J. Geophys. Res. 70 (11), 2535–2558. http://dx.doi.org/10.1029/JZ070i011p02535.

Mayaud, P.N., 1976. Magnetospheric and night-time induced effects in the regular daily variation S_R. Planet. Space Sci. 24, 1049–1057. http://dx.doi.org/10.1016/0032-0633(76)90123-9.

Onwumechili, C.A., 1992a. A study of rocket measurements of ionospheric currents —I. General setting and night-time ionospheric currents. Geophys. J. Int. 108 (2), 633–640. http://dx.doi.org/10.1111/j.1365-246X.1992.tb04642.x.

Onwumechili, C.A., 1992b. A study of rocket measurements of ionospheric currents —III. Ionospheric currents at the magnetic dip equator. Geophys. J. Int. 108 (2), 647–659. http://dx.doi.org/10.1111/j.1365-246X.1992.tb04644.x.

Onwumechili, C.A., Ezema, P.O., 1977. On the course of the geomagnetic daily variation in low latitudes. J. Atmos. Terr. Phys. 39 (9–10), 1079–1086. http://dx.doi.org/10.1016/0021-9169(77)90016-2.

Pfaff, R.F., Sobral, J.H.A., Abdu, M.A., Swartz, W.E., LaBelle, J.W., Larsen, M.F., Goldberg, R.A., Schmidlin, F.J., 1997. The Guará Campaign: a series of rocket-radar investigations of the Earth's upper atmosphere at the magnetic equator. Geophys. Res. Lett. 24 (13), 1663–1666. http://dx.doi.org/10.1029/97GL01534.

Pingree, J.E., Fejer, B.G., 1987. On the height variation of the equatorial F region vertical plasma drifts. J. Geophys. Res. 92 (A5), 4763–4766. http://dx.doi.org/10.1029/JA092iA05p04763.

Prakash, S., Gupta, S.P., Subbaraya, B.H., 1970. A study of the irregularities in the night time equatorial E-region using a Langmuir probe and plasma noise probe. Planet. Space Sci. 18 (9), 1307–1318. http://dx.doi.org/10.1016/0032-0633(70)90141-8.

Prakash, S., Subbaraya, B.H., 1967. Langmuir probe for the measurement of electron density and electron temperature in the ionosphere. Rev. Sci. Instrum. 38 (8), 1132–1136. http://dx.doi.org/10.1063/1.1721035.

Raghavarao, R., Anandarao, B.G., 1987. Equatorial electrojet and the Counter-Electrojet. Indian J. Radio Space Phys. 16, 54–75.

Rastogi, R.G., Chandra, H., James, M.E., 1996. Nocturnal variations of geomagnetic horizontal field at equatorial stations. Geophys. Res. Lett. 23 (19), 2601–2604. http://dx.doi.org/10.1029/96GL02390.

Rastogi, R.G., Iyer, K.N., 1976. Quiet day variation of geomagnetic H-field at low latitudes. J. Geomagn. Geoelectr. 28 (6), 461–479. http://dx.doi.org/10.5636/jgg.28.461.

Rastogi, R.G., Patil, A., 1986. Complex structure of equatorial electrojet current. Curr. Sci. 55 (9), 433–436.

Richmond, A.D., 1973. Equatorial electrojet—I. Development of a model including winds and instabilities. J. Atmos. Terr. Phys. 35 (6), 1083–1103. http://dx.doi.org/10.1016/0021-9169(73)90007-X.

Sampath, S., Sastry, T.S.G., 1979. AC electric fields associated with the plasma instabilities in the equatorial electrojet-III. J. Geomagn. Geoelectr. 31 (3), 391–400. http://dx.doi.org/10.5636/jgg.31.391.

Sastry, T.S.G., 1970. Diurnal changes in the parameters of the equatorial electrojet as observed by rocket-borne magnetometers. Space Res. X, 778–785.

Savitzky, A., Golay, M.J.E., 1964. Smoothing and differentiation of data by simplified least squares procedures. Anal. Chem. 36 (8), 1627–1639. http://dx.doi.org/10.1021/ac60214a047.

Sekar, R., Gupta, S.P., Acharya, Y.B., Chakrabarty, D., Pallamraju, D., Pathan, B.M., Tiwari, D., Choudhary, R.K., 2013. Absence of streaming plasma waves around noontime over Thumba in recent times: is it related to the movement of the dip equator?. J. Atmos. Sol.-Terr. Phys. 103, 8–15. http://dx.doi.org/10.1016/j.jastp.2013.02.005.

Shuman, B.M., 1970. Rocket measurement of the equatorial electrojet. J. Geophys. Res. 75 (19), 3889–3901. http://dx.doi.org/10.1029/JA075i019p03889.

Stening, R.J., Winch, D.E., 1987. Night-time geomagnetic variations at low latitudes. Planet. Space Sci. 35 (12), 1523–1539. http://dx.doi.org/10.1016/0032-0633(87)90078-X.

Subbaraya, B.H., Muralikrishna, P., Sastry, T.S.G., Prakash, S., 1972. A study of the structure of electrical conductivities and the electrostatic field within the equatorial electrojet. Planet. Space Sci. 20 (1), 47–52. http://dx.doi.org/10.1016/0032-0633(72)90139-0.

Subbaraya, B.H., Prakash, S., Gupta, S.P., 1983. Electron Densities in the Equatorial Lower Ionosphere from the Langmuir Probe Experiments Conducted at Thumba During 1966–1978. Scientific Report, ISRO-PRL-SR-15-83.

Subbaraya, B.H., Prakash, S., Gupta, S.P., 1985. Structure of the equatorial lower ionosphere from the Thumba Langmuir probe experiments. Adv. Space Res. 5 (7), 35–38. http://dx.doi.org/10.1016/0273-1177(85)90352-7.

Sudan, R.N., Akinrimisi, J., Farley, D.T., 1973. Generation of small-scale irregularities in the equatorial electrojet. J. Geophys. Res. 78 (1), 240–248. http://dx.doi.org/10.1029/JA078i001p00240.

Sugiura, M., Poros, D.J., 1969. An improved model equatorial electrojet with a meridional current system. J. Geophys. Res. 74 (16), 4025–4034. http://dx.doi.org/10.1029/JA074i016p04025.

Takeda, M., Araki, T., 1985. Electric conductivity of the ionosphere and nocturnal currents. J. Atmos. Terr. Phys. 47 (6), 601–609. http://dx.doi.org/10.1016/0021-9169(85)90043-1.

Electrical conductivity of the stratosphere over Hyderabad, India: Results from Balloon borne measurements

S P Gupta[1,$] & Smitha V Thampi[2,#,*]

[1]Physical Research Laboratory, Navarangpura, Ahmedabad 380 009, India
[2]Space Physics Laboratory, Vikram Sarabhai Space Centre, Indian Space Research Organization, Trivandrum 695 022, India
E-mail: [$]spg@prl.res.in; [#]smitha_vt@vssc.gov.in

The stratospheric conductivity is an important parameter of the global electric circuit. In this paper, the stratospheric conductivity measurements are presented, which were made using high altitude balloon flights from Hyderabad (geographic 17.5°N, 78.5°E; magnetic lat 8.5°N), India as a part of the IMAP (1982-1994) program of India. The vertical profiles of ion conductivity were measured from Hyderabad during periods with different solar activity levels and during different seasons using different techniques. It was observed that conductivity values in stratosphere are larger in high solar activity period as compared to low solar activity period. This is similar in nature to the observations from mid-latitudes. The observed positive correlation with solar activity is discussed in terms of composition changes due to the change in intensity of the UV (200-300 nm) radiation with solar activity. It was found that the dissociation of heavy cluster ions to lighter ions, as conjectured by Gupta [Solar cycle variation of stratospheric conductivity over low latitude, *Adv Space Res* (*UK*), 26 (2000.) pp 1225–1229] is the main reason for the observed positive correlation of stratospheric conductivity with solar activity. No significant seasonal effect was noticed. In addition, conductivity profile obtained from Hyderabad is compared to that obtained from Cachoeira Paulista, Brazil.

Keywords: Stratosphere, Electrical conductivity, Photo-dissociation, Ion conductivity, Solar activity

PACS Nos: *92.60.hd*; 96.60.Q–

1 Introduction

Electrical conductivity, which is proportional to the product of the ion concentration and the ion mobility increases exponentially with altitude in the troposphere and stratosphere. Variations in conductivity may be caused by factors that can change either or both of these quantities. For instance, the ion concentration can change as a result of the variations in the cosmic ray flux, which is the source of ionization in the stratosphere and troposphere[2,3]. The stratospheric conductivity is an important parameter of the global electric circuit[4-6]. The conductivity in the stratospheric region is measured using Balloon-borne experiments. In the past, there were several such campaign mode observations, which provided several new insights to this topic. For example, measurements of the atmospheric conductivity from nine high-altitude balloon flights obtained between the altitudes of 10 and 30 km at three locations widely separated in latitude provided the conductivity variations on local and global scales[7]. The observations were made during 1973-1981 period. The vector electric field and polar conductivities were measured

by balloon-borne payloads launched from Wallops Island, Virginia during the summers of 1987 and 1988[8]. Similarly, during the polar patrol balloon (PPB) campaigns, direct electric field and conductivity measurements were made from Antarctica[9,10]. Balloon-borne measurements of the conductivity from near ground level to 35 km were studied in conjunction with measurements of the ionization rate and the positive ion density and three parameters were used to calculate the average positive ion mobility profile and the effective recombination coefficient profile, using data from Laramie, from the flights during 1978-1979[11]. All these measurements pertain to the mid and polar latitudes.

One of the very important programs to study the variability of the middle atmospheric electrodynamics was the Indian Middle Atmospheric Program (IMAP), an important element of which was the Indian Middle Atmospheric Conductivity Campaign[1,12,13]. The two phases of this national program spanned from 1982 to1994, during which the vertical profiles of conductivity were measured using different techniques from a low-latitude station Hyderabad

(geographic 17.5°N, 78.5°E; magnetic lat 8.5°N). The uniqueness of this database is that it covers both the high and low solar activity periods as well as different seasons. Using the data from four flights, it was shown that conductivity values in stratosphere are larger in high solar activity period as compared to low solar activity period. It was suggested that during high solar activity period, the heavy cluster ions dissociate into lighter ions giving rise to the enhanced conductivity over this region[1]. The main objective of this paper is to further show the solar activity dependence of stratospheric conductivity. In the present paper, the data from the four flights already published by Gupta[1] is used and added from two more flights corresponding to low (daily mean sunspot number $R_z = 26$) and high ($R_z = 167$) solar activity periods to show that the results are consistent. Further, by extracting the altitude variation of the difference in conductivity during solar maximum and minimum, it is qualitatively proved that the composition changes due to the changes in the UV radiation intensity with solar activity[14,15] is a principal cause for the positive correlation of stratospheric conductivity with solar activity. It must be mentioned here that data obtained from same technique were compared for low and high solar activity periods. For example, the Langmuir probe (LP) data obtained on 6 December 1995 is compared with that on 22 April 1989, which was also obtained using LP. This was done to take care of the difference in values that may arise due to the difference in the measurement technique. Apart from this, conductivity profile obtained from Hyderabad on 5 January 1994 is compared to that obtained from Cachoeira Paulista, Brazil (geographic 22°44′S 44°56′W; geomagnetic 11°57′S, 22°32′E) for 26 January 1994 to show the longitudinal differences in conductivity.

2 Experimental technique

The list of observations along with the corresponding sunspot number is given in Table 1. The balloon flights on 8 April 1987 and 6 December 1989 used a 'long wire' probe and those on 17 October 1989 and 5 January 1994 used a 'spherical probe'. Both these measurements were based on relaxation time measurements. In this technique, one or more probes are driven to a potential different from the ground potential of the payload for a short period of time; the potential difference is then released and the probe potential is allowed to decay exponentially to a steady state value[16]. The sensor is a hollow

spherical copper sphere of 20 cm diameter, coated with aquadag and mounted on a boom of one meter length on balloon gondola. A voltage pulse of ±5 V is applied for a duration of 1 sec with an interval of 50 sec. The decay time constant is measured and the conductivity is calculated using the following equation[17]:

$$= - \qquad \qquad …(1)$$

where, , is the permittivity of the medium[1,18].

The balloon flights on 6 December 1985 and 22 April 1989 used Langmuir Probe (LP) for measuring the vertical profiles of polar conductivity. The payload consisted of an electrostatic sensor, which is hemi-spherical (10 cm diameter) in shape and made of stainless steel. In this technique, a suitable potential is applied to the sensor with reference to the reference electrode and the resulting current is measured. Depending on the potential of the probe, it would collect either positive or negative ions. The conductivities are derived from the resulting I-V characteristics:

$$\propto \frac{dI}{dV_P} \qquad \qquad …(2)$$

where, $V_{P,}$ is the probe voltage.

3 Results and Discussion

Figure 1(a-c) shows the vertical profiles of negative ion conductivity measured over Hyderabad during the IMAP campaigns. The daily sunspot number data are taken from NSSDC (http://omniweb.gsfc.nasa.gov/form/dx1.html). Figure 1(a) compares the profiles of negative ion conductivity on 8 April 1987 (low solar activity, $R_z=64$) with that on 6 December 1989 (high solar activity, $R_z=187$). As mentioned earlier, both are 'long wire' probe measurements based on relaxation time. It can be seen that the conductivity increases exponentially with altitude. It can also be seen that the conductivity is high at all altitudes during high solar

Table 1 — List of observations

Date of observation	Sunspot number
6 December 1985	26
8 April 1987	64
22 April 1989	167
17 October 1989	206
6 December 1989	184
5 January 1994	104

activity day compared to low solar activity day[1], and the difference increases with altitude. Figure 1(b) compares the vertical profiles of negative ion conductivity on 5 January 1994 (low solar activity, $R_z=107$) with that on 17 October 1989 (high solar activity, $R_z=206$). These are also 'relaxation time probe' measurements but with a spherical probe. Here also, the positive correlation with solar activity is evident. Figure 1(c) compares the vertical profiles of negative ion conductivity on 6 December 1985 (solar minimum, $R_z=26$) with that on 22 April 1989 (solar maximum, $R_z=167$). These are LP measurements, and hence one cannot compare the absolute value of conductivity with the previous ones. However, both the measurements shown in Fig. 1(c) can be compared, since both are LP measurements. It can be seen that the conductivity is high at all altitudes during high solar activity day compared to solar minimum and the difference increases with altitude.

Gupta[1] suggested that the dissociation of the heavy cluster ions into lighter ions plays a crucial role in enhancing the conductivity during solar maximum
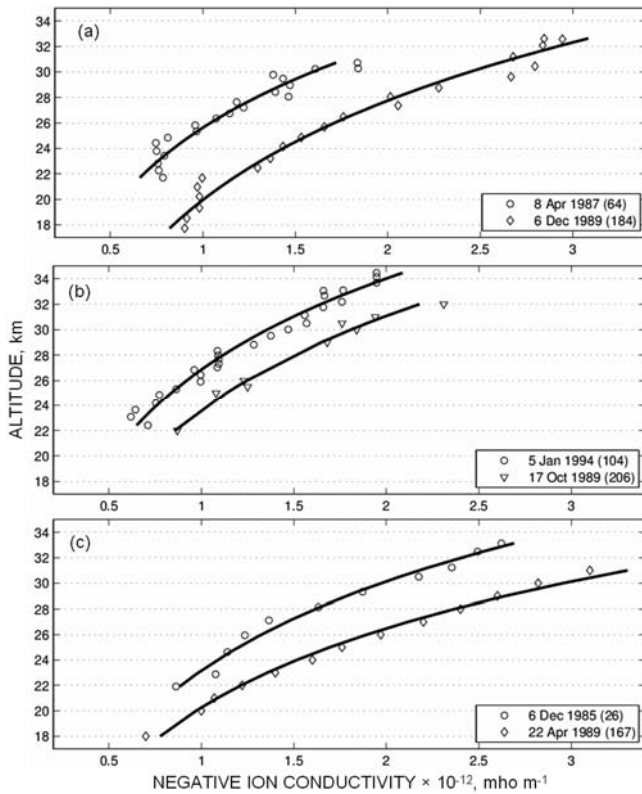
period. To substantiate this further, the mean profile of difference in negative ion conductivity with the standard deviations is taken and calculated at each km [Fig. (2)]. It can be seen that the difference increases exponentially with altitude with a scale height (distance over which a quantity decreases by a factor of e) of ~8 km. This value matches with the scale height of the UV radiation (decreases as one goes lower in altitude). The available flux UV radiation for dissociation of cluster ions will be more at higher altitudes and hence, one can expect the difference in conductivity also to be more at higher altitudes. In other words, the scale height of the difference in conductivity (between high and low solar activity) and scale height of the change in UV radiation with altitude are identical in nature, and this further adduce the role of dissociation of cluster ions by UV radiation in increasing the conductivity. It may be noted here that the percentage changes in UV radiation are not being related with that of stratospheric conductivity because the global or local variations in the ion mobility can occur due to changes in the ion recombination rate, and hence, any relationship between ion mobility change and percentage change in UV radiation would not be linear. However, if the cause of the positive correlation of conductivity with solar activity lies in the variability of UV flux, then both would show similar scale heights as it is observed. Hence, one can qualitatively conclude that dissociation of the cluster ions and the resultant enhancement in mobility causes the enhancement in the conductivity during solar maximum period.

Fig. 1 — Conductivity profiles observed from Hyderabad, India: Comparison of measurements using: (a) long wire probe; (b) spherical probe; and (c) LP for different solar activity levels [daily sunspot numbers corresponding to the days are given in legend; thick solid lines are exponential fits]
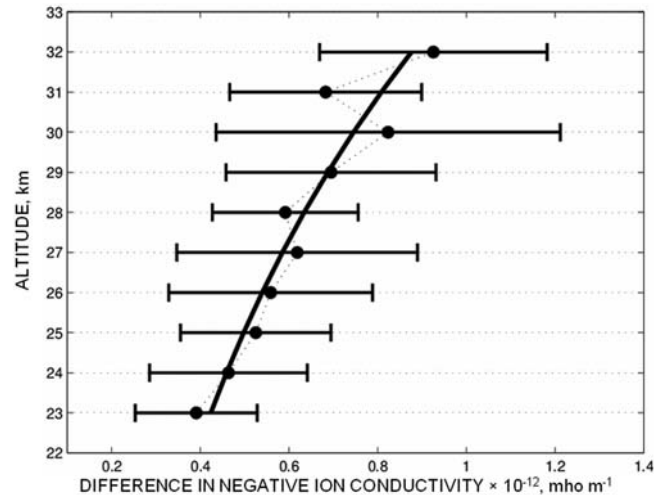

Fig. 2 — Profile of the mean difference in negative ion conductivity (between high and low solar activity days) with the standard deviations [thick solid line shows an exponential fit]

Another important aspect which needs to be considered while addressing the long term changes in the stratospheric conductivity is the variation in the ionization due to galactic cosmic rays. Cosmic ray parti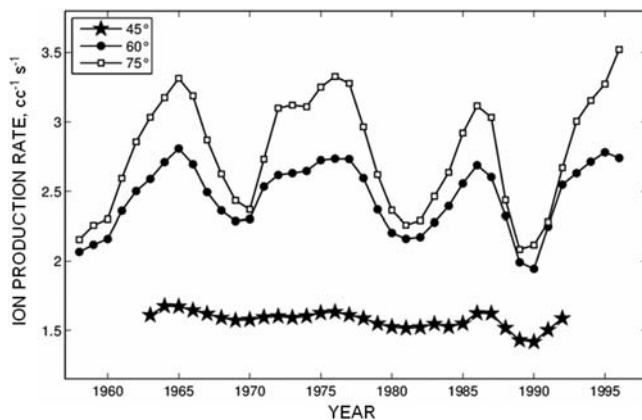cles with energy greater than 1 Gev can reach over equator. Figure 3 shows the yearly averaged maxima of ion production due to galactic cosmic ray in the stratosphere corresponding to three magnetic latitudes (75°, 60°, and 45°). This is reproduced from Krivolutsky[19]. It can be seen that the galactic cosmic ray intensity shows substantial solar cycle dependence only for 75° and 60° magnetic latitudes with maximum intensity on solar minimum period and minimum intensity during solar maximum period. Such clear solar activity dependence is not seen at 45° magnetic latitude. This indicates that the ion production in the stratosphere does not vary significantly with solar activity. The stratospheric conductivity is determined by the ionization produced by the galactic cosmic rays and the ion mobility. At high latitudes, the cosmic ray flux has an inverse correlation with solar activity, whereas at mid-latitudes, this inverse correlation is not seen. However, it is observed that stratospheric conductivity has a positive correlation with solar activity. In fact, the positive correlation holds good at mid-latitudes as well. For instance, if one compares the conductivity profiles from Palestine (32°N geographic)[20] for 1 September 1976 (low solar activity $R_z=17$) with that of 6 July 1999 (higher solar activity $R_z=141$), one can see that the conductivity is high in high solar activity period. These observations suggest that one cannot attribute the observation that the stratospheric conductivity has positive correlation with solar

activity to any changes in the cosmic ray fluxes. It must be mentioned here that similar trend can be seen in the conductivity variations over the South American sector as well. For instance, if one compares the conductivity value at 26 km reported by Pinto et al.[21] corresponding to high solar activity (April 1980, Rz=164) to that reported by Saba et al.[22], for low solar activity period (January 1994, Rz=67), a similar trend can be seen.

Figure 4 compares the conductivity profile obtained from Hyderabad on 5 January 1994 and that obtained from Cachoeira Paulista, Brazil (geographic 22°44′S, 44°56′W; geomagnetic 11°57′S, 22°32′E) for 26 January 1994. The measurement over Cachoeira Paulista, Brazil is reproduced from Saba et al.[22]. These are also made using a relaxation time probe[22]. Such a comparison of observations from two separate locations during same month and year was not done previously because the balloon-borne observations comprise only a very small database around the globe and near simultaneous measurements from two such locations were not available. An important point to be noted here is that the magnetic field strength is different at these two stations. It must also be mentioned here that the profile reported by Saba et al.[22] is obtained before the thunderstorm event when the balloon was ascending. The thunderstorm started after the balloon reached the float altitude[22]. Though the comparison is made using only one flight each for a location, considering the fact that very few observations are available over the world, this observation is considered very important. From this single observation, it appears that since
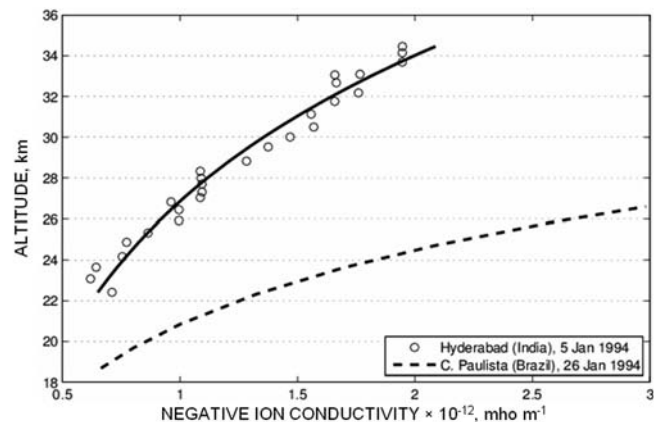

Fig. 3 — Yearly averaged maxima of ion production rate due to galactic cosmic rays in the stratosphere corresponding to three magnetic latitudes [*Source*: Krivolutsky, Large scale / long term ozone response in connection to comsic influence, in *Long term changes and trends in the atmosphere* Vol I, 2000]

Fig. 4 — Conductivity profile obtained from Hyderabad on 5 January 1994 and from Cachoeira Paulista, Brazil for January 26 1994 [*Source*: Saba et al., Stratospheric conductivity measurements in Brazil, *J Geophys Res* (USA), 104 (D22) (1999) pp 27203-27208, doi: 10.1029/1999JD900221]

magnetic field value at Brazil is lower than over Indian zone, the conductivity is also higher over Brazil compared to India. However, more coordinated observations are needed to further confirm the differences.

4 Conclusion

The stratospheric conductivity measurements made using high altitude balloon flights from Hyderabad, India as a part of the IMPAP (1982-1994) program of India show that conductivity values in stratosphere are larger in high solar activity period compared to low solar activity period. This observation is similar in nature to that observed at mid-latitudes. The mean differences in negative ion conductivity increases exponentially with altitude and has a scale height of ~8 km. This value matches with the scale height of the UV radiation. This confirms the role of dissociation of cluster ions by UV radiation in increasing the conductivity. Another important aspect revealed by the present investigation is that the conductivity over Cachoeira Paulista, Brazil is significantly higher, than that observed over Hyderabad.

Acknowledgement

References

1   Gupta S P, Solar cycle variation of stratospheric conductivity over low latitude, *Adv Space Res (UK)*, 26 (2000.) pp 1225–1229.

2   Bazilevskaya G A, Usoskin I G, Flueckiger E O, Harrison R G, Desorgher L, Buetikofer R, Krainev M B, Makhmutov V S, Stozhkov Y I, Svirzhevskaya A K, Svirzhevsky N S & Kovaltsov G A, Cosmic ray induced ion production in the atmosphere, *Space Sci Rev (Netherlands)*, 137 (2008) pp 149-173.

3   Harrison R G & Bennett A J, Cosmic ray and air conductivity profiles retrieved from early twentieth century balloon soundings of the lower troposphere, *J Atmos Sol-Terr Phys (UK)*, 69 (2007) pp 515-527.

4   Aplin K L, Harrison R G & Rycroft M J, Investigating Earth's atmospheric electricity: A role for model planetary studies, *Space Sci Rev (UK)*, 137 (2008) pp 11-27.

5   Rycroft M, Harrison R G, Nicoll K A & Mareev E A, An overview of Earth's global electric circuit and atmospheric conductivity, *Space Sci Rev (UK)*, 137 (2008) pp 83-105.

6   Nicoll K A, Measurements of atmospheric electricity aloft, *Surv Geophys (Netherlands)*, 33 (2012), pp 991-1057.

7   Byrne G J, Benbrook J R, Bering III E A, Oro´ D M, Seubert C O & Sheldon W R, Observations of the stratospheric conductivity and its variation at three latitudes, *J Geophys Res (USA)*, 93 (1988) pp 3879-3892.

8   Hu H, Holzworth R H & Li Y Q, Thunderstorm-related variations in stratospheric conductivity measurements, *J Geophys Res (USA)*, 94 (1989) pp 16429-16435.

9   Fujii R, Miyaoka H, Kadokura A, Ono T, Yamagishi H, Sato N, Ejiri M, Hirasawa T, Nishimura J, Yajima N, Yamagami T, Ohta S, Akiyama H, Tsuruda K, Kodama M, Fukunishi H, Yamanaka M D & Kokubun S, Polar Patrol Balloon experiment during 1991–1993, *Nankyoku Siryo (Antarctic Record) (Japan)*, 33 (2) (1989) pp 320-328.

10   Holzworth R H, Bering III E A, Kokorowski M F, Lay E H, Reddell B, Kadokura A, Yamagishi H, Sato N, Ejiri M, Hirosawa H, Yamagami T, Torii S, Tohyama F, Nakagawa M, Okada T & Dowden R L, Balloon observations of temporal variation in the global circuit compared to global lightning activity, *Adv Space Res (UK)*, 36 (2005) pp 2223-2228

11   Rosen J M & Hofmann D J, Balloon-borne measurements of electrical conductivity, mobility, and the recombination coefficient, *J Geophys Res (USA)*, 86 (C8) (1981) pp 7406-7410, doi: 10.1029/JC086iC08p07406.

12   Gupta S P, Chakravarty S C & Chandrasekaran S (Eds), *Balloon-borne experiments for middle atmospheric conductivity Campaign* (ISRO IMAP Scientific Report) (ISRO, Bangalore), vol 39, 1992.

13   Gupta S P, Solar activity and atmospheric tide effect on the polar conductivity and the vertical electric field in the stratosphere over low latitude, *Adv Space Res (UK)*, 34 (2004) pp 1798-1800.

14   Heath D F & Thekaekara M P, *The solar spectrum between 1200 and 3000 & in the solar output and its variation*, edited by O R White (Colorado Associated University Press, Boulder), 1977, pp 193-212.

15   Pap J M & Frohlich C, Total solar irradiance variations, *J Atmos Sol-Terr Phys (UK)*, 61 (1999) pp 15-24.

16   Norville K & Holzworth R, Global circuit variability from multiple stratospheric electrical measurements, *J Geophys Res (USA)*, 92 (1987) pp 5685-5695.

17   Gupta S P & Narayan A, Balloon-borne measurements of ion conductivity over low latitude stratosphere, *Planet Space Sci (UK)*, 35 (1987) pp 439-443.

18   Narayan A, Acharya Y B & Gupta S P, A technique for measurement of electrical potential of balloon-borne gondola, *Rev Sci Instrum (USA)*, 61 (1990) pp 3866-3870.

19   Krivolutsky A A, *Large scale / long term ozone response in connection to comsic influence, in Long term changes and trends in the atmosphere Vol I*, edited by G Beig, (New Age International, New Delhi), 2000.

20   Bering III E A, Holzworth R H, Reddell B D, Kokorowski M F, Kadokura A, Yamagishi H, Sato N, Ejiri M, Hirosawa H, Yamagami T, Torii S, Tohyama F, Nakagawa M & Okada T, Balloon observations of temporal and spatial

fluctuations in stratospheric conductivity, *Adv Space Res (UK)*, 35 (2005) pp 1434-1449.

21   Pinto I R C A, Pinto Jr O, Gonzalez W D, Dutra S L G, Wygant J & Mozer F S, Stratospheric electric field and conductivity measurements over electrified convective clouds in the South American region, *J Geophys Res (USA)*, 93(D1) (1988) pp 709-715, doi: 10.1029/JD093iD01p00709.

22   Saba M M F, Pinto Jr O & Pinto I R C A, Stratospheric conductivity measurements in Brazil, *J Geophys Res (USA)*, 104 (D22) (1999) pp 27203-27208, doi: 10.1029/ 1999JD900221.
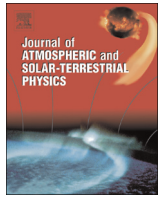
Short Communication

On the altitude of initiation of the gradient drift waves at different longitude sectors in the vicinity of the dip equator

CrossMark

R. Sekar *, S.P. Gupta, D. Chakrabarty

Physical Research Laboratory, Ahmedabad 380009, India

A B S T R A C T

In order to understand the variation in the altitudes of initiation (h_{aoi}) of E region gradient drift (GD) waves at different longitude sectors in the vicinity of the dip equator, the linear growth rate expression was examined. This revealed that the growth rate of the primary GD waves in an altitude region of 85–93 km depends on the square of the geomagnetic field strength (B). This is shown to explain the lower h_{aoi} of GD waves over Indian longitude vis-a-vis American longitudes. The available observations on the GD waves from different longitude sectors reveal that the h_{aoi} is inversely proportional to B^2.

© 2014 Elsevier Ltd. All rights reserved.

1. Introduction

It is well known that E-region of ionosphere over equatorial regions supports the generation of plasma waves. The streaming plasma waves and the gradient drift waves have been measured over several years using radar (Fejer et al., 1975; Krishna Murthy et al., 1998; Tiwari et al., 2003) and *in situ* probes (Prakash et al., 1969; Klaus and Smith, 1978; Pfaff et al., 1985). The streaming plasma waves are generated in closest vicinity of the dip equator (Sekar et al., 2013), while the gradient drift waves are observed at low latitude region as well. The characteristics of these waves and the generation mechanisms are well documented (Kelley, 2009). Linear and nonlinear theories were developed to understand the measured characteristics of these waves using radar and *in situ* probes. The present investigation deals with the gradient drift waves in the lower altitude region where collisions play an important role.

The *in situ* measurements of electron densities and their fluctuations using rocket flight from Thumba, India, revealed the presence of electron density fluctuations from 87 km onwards (Prakash et al., 1969). The results from the same flight also revealed the co-existence of large (30–300 m) and small (3 m) size irregularities at 87 km altitude. The amplitude of the former is ~10–20% (Prakash et al., 1971) and the latter is 1–2%. Subsequently, the presence of electron density fluctuations at 87 km altitudes in the positive electron density gradient region during normal electrojet condition (eastward electric field) and the

absence of them during counter-electrojet (westward electric field) condition (Prakash et al., 1979) suggest that the plasma instability process governs their generation. The spectral analysis based on several rocket flights conducted from Thumba revealed (Prakash et al., 1980) that the spectral indices of fluctuations above 87 km lie between -3.5 ± 1.5 indicating the plasma turbulence. On the other hand, the spectral indices of the fluctuations below 80 km lie between -1.6 ± 0.7 indicating that causative mechanism is due to neutral turbulence. Thus, the presence of these irregularities observed around 87 km is due to the gradient drift waves. These waves at lower altitude could not be damped by enhanced neutral collisions and/or by increased recombination effect in the presence of sunlit condition. In contrast to these observations over Indian sector, large and small scale size irregularities were observed only above 93 km during afternoon hours over the American sector (Klaus and Smith, 1978). The VHF radar observation from Jicamarca consisting of the temporal sequence of backscatter power of small scale size irregularities (Fejer et al., 1975) supports the above findings. The linear growth rates were evaluated based on the measurements from three different rocket flights and radar observations (Pfaff et al., 1985). Their work indicated that the growth of the irregularities by gradient drift mechanism is possible only above 93 km altitude in the American zone.

It is to be noted here that the present investigation is restricted to the vicinity of the dip equator as the vertical polarization electric field that drives the gradient drift waves is substantially reduced at the off-equatorial region. Further, it is assumed following Sudan et al. (1973) that the small-scale irregularities (a few meters) are generated as a consequence of primary gradient drift

waves with sufficient amplitudes. In addition, as the present investigation pertains to 85–93 km altitude region where collisions dominate, isothermal condition is assumed. Based on these assumptions, the linear growth rate expression of the primary gradient drift waves is examined to address the differences in the h_{aoi} of the generation of gradient drift waves over Indian and American sectors. In this short note, the possible explanation for this difference is provided.

2. Examination of growth rate expression

The growth rate (γ_k) of the primary waves of equatorial electrojet irregularities (Sudan et al., 1973; Rogister and D'Angelo, 1970) is as follows:

$$\gamma_k = \frac{\Psi}{1 + \Psi}\left[\frac{\Omega_e}{\nu_e} \cdot \frac{\omega_k}{kL} + \left(\omega_k^2 - k^2C_s^2\right)\frac{1}{\nu_i}\right] \tag{1}$$

where

$$\omega_k = \frac{kv_d}{1 + \Psi} \tag{2}$$

$$\Psi = \frac{\nu_i\nu_e}{\Omega_i\Omega_e} \tag{3}$$

and plasma scale length (L) in the vertical direction (Z) is given by

$$L = \left(\frac{1}{N}\frac{dN}{dZ}\right)^{-1} \tag{4}$$

The symbols N, ν, and Ω represent plasma density, collision frequency and gyro frequency respectively. The subscripts i and e correspond to the species ions and electrons, respectively. The symbols k, v_d and C_s denote wave number, electron drift in the zonal direction and ion acoustic speed, respectively. The primary waves in the zonal direction grow in the region whenever the growth rate γ_k is larger than the recombination rate ($2\alpha N$, where α is the recombination coefficient). The first term in Eq. (1) represents the growth of gradient drift waves while the second term corresponds to the growth of two stream waves. In the lower altitude (85–95 km) region, for the generation of gradient drift the first term is important.

The altitude variation of Ψ is large due to the exponential variation of collision frequencies. In earlier studies on equatorial electrojet, the value of Ψ is taken to be 1 around 100 km altitude (Rogister and D'Angelo, 1970) and 0.22 at 105 km (Kelley, 2009). However, the value of Ψ is much higher in the altitude range of 85–93 km, the region where the initiation of the gradient drift waves occur at different longitude sectors (to be discussed later). The present investigation aims to understand this longitudinal variation. Therefore, the values of Ψ fall in the range of a few hundred at 85 km to ~10 at 93 km. Thus, in this altitude range, the value of $1 + \Psi$ can be assumed to be equal to Ψ.

Thus

$$\gamma = \frac{v_d\Omega_e}{\Psi\nu_e L} \tag{5}$$

in other words

$$\gamma = \frac{\left(\frac{E_z}{B}\right)\Omega_e}{\Psi\nu_e L} \tag{6}$$

or

$$\gamma = \frac{E_z}{BL}\frac{\Omega_i\Omega_e^2}{\nu_i\nu_e^2} \tag{7}$$

Here E_z and B are the vertical polarization field and strength of geomagnetic field respectively. Since the gyro frequencies (Ω_i, Ω_e) of ions and electrons are proportional to B, the growth rate (γ) at lower altitude is proportional to B^2.

Simultaneous measurements of electric field, electron density profiles and neutral densities from Indian and American sectors are not available to evaluate the growth rate over American (γ_A) and Indian (γ_I) sectors. Therefore, the growth rate at 93 km altitude over American zone (γ_{93A}) is taken as a reference growth rate where the systematic measurements using Jicamarca radar reveal the initiation of Type-II echoes. The other growth rates are normalized to these values.

Examining Eq. (7), it is found that the variation of collision frequencies with altitude is dominant and hence this variation is only considered for further analysis. ν_i and ν_e are proportional to neutral densities which increase exponentially as the altitude decreases with respect to the reference altitude of 93 km. Thus, the altitude variation of the growth rate can be expressed as

$$\gamma_{hA}^h = \left(\frac{E_z}{BL}\right)_A \times \frac{\Omega_i\Omega_e^2}{(\nu_{i93})(\nu_{e93})^2 e^{(3(93-h))/H}} \tag{8}$$

where 'h' is the altitude lower than the reference altitude 93 (i.e. $93 \geq h > 85$) and H is the neutral density scale height.

Therefore,

$$\frac{\gamma_{hA}}{\gamma_{93A}} = \frac{1}{e^{(3(93-h))/H}} \tag{9}$$

Assuming the similar neutral atmospheric parameters over the Indian sector, the corresponding variation of growth rate can be written as

$$\frac{\gamma_{hI}}{\gamma_{93I}} = \frac{1}{e^{(3(93-h))/H}} \tag{10}$$

3. Results and discussion

It is clear from Eq. (7) that the growth rate of primary GD waves is proportional to the square of the strength of the geomagnetic field. As the growth rate increases with geomagnetic field strength, the h_{aoi} can be expected to be less. In order to verify the possible relation between the square of the geomagnetic field strength and h_{aoi}, observations where either radar or rocket data is available in the literature containing the h_{aoi} over certain dip equatorial stations are compiled and provided in Table 1 along with the strengths of the magnetic field based on the International Geomagnetic Reference Field (IGRF) model. Fig. 1 depicts the

Table 1

Location, geographic latitude and longitude, magnetic field strength (Gauss) obtained from the IGRF model, h_{aoi} of gradient drift waves obtained from either radar or in situ measurements and the relevant references are given.

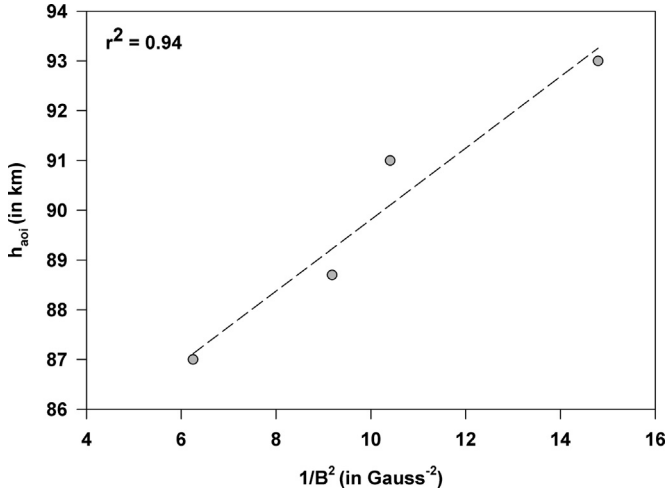| Location	Geog. lat./long. (deg)	B (Gauss)	h_{aoi} (km)	References
Thumba	8.5N/77E	0.40	87.0	Prakash et al. (1969) and Tiwari et al., 2003
Pohnpei	6.95N/158.2E	0.33	88.7	St. Maurice et al. (2003)
Alcantara	2.33S/44.4W	0.31	91.0	Lehmacher et al. (1997)
Jicamarca	12.5S/76.8W	0.26	93.0	Fejer et al. (1975) and Klaus and Smith (1978)

Fig. 1. The relation between altitude of initiation h_{aoi} of the gradient drift waves gleaned from different sources (see Table 1) and the inverse of the square of the strength of the geomagnetic field over corresponding longitude sectors.

relationship between geomagnetic field strength and h_{aoi}. The linear relation in Fig. 1 suggests that h_{aoi} is mainly controlled by the square of the strength of the magnetic field. This probably explains the variation in the lowermost altitude for the generation of gradient drift waves over Indian and American zones.

In order to ascertain this point, the growth rates of the primary GD waves over Indian and American longitudes need to be evaluated at the same time. As mentioned earlier, simultaneous measurements of all the parameters are not available from both sectors. Therefore, certain assumptions are made to evaluate the ratio of the growth rates of the primary GD waves over Indian and American zones (γ_I/γ_A). The neutral atmosphere is assumed to remain same over Indian and American zones. The plasma scale lengths observed around noon hours over Indian (Subbaraya et al., 1983) and American zones (Klaus and Smith, 1978) are nearly same probably due to similar photochemical equilibrium which governs the E-region ionosphere and its altitude structure. Therefore, the plasma scale length L is assumed to be the same over these two sectors. Using Eq. (7) and the values of B over Indian and American zones from Table 1, the ratio γ_I/γ_A turns out to be 2.4*(E_{zI}/E_{zA}), where E_{zI} and E_{zA} are the vertical polarization electric fields over Indian and American zones, respectively. The direct measurement of vertical polarization field is extremely sparse. The available values in the literature over Indian zone (Sartiel, 1977) and American zone (Pfaff et al., 1997) reveal the same value of ~5 mV/m at 99 km altitude and 10 mV/m at the altitude where the electrojet current is maximum. In general, the vertical polarization fields ($E_z = E_{sq}*\Sigma_H/\Sigma_P$) are inferred by using the product of global tidal zonal electric field (E_{sq}) and the ratio of integrated Hall (Σ_H) to Pedersen (Σ_P) conductivities (Σ_H/Σ_P). The calculated ratios of integrated conductivities over Indian zone (Anandarao et al., 1977) and over south American longitudes (Denardini, 2007) are estimated to be ~10 and ~15 at 90 km altitude, respectively. Assuming that the off-equatorial E_{sq} electric fields map over equatorial F region, the E_{sq} fields over Indian and American longitudes can be obtained by multiplying the corresponding geomagnetic field strengths with the drifts obtained from the Scherliess and Fejer model (Scherliess and Fejer, 1999). The maximum deviation in the E_{sq} fields over Indian and American zones during daytime, thus obtained, is ~1.0 mV/m and ~0.6 mV/m, respectively. Therefore, the ratio of the vertical polarization fields over Indian and American zones can be expected to vary within 10% that appears to have secondary effect in the determination of h_{aoi}. Thus, h_{aoi} at different longitudes in the vicinity of the

dip equator appears to be independent of dynamically varying paramater like vertical polarization electric field. Most importantly, this inference gets support from a number (16) of daytime rocket flight measurements conducted at different local times (between 0600 and 1800 h) on normal electrojet days from Thumba (Gupta, 2001) revealing electron density fluctuations with the characteristic of plasma turbulence (as described in the Introduction section) and h_{aoi} to be at 87 km irrespective of having different strengths of vertical polarization electric fields during daytime. This suggests that if one neglects the effects of collision, the vertical polarization electric field in the vicinity of the dip equator over Indian and American longitudes will be sufficient for the generation of GD waves at the base of E-region (~87 km) under suitable plasma density gradients to overcome the effects due to recombination. However, the growth of GD waves will be impeded by collisions where the ratio of collision to gyro frequencies is larger. Assuming that the collision frequencies are same over Indian and American longitudes, the larger gyro frequencies of electrons and ions bring down the h_{aoi} to 87 km over Indian sector in comparison to 93 km over American sector. For the calculation of relative growth rate (γ_I/γ_A) and discussion in the subsequent paragraph, the ratio of polarization electric field over Indian and American zone is assumed to be unity. The consequences of relaxing this assumption are also discussed.

In order to examine whether the increase in the growth rate over Indian zone compared to the American zone is sufficient to explain the initiation of gradient drift waves over Indian zone at lower altitude, the following exercise is carried out. The relative growth rates (compared to 93 km, where the value is taken as unity) over the American zone are calculated using Eq. (9) with a neutral scale height value of 6 km (H=6 km). Similar calculations were done over Indian longitudes using Eq. (10) and taking $\gamma_{93I} = 2.4\gamma_{93A}$ due to the differences in the strength of the geomagnetic field over these regions. Fig. 2 depicts the altitude profiles of the relative growth of gradient drift waves over American and Indian zones. In order to compare with the normalized decay rate, the relative recombination rates ($2\alpha N_{eh}/2\alpha N_{e93}$) are overlaid in Fig. 2. This curve based on average electron number densities during daytime is obtained from several rocket flight measurements (Subbaraya et al., 1983) carried out from Thumba. It may also be noted that based on the calculation of differences in the growth rate with respect to recombination rate (~25%) around
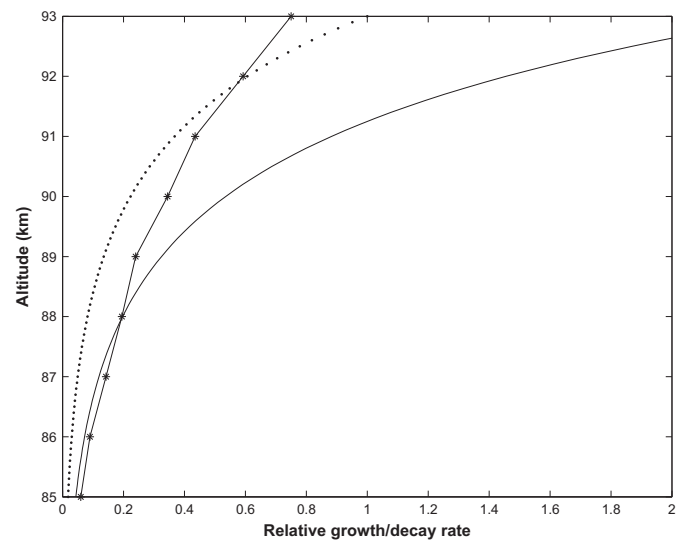

Fig. 2. Altitude of variation of relative growth rates over Indian (solid line) and American (dotted line) sectors based on Eqs. (9) and (10). Relative decay rate (marked by asterisks) obtained based on electron densities obtained from Thumba is also overlaid.

95 km (Pfaff et al., 1985), it is assumed that there exists 10% difference at 93 km between them to explain the observations over Jicamarca. From Fig. 2, it is clear that the relative growth rate of the gradient drift waves is larger than the relative recombination rate at 88 km over Indian longitudes while the same over American longitude is around 92 km. Thus, the combined effects of increased growth rate due to the strength of the magnetic field and the reduction in the decay rate due to the low electron number densities contribute to the initiation of gradient drift waves as low as about 88 km over Indian longitudes. The slight departure from the observation in the lowermost altitudes over Indian and American zones is probably due to various assumptions involved in obtaining Fig. 2.

The assumption of same vertical polarization field over Indian and American zones is not expected to alter the conclusion on h_{aoi} as long as the vertical electric fields are significant. This happens in the vicinity of the dip equator above certain altitudes probably ~88 km. At altitudes lower than this, certain variations are expected with the strength of the electric field. Further, h_{aoi} over off-equatorial station like Gadanki (12.5° dip), India, where the vertical electric fields are small compared to dip equatorial stations, h_{aoi} is expected to vary with local time with the variation of electric field and plasma density. The observations over Gadanki by Choudhary et al. (1996) reveal a decrease in h_{aoi} with time.

Finally, it is to be noted that the dependence on the square of the strength of the magnetic field is essentially applicable at lower altitude ($93 \geq h > 85$ km) where the approximation $(1 + \Psi) \approx \Psi$ can be made. Thus, the dependence will not be entirely agreeable at the equatorial electrojet altitude region (~105 km) as $\Psi < 1$ at this height. Further, examination of the growth rate expression (Sudan et al., 1973) of the vertically propagating secondary waves, the growth rate corresponding to secondary waves is proportional to cube of strength of magnetic field at lower altitudes and square of the amplitude of the primary waves. Thus, even smaller amplitudes of primary waves at lower altitude can lead to significant secondary waves where the strength of the magnetic fields is stronger.

4. Conclusions

Examination of linear growth rate expression of the gradient drift waves in the range of 85–93 km in the vicinity of the dip equator reveals that the growth rate depends on the square of the magnetic field strength. The increase in the growth rate over Indian longitudes due to geomagnetic field strength in conjunction with the lower decay rate due to less electron densities at lower altitudes explains the initiation of these waves at a lower altitude compared to their counterpart over Jicamarca.

Acknowledgments

References

Anandarao, B.G., Desai, J.N., Giles, M., Martelli, G., Raghavarao, R., Rothwell, P., 1977. Electric fields in the equatorial ionosphere. J. Atmos. Terr. Phys. 39, 927–933.

Choudhary, R.K., Mahajan, K.K., Singh, Sachchidanand, Kumar, Keshav, Anandan, V. K., 1996. First VHF radar observations of tropical latitude E-region field aligned irregularities. Geophys. Res. Lett. 23, 3683–3686.

Denardini, C.M., 2007. A conductivity model for the Brazilian equatorial E-region: initial results. Rev. Bras. Geof. 25, 87–94.

Fejer, B.G., Farley, D.T., Balsley, B.B., Woodman, R.F., 1975. Vertical structure of the VHF backscattering region in the equatorial electrojet and the gradient drift instability. J. Geophys. Res. 80, 1313–1324.

Gupta, S.P., 2001. Collected Works. Physical Research Laboratory, India.

Kelley, M.C., 2009. The Earth's Ionosphere: Plasma Physics and Electrodynamics. Academic Press, San Diego, USA.

Klaus, D.E., Smith, L.G., 1978. Rocket Observations of Electron-Density Irregularities in the Equatorial Ionosphere Below 200 km. Aeronomy Report No. 80, University of Illinois, Urbana.

Krishna Murthy, B.V., Ravindran, Sudha, Viswanathan, K.S., Subbarao, K.S.V., Patra, A.K., Rao, P.B., 1998. Small-scale (~3 m) irregularities at and off the magnetic equator. J. Geophys. Res. 103, 20761–20772.

Lehmacher, G.A., Goldberg, R.A., Schmidline, F.J., Croskey, C.L., Mitchell, J.D., Swartz, W.E., 1997. Electron density fluctuations in the equatorial mesosphere: neutral turbulence or plasma instabilities. Geophys. Res. Lett. 94, 1715–1718.

Pfaff Jr., R.F., Acuña, M.H., Marionni, P.A., Trivedi, N.B., 1997. DC polarization electric field, current density, and plasma density measurements in the daytime equatorial electrojet. Geophys. Res. Lett. 24, 1667–1670.

Pfaff, R.F., Kelley, M.C., Fejer, B.G., Maynard, N.C., Brace, L.H., Ledley, B.G., Smith, L.G., Woodman, R.F., 1985. Comparative in situ studies of the unstable day-time equatorial E-region. J. Atmos. Terr. Phys. 47, 791–811.

Prakash, S., Gupta, S.P., Subbaraya, B.H., 1969. Irregularities in E region over Thumba. Radio Sci. 4, 791–796.

Prakash, S., Gupta, S.P., Subbaraya, B.H., 1971. Experimental evidence for cross field instability in the equatorial ionosphere. Space Res. XI, 1139–1145.

Prakash, S., Gupta, S.P., Subbaraya, B.H., Pandey, R., 1979. Electric fields in the E-region during counter electrojet. Space Res. 19, 279–282.

Prakash, S., Gupta, S.P., Subbaraya, B.H., Pandey, R., 1980. A review of the electron density irregularities in the equatorial D and E regions. Adv. Space Explor. 8, 3–16.

Rogister, A., D'Angelo, N., 1970. Type II irregularities in the equatorial electrojet. J. Geophys. Res. 75, 3879–3887.

Sartiel, J., 1977. Champs Electrques Dan La Region de L' electrojet Equatorial (Ph.D. thesis). L'Université Pierre et Marie Curie, Paris VI, France.

Scherliess, L., Fejer, B.G., 1999. Radar and satellite global equatorial F region vertical drift model. J. Geophys. Res. 104, 6829–6842.

Sekar, R., Gupta, S.P., Acharya, Y.B., Chakrabarty, D., Pallamraju, D., Pathan, B.M., Tiwari, Diwakar, 2013. Absence of streaming plasma waves around noon time over Thumba in recent times: is it related to the movement of the dip equator?. J. Atmos. Sol-Terr. Phys. 103, 8–15.

St. Maurice, J.P., Choudhary, R.K., Ecklund, W.L., Tsunoda, R.T., 2003. Fast Type I waves in the equatorial electrojet: evidence for the non isothermal ion acoustic speeds in the lower E region. J. Geophys. Res. 108, A5. http://dx.doi.org/10.1029/2002JA009648 1170.

Subbaraya, B.H., Prakash, S., Gupta, S.P., 1983. Electron Densities in the Equatorial Lower Ionosphere from the Langmuir Probe Experiments Conducted at Thumba During 1966–1978, ISRO Scientific Report, ISRO-PRL-SR-15-83.

Sudan, R.N., Akinrimisi, J., Farley, D.T., 1973. Generation of small-scale irregularities in the equatorial electrojet. J. Geophys. Res. 78, 240–248.

Tiwari, D., Patra, A.K., Viswanathan, K.S., Jyoti, N., Devasia, C.V., Subbarao, K.S.V., Sridharan, R., 2003. Simultaneous radar observations of the electrojet plasma irregularities at 18 and 54.95 MHz over Trivandrum, India. J. Geophys. Res. 108, 1368. http://dx.doi.org/10.1029/2002JA009698, A10.
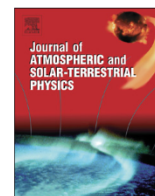
Characteristics of E-region background ionosphere and plasma waves measured over the dip equator during total solar eclipse campaign

R. Sekar *, S.P. Gupta, D. Chakrabarty

Physical Research Laboratory, Ahmedabad 380009, India

ABSTRACT

A unique set of rocket flight measurements of plasma parameters from the dip equator (Thumba; 8.5°N, 76.5°E, dip 0.5°S) was carried out at two obscuration levels (40% and 72%) on a total solar eclipse day (16 February 1980) which was also under a moderately disturbed geomagnetic condition. The path of totality was 400 km north of Thumba. Another rocket flight was conducted on 17 February 1980 to obtain the control day measurement at the same local time. As expected, the electron densities are found to be less throughout the measured altitude region on a solar eclipse day with the 72% obscuration level compared to the control day at the same local time (same solar zenith angle). In the presence of average electron density scale length of 10 and 9 km in the altitude region of 88–100 km, the initiation of the gradient drift waves is observed at altitudes of 91 and 93 km during 40% and 72% obscuration levels respectively on a solar eclipse day. However, on a control day, in the presence of average electron density scale length of 9 km, these waves are found at altitude as low as 88 km. In addition, the amplitude of the gradient drift waves is found to be the largest during the 72% obscuration level compared to those during the 40% obscuration level and control day. In the absence of electric field measurements, the magnetometer observations are used to infer an increase in the polarization electric field when the obscuration level is around 72%. This along with steeper gradient can account for the increase in the amplitude of gradient drift waves during 72% obscuration compared to 40% obscuration. The relative role of the growth and decay of the gradient drift waves is discussed in the context of these observations.

© 2014 Elsevier Ltd. All rights reserved.

1. Introduction

It is well known that a jet of current flows in a narrow altitude region (~ 105 km) over the dip equator owing to the development of a strong vertical polarization electric field due to the abatement of vertical flow of electrons by inhibiting boundaries. The maximum magnitude of this vertical electric field is about 30 times larger than the S_q electric field driven by global tidal winds through dynamo action. The existence of the vertical electric field for the development of equatorial electrojet was realized by the theories (Forbes, 1981) and numerical models (e.g. Sugiura and Cain, 1966; Richmond, 1973a,b; Anandarao and Raghavarao, 1987). However, direct measurements of vertical electric fields (e.g. Sartiel, 1977; Pfaff et al., 1997) are sparse owing to various technical difficulties. Inferences (e.g. Prakash et al., 1970, 1972, 1979) of the polarity of this electric field have been obtained by the measurements of the plasma waves that are associated with the equatorial electrojet. It is well-known that the E-region of the ionosphere supports two types of plasma waves over a dip equatorial station like Thumba. These are the gradient drift and streaming plasma waves (Kelley, 2009).

Simultaneous measurements of electron density and the normalized fluctuations in the gradient drift wave are extremely useful to understand generation processes of gradient drift waves in the E-region. The laboratory simulation of gradient drift waves was obtained initially by Simon (1963). Later, these waves have been observed in ionosphere at the locations where the background electric fields are parallel to the gradient in the electron density (e.g. Reid, 1968; Prakash et al., 1972; Fejer and Kelley, 1980; Kelley, 2009). In addition, the earlier rocket measurements (Prakash et al., 1979) from India revealed that the gradient drift waves are absent in the positive density gradient region during afternoon counter-electrojet event when the vertical polarization field is directed downward. Further, earlier work (Prakash et al., 1970) also revealed the simultaneous presence and absence of gradient drift waves in the negative and positive density gradient regions respectively below the valley region of the electron density profile during nighttime. These aspects were also confirmed over the American zone (Kelley, 2009). However, the in situ measurements of gradient drift waves at two obscuration levels during a solar eclipse are not reported so far.

The characteristics of the gradient drift waves had been investigated using Langmuir probe measurements from Thumba,

* Corresponding author: Tel.: +91 79 26314653; fax: +91 79 26314659.
E-mail address: rsekar@prl.res.in (R. Sekar).

India (e.g. Prakash et al., 1972; Subbaraya et al., 1983) and other places (e.g. Pfaff and et al., 1987). The characteristics of plasma waves at and off the equator were also obtained by in situ measurements (Gupta, 1997). The normalized fluctuations of the gradient drift waves were found to increase with scale sizes in the range of 1–15 m. Such simultaneous measurements of electron density profiles and the normalized fluctuations in gradient drift waves were obtained over Thumba over the years. Among the several rocket flight measurements that have been conducted from Thumba, a few of them were flown during total and annular solar eclipse events to understand the variations in the ionosphere when there is a change in the intensity level of the incoming solar radiation. Recently conducted rocket flight from Thumba during an annular solar eclipse event on 15 January 2010 indicated that the strength of gradient drift waves was less on this day compared to the control day (Sekar et al., 2011). As there were no multiple rocket flights with identical payloads at different obscuration levels during the 15 January 2010 event, the progressive change in the characteristics of gradient drift waves could not be ascertained unambiguously based on this rocket data. This stimulated us to re-look into the measurements obtained on a total solar eclipse event on 16 February 1980 when two rocket flights were conducted from Thumba at two obscuration levels. This campaign provided a unique opportunity to capture the changes in the development of E-region gradient drift waves during the solar eclipse. In addition, comparison of the development of these waves at a given local time during a solar eclipse day vis-a-vis a control day, is possible based on the measurements obtained in this campaign. Interestingly, both the solar eclipse events are concomitant with space weather disturbances in varying degrees. It must be noted here that some of the results obtained based on the 16 February 1980 event like the variations in the ratio of negative ions to electron density in the mesospheric altitudes (Gupta and Chakrabarty, 1982) and the geomagnetic field variations over the Indian zone (Rastogi et al., 1982), were already reported. However, as mentioned earlier, the issue of the changes in the characteristics of E-region gradient drift waves at different levels of solar obscuration and on control day was not addressed earlier. In the present work, the measured ionospheric electron density profiles and the normalized fluctuations in the gradient drift waves on 16 and 17 February 1980 are presented. The present work highlights the decay process of the gradient drift waves at lower altitudes with the progress of solar eclipse. Further, the increase in magnitude of vertical electric field around 100 km in the E-region is inferred from ground based magnetometer observations.

2. Details of observations

Two Centaure rockets were launched from Thumba (8.5°N, 76.5°E, dip 0.5°S) on 16 February 1980 at 1454 and 1522 IST (Indian Standard Time, IST=Universal time, UT + 5.5 h) at 40% and 72% obscuration of solar disc. Another Centaure rocket was launched on 17 February 1980 at 1522 IST from Thumba to get the corresponding observations on control day. These rockets were containing Langmuir probes as payload to measure electron densities and plasma waves. The probe sensor was connected to the electrometer amplifier to measure probe current whose dynamical range was 10^{-9}–2×10^{-5} A. This large dynamical range was achieved by using an automatic gain switching system which connects to different feedback resistances. The switching system was made to reset electronically after every second. The output voltage of the main channel was telemetered to the ground station. The main channel provided the background electron density (N_o). For the measurements of the plasma waves, the

voltage output from the electrometer was passed through a band-pass filter with a 3 dB bandwidth of 70–1000 Hz. In order to accommodate the output voltage within the telemetered range, the filtered output was fed to an AC amplifier with a gain of 40. Subsequently, the AC amplifier output was telemetered to the IRIG channel which had an acceptance limit up to 1 kHz. As the rocket velocities for these three flights were ∼1 km s^{-1} between the altitude region of 85–110 km, the scale sizes of the measured irregularities correspond to around 15 to 1 m for the AC channel of 70–1000 Hz. The normalized percentage fluctuations ($\Delta N/N_o \times 100$) are evaluated to quantify the plasma waves.

Several rocket flights were conducted using similar probes at various times (Subbaraya et al., 1983). The absence of fluctuations in electron density in the altitude region above 85 km during counter electrojet times (Prakash et al., 1976) and during nighttime above 85 km in the positive gradient region reveals that the ac channel of the probe is sensitive to plasma processes above 85 km altitude. In addition, the detection of type-II echoes in an altitude as low as 87 km (Choudhary et al., 1996; Patra et al., 2006) using a radar beam orthogonal to geomagnetic field by 53 MHz VHF radar over Indian low latitude station supports the observations by Langmuir probes over the Indian sector.

A network of observatories to continuously monitor the geo-magnetic variations at several Indian stations, is operated by the Indian Institute of Geomagnetism. During this solar eclipse period, magnetic measurements were carried out from Trivandrum in the equatorial region. These measurements were carried out using an analog classical magnetometer with the resolution of 1 nT and the magnetograms were digitized for 3-min intervals for 13, 15 and 16 February 1980 (Rastogi et al., 1982). The support is taken from the published work of Rastogi et al. (1982) to infer the variations in the E-region of the ionosphere on 16 February 1980. Fig. 1 depicts the map of Indian subcontinent showing the path of totality of the solar eclipse of 16 February 1980 and the network of Indian magnetic observatories used in the present investigation. The rocket launch station (TRD) and the position of the dip equator in 1980 are also marked in Fig. 1. The ground projection of rocket trajectory and the range corresponding to 100 km are marked in this figure. These details are nearly the same within ± 3° in launch azimuth for all the three rocket flights. In addition to these observatories shown in Fig. 1, magnetometer observations from Tashkent (TAS) (presently in Uzbekistan) along the similar long-itudinal chain were also used. It is to be noted that the rocket flights were flown from Thumba (TRD), a station around 400 km away from the path of totality.

3. Results

The altitude profiles of electron densities along with the percentage of normalized fluctuations due to the plasma waves on the solar eclipse day at 40% and 72% obscuration levels are depicted in Fig. 2a and b respectively. These profiles correspond to upleg of the rocket trajectory. The decrease in the electron density with the increase in obscuration is more pronounced at 85 km compared to 105 km. Further, the valley region in the electron density profile around 120 km becomes slightly deeper with the increase in the obscuration level. The fluctuations associated with the streaming waves in the altitude region of 105–107 km are found to be absent. Further, the fluctuations in the altitude region in the presence of positive density gradients are due to gradient drift waves. The altitude extent of the gradient drift waves was found to change from 91–102 km at the 40% obscuration level to 93–102 km at the 72% obscuration level. Even though a strong plasma density gradient is present at the lower altitude region (85–88 km), the gradient drift waves are found to be absent. The
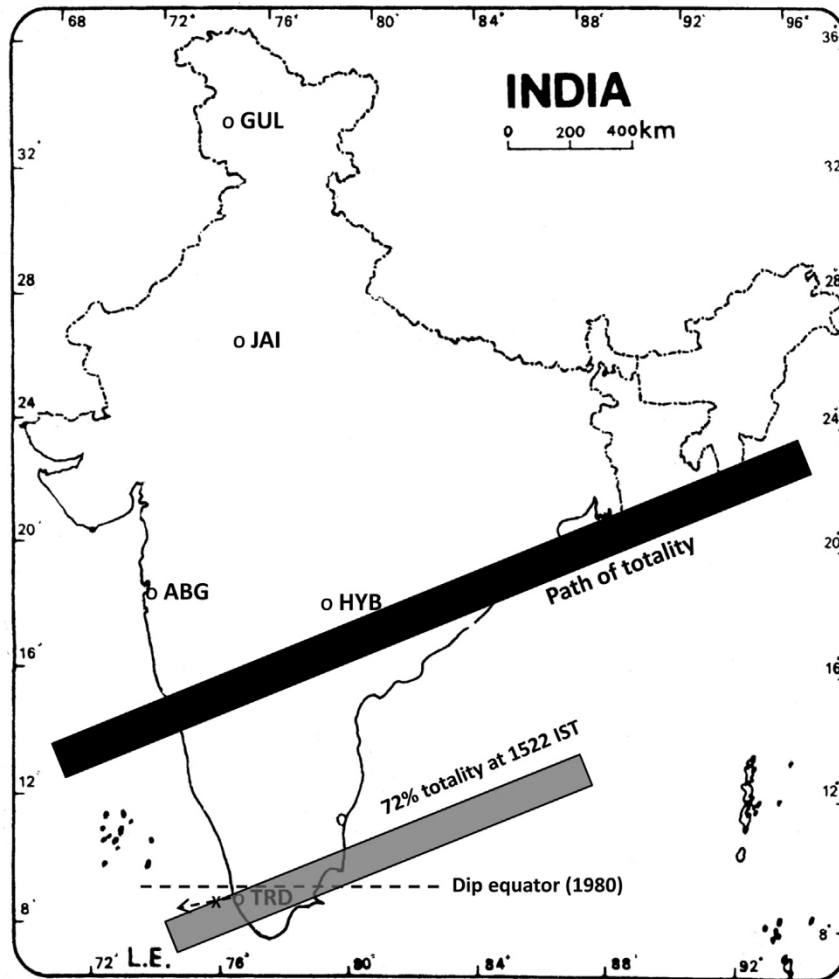
Fig. 1. The map of the Indian subcontinent showing the path of totality of the solar eclipse of 16 February 1980 and the network of magnetic observatories used in the present investigation. The locations of the dip equator and the rocket launch station are marked. The ground projection of the rocket trajectory and the range corresponding to 100 km altitude (marked by triangle) are shown.

average plasma scale lengths, in the altitude regions of 88–100 km where the gradient drift waves were present, were around 10 and 9 km at 1454 and 1522 IST respectively. Further, the amplitude of fluctuations of the gradient drift plasma waves at 100–101 km was found to be large when the obscuration level increases. The roles of plasma density gradient and electric field will be discussed in the discussion section.

The altitude profiles of the electron density and the percentage of fluctuations of the gradient drift waves measured at the same local time (1522 IST) on the solar eclipse day (at the 72% obscuration level on 16 February, 1980) and on a control day (17 February 1980) are depicted in Fig. 3a and b respectively. These profiles correspond to upleg of the rocket trajectory. The electron density was found to reduce considerably all through the altitude on solar eclipse day compared to the control day. The plasma density gradient on the eclipse day is slightly more around 85 km altitude compared to the control day. However, the average plasma scale length between 88 and 100 km is nearly the same (~9 km) on both the days. However, the altitude extent of the existence of gradient drift waves was found to be larger on control day (88–103 km) compared to the solar eclipse day with 72% obscuration. In addition, the amplitudes of fluctuations were, on and average, more on 16 February and the valley region was slightly deeper on the solar eclipse day compared to the control day. The relative roles of the growth and decay of the gradient drift waves will be addressed in the discussion section.

In the absence of electric field measurement which drives the gradient drift wave, the magnetometer data are used to infer the polarity and the relative strength of the electric field. Fig. 4 is reproduced from Rastogi et al. (1982) wherein the temporal variation of differences between the horizontal components of geomagnetic field (H) from various stations with respect to the same at Gulmarg (GUL) station are plotted for 13, 15 and 16 February 1980. It may be noted that in order to extract the ionospheric part and to eliminate the magnetospheric contribution, the Gulmarg station is chosen as the reference where solar eclipse effects are considered negligible for this event (Rastogi et al., 1982). In this figure, TAS, JAI, ABG, HYB and TRD stand for Tashkent, Jaipur, Alibag, Hyderabad and Trivandrum respectively. As these observations were not compared with the simultaneous in situ ionospheric measurements, definite eclipse induced effects in the geomagnetic field (Rastogi et al., 1982) could not be identified by them. It is of interest to note from Fig. 4 that after the first contact, the decrease in the geomagnetic field variation at TRD with respect to GUL (henceforth, denoted by ΔH_{TRD}) is found to be steeper than the other stations and a small but noticeable increase is also observed only over Thumba at around 70% obscuration level. The importance of this observation in terms of the modification of the vertical polarization field will be discussed in the subsequent section. Further, the control day geomagnetic field observations on 13 February 1980 over different stations were found to be smooth. In contrast, the geomagnetic field observations over different stations on 16 February 1980 revealed small scale fluctuations. Particularly,
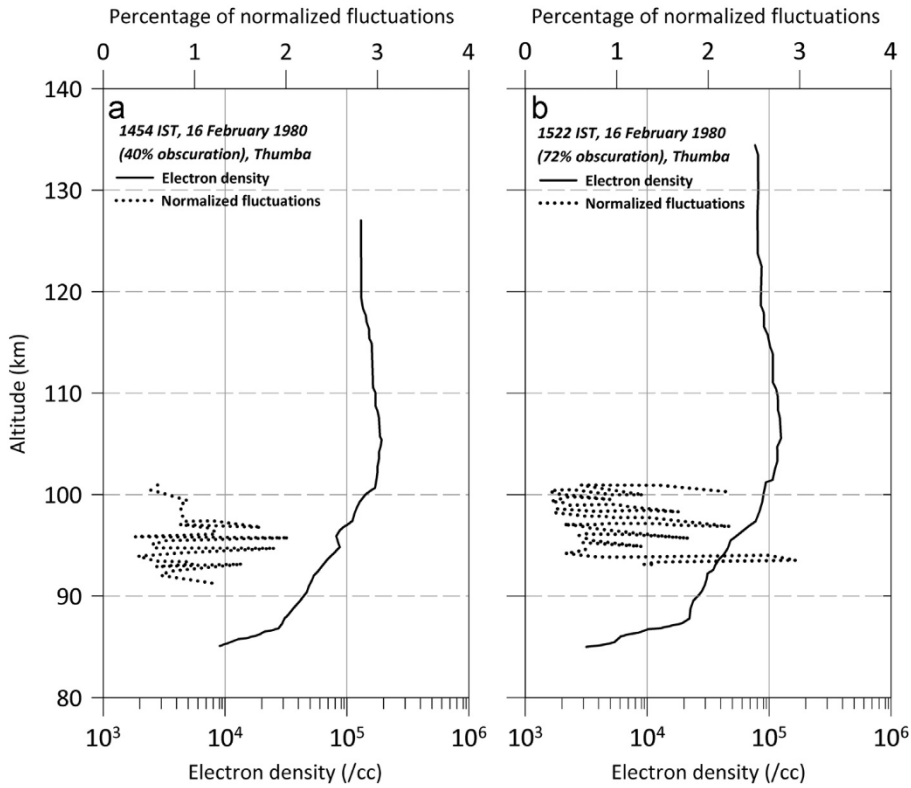
Fig. 2. Altitude profiles of electron densities (solid line) and percentage of normalized fluctuations (dotted line) on the solar eclipse event (16 February 1980) at (a) 40% obscuration level and (b) 72% obscuration level.
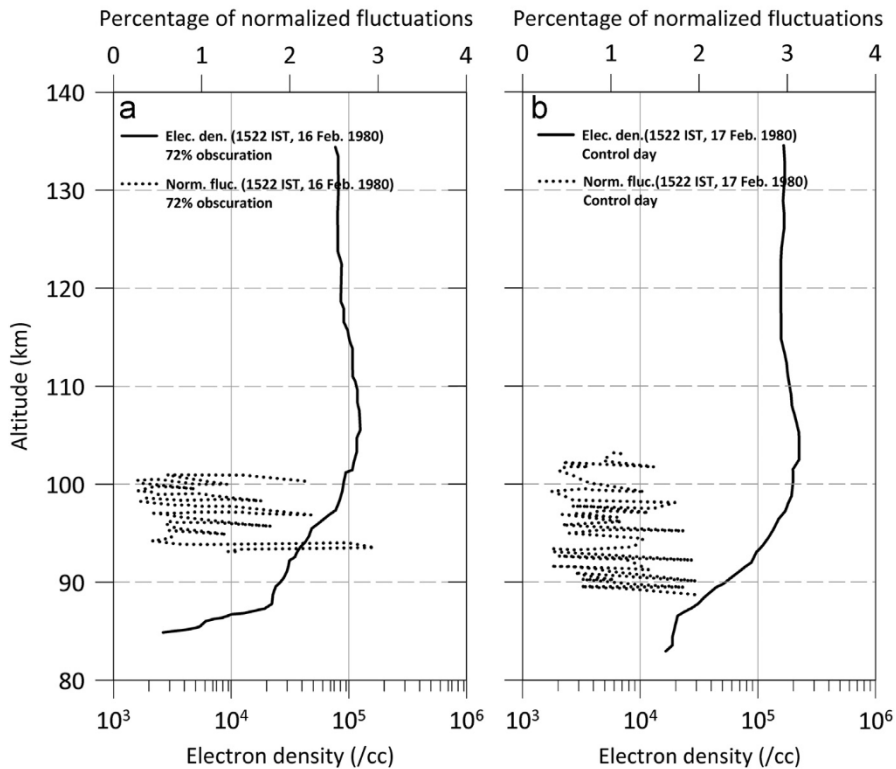

Fig. 3. Comparison of the profiles of electron densities and the percentage of normalized fluctuations obtained at the same time (1522 IST) over Thumba (a) on a solar eclipse day (16 February 1980), (b) with a control day (17 February 1980).

the temporal variations in ΔH_{TRD} over Thumba on 16 February seem to have additional periodicities besides having similar periods observed over other stations.

The equatorial electric field can be modified by penetration electric fields associated with geomagnetic storms and substorms and also due to the waves in the neutral atmosphere during solar
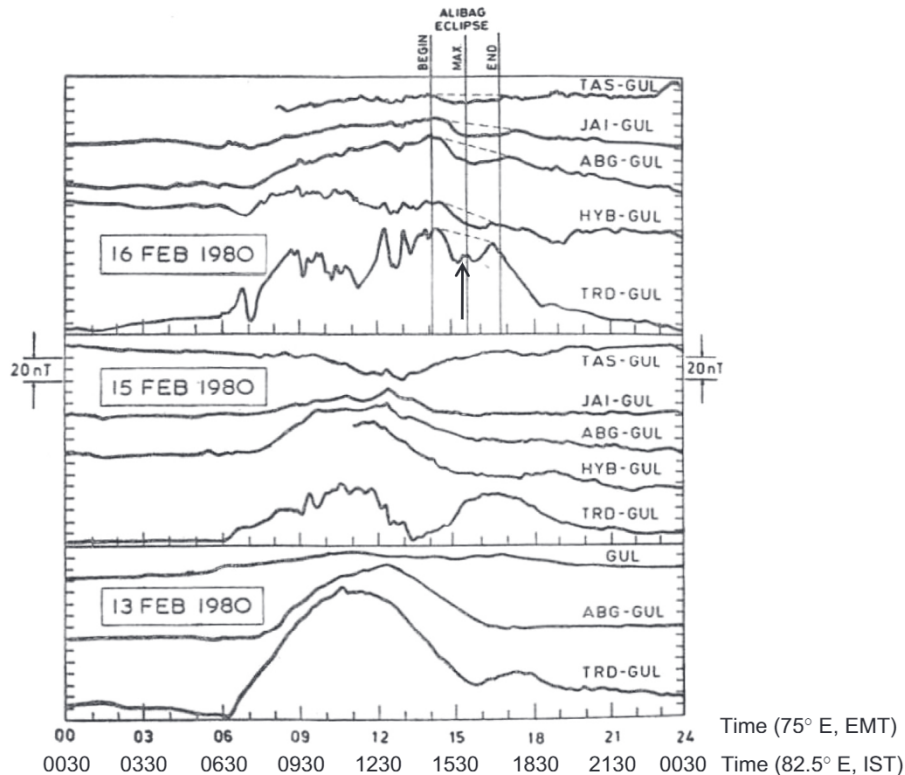
Fig. 4. Temporal variations of differences between the horizontal component of geomagnetic field from various stations (defined in the text) with respect to Gulmarg (GUL) station for 13, 15 and 16 February 1980. The temporal resolution is 3 min. The eclipse duration is marked by vertical lines on 16 February 1980. The abbreviations "TAS", "JAI", "ABG", "HYB" and "TRD" stand for Tashkent, Jaipur, Alibag, Hyderabad and Trivandrum respectively. The arrow indicates the time of launch of the second rocket. Reproduced from Rastogi et al. (1982).

eclipse and/or geomagnetic storm which was prevalent during this campaign. In order to delineate the source, an attempt is made to carry out spectral analyses on the magnetometer data as the direct electric field measurements are not available. As the common periodic components over all the stations may be attributed to the global storm time electric field variations, periodogram analyses of geomagnetic field variations observed over different latitudes are performed using a standard methodology (Schulz and Stattegger, 1997). In the absence of the ascii data, the magnetograms are digitized with high resolution and the corresponding time series of the magnetic variations for all the stations are generated for the 0600–1800 h duration. As the digitization process could not generate evenly sampled data, the above algorithm is chosen which can handle unevenly sampled data to obtain periodic components. Further, the spectral analysis was done after detrending (filtering out in the spectral domain) the tidal components (> 3.0 hr). The spectral analyses generate normalized periodograms in which power contained in each spectral element is normalized with respect to the total power contained in all the spectral elements taken together. This technique, thus, renders the relative distribution of the spectral power independent of the spectral windowing applied to avoid spectral leakage. The normalized periodograms for Thumba (TRD), Alibag (ABG), Jaipur (JAI) and Taskhent (TAS) are shown in Fig. 5. The magnetic variations over Hyderabad (HYB) are not considered as the latitudinal separation of ABG and HYB is not substantial. "Significant" frequency components in the periodograms exceed the critical level (marked by dotted lines) determined by Fisher's test. Therefore, Fig. 5 reveals the relative dominance of each periodic component in the time series. It is clear from Fig. 5 that the ~ 1.0 h periodicity is present over all the stations although it is significantly enhanced (above the critical level determined by Fisher's test) over Thumba. Further, the progressive decrease of

the normalized spectral power in the ~ 1.0 h component from TAS till ABG and then enhancement at the dip equatorial station TRD strongly suggest that this magnetic signature is associated with DP2 current fluctuations over low latitudes (e.g. Mene et al., 2011, and references cited therein). DP2 periodicities ranging from 0.5–1.0 h have been reported earlier (e.g. Chakrabarty et al., 2005, 2008) from low-equatorial latitude stations in India. In addition to this, ~ 2.0 periodicity is found to be present over TRD, ABG and JAI but not over TAS. Further, the normalized spectral power at this period is found to be maximum over TRD. At this juncture, it is interesting to note that the presence of ~ 64 min periodicity in the HF (5 MHz) Doppler velocity over Trivandrum was reported by Balan and Krishna Murthy (1982) and the presence of ~ 2.25 h periodicity was evident from the TEC variation over low latitudes (Deshpande et al., 1982) during this eclipse. Thus, the periodicities obtained in the present investigation get support from other independent measurements.

4. Discussion

As the observational time is around 1500 IST, the absence of streaming waves in all the three rocket flights is attributed to low level Sq electric field in the afternoon hours. The low level S_q electric field in the afternoon hours over Thumba is supported by the in situ magnetometer experiments conducted earlier (Sastry, 1970) and by the global empirical model of Scherliess and Fejer (1999). This is consistent with the earlier observations by rocket (Prakash et al., 1972) and radar (KrishnaMurthy et al., 1998) wherein the streaming waves are observed between 0900 and 1300 IST during daytime over Thumba. Thus, this indicates the observation was done in the descending phase of the tidally generated S_q electric field and required threshold electric field
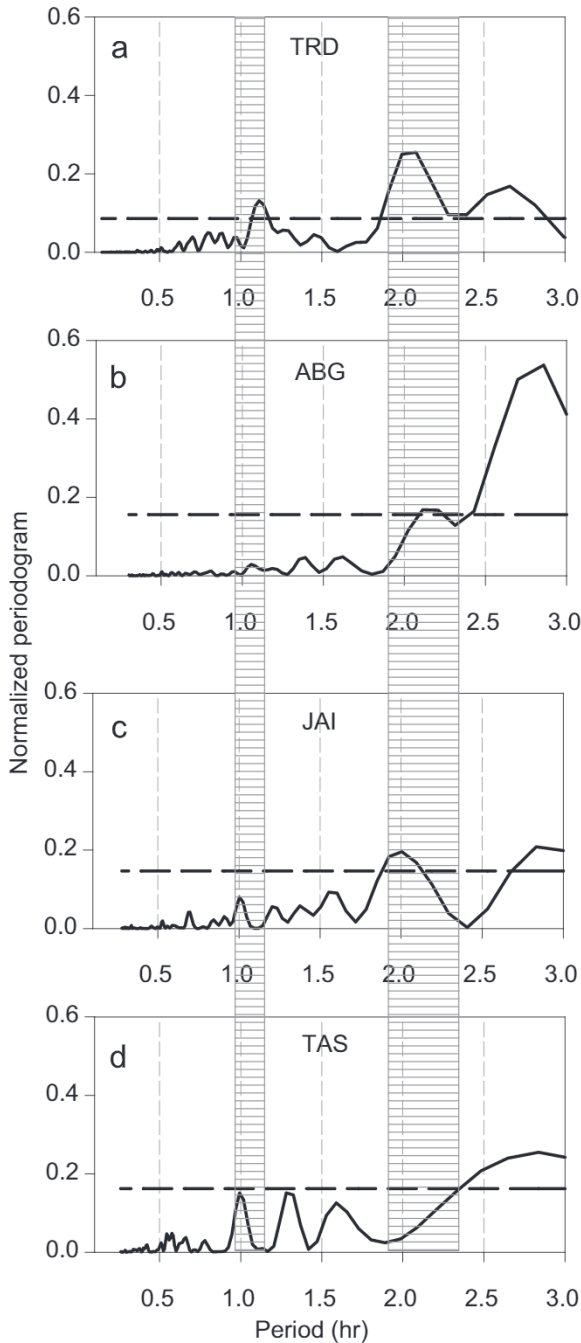
Fig. 5. Normalized periodograms of the daytime (0600–1800 h) magnetometer data from TRD, ABG, JAI and TAS with respect to GUL on 16 February 1980. Periodicities of ~1.0 and ~2.0 h are marked by hatched boxes. The critical levels determined by Fisher's test are marked by dashed lines in each subplot.

was not present to excite streaming plasma waves. Further, it is clearly evident from Fig. 2 that the E-region electron densities and therefore the conductivities were reducing with the degree of obscuration on solar eclipse day. Therefore, one expects a decrease in current density in the ionosphere which is evident from the rate of decrease of ΔH_{TRD} after the first contact as revealed in Fig. 4. The increase observed in the ΔH_{TRD} (see Fig. 4) at around 1522 IST can only be accounted by the increase in the electrojet current density owing to the enhancement in the vertical polarization electric field. The increase in the vertical electric field over the dip equator at the time of decreasing S_q electric field is possible through local winds (Anandarao, 1977; Reddy and Devasia, 1981;

Anandarao and Raghavarao, 1987; Raghavarao and Anandarao, 1987) in the altitude region of 100–105 km.

The role of local winds in the modification of the vertical polarization field is discussed by earlier researcher (Anandarao, 1977) by solving the current conservation equation under electrostatic condition and the following expression (Raghavarao and Anandarao, 1987) for the vertical electric field (E_r) is obtained.

$$E_r = -(W \times B)_r + \frac{\sigma_H}{\sigma_P} C[E_\phi + (W \times B)_\phi] + J_r(\rho_P C^2 + \rho_O S^2) - J_\theta(\rho_O - \rho_P)SC \tag{1}$$

In the above expression, (r, θ, ϕ) defines a geocentric coordinate system where r is the radial distance of the electrojet height region from the center of the earth (positive upward), θ is the co-latitude (positive northward) and ϕ is the longitude (positive eastward). Moreover, $\rho_O = 1/\sigma_O$, $\rho_P = 1/\sigma_P$, $S = \sin I$ and $C = \cos I$ where I, σ_O, σ_P, σ_H, W, B and J are the dip angle (positive southward), direct conductivity, Pedersen conductivity, Hall conductivity, neutral wind, geomagnetic field strength and electrojet current density respectively. It may be noted that the local and field-integrated conductivities yielded similar results in the E-region up to 120 km altitude (Anandarao et al., 1977). Therefore, only local values are considered for the present discussion. Examination of Eq. (1) reveals that the local westward wind at 100–105 km can enhance the polarization field E_r. The increase in ΔH_{TRD} over Thumba (not over other places, see Fig. 4) lasted for ~30 min only. The spectral analyses of magnetometer data revealed 1.0 h periodicity over all stations probably due to DP2 fluctuations and significant 2.0 h periodicity over Thumba. Thus, it is not clear that the increase in ΔH_{TRD} is due to the effects associated with geomagnetic storm or solar eclipse.

The presence and sustenance of a few meter scale sizes plasma waves in the lower altitude region (< 93 km) are not clearly understood. Earlier in situ measurements conducted from Chilca, Peru during afternoon hours (Klaus and Smith, 1978) revealed the presence of such plasma waves only above 93 km. The temporal sequence of the backscattered power from the electrojet region (Fejer et al., 1975) using 50 MHz Jicamarca radar also confirms the absence of 3 m plasma waves below 93 km during afternoon hours over American sector. However, the presence of such waves was noticed slightly below 93 km after midnight and early morning hours. Comparative studies of the unstable daytime equatorial E-region over American sector were carried out (Pfaff et al., 1985) using Jicamarca radar and in situ rocket measurements conducted from Peru at different local times. Calculations of linear growth rate of gradient drift waves at different altitudes based on these measurements revealed that the growth of scale sizes of a few meter is not conducive at lower altitudes as the growth rate of these waves is less compared to recombination rate. Further, the growth rate is less due to an increase in damping by collisions with decreasing altitude. In this context, it may be noted such growth rate calculation is not possible for the observations presented in this work as supporting measurements are not available. Thus the absence of plasma waves in spite of the presence of unstable gradient may be associated with damping effects. On the other hand, the presence of plasma waves over Thumba, India was reported even at 87 km altitude by Prakash et al. (1969) using in situ measurements. Based on many rocket flights from Thumba, the spectral indices of the small scale sizes were shown (Prakash et al., 1980) to lie between -3.5 ± 1.5 for the plasma waves obtained at 87 km and above. This is in contrast to the neutral turbulence induced small scale waves below 80 km whose spectral indices lie between -1.6 ± 0.7 (Prakash et al., 1980). Subsequently, VHF radar (53 MHz) experiments from Gadanki (6.3°N dip latitude) using a beam perpendicular to geomagnetic field also revealed the presence of ~3 m plasma waves at heights as low

as 87 km (Choudhary et al., 1996; Patra et al., 2006) in spite of the magnitude of the vertical electric field being less over a low latitude station like Gadanki. However, these works could not provide conclusively the reason for the presence and sustenance of the observed 3 m plasma waves at the lower altitude region over the Indian sector.

The differences in the generation of gradient drift waves during the flights can only be qualitatively discussed in the absence of rigorous electric field measurements. The average plasma scale length is slightly less during 72% obscuration compared to the measurement at 40% obscuration. Further, the relative strength of the electric field as inferred from the magnetometer measurements revealed that an increase in the vertical polarization field during the 72% obscuration level. Thus, it appears that higher plasma density gradient and relatively stronger vertical polarization field can account for the strongest amplitude of gradient drift waves observed during the 72% obscuration level. Despite these favorable conditions, the initiation of the gradient drift waves is observed at 93 km during 72% obscuration compared to the observation of 91 km during the 40% obscuration level. This suggest the decay of the gradient drift waves at lower altitude during the 72% obscuration level. This suggestion gets further support from the comparison of the measurements on eclipse (72%) and control day (at the same local time) wherein the initiation of gradient drift wave changed from 93 to 88 km altitude respectively. Thus the absence of the gradient drift waves at lower altitude is either due to increased recombination rate or due to the damping of these waves by collisions. The recombination rate coefficient (α), though depends on electron temperature (Torr and Torr, 1979), is not very sensitive to temperature variation associated with eclipse around 90 km altitude and below. Further, as the recombination rate (αN) is proportional to the electron density, it is expected to decrease with the obscuration level as evident in Figs. 2 and 3. This is conducive for the growth of plasma waves at a lower altitude. Therefore, at a given altitude, a recombination process cannot be the cause for the disappearance of plasma waves with the decrease in electron densities associated with the increasing obscuration during total solar eclipse. On the other hand, the growth rate expression (Sudan et al., 1973) depends on $\psi_o (= (\nu_e \nu_i / \omega_e \omega_i))$ where ν and ω are collision and gyrofrequencies respectively. The subscripts i and e denote ions and electrons respectively. It is suggested that the propagation of neutral waves might have altered neutral densities in the altitude region of 88–93 km with the progress of solar eclipse. Thus, the present set of measurements indicates the importance of quenching of gradient drift waves by collisions at lower altitudes with the progress of solar obscuration.
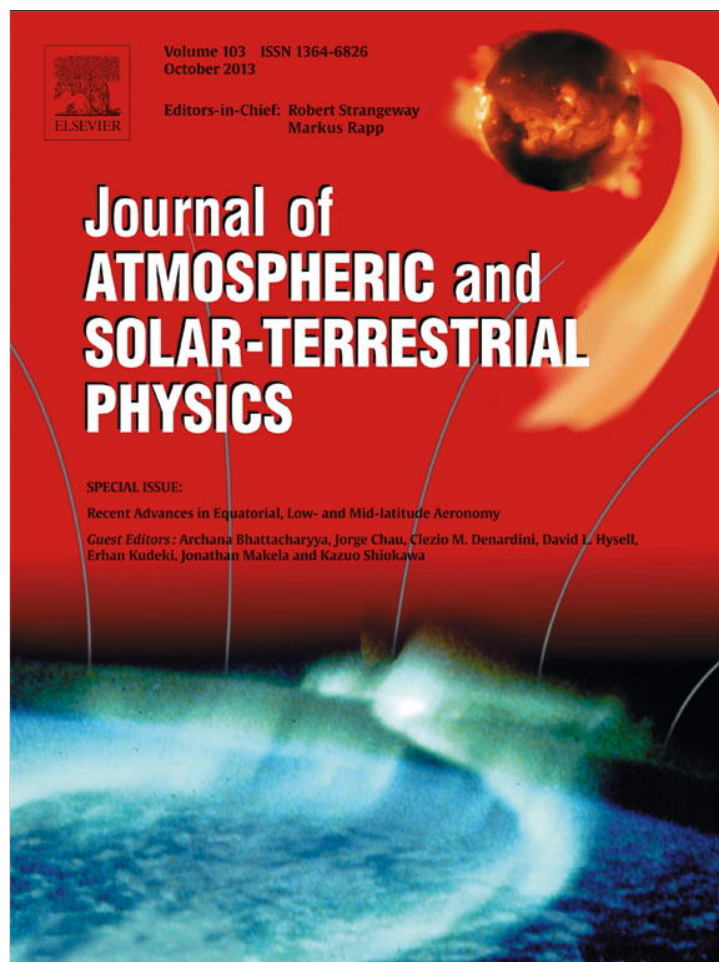
5. Summary

Three rockets containing Langmuir probes were flown from Thumba, India to measure electron densities and plasma waves during 16 and 17 February 1980. Two of the rockets were launched on a total solar eclipse day (16 February 1980) at 1454 IST (40% obscuration) and at 1522 IST (72% obscuration) respectively. The third rocket was flown on a control day (17 February 1980) at 1522 IST which is the same time as that of the rocket flight at an obscuration level of 70% on the previous day. As expected, the electron densities are found to be less throughout the measured altitude region on a solar eclipse day compared to the control day measured at the same local time. The streaming waves were absent in all the three flights probably due to low level S_q electric field during afternoon hours. The average electron density scale lengths in the altitude region of 88–100 km are 10 and 9 km on a solar eclipse day and ∼9 km on a control day. However, the

initiation of the gradient drift waves are observed at 91 and 93 km during the first two flights on solar eclipse day and 88 km on the control day. Further, the amplitude of the gradient drift waves is found to be the largest during the 72% obscuration level compared to the other two flights. The inferred polarization electric field was found to be more when the obscuration level was 72%. The largest amplitude can be attributed to the enhanced polarization field along with the steeper electron density gradient. The relative role of growth and the decay of the gradient drift waves is qualitatively discussed. These measurements indicate the importance of quenching of gradient drift waves by collisions at lower altitudes with the progress of solar obscuration levels.

References

Anandarao, B.G., 1977. Studies on the Dynamics of the Equatorial Ionosphere (Ph.D. thesis), Gujarat University.

Anandarao, B.G., Desai, J.N., Giles, M., Martelli, G., Raghavarao, R., Rothwell, P., 1977. Electric fields in the equatorial ionosphere. J. Atmos. Terr. Phys. 39, 927–933.

Anandarao, B., Raghavarao, R., 1987. Structural changes in the currents and fields of the equatorial electrojet due to zonal and meridional winds. J. Geophys. Res. 92, A3, http://dx.doi.org/10.1029/JA092iA03p02514.

Balan, N., Krishna Murthy, B.V., Raghava Reddi, C., Rao, P.B., Subbarao, K.S.V., 1982. Ionospheric disturbances during the total solar eclipse on 16 February 1980, Proc. Indian Natl. Sci. Acad. 48A (Suppl. 3), 406–415.

Chakrabarty, D., Sekar, R., Narayanan, R., Devasia, C.V., Pathan, B.M., 2005. Evidence for the interplanetary electric field effect on the OI 630.0 nm airglow over low latitude. J. Geophys. Res. 110, A11301, http://dx.doi.org/10.1029/2005JA011221.

Chakrabarty, D., Sekar, R., Sastri, J.H., Ravindran, S., 2008. Distinctive effects of interplanetary electric field and substorm on nighttime equatorial F layer: a case study. Geophys. Res. Lett. 35, L19108, http://dx.doi.org/10.1029/2008GL035415.

Choudhary, R.K., Mahajan, K.K., Singh, S., Kumar, K., Anandana, V.K., 1996. First VHF radar observations of tropical latitude E-region field-aligned irregularities. Geophys. Res. Lett. 23, 3683–3686.

Deshpande, M.R., Chandra, H., Sethia, G., Vats, H.O., Vyas, G.D., Iyer K.N., Janve, A.V., 1982. Effects of the total solar eclipse of 16 February 1980 on TEC at low latitudes, Proc. Indian Natl. Sci. Acad. 48A (Suppl. 3), 427–433.

Fejer, B.G., Farley, D.T., Balsley, B.B., Woodman, R.F., 1975. Vertical structure of the VHF backscattering region in the equatorial electrojet and the gradient drift instability. J. Geophys. Res. 80, 1313–1324.

Fejer, B.G., Kelley, M.C., 1980. Ionospheric irregularities. Rev. Geophys. Space Phys. 18, 401–454.

Forbes, J.M., 1981. The equatorial electrojet. Rev. Geophys. Space Phys. 19, 469–504.

Gupta, S.P., 1997. Features of E region irregularities at the magnetic equator and in its vicinity. Adv. Space Res. 20 (11), 2195–2198.

Gupta, S.P., Chakrabarty, D.K., 1982. On variation of λ and α_{eff} in the mesosphere during the solar eclipse of 16 February 1980 over India, Proc. Indian Natl. Sci. Acad., 48A (Suppl. 3), 518–522.

Kelley, M.C., 2009. The Earth's Ionosphere: Plasma Physics and Electrodynamics. Academic Press, San Diego, USA.

Klaus, D.E., Smith, L.G., 1978. Rocket observations of electron-density irregularities in the equatorial ionosphere below 200 km. Aeronomy Report No. 80, University of Illinois, Urbana.

KrishnaMurthy, B.V., Ravindran, S., Viswanathan, K.S., Subbarao, K.S.V., Patra, A.K., Rao, P.B., 1998. Small-scale (∼3 m) irregularities at and off the magnetic equator. J. Geophys. Res. 103, 20761–20772.

Mene, N.M., Kobea, A.T., Obrou, O.K., Zaka, K.Z., Boka, K., Amory-Mazaudier, C., Assamoi, P., 2011. Statistical study of the DP2 enhancement at the dayside dip-equator compared to low latitudes. Ann. Geophys. 29, 2225–2233, http://dx.doi.org/10.5194/angeo-29-2225-2011.

Patra, A.K., Sripathi, S., Rao, P.B., Choudhary, R.K., 2006. Gadanki radar observations of daytime E region echoes and structures extending down to 87 km. Ann. Geophys. 24, 1861–1869.

Pfaff, R.F., Kelley, M.C., Fejer, B.G., Maynard, N.C., Brace, L.H., Ledley, B.G., Smith, L.G., Woodman, R.F., 1985. Comparative in situ studies of the unstable day-time equatorial E-region. J. Atmos. Terr. Phys. 47, 791–811.

Pfaff, R.F., et al., 1987. Electric field and plasma density measurements in the strongly driven daytime equatorial electrojet: 1. The unstable layer and gradient drift waves. J. Geophys. Res. 92, 13578–13596.

Pfaff Jr., R.F., Acuña, M.H., Marionni, P.A., Trivedi, N.B., 1997. DC polarization electric field, current density, and plasma density measurements in the daytime equatorial electrojet. Geophys. Res. Lett. 24, 1667–1670.

Prakash, S., Gupta, S.P., Subbaraya, B.H., 1969. Irregularities in E region over Thumba. Radio Sci. 4, 791–796.

Prakash, S., Gupta, S.P., Subbaraya, B.H., 1970. A study of the irregularities in the nighttime equatorial E-region using a Langmuir probe and plasma noise probe. Planet Space Sci. 18, 1307–1318.

Prakash, S., Subbaraya, B.H., Gupta, S.P., 1972. Rocket measurements of ionization irregularities in the equatorial ionosphere at Thumba and identification of plasma instabilities. Indian J. Radio Space Phys. 1, 72–80.

Prakash, S., Gupta, S.P., Sinha, H.S.S., Rao, T.R., 1976. Ionization irregularities in the E region during counter electrojet. Space Res. XVI, 401–404.

Prakash, S., Gupta, S.P., Subbaraya, B.H., Pandey, R., 1979. Electric fields in the E-region during counter electrojet. Space Res. 19, 279–282.

Prakash, S., Gupta, S.P., Subbaraya, B.H., Pandey, R., 1980. A review of the electron density irregularities in the equatorial D and E regions. Adv. Space Explor. 8, 3–16.

Raghavarao, R., Anandarao, B.G., 1987. Equatorial electrojet and the counter-electrojet. Indian J. Radio Space Phys. 16, 54–75.

Rastogi, R.G., Rangarajan, G.K., Agarwal, A.K., 1982. Geomagnetic field observations in the Indian zone during the total solar eclipse of 16 February 1980, Proc. Indian Natl. Sci. Acad., 48A (Suppl 3), 482–488.

Reddy, C.A., Devasia, C.V., 1981. Height and latitude structure of electric fields and currents due to local east-west winds in the equatorial electrojet. J. Geophys. Res. 86, 5751–5767.

Reid, G.C., 1968. The formation of small scale irregularities in the ionosphere. J. Geophys. Res. 73, 1627–1640.

Richmond, A.D., 1973a. Equatorial electrojet, I, development of a model including winds and instabilities. J. Atmos. Terr. Phys. 35, 1083–1103.

Richmond, A.D., 1973b. Equatorial electrojet, II, use of the model to study the equatorial ionosphere. J. Atmos. Terr. Phys. 35, 1105–1118.

Sartiel, J., 1977. Champs Electrques Dan La Region de L' electrojet Equatorial (Ph.D. thesis), L'Universite' Pierre et Marie Curie - Paris VI, France.

Sastry, T.S.G., 1970. Diurnal changes in the parameters of the equatorial electrojet as observed by rocket-borne magnetometer. Space Res. 10, 778–785.

Scherliess, L., Fejer, B.G., 1999. Radar and satellite global equatorial F region vertical drift model. J. Geophys. Res. 104, 6829–6842.

Schulz, M., Stattegger, K., 1997. Spectrum: spectral analysis of unevenly spaced paleoclimatic time series. Comput. Geosci. 23, 929.

Sekar, R., Acharya, Y.B., Chakrabarty, D., Pallamraju, D., Gupta, S.P., Pathan, B.M., 2011. Investigations on the effects of annular solar eclipse in the equatorial ionosphere. In: Proceedings of the National Workshop: Results on Solar Eclipse (NaWRoSE), SPL, VSSC, pp. 59, January 27–28.

Simon, A., 1963. Instability of a partially ionized plasma in cross electric and magnetic field. Phys. Fluids 6, 382–388.

Subbaraya, B.H., Prakash, S., Gupta, S.P., 1983. Electron densities in the equatorial lower ionosphere from the Langmuir probe experiments conducted at Thumba during 1966–1978. ISRO Scientific Report, ISRO-PRL-SR-15-83.

Sudan, R.N., Akinrimisi, J., Farley, D.T., 1973. Generation of small-scale irregularities in the equatorial electrojet. J. Geophys. Res. 78, 240–248.

Sugiura, M.M., Cain, J.C., 1966. A model equatorial electrojet. J. Geophys. Res. 71, 1869–1877.

Torr, D.G., Torr, M.R., 1979. Chemistry of thermosphere and ionosphere. J. Atmos. Terr. Phys. 41, 797–839.

Absence of streaming plasma waves around noontime over Thumba in recent times: Is it related to the movement of the dip equator?

CrossMark

R. Sekar [a,*], S.P. Gupta [a], Y.B. Acharya [a], D. Chakrabarty [a], D. Pallamraju [a], B.M. Pathan [b], Diwakar Tiwari [b,1], R.K. Choudhary [c]

[a] Physical Research Laboratory, Ahmedabad 380009, India
[b] Indian Institute of Geomagnetism, Navi Mumbai 410218, India
[c] Space Physics Laboratory, Vikram Sarabhai Space Center, Thiruvananthapuram 695022, India

ARTICLE INFO

ABSTRACT

Systematic ground-based magnetometer measurements from Thumba (8.47°N, 76.6°E) and Tirunelveli (8.73°N, 77.8°E), India, revealed a movement of the magnetic dip equator towards the south. The magnetic dip angle measured over Thumba increased by about 2° during 1985–2010. In view of the movement of the dip equator over Thumba, the dependence of the generation of streaming plasma waves on the dip angle is examined. An order of magnitude calculation using the results obtained from the thin-shell model of the electrojet is performed. The calculation suggests that the streaming waves over Thumba during magnetically quiet periods at noontime exist when the dip angle is $< 1.5°$ and that these waves are generally absent whenever the dip angle is $\geq 1.5°$. Evidence based on in situ rocket and ground-based radar measurements is provided by comparing earlier and recent observations.

© 2013 Elsevier Ltd. All rights reserved.

1. Introduction

The movement of the location of the dip equator over the southernmost part of India in the last two decades has been reported in the recent past (Rangarajan and Deka, 1991; Deka et al., 2005) using ground-based geomagnetic observations. A ground magnetic survey was conducted (Deka et al., 2005) on the landmass in the southernmost part of India between 8°N and 9°N latitudes and compared with the International Geomagnetic Reference Field (IGRF) model. This survey revealed a well-defined southward migration of the dip equator over three and a half decades (Deka et al., 2005). Though the movement of the dip equator is less than 1° in latitude, it affects the geometry of the geomagnetic field over the well-known dip-equatorial rocket launching station Thumba by making it less horizontal. This affects the development of plasma waves associated with the equatorial electrojet, particularly those waves whose development depends on a large threshold value of electron drift.

Two types of plasma waves over the magnetic dip equator are excited with scale sizes ranging from few tens of meters to a few meters. One of them is due to the streaming of electrons (also known as the Type-I or Farley–Buneman wave), caused by the enhanced electrical conductivity (Cowling conductivity) over the dip equator, giving rise to electrons speed exceeding the ion acoustic speed of the plasma (Farley, 1963; Buneman, 1963). The other plasma wave is known as the gradient drift (Simon, 1963; Reid, 1968) or Type-II wave. This wave has been observed either in the positive or the negative gradient regions whenever the vertical electric field is non-zero (Prakash et al., 1972) and parallel to the background electron density gradient (Reid, 1968). The characteristics of these two plasma waves have been investigated using rocket-borne probes, ground-based VHF radars at different frequencies (Balsley and Farley, 1971) and HF radars. Ground-based radar measurements with different frequencies, although technically challenging, provide information only on a small number of scale sizes. On the other hand, in situ rocket-based measurements provide complementary information on the spectrum of irregularities, although restricted to the time of the experiment. Hence, it becomes necessary to make use of all the relevant techniques in order to understand the equatorial electrodynamics.

Rocket-borne probe measurements have been conducted from Thumba, India (Prakash et al., 1972; Subbaraya et al., 1983), Punta Lobos, Peru (Pfaff et al., 1987) and Alcantara, Brazil (Pfaff et al., 1997). The co-existence of fluctuations in the electric field and plasma densities (Kelley, 2009) revealed the electrostatic nature of the plasma waves. Further, the results obtained from the rocket flights revealed that, within 1–15 m scale sizes, the streaming wave amplitudes increase with a decrease in scale sizes, while that of

the gradient drift waves increase with increasing scale sizes (Prakash et al., 1972).

The initial investigations of these plasma waves with the ~ 3 m scale size were carried out using VHF radars over Jicamarca, Peru (Cohen and Bowles, 1967) and Thumba, India (Prakash et al., 1974). Subsequently, observations have been made for more than two decades from India (e.g. Reddy and Devasia, 1981; Krishna Murthy et al., 1998) and Jicamarca (e.g. Fejer and Kelley, 1980; Kelley, 2009). At a later time, these waves with scale size of 8.3 m were also investigated using the HF backscatter radar measurements from Thumba (Tiwari et al., 2003). These investigations revealed that the gradient drift waves were observed during day and night even with small electric field values. Further, the gradient drift waves or their manifestation on the ionograms, the E_{sq} traces, (Krishna Murthy and Sen Gupta, 1972) are observed well beyond the dip equator (Krishna Murthy et al., 1998; Gupta, 1997). Furthermore, the VHF radar observations (Choudhary et al., 1996) from Gadanki (12.5° dip angle) confirm this inference. On the other hand, the streaming waves are generated only when the electron velocity exceeds the ion acoustic velocity of the medium and are observed during the daytime for a finite period around 0900–1300 IST, (Indian Standard Time=UT+5.5 h) over the dip equator (Krishna Murthy et al., 1998) in the Indian sector. It is difficult to measure the possible latitudinal extent of the existence of streaming waves with respect to the magnetic dip equator. It is envisaged that the generation of the streaming waves is likely to get affected by the movement of the dip equator as the generation of these waves requires a large threshold value of electron drift, while the generation of the gradient drift wave is less likely to be affected.

Linear (Farley, 1963; Buneman, 1963; Simon, 1963; Reid, 1968) and non-linear (Sudan, 1983) theories were developed to understand the observed characteristics of these plasma waves. The linear theory suggests (Reid, 1968) that the gradient drift waves exist in the E-region of the ionosphere at locations where the background electric field is parallel to the gradient in the electron density. However, the linear theory on the gradient drift waves is not adequate to explain the generation of vertically propagating waves as observed by both rocket and radar measurements. A two-step instability process was developed by Sudan et al. (1973) to explain these measurements. In this approach, the primary horizontal waves grow in amplitude, causing local horizontal gradients and thereby assisting the growth of vertically propagating waves. Further, the perturbation electric fields become comparable to that of the background electric fields and thereby assist the generation of streaming waves. Experimental evidences of streaming wave structure embedded in kilometers scale gradient drift waves are obtained (Kudeki et al., 1982) using radar interferometry. Recently, the east–west asymmetry of spectral shapes (Choudhary et al., 2006; St.-Maurice and Choudhary, 2006) is ascribed to the embedding of streaming waves in gradient drift waves. Another important aspect, which affects the threshold condition of the streaming waves, is the effect due to non-isothermal electrons. St.-Maurice et al. (2003) showed evidence for the increase in the phase velocity of the waves of 1.46 times at ~ 100 km when the electron thermal fluctuations are included in the evaluation of the acoustic speed of ions. Many nonlinear models of streaming waves which bring out evolution of these waves and the saturation of phase velocity of the waves are available in literature (e.g. see Kelley, 2009). In contrast, the linear theory of streaming waves provides the necessary condition for the onset of these waves when the electron drift velocity exceeds the characteristic sound speed of the medium.

The generation of streaming plasma waves is decided by the magnitude of the drift velocity of electrons in the E-region, which is inversely proportional to the geomagnetic field strength. This magnetic field strength is larger over the Indian longitudes in comparison with the American longitudes. Further, the rate of change of magnetic dip angle with latitude varies differently over the Indian zone in comparison with the American zone (Forbes, 1981). In the present work, the possible association of the generation of the streaming waves with the dip angle is addressed over the Indian sector. This kind of investigation could not be carried out earlier over the Indian region due to the lack of steerable radar close to the dip equator. Further, rocket-borne experiments from a ship around the dip equator such as those reported by Davis et al. (1967) have never been conducted over Indian longitudes. Moreover, accurate measurements of the altitude profile of the electric field in the E-region from close-by latitudes centered around the dip equator are difficult to obtain. In spite of these constrains, the existing set of available measurements provides one with an opportunity to estimate the limiting dip angle up to which the generation of streaming waves is possible over the Indian region.

The scope of this communication is as follows. In Section 2, the dependence of the generation of streaming waves on the dip angle is examined. In Section 3, the details of the observations used to support the movement of the dip equator are described. Further, details of the observations made on the presence of the streaming waves using in situ probes and ground-based radar are also described. The results obtained from those observations are presented in Section 4. The effect of movement of the dip equator in the generation of streaming waves is discussed in Section 5 and results of the investigation are summarized in Section 6.

2. Dependence of the generation of streaming waves on the dip angle

The condition for the generation of streaming plasma waves obtained by earlier works is that they are generated when the drift velocity of electrons exceeds the sound velocity (Farley, 1963). Detailed theoretical studies (Farley, 1963; Sudan, 1983) reveal that the electron drift velocity needs to exceed the velocity of sound by $(1+\psi_0)$ times. The ψ_0 is given by the following equation:

$$\psi_0 = \frac{v_e v_i}{\omega_e \omega_i} \tag{1}$$

In the above expression, v and ω represent collision and gyration frequencies and the subscripts e and i represent electrons and ions, respectively. The value of ψ_0 is about 0.1 at 105 km altitude over Thumba, and increases at altitudes of 90 km and below. Mathematically, the condition for the generation of streaming waves can be written as:

$$\frac{E_z}{B} > (1+\psi_0) C_s \tag{2}$$

where E_z is the vertical electric field. B and C_s denote the strength of geomagnetic field and the sound speed, respectively. According to the thin shell dynamo equation, the vertical electric field (E_z) is related to zonal (E_λ) and meridional (E_θ) electric field components by the following expression (based on equation 14 in Forbes (1981)):

$$E_z = -\frac{(\sigma_{z\lambda}E_\lambda + \sigma_{z\theta}E_\theta)}{\sigma_{zz}} \tag{3}$$

where the relevant terms in the conductivity tensor ($\hat{\sigma}$) are as follows (based on equation (10) in Forbes (1981)):

$$\sigma_{\lambda z} = -\sigma_{z\lambda} = \sigma_2 \cos I \tag{4}$$

$$\sigma_{z\theta} = \sigma_{\theta z} = (\sigma_0 - \sigma_1) \sin I \cos I \tag{5}$$

$$\sigma_{zz} = \sigma_1 \cos^2 I + \sigma_0 \sin^2 I \tag{6}$$

Here, σ_0, σ_1 and σ_2 refer to parallel, Pedersen and Hall conductivities, respectively. As the magnetic field lines are equipotential, the E_θ term in Eq. (3) can be neglected. Under these conditions, Eqs. (2) and (3) can be reduced to reach the following condition:

$$\frac{\sigma_{\lambda z}}{\sigma_{zz}} \times \left(\frac{E_\lambda}{B}\right) > (1+\psi_0)C_s \qquad (7)$$

The left hand side of Eq. (7) represents the horizontal plasma drift due to the vertical polarization electric field (E_z). This vertical polarization field over the dip equatorial E region arises owing to the modification of the zonal electric field by a factor R due to the geometry of geomagnetic field. The factor R (which is a function of the dip angle I) is given by

$$R(I) = \frac{E_z}{E_\lambda} = \frac{\sigma_{\lambda z}}{\sigma_{zz}} = \frac{\sigma_2 \cos I}{\sigma_1 \cos^2 I + \sigma_0 \sin^2 I} \qquad (8)$$

The factor, $R(I)$ (henceforth denoted by R), over the dip equator attains a maximum value of about 30–35 (Anandarao et al., 1977), and this critically depends on the horizontal nature of the geomagnetic field. At locations where the magnetic dip angle (I) values are non-zero, this factor R will decrease from the maximum value. Further, even when R is at its maximum, the strengths of the electric and magnetic fields also determine the existence of the streaming waves. Thus, on a given day, as the strength of the zonal electric field (E_λ) changes diurnally, only a certain duration is suitable for the generation of streaming waves. This duration of the existence of streaming waves during the daytime is from around 0900 to 1300 IST over the Indian longitudes (Krishna Murthy et al., 1998) and it can be used to determine one of the limiting values for condition (7) to be satisfied.

Combining Eqs. (7) and (8) the following condition needs to be satisfied for the generation of streaming waves.

$$\frac{E_\lambda/B}{C_s} > (1+\psi_0)\frac{\sigma_1}{\sigma_2}\left(\cos I + \frac{\sigma_0}{\sigma_1}\frac{\sin^2 I}{\cos I}\right) \qquad (9)$$

It can be seen from the condition that the requirement of zonal electric field to satisfy Eq. (9) [$(E_\lambda)_{min}$] is independent of electron number densities, as the right hand side (RHS) depends on the ratios of conductivities. Thus, the required electric field [$(E_\lambda)_{min}$] is not expected to change with the changes in the electron densities associated with the solar cycle. As $(1+\psi_0)$ increases exponentially below 90 km, the generation of streaming waves is not conducive at altitudes of 90 km and below. Further, it is clear from Eq. (9) that the requirement of [$(E_\lambda)_{min}$] increases with the increase in dip angle, irrespective of its polarity. Furthermore, the second term in the parenthesis on the RHS increases rapidly with the increase in the dip angle due to large values of direct conductivity (σ_0). In other words, the development of the vertical polarization field is inhibited by large values of direct conductivity as dip angle increases, and thereby makes the condition non-conducive for the generation of streaming waves. As the dip angle deviates from 0° to 2° the second term becomes large and thereby the requirement of zonal electric field for the generation of streaming waves increases beyond the observed values. This aspect is discussed in the ensuing paragraph.

An order of magnitude calculation is performed by making use of the results of the thin shell model wherein complete inhibition of vertical current is assumed. Using the expression given in Eq. (8) and also the conductivity profiles given in Figure 28 of Forbes (1981), the factor R that enhances the primary zonal electric field is calculated for a few values of dip angle. It is shown by Anandarao et al. (1977) that the local and field line

integrated values of various parameters, including conductivities, yield similar R values in the E-region. Therefore, only local values are used for the present calculations. This value of R is around 32, corresponding to 100 km altitude over the dip equator. The calculated R is found to reduce to 18, 11.4, and 8 for the dip angle values 1°, 1.5°, and 2°, respectively. The model calculations reveal that the altitude, where the vertical electric field maximizes, is about 5 km lower than the corresponding value deduced from the measurements of current and electron densities (Subbaraya et al., 1972; Forbes, 1981). In order to account for this discrepancy, it is assumed that the above calculated R values correspond to 105 km altitude. Using these R values and the value of ψ_0 (0.1) at 105 km over Thumba, the requirements of zonal S_q electric fields are found out so that the electrons drift is $(1+\psi_0)$ times the speed of sound ($C_s=330$ m s^{-1} at 105 km). Thus, obtained zonal S_q electric field values are 0.79, 1.24 and 1.8 mV m^{-1} when the dip angle becomes 1°, 1.5° and 2°, respectively. These zonal electric fields correspond to the vertical plasma drifts of 20, 32 and 45 m s^{-1} at 1°, 1.5° and 2° dip angles, respectively over the Indian region. However, the maximum vertical drift velocity over Indian longitudes during the magnetically quiet period around noon time by the global empirical model (Scherliess and Fejer, 1999) is only around 25–30 m s^{-1}. This empirical model velocity (and E_λ) does not change within a few degrees of the dip angle. Thus, it is estimated that the signatures of the streaming waves disappear when the dip angle is between 1° and 1.5°. Incidentally, a similar result is shown in Fig. 1 (private communication from St.-Maurice, 2012) with the magnetic field strength of 0.35×10^{-4} T and with more refined calculations of minimum E_λ/B, including non-isothermal conditions and allowance for the assistance by gradient drift waves using the conditions given by St.-Maurice et al. (2003). Fig. 1 depicts the altitude-dip angle variations of contours of minimum vertical drift $(E_\lambda/B)_{min}$ corresponding to the minimum horizontal electric field $(E_\lambda)_{min}$ in order to excite the streaming waves with a
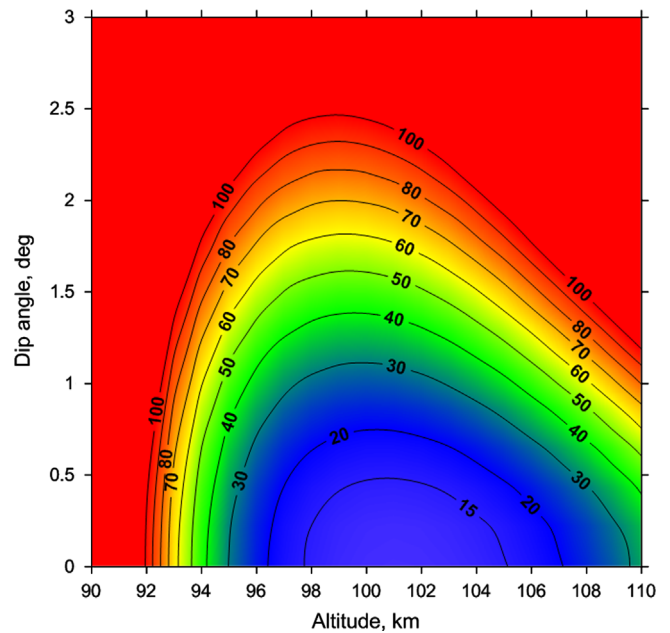

Fig. 1. Altitude-dip angle variations of contours of minimum vertical drift $(E_\lambda/B)_{min}$ corresponding to the minimum horizontal electric field $(E_\lambda)_{min}$ in order to excite the streaming waves with a 8.3 m scale size. The calculation is based on conditions given in St.-Maurice et al. (2003), which includes non-isothermal conditions and allowance for the assistance by gradient drift waves. The strength of the magnetic field assumed is 0.35×10^{-4} T (courtesy: St.-Maurice, private communication, 2012).

8.3 m scale size. Considering the maximum vertical drift values of 30 m s^{-1} (Scherliess and Fejer, 1999), it is clear from Fig. 1 that the transition from appearance to disappearance of streaming waves occurs between 1° and 1.5° dip angle. Interestingly, this inference from Fig. 1 is similar to the estimation given based on the order of magnitude calculation presented here. However, taking into account the over-estimation of R due to the limitations of the thin shell model as discussed in Section 5, it can be taken that the transition is around the 1.5° dip angle. In other words, the detection of streaming waves was possible at an earlier time when the dip angle was < 1.5° and the same waves are unlikely to be present in the recent past when the dip angle is ≥ 1.5°. In order to examine this proposition, in situ and ground-based measurements are used. The details of observations along with the results are presented in the following sections.

3. Details of observations

A network of observatories, monitoring geomagnetic field variations in the Indian subcontinent on a continuous basis, is operated by the Indian Institute of Geomagnetism. During the period 1957–1999, magnetic measurements in the equatorial region were carried out from Thumba (TRD 8.47°N, 76.6°E) using an analog classical magnetometer having a resolution of 1.0 nT. Subsequently, in the year 1999, the equatorial magnetic observatory was shifted to Tirunelveli (TIR 8.73°N, 77.8°E), where proton precession and fluxgate magnetometers are being operated routinely to measure the magnetic field with a resolution of 0.1 nT.

The characteristic signatures of the plasma waves were detected using in situ probes and a ground based radar. The details of these experiments are briefly discussed in the following paragraphs.

A modified Langmuir probe system was designed and developed (Prakash and Subbaraya, 1967; Subbaraya et al., 1983) at the Physical Research Laboratory, India, to measure electron densities and plasma waves in the ionosphere. In this system, internal leakage current and capacitance leakage are reduced and thus, it enables measurements of variations in the electron densities due to the presence of plasma waves. The dc component of the probe current is calibrated with a ground-based ionosonde to obtain electron density (N). The fluctuations in the probe current (proportional to the electron density fluctuations, ΔN) are separated using a band-pass filter ($\sim$70–1000 Hz) and telemetered after suitable amplification. Thus, the scale sizes of the fluctuations corresponding to these frequencies turn out to be 15–1 m for a typical rocket velocity of 1 km s^{-1}. The percentage amplitudes of normalized electron density fluctuations are deduced from (ΔN/N) × 100. Probes of such type have been flown over the years from Thumba and also from another low latitude station, SHAR (13.8°N, 80.2°E). A similar Langmuir probe was flown during the rocket flight on 16th January, 2010. In this communication, the latest results obtained on 16th January, 2010, are presented and compared with the typical results obtained during earlier periods from Thumba.

Coherent backscatter radar in the HF range was designed and fabricated at Thumba by the Space Physics Laboratory, India. This is a coherent pulsed Doppler radar capable of operating either at 18 or at 9 MHz. The power aperture product of this system can be as high as 5 × 10^8 W m^2. The complete details of this radar, along with the scientific results, are available in literature (Janardhanan et al., 2001; Tiwari et al., 2003). The results obtained from this radar operating at 18 MHz with the beam orientation of 15° west off-zenith in the recent (2010) years are presented and compared with the typical spectra obtained at an earlier time. Further, support is also taken from published results (e.g., Krishna Murthy et al., 1998) using the backscatter VHF radar operating at 54.95 MHz from Thumba. The system details of the VHF radar are available in literature (Prakash et al., 1974; Reddy et al., 1990).

4. Results

Fig. 2(a) depicts the location of the dip equator in geographic latitudes over the Indian longitude (77.5°E) from the International Geomagnetic Reference Field model. The location of the rocket launch station at TRD is marked by the horizontal line. The annual mean of the measured values of the dip angle of the geomagnetic field at TRD (geographic 8.47°N) from 1957 to 1998 and the same at the nearby station TIR (geographic 8.73°N) from 1999 to 2010 are depicted in Fig. 2(b). It is noted that the variation of the dip angle over TIR maintained a steady increase till 2010, indicating a southward movement of the dip equator in conformity with earlier work (Deka et al., 2005). Therefore, in order to have continuity, the dip angle over TRD should increase from 1999 to 2010. Assuming the same slope with time as that of TIR, the dashed curve has been plotted in Fig. 2(b) to represent the change in the dip angle over TRD. It is also conspicuous from Fig. 2(b) that the dip angle (I) over TIR is smaller than that over TRD, although one would expect it to be greater, as TIR is north of TRD and the dip equator has moved further southward from this region. This difference in the dip angles between TIR and TRD is believed to originate from the magnetic Z-component anomaly (e.g. Arora and Subba Rao, 2002; Rastogi et al., 2004; Deka et al., 2005; Kuvshinov et al., 2007) over the Indian subcontinent, as the changes in the magnitude of H with
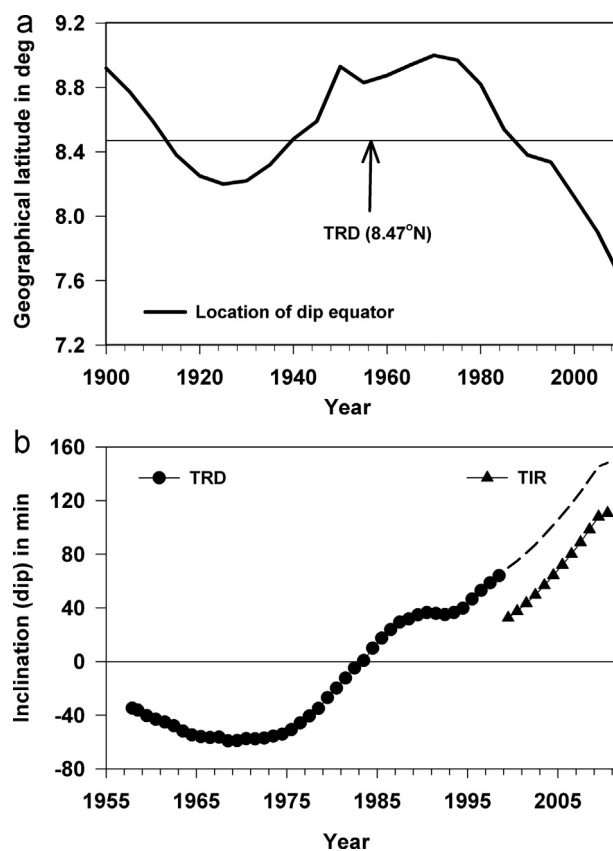

Fig. 2. (a) Location of the dip equator over the Indian longitude (77.5°E) obtained by the International Geomagnetic Reference Field Model. The horizontal line refers to the location of the rocket launching station, Thumba (TRD). (b) Annual mean of the measured dip angle from Thumba (TRD; filled circle) and Tirunelveli (TIR, 8.73°N; filled triangle). The projected dip angle over TRD after 1999–2010 is denoted by a dashed line.

latitude are smaller in the equatorial region as compared to that in the Z-component. It is known that the magnetic dip angle (I) is related to the Z-component (vertical component) and the H-component (horizontal component) through the following relationship:

$$I = \tan^{-1}\left(\frac{Z}{H}\right) \tag{10}$$

In contrast to the expectation over a station in the northern hemisphere, observations from the Indian magnetic observatories reveal that Z is positive over Thumba (e.g. Rastogi et al., 2004) and nearby places. This is the Z-anomaly which alters the polarity and magnitude of the Z-values (and, as a consequence, the dip angle) over the southern peninsular region of India. Many hypotheses like the induction effects of the equatorial electrojet (EEJ) current along the Palk strait (the narrow sea channel between India and Sri Lanka), sub-surface conductivity anomalies in this region, etc. have been invoked to explain this Z-anomaly (for a detailed discussion on this, see Rastogi et al. (2004) and Kuvshinov et al. (2007), and references cited therein). The peculiar variation of the dip angle over the Indian subcontinent is expected to have localized effects on the development of streaming waves. As this aspect is not directly relevant to the present investigation, it is not discussed further. Nevertheless, it is worthwhile to note from Fig. 2 that the dip angle value over TRD/TIR in the year 2010 is far from zero, indicating that the dip equator has deviated southward of these locations.

Fig. 3(a) depicts the altitude profiles of electron density and percentage amplitudes of normalized electron density fluctuations (as defined in Section 3) measured by the Langmuir probe on-board a RH-300 MKII rocket flight conducted at 1220 IST on 16th January, 2010. A steep electron density gradient between 85 and 92 km followed by a lesser gradient between 93 and 98 km altitude region is recorded. Enhancements in the amplitudes of normalized electron density fluctuations are seen in Fig. 3(a) corresponding to these gradient regions. Note that the amplitude is larger in the altitude region of 85–92 km where electron density gradients are steeper. These are signatures of gradient drift waves. The magnetic observation (not shown here) at Tirunelveli (with a maximum $\Delta H \sim 40$ nT at around 1100 IST) reveals that a normal electrojet condition was prevalent on this day, indicating the presence of an eastward electric field. Thus, the vertical polarization electric field is expected to be upward. The presence of gradient drift waves in the scale size of 1–15 m in the positive gradient region of the electron density profile confirms the existence of the upward polarization field. Further, the amplitudes of these gradient drift waves are found to reduce with the reduction in the gradients. Surprisingly, the expected increase in the amplitude of the waves around the 105–106 km altitude region corresponding to the streaming plasma waves was found to be absent. In fact, after 100 km, until the apogee of the rocket trajectory, only non-geophysical noise was found. Importantly, the absence of streaming wave signatures on 16th January, 2010, at around 105–106 km is in sharp contrast with the results obtained from the earlier rocket measurements from Thumba, wherein the signatures of streaming waves were always found at the said altitude region during noon time. One such example (Gupta, 2000) based on the rocket measurement using a similar probe under similar conditions of season and solar epoch (1105 IST on 19th February, 1975) is presented as Fig. 3(b). It is worth mentioning here that, similar to 2010, the period around the rocket campaign in 1975 was also marked by very low solar activity when the sunspot numbers were very small for a prolonged duration. In this figure, it can be seen that in addition to the two peaks below 100 km in the amplitudes of normalized fluctuations (which corresponds to gradient drift waves), an additional peak at 104–105 km corresponding to
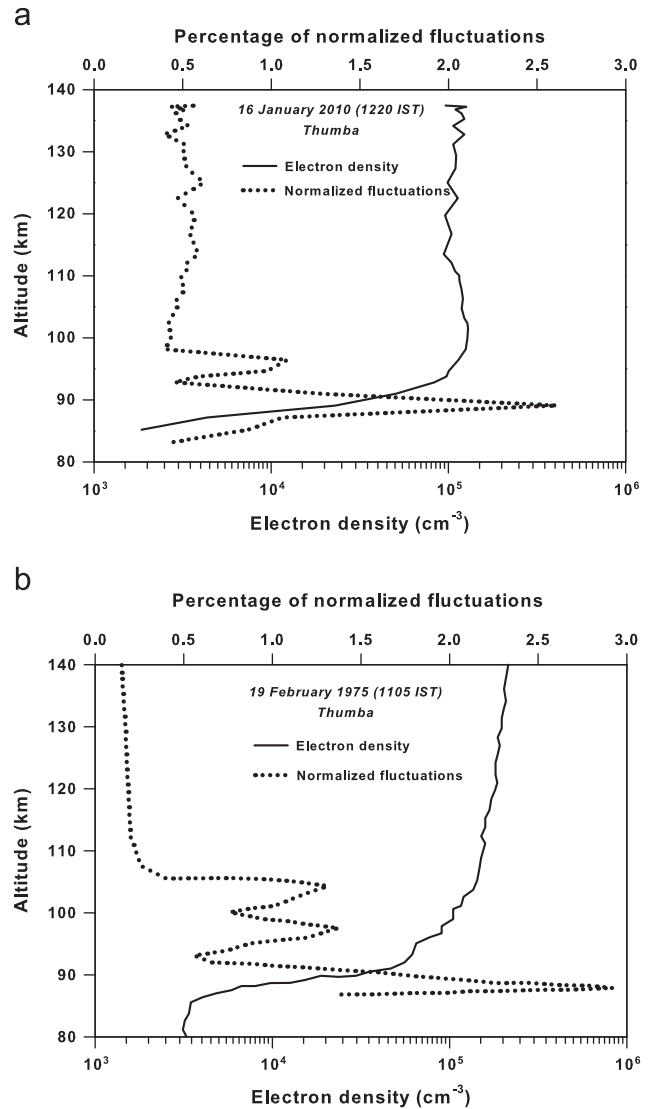

Fig. 3. Altitude profiles of electron densities and percentage amplitudes of plasma waves measured over Thumba (a) on 16th January, 2010, at 1220 IST and (b) on 19th February, 1975, at 1105 IST using Langmuir probes. Comparison of Fig. 2(a) and (b) reveals two peaks below 100 km in the normalized fluctuations in the electron densities that correspond to the presence of gradient drift waves on these two occasions. However, the absence of the third peak in the amplitudes of fluctuations at ~105 km in Fig. 2(a) indicates the absence of the streaming waves on 16th January, 2010.

streaming plasma waves is present. The amplitude of these waves at the 105 km altitude region in general increases with decreasing scale sizes. One clear example of such characteristics is provided by Prakash et al. (1972). Furthermore, the decrease in the percentage of normalized fluctuations (from 1.4 at 97 km to 0.75 at 101 km) and subsequent increase in the same (from 0.75 at 101 km to 1.25 at 105 km) despite the monotonic decrease in the electron density gradient, shows that the gradient-drift mechanism is not probably associated with the peak at 105 km.

Fig. 4 brings out a comparison of the typical spectra obtained from the measurements by the HF backscatter radar at Thumba on 3rd February, 1999, with that on 17th January, 2010. The comparison of the spectra obtained on these two days is done to highlight the fact that the HF backscatter radar, which is capable of picking up the characteristic signature of streaming waves, detected the presence of streaming waves on 3rd February, 1999, and not on 17th January, 2010. Fig. 4(a) depicts a temporal sequence of Doppler spectra obtained on 3rd February,
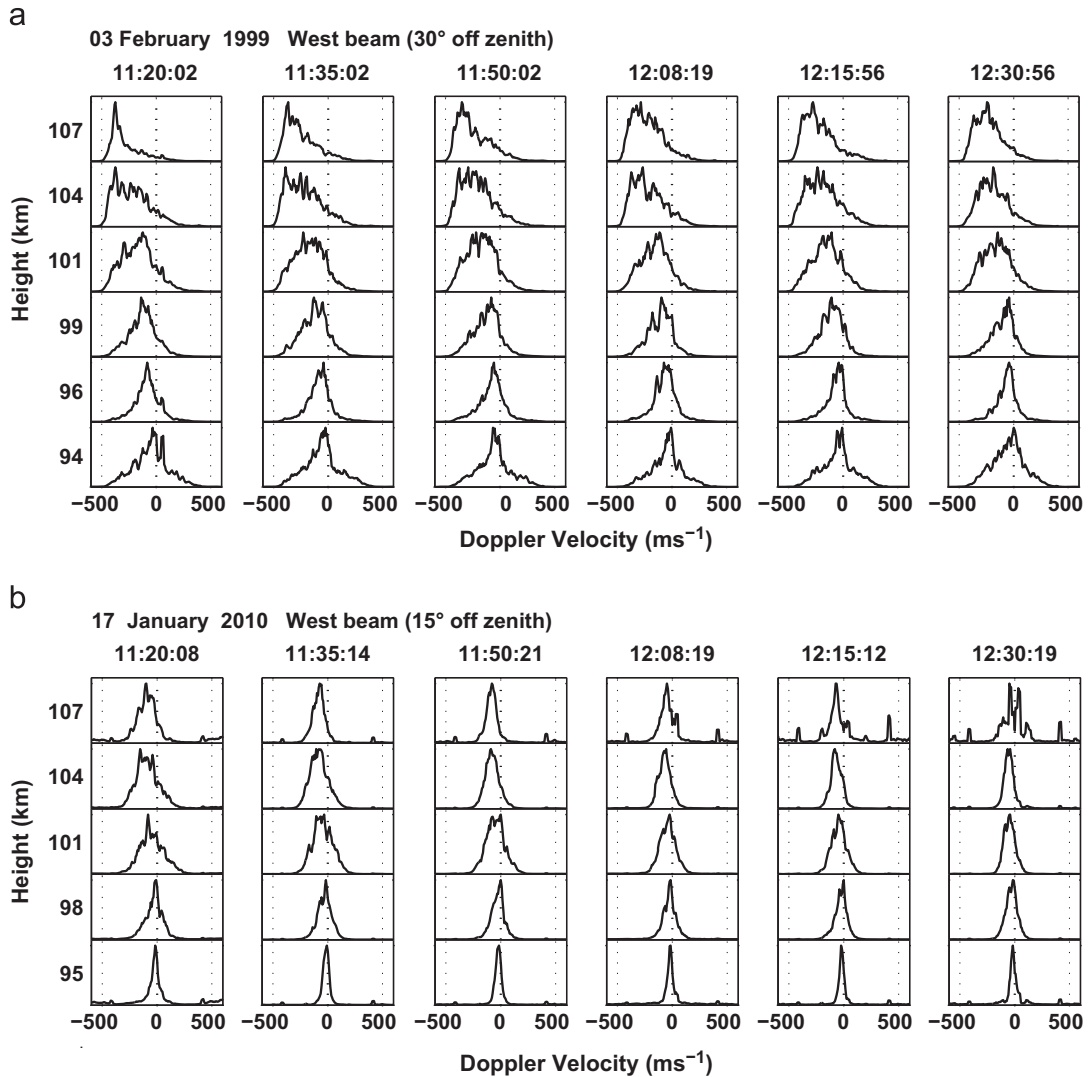
Fig. 4. Doppler spectra at different altitudes around noon hours obtained using HF (18 MHz) backscatter radar over Thumba on 3rd February, 1999, (Fig. 4a) and 17th January, 2010 (Fig. 4b). The former revealed the presence of streaming waves around 104 and 107 km altitudes. The absence of streaming waves is evident on 17th January, 2010. The vertical dotted lines correspond to ± 500 and $0\ \text{m s}^{-1}$.

1999, at different altitudes with the beam orientation toward west and a zenith angle of 30°. This provides sample spectra containing the signatures of streaming plasma waves at 104 and 107 km altitudes, as observed by the HF backscatter radar operating at 18 MHz, which corresponds to the 8.3 m scale size (half of the probing wavelength). Gradient drift waves have also been observed all through the altitudes, particularly at lower heights. It can be seen that the gradient drift waves are observed to move westward (moving away from the viewing direction, as indicated by the negative Doppler velocity) during the daytime, indicating an eastward electrojet on this day. Fig. 4(b) depicts a temporal sequence of Doppler spectra obtained at E-region altitudes on 17th January, 2010, using the same HF backscatter radar with the beam orientation towards west, but with a zenith angle of 15°. However, the spectra obtained on this day indicate the presence of only the gradient drift waves and the absence of streaming waves. A general verification is also made on the occurrence of the spectral signatures corresponding to the streaming waves during 2001–2005. Based on the sporadic observations made during this period, it is noted that the signatures of streaming plasma waves are seen around noon time on all the observed days till 2001, intermittently during 2002 and absent whenever the HF radar was operated during 2003–2005,

encompassing different months of the year. More than 30 days of operation of this HF backscatter radar during 2010 revealed the total absence of streaming waves.

5. Discussion

It has been shown (Yacob and Khanna, 1963; Rabiu and Nagarajan, 2007) that the half-width where the current density value falls to one-half of the value at the dip equator is ~2.6° latitude over the Indian region. However, the streaming plasma waves were not observed by the VHF radar (Krishna Murthy et al., 1998) at Gadanki (13.5°N, 79.2°E, dip 12.5°N), which is located at a low latitude region and also by in situ measurements over SHAR (dip: 11°N) using rocket-borne Langmuir probes (Gupta, 1997). The absence of these waves is essentially due to the fact that the threshold values of the electric fields as required by Eq. (9) for the generation of streaming plasma waves at these dip angles are not satisfied when one moves away from the dip equator. This is owing to the fact that the modification of the zonal component of the electric field critically depends on the horizontal nature of the geomagnetic field (see Eq. (9)) to generate the upward polarization field that drives the electrojet.

In the absence of systematic observations of zonal electric field over Thumba, the global empirical model (Scherliess and Fejer, 1999) for the quiet time F-region equatorial vertical drifts corresponding to the zonal electric field is used to estimate electric field variations during the daytime. This empirical model is based on combined incoherent scatter radar observations at Jicamarca and ion drift meter observations on-board the Atmospheric Explorer-E satellite. Further, the model drift amplitudes are constrained using the curl-free condition of the electric field. The model values corresponding to 60°E longitudes are considered to represent the Indian longitudes. These model values reveal that the daytime drifts (E_λ/B) have maximum values between 0900 and 1100 LT in the Indian sector. Further, daytime drifts (E_λ/B) are shown to be independent of solar activity, except for a small increase during the June solstice in solar minimum condition. Considering various seasons and epochs, this drift value (E_λ/B) attains a noontime maximum of $\sim$30 m s^{-1} between 0900 and 1100 LT and a value of $\sim$15 m s^{-1} at 1300 LT when the streaming waves cease to exist over Indian longitudes. This amounts to reduction of drift by $\sim$50% from the maximum value, which will result in the absence of streaming waves after 1300 LT in spite of the maximum value of R. In other words, if the maximum value R falls from 32 to 16 (by 50%), then the generation of streaming waves will cease to exist. Therefore, as the value of R reduces to 16 when the dip angle is between 1° and 1.5°, the streaming waves are expected to be absent. As the existence of streaming waves was detected (Prakash et al., 1971) by the rocket flight (28th January, 1971, at 1110 IST) when the dip angle (I) was $-1°$, their existence is expected until 1997, considering a similar magnitude ($+1°$) of the dip angle, as can be seen from Fig. 2(b). The observation provided in Fig. 4(a) reveals the presence of streaming waves even in 1999. Thus, the streaming waves continued to get generated even when the magnetic dip angle was greater than 1°. In spite of the sporadic nature of measurements, the radar observations during 2001–2005, reveal a systematic transition from the occurrence to the non-occurrence in the signatures of streaming waves over Thumba. It appears that when the value of the dip angle reaches $\geq$ 1.5° over the Indian zone, the electron drift velocity is reduced to such an extent that the generation of streaming waves would not take place. The 2010 rocket measurement (see Fig. 3a) was conducted during a period when the magnetic dip angle was $>2°$ (see Fig. 2b). Thus the absence of the streaming plasma waves at all scale lengths during this rocket flight is consistent with the estimated criterion of the dip angle $\geq$ 1.5°, as described above.

An attempt was made to obtain the signature, if any, of the movement of the dip equator with the mean peak value of the strength of the EEJ during the daytime, derived using ground-based magnetometer data from a dip equatorial station (Thumba or Tirunelveli) and a low latitude station (Alibag). The variation of the mean peak value of the EEJ strength (not shown here) reveals dominant periodicity of $\sim$11 years that is believed to be associated with the changes in the plasma density during the solar cycle. It is known that the daytime plasma drifts are almost independent of solar activity (Scherliess and Fejer, 1999). Therefore, the signature, if any, of the movement of the dip equator on the EEJ strength will be extremely small and will be difficult to delineate. More importantly, ground-based magnetometers will register changes in the overhead current flowing within $\pm$1° latitude, and hence the small changes in the ionospheric current and electric field as a consequence of the movement of the dip equator, as in the present case, may get integrated out in the magnetic measurements of ΔH. Thus, it is rather difficult to decipher the impact of the movement of the magnetic dip equator (which is $<$1° latitude) using ground-based measurements of ΔH.

The thin shell model overestimates the decrease of the factor R with the increase of the dip angle. The limitations of the thin shell model and subsequent development of models allowing vertical current with various other assumptions are amply discussed by Forbes (1981). One such model (Richmond, 1973a, 1973b) overestimates the current over the dip equator even with smaller E_λ. The other model which is applicable over the Indian zone (Anandarao, 1977; Anandarao and Raghavarao, 1987) reveals that the factor R does not reduce rapidly as predicted by the thin shell model. However, the latitudinal resolution (0.5° latitude resolution that corresponds to 1.25° dip angle over the Indian region) of the calculations performed so far with this model (Anandarao, 1977) does not permit investigations on the sensitivity of the generation of plasma waves with respect to the dip angle. A high spatial resolution model calculation is needed to investigate this sensitivity. The high resolution calculations based on the improved models on the vertical electric field at off-dip equatorial locations are beyond the scope of this communication.

Finally, it is to be noted that the inference drawn in the present investigation pertains to daytime and geo-magnetically quiet conditions. However, in the presence of penetration electric fields and during twilight/post-sunset hours, signatures of the streaming plasma waves may still be obtained. These are, of course, special circumstances wherein changes in the electric field are significant (e.g. Simi et al., 2012). The present investigation precludes these possibilities.

6. Summary

Systematic magnetic observations over Thumba and a nearby station revealed a movement of the dip equator towards south of Thumba, which correspond to a change in the dip angle of more than 2° in recent times. The calculation based on the thin shell model suggests that the streaming waves are unlikely to exist over Thumba when the magnetic dip angle is $\geq$ 1.5°. As expected from the magnetic observation and the thin shell estimates, there has not been a single instance of detection of streaming waves during the daytime over Thumba since 2003, either with radar or with rocket measurements, as illustrated by Figs. 3 and 4.

References

Anandarao, B.G., 1977. Studies on the dynamics of the equatorial ionosphere. Ph.D. Thesis. Gujarat University.
Anandarao, B.G., Desai, J.N., Giles, M., Martelli, G., Raghavarao, R., Rothwell, P., 1977. Electric field in the equatorial ionosphere. Journal of Atmospheric and Terrestrial Physics 39, 927–931.

Anandarao, B., Raghavarao, R., 1987. Structural changes in the currents and fields of the equatorial electrojet due to zonal and meridional winds. Journal of Geophysical Research 92, A3, http://dx.doi.org/10.1029/JA092iA03p02514.

Arora, B.R., Subba Rao, P.B.V., 2002. Integrated modeling of EM response functions from Peninsular India and Bay of Bengal. Earth Planets Space 54, 637–654.

Balsley, B.B., Farley, D.T., 1971. Radar studies of the equatorial electrojet at three frequencies. Journal of Geophysical Research 76, 8341–8351.

Buneman, O., 1963. Excitation of field-aligned sound waves by electron streams. Physical Review Letters 10, 285–287.

Choudhary, R.K., Mahajan, K.K., Singh, S., Kumar, K., Anandan, V.K., 1996. First VHF radar observations of tropical latitude E-region field aligned irregularities. Geophysical Research Letters 23 (25), http://dx.doi.org/10.1029/96GL02625.

Choudhary, R.K., St.-Maurice, J.-P., Ecklund, W.L., Tsunoda, R.T., 2006. East-west and vertical spectral asymmetry associated with equatorial type I waves during strong electrojet streaming: 1. Pohnpei radar observations. Journal of Geophysical Research 111, A11303, http://dx.doi.org/10.1029/2006JA011842.

Cohen, R., Bowles, K.I., 1967. Secondary irregularities in the equatorial ionosphere. Journal of Geophysical Research 72, 885–894.

Davis, T.N., Burrows, K., Stolarik, J.D., 1967. A latitude survey of the equatorial electrojet with rocket-borne magnetometers. Journal of Geophysical Research 72, 1845–1861.

Deka, R.C., D'Cruz, L.A., Jacob, V.J., Iype, A., Elango, P., 2005. Location of the dip equator over peninsular India. Journal of Indian Geophysical Union 9, 41–46.

Farley, D.T., 1963. A plasma instability resulting in field-aligned irregularities in the ionosphere. Journal of Geophysical Research 68, 6083–6097.

Fejer, B.G., Kelley, M.C., 1980. Ionospheric irregularities. Reviews of Geophysics and Space Physics 18, 401–454.

Forbes, J.M., 1981. The equatorial electrojet. Reviews of Geophysics and Space Physics 19 (3), 469–504.

Gupta, S.P., 1997. Features of E region irregularities at the magnetic equator and its vicinity. Advances in Space Research 20, 2195–2198.

Gupta, S.P., 2000. Features of lower ionosphere during day and night over magnetic equator. Advances in Space Research 25, 53–63.

Janardhanan, K.B., et al., 2001. HF backscatter radar at the magnetic equator: system details and preliminary results. Indian Journal of Radio & Space Physics 30, 77–90.

Kelley, M.C., 2009. The Earth's Ionosphere: Plasma Physics and Electrodynamics. Academic Press, San Diego, USA.

Krishna Murthy, B.V., Sen Gupta, K., 1972. Disappearance of Es associated with magnetic field depressions. Planetary and Space Science 20, 371–378.

Krishna Murthy, B.V., Sudha Ravindran, K.S., Viswanathan, K.S.V., Subbarao, A.K., Patra, Rao, P.B., 1998. Small-scale (~ 3 m) irregularities at and off the magnetic equator. Journal of Geophysical Research 103, 20761–20772.

Kudeki, E., Farley, D.T., Fejer, B.G., 1982. Long wavelength irregularities in the equatorial electrojet. Geophysical Research Letters 9, 684–687.

Kuvshinov, A., Manoj, C., Olsen, N., Sabaka, T., 2007. On induction effects of geomagnetic daily variations from equatorial electrojet and solar quiet current sources at low and middle latitudes. Journal of Geophysical Research 112, B10102, http://dx.doi.org/10.1029/2007JB004955.

Pfaff, R.F., et al., 1987. Electric field and plasma density measurements in the strongly driven daytime equatorial electrojet: 1. The unstable layer and gradient drift waves. Journal of Geophysical Research 92, 13578–13596.

Pfaff, R.F., Acuna, M.H., Marionni, P.A., Trivedi, N.B., 1997. DC polarization electric field, current density, and plasma density measurements in the daytime equatorial electrojet. Geophysical Research Letters 24, 1667–1670.

Prakash, S., Subbaraya, B.H., 1967. Langmuir probe for the measurement of electron density and electron temperature in the ionosphere. Review of Scientific Instruments 38, 1132–1136.

Prakash, S., Gupta, S.P., Subbaraya, B.H., Jain, C.L., 1971. Electrostatic plasma instabilities in the equatorial electrojet. Nature 233 (38), 56–58.

Prakash, S., Subbaraya, B.H., Gupta, S.P., 1972. Rocket measurements of ionization irregularities in the equatorial ionosphere at Thumba and identification of plasma instabilities. Indian Journal of Radio & Space Physics 1, 72–80.

Prakash, S., Jain, C.L., Balsley, B.B., Greenwald, R.A., 1974. Evidence of two types of electron density irregularities in the electrojet over India. Journal of Geophysical Research 79, 4334–4336.

Rabiu, A.B., Nagarajan, Nandini, 2007. Inter-relationships between the thickness, width and intensity of the equatorial electrojet in Indian sector. Bulletin of the Astronomical Society of India 35, 645–654.

Rangarajan, G.K., Deka, R.C., 1991. The dip equator over peninsular India and its secular movement. Proceedings of the Indian Academy of Sciences (Earth and Planetary Sciences) 100, 361–368.

Rastogi, R.G., Kitamura, T., Kitamura, K., 2004. Geomagnetic field variations at the equatorial electrojet station in Sri Lanka, Peredinia. Annales Geophysicae 22, 2729–2739.

Reddy, C.A., Devasia, C.V., 1981. Height and latitude structure of electric fields and current due to local east-west winds in the equatorial electrojet. Journal of Geophysical Research 86, 5751–5767.

Reddy, C.A., Janardhanan, K.V., Mukundan, K.K., Shenoy, K.S.V., 1990. Concept of an interlaced phased array for beam switching. IEEE Transactions on Antennas and Propagation 38, 573–575.

Reid, G.C., 1968. The formation of small scale irregularities in the ionosphere. Journal of Geophysical Research 73, 1627–1640.

Richmond, A.D., 1973a. Equatorial electrojet, I, development of a model including winds and instabilities. Journal of Atmospheric and Terrestrial Physics 35, 1083–1103.

Richmond, A.D., 1973b. Equatorial electrojet, II, use of the model to study the equatorial ionosphere. Journal of Atmospheric and Terrestrial Physics 35, 1105–1118.

Scherliess, L., Fejer, B.G., 1999. Radar and satellite global equatorial F region vertical drift model. Journal of Geophysical Research 104, 6829–6842.

Simi, K.G., Thampi, S.V., Chakrabarty, D., Pathan, B.M., Prabhakaran Nayar, S.R., Pant, T.K., 2012. Extreme changes in the equatorial electrojet under the influence of interplanetary electric field and the associated modification in the low-latitude F region plasma distribution. Journal of Geophysical Research 117, A03331, http://dx.doi.org/10.1029/2011JA017328.

Simon, A., 1963. Instability of a partially ionized plasma in cross electric and magnetic field. Physics of Fluids 6, 382–388.

St.-Maurice, J.P., Choudhary, R.K., Ecklund, W.L., Tsunoda, R.T., 2003. Fast type-I waves in the equatorial electrojet: evidence for nonisothermal ion-acoustic speeds in the lower E region. Journal of Geophysical Research 108 (A5), 1170, http://dx.doi.org/10.1029/2002JA009648.

St.-Maurice, J.-P., Choudhary, R.K., 2006. East–west and vertical spectral asymmetry associated with equatorial type I waves during strong electrojet conditions: 2. Theory. Journal of Geophysical Research 111, A11303 http://dx.doi.org/10.1029/2006JA011843.

Subbaraya, B.H., Muralikrishna, P., Sastry, T.S.G., Prakash, S., 1972. A study of the structure of electrical conductivities and the electrostatic field within the equatorial electrojet. Planetary and Space Science 20, 47, http://dx.doi.org/10.1016/0032-0633(72)90139-0.

Subbaraya, B.H., Prakash, S., Gupta, S.P., 1983. Electron densities in the equatorial lower ionosphere from the Langmuir probe experiments conducted at Thumba during 1966–1978. ISRO Scientific report. ISRO-PRLSR-15-83.

Sudan, R., Akinrimisi, J., Farley, D., 1973. Generation of small-scale irregularities in the Equatorial Electrojet. Journal of Geophysical Research 78, 240–248.

Sudan, R.N., 1983. Unified theory of type 1 and type 2 irregularities in the equatorial electrojet. Journal of Geophysical Research 88, 4853–4860.

Tiwari, D., Patra, A.K., Viswanathan, K.S., Jyoti, N., Devasia, C.V., Subbarao, K.S.V., Sridharan, R., 2003. Simultaneous radar observations of the electrojet plasma irregularities at 18 and 54.95 MHz over Trivandrum, India. Journal of Geophysical Research 108, 1368, http://dx.doi.org/10.1029/2002JA009698.

Yacob, A., Khanna, K.B., 1963. Geomagnetic S_q variations and parameters of the Indian electrojet for 1958-1959. Indian Journal of Meteorology and Geophysics 14, 470–477.

Preface

A number of papers were presented in the Symposium on Atmospheric Electrodynamics and Climate Change held during the COSPAR Assembly in Paris on July 2004. The phenomenon of global thunderstorm activity was discussed by several authors. In this context many new findings were presented. The maximum thunderstorm activity is mainly confined along the magnetic equator (in contrast to the geographic equator as believed earlier), with a latitudinal extent of 15° on both the sides of the magnetic equator. On the globe there are mainly three centres of thunderstorm activity, namely over South America, Central Africa and Asia/Australia. E. Williams suggested that thunderstorm activity is maximum over the wetter Amazon region (Brazil) compared to the drier Congo region (Africa). This can explain the observed vertical electric field variation at the surface of earth with Universal Time. Based on the results from the American Zone, M.D. Kartalev and co-workers have shown that thunderstorms at the magnetic equator can affect the electric field at E-region heights. P. Velinov and P. Tonev presented a theoretical model for thunderstorm generated electric-fields in the ionosphere and particularly the effect on the east-west electric field. D. Rowland and co-workers presented rocket borne results of the effect of thunderstorms on the generation of parallel electric-fields (along magnetic field lines) in the ionosphere over high latitudes. (This paper was presented by C. Steigies of Germany who has worked earlier in NASA.).

L. Makarova discussed the effect of the solar wind on the conductivity of the stratosphere. Thermal structure in the stratosphere over high latitude regions can be modified by solar wind penetration and can cause climate variation. Temporal and spatial fluctuations in stratospheric conductivity over the South Pole were discussed by E.A. Bering. The solar activity dependence on stratospheric electrical conductivity was presented by S.P. Gupta based on the balloon borne experiments using three different types of techniques covering a period of high and low solar activity over low latitude regions.

The effect of cosmic rays on the ionisation production process was discussed by R.G. Harrison and K.L. Aplin. New results on 'sprites' from the International Space Station were presented by E. Blanc and M.J. Rycroft discussed results obtained from the "Sprite 2003" ground-based campaign in Southern Europe.

I am thankful to Prof. M.J. Rycroft for organising this symposium. The chairmen for the two sessions were Prof. Rycroft and Dr. S.P. Gupta. I sincerely appreciate the work of the referees for these papers, namely Prof. M.J. Rycroft, M. Parrot, K.I. Oyama, V. Pasko, R. Holzworth, H. Chandra and S.P. Gupta.

Guest Editor
S.P. Gupta
Physical Research Laboratory
Ahmedabad 380 009
India

Latitude gradients in the natural variance in stratospheric conductivity – Implications for studies of long-term changes

E.A. Bering III [a,*], J.R. Benbrook [a], R.H. Holzworth [b], G.J. Byrne [c], S.P. Gupta [d]

[a] Physics Department, University of Houston, 617 Science and Research I, Houston, TX 77204-5005, USA
[b] Department of Earth and Space Sciences, University of Washington, Room 346A, Johnson Hall, Box 351310, Seattle, WA 98195-1310, USA
[c] NASA Johnson Space Center, 2101 NASA Rd. 1, Houston, TX 77058, USA
[d] Physical Research Laboratory, Navarangpura, Ahmedabad 380 009, Gujarat, India

Abstract

Stratospheric electrical conductivity measurements have been made from high altitude research balloons at various locations around the world for more than 40 years. In the stratosphere, conductivity changes may indicate changes in aerosol or water vapor content. In this paper, we will compare the short term variation amplitude in data taken at several latitudes from equatorial to polar cap. Short term variations that occur on time scales of weeks to months (10^5–10^7 s) can be attributed to Forbush decreases, geomagnetic storms, aerosol injections by volcanos and forest fires, etc. Variations with time scales of minutes to days (10^3–10^5 s) can have amplitudes of a factor of $\sim$2 or more at high magnetic latitude. The variance at equatorial latitude is much smaller. The sources of these fluctuations and the latitude gradient remain unknown. Variations of all origins completely obscure any long-term climatic trend in the data taken in the previous four decades at both mid and high latitude.
© 2005 COSPAR. Published by Elsevier Ltd. All rights reserved.

Keywords: Balloon; Stratosphere; Conductivity; Spatial structure; Time variations; Solar cycle variations; Latitude gradient of variance

1. Introduction

Balloon-borne measurements in the past have consistently shown that the atmospheric electrical conductivity generally increases exponentially with altitude through the troposphere and stratosphere. However, there are considerable uncertainties in the nature of the conductivity because of spatial and temporal variations that are not well understood. In this paper we report measurements of the stratospheric conductivity by more than 40 high-altitude balloons, launched from eight locations widely separated in latitude over a period of nearly 40 years. The measurements provide the opportunity to investigate long-term variations in conductivity profiles on local and global scales. This paper will focus on evidence for a geographically organized latitude gradient in the natural variance of the conductivity measurements. This research was motivated by the lack of global measurements of the atmospheric conductivity and its variations, which are crucial to our understanding of the global electrical environment (Hays and Roble, 1979; Roble and Tzur, 1986).

The atmospheric conductivity is proportional to the product of the ion concentration and the ion mobility. Variations in conductivity may be caused by a variety of factors that alter either of these two basic quantities.

* Corresponding author. Tel./fax: +1 713 743 3543.
  E-mail address: ebering@mail.uh.edu (E.A. Bering III).
  URL: http://www.uh.edu/~ebering/beringps.html (E.A. Bering III).

These factors include latitudinal and temporal variations in the ionizing cosmic ray flux, global or local variations in the ion mobility due to ion attachment to aerosols (Gringel et al., 1986), and changes in the ion mobility and ion recombination rate as functions of temperature (Israel, 1973). In previous publications (Byrne et al., 1988, 1991; Bering et al., 2003), we investigated these and other effects extensively with regard to their effects on our conductivity data from the earlier flights (prior to 1987). In our most recent survey paper, it was suggested that there may be a latitude gradient in the natural variance of stratospheric conductivity (Bering et al., 2003). The major objectives of this paper are to investigate this suggestion in quantitative detail, to expand the temporal range of our prior survey, and to present the data as a function of geomagnetic rather than geographic latitude.

The balloon flights were conducted during many separate balloon campaigns, some by our groups and others taken from the literature: 1973, 1976, and 1999 at Palestine, Texas; 1975 at Roberval, Quebec; 1980–1981 at Siple Station, Antarctica, 1985–1986 at South Pole, 1990–2003 from Syowa Station, Antarctica, 1999 at Ottumwa, Iowa, 1983–84 and 1992–93 from Christchurch, New Zealand, six flights from 1986 to 1994 from Hyderabad, India, and several flights from 1978, 1979, and 1983 from Laramie, Wyoming (Paltridge, 1965; Benbrook et al., 1974; Morita and Ishikawa, 1976; Widdell et al., 1976; Rosen et al., 1978, 1982, 1985; Bering et al., 1980, 1987, 2003, 2005; Holzworth, 1981, 1991; Rosen and Hofmann, 1981; Holzworth et al., 1984, 1986, 1992, 2005; Gupta and Narayan, 1987; Norville and Holzworth, 1987; Byrne et al., 1990, 1991; Udare et al., 1991; Holzworth and Hu, 1992; Holzworth and Norville, 1992; Gupta et al., 1992; Ejiri et al., 1995; Ebihara et al., 1996; Chakravarty et al., 1997; Gupta, 2000, 2004). The locations of the launch sites, dates and times of the balloon flights are summarized in Table 1.

2. Instrumentation

On most of the flights the conductivity measurements were obtained by the relaxation time method (Mozer and Serlin, 1969, Benbrook et al., 1974, Bering et al., 1980, Holzworth, 1981, Rosen et al., 1982, Holzworth et al., 1986, Norville and Holzworth, 1987). Various types of probes were used on the flights. Both flat plates 30 cm square and spherical probes of various diameters (15–30 cm) were used in various University of Houston (UH) and University of Washington (UW) campaigns. The UH and UW probes were coated with a colloidal suspension of carbon (Aquadag) to increase the surface work function, thereby suppressing the emission of photoelectrons which contaminate the positive ion conductivity measurements. The payload ground consisted of four similarly coated aluminum plates, typically $30 \, \text{cm} \times 60 \, \text{cm}$, mounted on the payload body. The probes were configured on the payload to enable the measurement of the electrical potential difference in the atmosphere between two points on three orthogonal axes. For this purpose each of five (Siple, Roberval) or six (Palestine, Iowa, southern ocean) probes was mounted on 2-m-long phenolic insulating booms, two

Table 1
Summary of the balloon flights

Campaign	Location	Month	Year(s)	Latitude	Number
Melbourne	Australia	February	1964	38°S	4
Perdasdefogu	Sardinia	May	1968	39°N	1
Palestine	Texas	July	1973	32°N	1
Sanriku	Japan	October	1973	39°N	1
El Aremosillo	Spain	June	1975	37°N	1
Roberval	Quebec	July	1975	48°N	3
Laramie	Wyoming	July	1975	41°N	1
Palestine	Texas	September	1976	32°N	1
Laramie	Wyoming	May–Aug.	1978	41°N	4
Laramie	Wyoming	May	1979	41°N	1
Laramie	Wyoming	March	1983	41°N	2
Siple Station	Antarctica	Dec.–Jan.	1980–81	80°S	5
EMA	S. Ocean	Dec–Jan.	1985–86	<45°S	8
South Pole	Antarctica	Dec.–Jan.	1985–86	90°S	8
Hyderabad	India	Dec., Jan., Apr., Oct.	1986, 87, 1989, 94	17°N	6
PPB	Antarctica	Dec.–Jan.	1990, 92	78°S	3
	Antarctica	Jan.–Feb.	2003	78°S	2
ELBBO Sprites 99	S. Ocean	Nov.–Feb.	1992–93	<45°S	5
Palestine	Texas	July	1999	32°N	1
Ottumwa	Iowa	August	1999	41°N	1

probe pairs horizontally and one probe-pair (probe) vertically (downward). All of the flat plate probes lay in a vertical plane. The payloads were rotated about the vertical axis at a period of typically 20 s in order to permit removal of DC offsets from the horizontal probe data. This type of double-probe system has been used frequently during the past 40 or so years to measure stratospheric electric fields (Paltridge, 1964, 1965; Mozer and Serlin, 1969; Benbrook et al., 1974; Holzworth and Mozer, 1979; Bering et al., 1980, 1987; Holzworth, 1981; Holzworth et al., 1984, 1986). The electric field was passively measured, so that the conductivity in the vicinity of the probes was not disturbed.

In the relaxation time technique, one or more probes are driven to a potential different from the "ground" potential of the payload for a short period of time and then released and allowed to lose their excess charge by conduction through the atmospheric medium. In order for the technique to work, the voltmeter that senses the potential difference between the driven probe and the payload ground must draw significantly less current than the current that flows from the probe to the medium. This is achieved by using MOSFET preamplifiers with input impedances $>10^{13}\,\Omega$. The resistance to infinity from the probe through the medium is of order $10^{11}\,\Omega$ at float altitude, but it increases roughly exponentially with decreasing altitude, with an e-folding distance of order 7–10 km. Thus this technique is useful only for altitudes above 10 km. An extensive discussion of the expected response of the probes and the methods used to obtain the conductivity data can be found in Byrne et al. (1988, 1990, 1991).

3. Observations

The conductivity measurements during the ascent or descent of a few of the balloon flights are presented as a function of altitude in Figs. 1–3. Each conductivity measurement was individually plotted and examined to see how well the fitted exponential matches the data. Those measurements that did not fit well were omitted from the data base, as discussed below and in detail by Byrne et al. (1988, 1991).

All measurements in this paper were obtained in fair-weather conditions, i.e., there were no direct effects of thunderstorms on the local electrical conditions of the atmosphere. Bering et al. (1980) have reported stratospheric conductivity measurements obtained in the vicinity of a thunderstorm during the 1975 balloon campaign. In Fig. 1, the measured conductivity profiles are compared with two model profiles. One model was derived by Cole and Pierce (1965) from microphysical considerations. The other, by Hays and Roble (1979), is an empirical model which includes a correction for latitudinal variations of cosmic ray ionization. Both model pro-
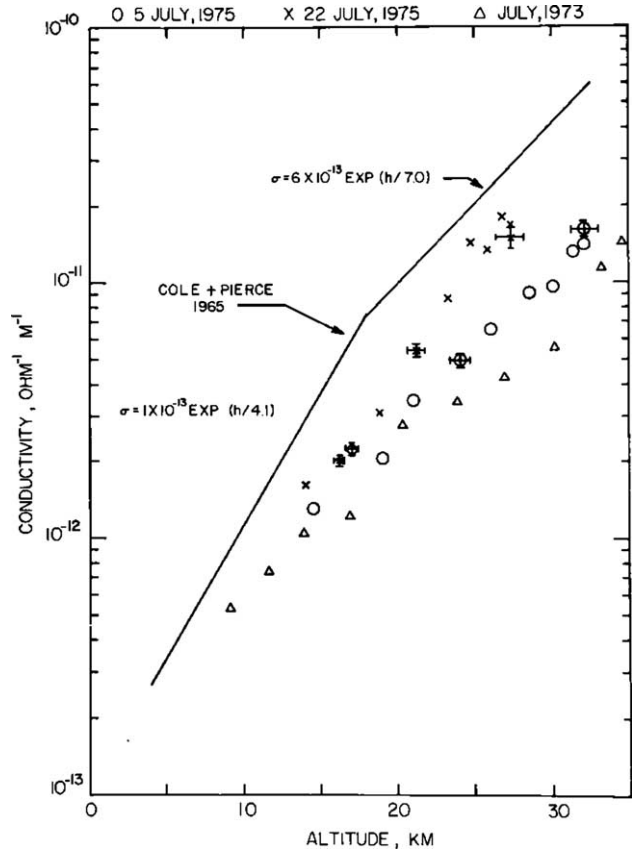
Fig. 1. Total conductivity versus altitude measured by two balloon flights during the 1975 Roberval, Quebec, campaign. The solid and open circles represent data points obtained during ascent and descent, respectively, on July 22. For comparison, the Cole and Pierce (1965) model profile and the 10 July 1973 Palestine data are also shown. (Byrne et al., 1988, ©1988 AGU, Fig. 1 reproduced with permission.)
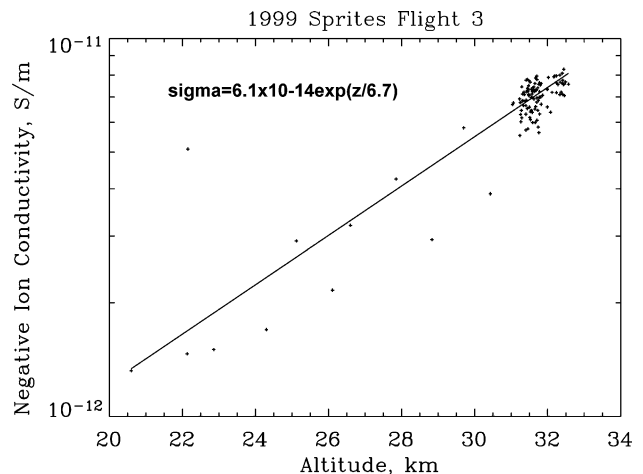
Fig. 2. Negative polar conductivity versus altitude measured at night during a flight in 1999 from Ottumwa, Iowa. The cluster of points above 30 km is the float data accumulated throughout the flight.

files are of the functional form $\sigma(z) = \sigma_\circ \exp(z/h)$, where $\sigma_\circ$ is a reference conductivity, z is the altitude above mean sea level, and h is the conductivity scale height.
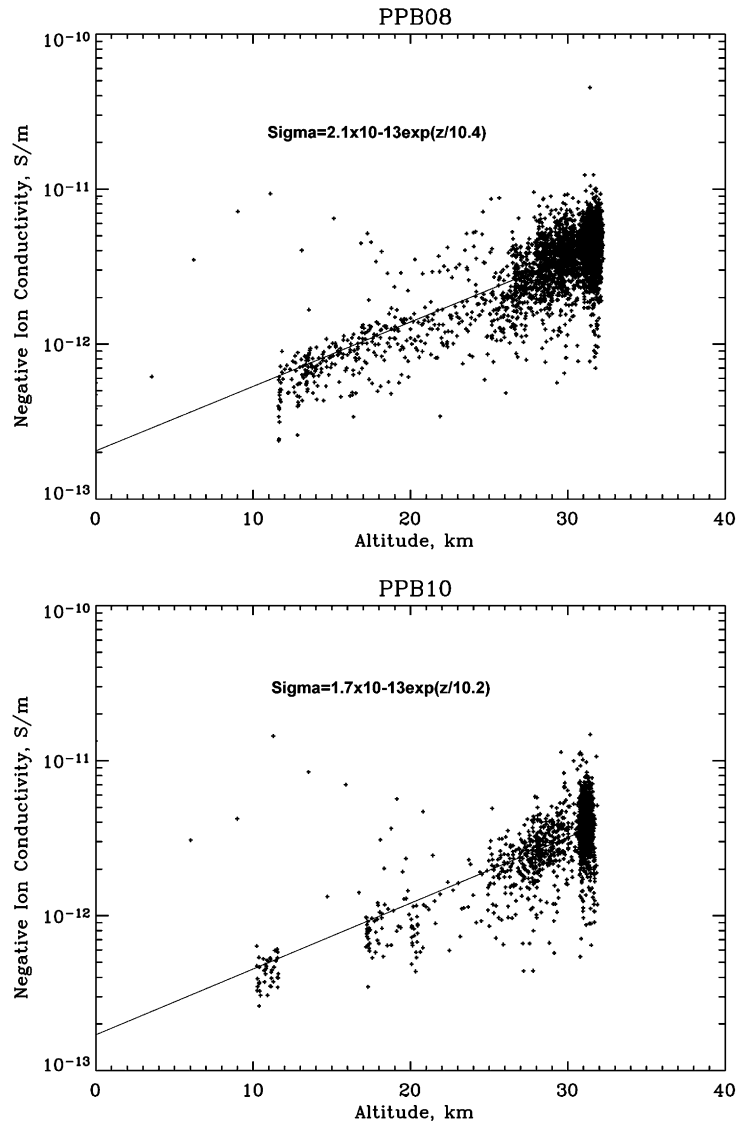
Fig. 3. Negative polar conductivity versus altitude measured by PPB 8 (top panel) and PPB 10 (bottom panel). Least-squares fits of exponential profiles are shown as solid lines with legends giving the fit coefficients.

In the Cole and Pierce model these parameters have the values

$$\sigma_\circ = 1 \times 10^{-13}, \quad h = 4.1, \quad 3.6 < z < 17.7,$$
$$\sigma_\circ = 6 \times 10^{-13}, \quad h = 7, \quad 17.7 < z < 40, \tag{1}$$

where the units for $\sigma_\circ$ are $\Omega^{-1}\,m^{-1}$, and the units for h and z are km. In the Hays and Roble model

$$\sigma_\circ = 1.14 \times 10^{-14}, \quad h = 3.5, \quad 0 < z < 8,$$
$$\sigma_\circ = 1.14 \times 10^{-13}, \quad h = 6, \quad 8 < z < 60. \tag{2}$$

The variation with latitude in the Hays and Roble model enters as a multiplying factor to (2). For Palestine, Roberval, and Siple Station latitudes, these factors are 1.2, 1.34, and 1.4, respectively, during solar quiet conditions.

For simplicity the model assumes coincident geographic and geomagnetic latitudes. The model profiles are included here as references for comparison with our data; however, neither model supposes to be a complete representation of the actual conductivity. For example, the Cole and Pierce model does not consider latitudinal variations, while the Hays and Roble model is oversimplified for mathematical expediency in their global model of atmospheric electricity (R.G. Roble, personal communication, 1987). A more complete representation of the atmospheric conductivity is lacking at this time.

Fig. 1 presents the total conductivity profiles measured during two flights of the July 1975 Roberval balloon campaign, as well as the 10 July 1973 Palestine flight for comparison. The July 5 flight attained a

maximum altitude of 32 km. This conductivity profile agrees well with the Hays and Roble model up to 17 km and between 22 and 24 km. Above 24 km the conductivity remained below the Hays and Roble profile. The July 22 flight attained a maximum altitude of 27 km before slowly descending as a result of a helium leak. Both the ascent and descent data of this flight are shown and are in good agreement. The conductivity profile measured in this flight is in good agreement with the Hays and Roble model for this latitude and is substantially different from the July 5 profile. Most notable is the lack of significant departures from an exponential increase in conductivity with altitude. The measured conductivities from both flights are below the Cole and Pierce model values by more than a factor of 2 (see 4 below) and are above the lower latitude Palestine data, as expected. Note that the scale height was ~7 km in both models and the data.

Space does not permit us to show the ascent profiles from all of the flights that we have included in this study. The data from a recent flights are shown in Fig. 2 (Ottumwa, Iowa). Two improvements in the precision of conductivity determination were incorporated in these results. The PCM telemetry system used on these flights was a 16 bit 1 kHz system, which provided a two order of magnitude increase in the resolution of the time constant measurements. Second, precise, high resolution altimetry was provided by GPS tracking, which is very much more accurate than barometric altimetry at these altitudes. In addition to the ascent profiles, the float interval data have also been included in the figures. This figures shows, first, that the conductivity over central North America has not changed significantly in nearly 30 years. Second, the fluctuations in the conductivity that occurred at a fixed altitude during the night were nearly a factor of 2. Owing to the technical refinements just mentioned, these fluctuations must be the result of actual ambient variations, rather than random measurement errors. This point will be explored further below. Note that the scale height observed by this payload was very similar to the scale heights observed elsewhere over North America in prior campaigns.

We have observed over the years that our probe voltages are at times noisy and rapidly time varying during the high-velocity ascent stage of a balloon flight. There are probably very good reasons for this, such as passage through wind-shears, aerosol layers, swinging of the payload, etc. It has been the case that much of the electric field data during the ascent portion of a given flight is simply too noisy to be useful, and few or none of the conductivity cycles (relaxation of the probe potential) could be adequately fitted to an exponential. The latter is because one has to be a bit lucky to have the infrequent conductivity measurement cycle occur during a period of reasonable stability (a time which is long compared to the relaxation time of a few seconds) of the electric field in order to get a reliable conductivity data point at low altitudes during ascent. This situation is one that varies from flight to flight. On the other hand, during times of float or slow descents, these types of noise signals (rapid, large excursions in potential) are not introduced, so that the electric field signal is stable and time constants can be determined unambiguously. We have taken the position that a conductivity data point is presented only if the exponential relaxation of the probe potential during a measurement cycle meets stringent goodness-of-fit criteria. Each of the conductivity measurement cycles during ascent or descent have been visually examined to see how well the fitted exponential of the probe potential during relaxation matches the data and how the basic data look. Those cycles that are too variable are simply omitted from the data base. This failure to fit occurred mostly during ascent. The number of missing points can be assessed by noting the gaps in otherwise regular data point in previously published individual ascent profiles (Byrne et al., 1988, 1991; Bering et al., 2003). At float and during slow altitude variations, the number of points omitted was typically a few percent of the total number of observations.

During the 2nd-PPB campaign (Bering et al., 2005; Holzworth et al., 2005), the PPB 8 and 10 flights remained aloft after the ballast supply was exhausted for 14 and 8 days, respectively. The resulting diurnal cycling in altitude afforded multiple slow rate scans over the 10–32 km altitude range. The vertical profiles of σ_- measured during these intervals of diurnal cycling are shown are shown in Fig. 3. On average, σ_- increased exponentially with increasing altitude, and over the range from 10 to 32 km can be expressed by

$$\sigma_- = \sigma_0 \exp(z/h), \tag{3}$$

where $\sigma_0 = 1.9 \times 10^{-13} \, \Omega^{-1} \, m^{-1}$, z is the altitude in km, and the scale height $h = 10.3$ km. Note that this scale height is in agreement with the scale height observed above South Pole in 1985–86 (Byrne et al., 1991), and in disagreement with the scale height observed above Siple Station in 1981 (Byrne et al., 1988).

In order to compare data from different times and places, the data must be normalized to a chosen altitude. Since the two largest data sets used in this study, EMA and ELBBO, were super-pressure balloons that floated at an altitude of 26 km, this height has been selected as the common reference height. This choice has the added advantage that the positive conductivity data are only slightly affected by photo-emission effects (Byrne et al., 1990). In order to display the entire data base in as comprehensible a way as possible, data from all of the flights in Table 1 have been plotted as a function of time (Fig. 4) and as functions of both time and geomagnetic latitude using a projected trimetric plot (Fig. 5). In both of these figures, a single point has been plotted for each zero-pressure balloon flight. Since the
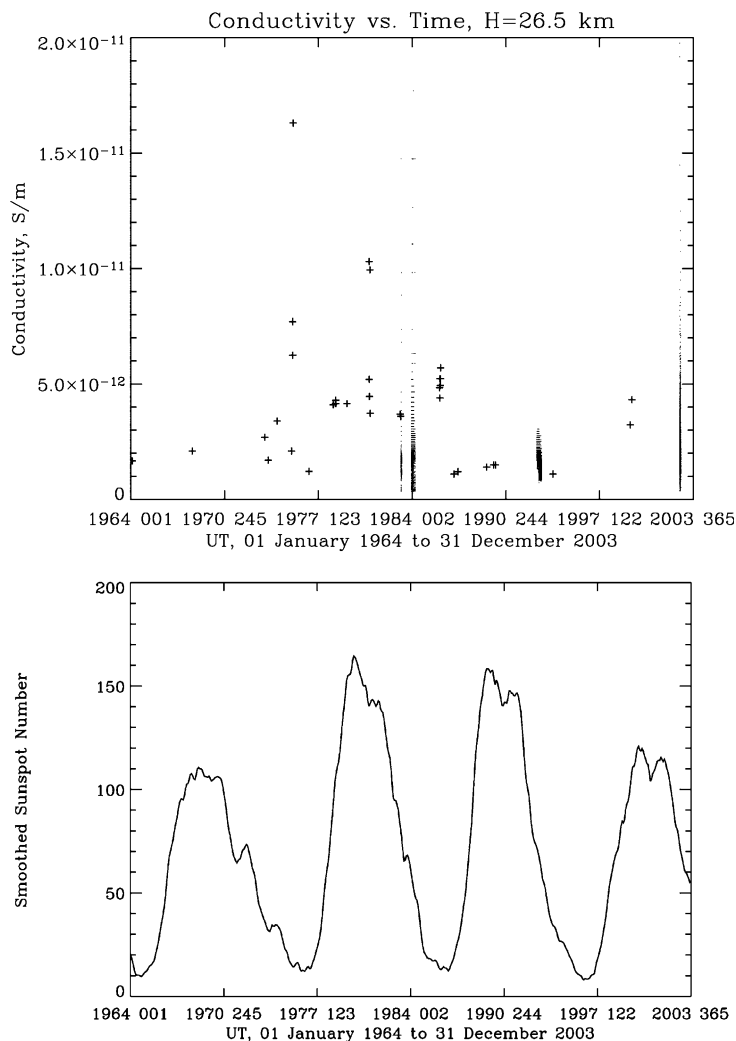
Fig. 4. Top panel shows conductivity at 26 km altitude is plotted vs. time from all flights considered in this study. Negative polar conductivity is plotted for all flights except the Laramie, Wyoming results (41°N, 1978–1983). All float altitude points from EMA and ELBBO have been plotted, using smaller dots. Bottom panel shows the smoothed monthly sunspot number for the same time interval. The format of the time axis tick mark labels is "year DOY", where DOY means day of year.

super-pressure flights covered a period of months, every data point from these flights was plotted using smaller symbols in Fig. 4. The smoothed sunspot number is plotted in the lower panel Fig. 4 in order illustrate possible solar cycle effects on the data (see below).

In Section 1, it was noted that a previous study had uncovered evidence for a latitude gradient in the naturally occurring fluctuations that are observed in the conductivity of the stratosphere (Bering et al., 2003). In order to investigate this question further, three flights were selected for detailed comparison: IMAP C-7, launched from Hyderabad on 17 October, 1989; Sprite Flight 3 launched from Ottumwa, Iowa on 21 August 1999; and PPB 8 launched from Syowa Station on 13 January, 2003. Since each of these flights flew at or near 32 km altitude, all data from these flights were normalized to exactly 32 km using the scale height appropriate to each flight. IMAP C-7 was altitude-controlled to stay

within 50 of 32 km, so no normalization was required for those data. The first two of these flights were both less than 24 h in duration, whereas the PPB flight produced 26 days of data. A comparison of the IMAP, Sprites balloon and one day of PPB data plotted as functions of universal time is shown in Fig. 6. It is evident in this Figure that the low latitude conductivity is both smaller and less variable the higher latitude data. Recall that the Sprites flight had a 1 kHz data sampling rate, which implies a very small error in estimating the exponential decay time constant.

The spatial averages and corresponding standard deviations of the data shown in Figs. 6 and 7 along with the other 25 days of data from PPB # 8 have been computed using 5° latitude bins, using both geographic and geomagnetic latitude. The resulting means and normalized variances were plotted as functions of both signed and absolute value of both types of latitude.
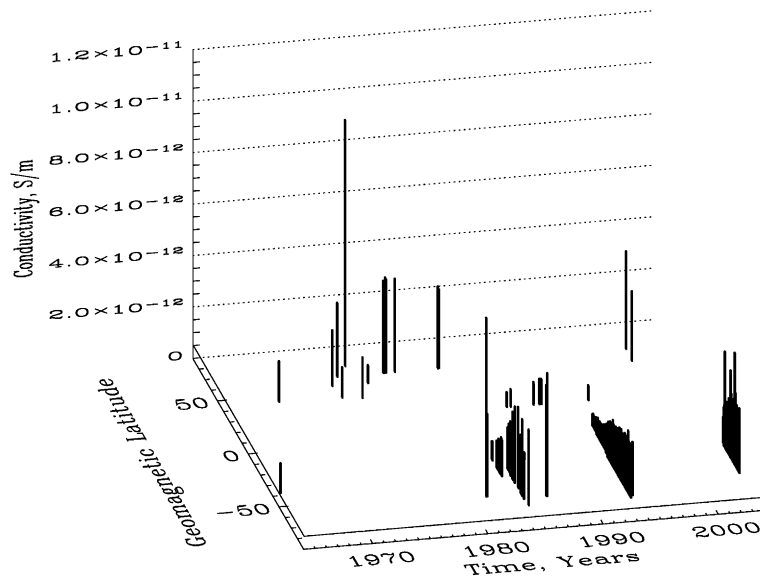
Fig. 5. Conductivity at 26 km altitude is plotted as a function of geomagnetic latitude and time using a projected trimetric view from all flights considered in this study. Negative polar conductivity is plotted for all flights except the Laramie, Wyoming results (41°N, 1978–1983).
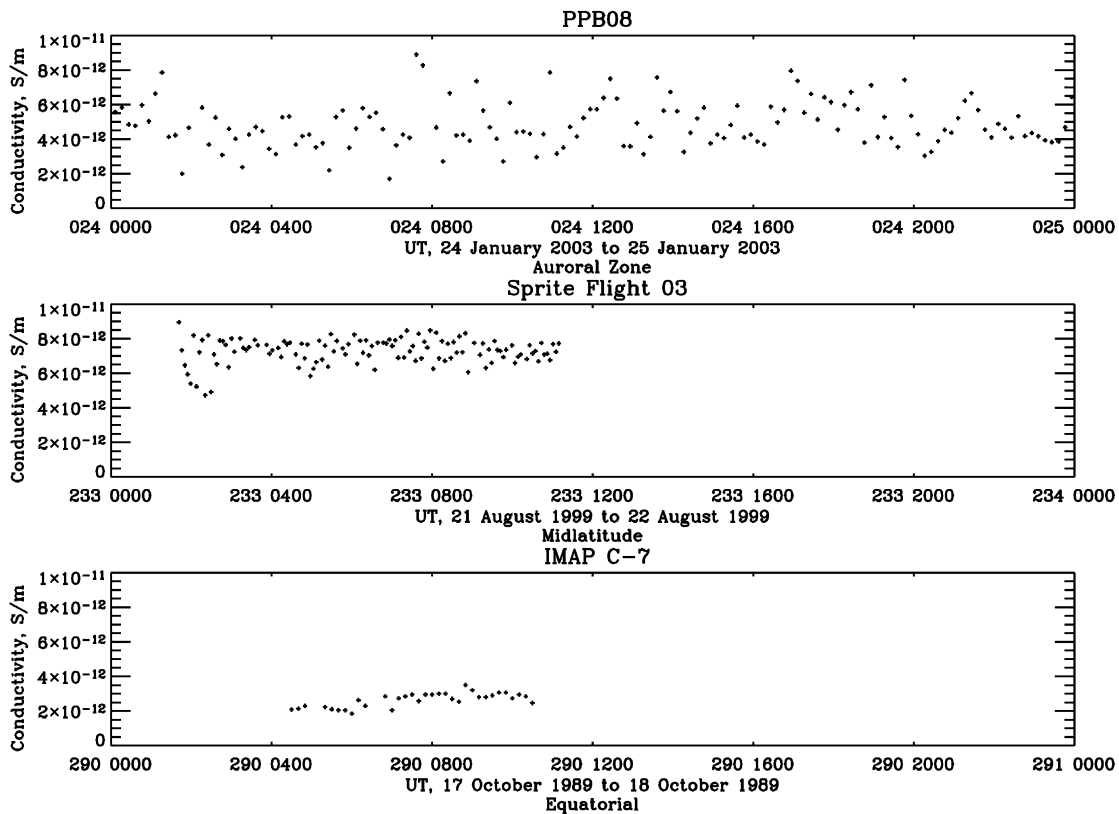
Fig. 6. Negative polar conductivity at 32 km altitude is plotted as a function of Universal Time. From bottom to top, the panels show the data measured by IMAP C-7 near Hyderabad, India, Sprite Flight 3 near Ottumwa, Iowa, and PPB 8 off the coast of Antarctica.

Fig. 8 shows the means and standard deviations plotted as functions of geomagnetic latitude. The figure indicates that the conductivity increased with increasing geomagnetic latitude. It also confirms what Fig. 5 shows that conductivity tends to be larger in the northern hemisphere than the southern. The plots of the 5° means versus absolute value of geomagnetic latitude and both signed and absolute geographic latitude are
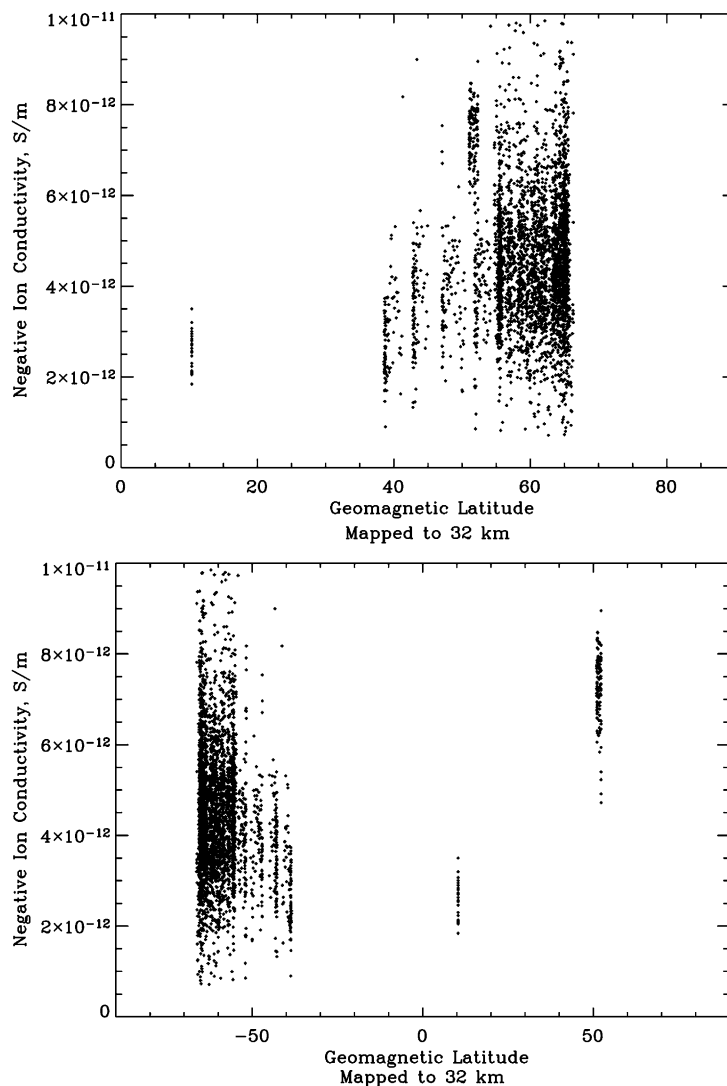
Fig. 7. Negative polar conductivity at 32 km altitude from the three flights shown in Fig. 6, plotted as functions of the absolute value of geomagnetic latitude (top panel), and geomagnetic latitude (bottom panel). All 26 days of data from flight PPB # 8 are shown.

not as well organized and not shown. The error bars plotted correspond to the standard deviation or natural variance of the data. These error bars are comparable in magnitude to the latitude variations. However, the observed curve is smooth and well ordered. The reason is that the errors in the mean are much smaller than the plotted error bars. Since the means are computed from hundreds of data points, the errors in the mean are at least an order of magnitude smaller than the standard deviations.

The normalized variance is shown as a function of the absolute value of geomagnetic latitude in Fig. 9. It should be noted that the estimated normalized experimental error of the individual data points is ∼3%. The figure shows that the variance is well organized by geographic latitude, and there is no detectable hemispheric difference. The normalized variance was ∼5–10 times the estimated experimental error.

4. Discussion

4.1. Early Palestine, Roberval and Siple flights

In our earlier papers that focused on flights prior to 1985, electrical conductivity profiles in the stratosphere were obtained from nine high-altitude balloons launched from three locations, widely separated in latitude (Byrne et al., 1988, 1991; Bering et al., 2003). Variations in the conductivity profiles were examined on local and global scales. The major conclusions of this prior work that are germane to the present paper are as follows:

1. The average profile at high latitude (76°S) was found by Byrne et al. (1988) to be in good agreement with the Hays and Roble (1979) model profile. The disagreement between their model and the measured profiles increases with decreasing latitude. The Cole
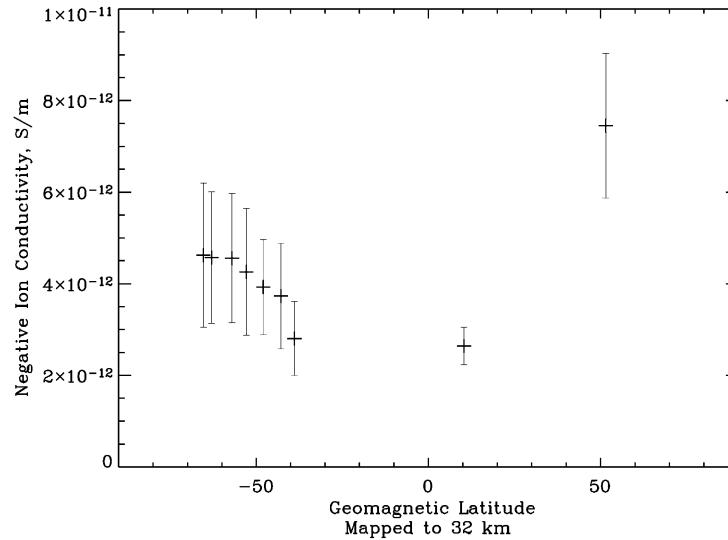
Fig. 8. Mean of 5° bins of the data shown in Fig. 7 plotted as a function of magnetic latitude. Error bars indicate the standard deviation of the data in each bin.
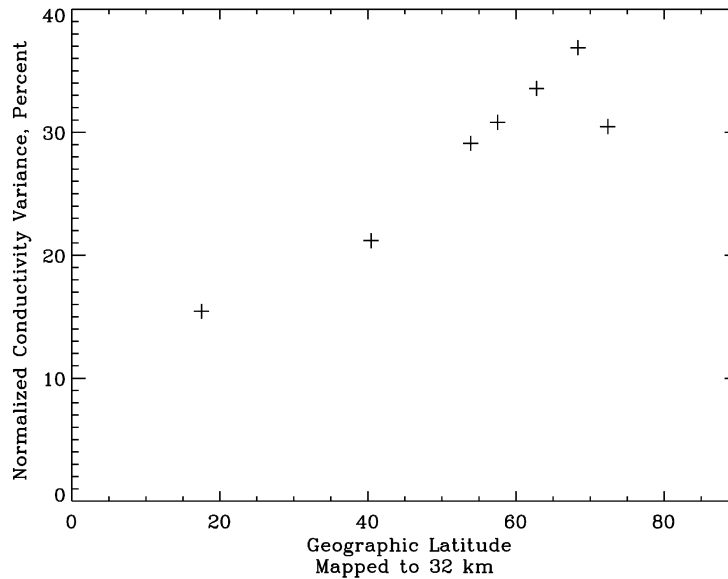
Fig. 9. Normalized variance in 5° bins of the data shown in Fig. 7 plotted as a function of the absolute value of geographic latitude.

and Pierce (1965) model appears to significantly over-estimate the conductivity for all latitudes. We specu-late that the reason for this overestimate is probably an incomplete or inaccurate consideration of the role of aerosols and molecular ion clusters in the micro-physics of the model.

2. The conductivity profiles at each latitude in Byrne et al. (1988) exhibited a significant day-to-day scatter. The measurements over Palestine and Roberval were made during quiet solar and geomagnetic conditions. Therefore the major differences in these profiles do not appear to be explained by this type of activity. The measurements over Siple Station were made during periods of variable geomagnetic conditions, which

may partly account for the observed scatter in the con-ductivity profiles. However, the scatter cannot be explained simply on the basis of changes in the ioniz-ing cosmic ray flux, which did not vary significantly from flight to flight. The day-to-day variations in con-ductivity were apparently dominated by local effects.

3. The effect of cosmic ray ionization on the latitudinal variation of the conductivity was examined by Byrne et al. (1988). The observed latitudinal variation in conductivity is not explained by a latitudinal distribu-tion of cosmic ray ionization alone.

4. The effects of aerosols and temperature on the lati-tudinal variation of the conductivity were examined by Byrne et al. (1988). A background distribution of

aerosol concentrations as a function of altitude and latitude was estimated and parameterized. By including the effects of aerosols, the agreement between the observed and calculated variation of the conductivity with latitude was improved although, the effect is too small to account for the observed variation. At high latitudes the conductivity may be maintained by a balance of ion recombination and cosmic ray ionization, while ion-aerosol attachment is insignificant. The role of aerosols becomes more important with decreasing latitude. The large variation in stratospheric temperatures with latitude was found to be a more important factor than the background aerosols. Overall, the addition of both aerosol and temperature effects results in a significant improvement in the agreement between the calculated and observed variation in conductivity. The implication of this work is that although the conductivity is quite variable due to many meteorological factors (Roble and Tzur, 1986), global models of conductivity may be improved by including the effects of a latitudinal distribution of aerosols and temperature.

4.2. Later flights

Most of the recent discussion of the results used in this paper have focused on issues such as the effect of thunderstorms on stratospheric conductivity, which are not germane to the results of this study. One interesting result is that geomagnetic latitude is the dominant organizer of the ELBBO data (Holzworth et al., 1992; Holzworth and Hu, 1992; Hu, 1994). The basic source of stratospheric conductivity is ionization owing to cosmic ray bombardment (Datta et al., 1984, 1987). As one moves to lower latitudes, the geometry of the Earth's magnetic field is such that there is a minimum momentum, termed cutoff rigidity, required for cosmic rays to reach the atmosphere. Thus the ionization rate and, therefore, the conductivity are expected to decline with latitude. In addition, solar cycle variations of the fluctuation amplitude of the interplanetary magnetic field act to modulate only the lower momentum portion of the cosmic ray spectrum. Thus solar cycle modulation of stratospheric conductivity owing to ionization rate variations is only expected poleward of 50° geomagnetic latitude (Datta et al., 1984, 1987). Ionization rate variations associated with cosmic ray cut-off rigidity variations appear to be sufficient to account for the latitude variations encountered by ELBBO, without the necessity of considering latitude gradients of temperature and aerosol content. The latitude variation of the 2003 PPB data also appears to be consistent with cosmic ray ionization rate variations (Bering et al., 2005).

The variance in the data is difficult to account for. For all of the flights, the variance is larger than the formal errors in the least squares fit parameters by a factor of at least 5. It is possible that the small size of the formal errors reflects inaccurate assessment of the uncertainty in the individual data points. Two uncertainties must be accounted for, the uncertainty in the relative timing of the data sampling, and the measurement uncertainty of the probe voltage. Since the former is established by crystal controlled on-board clocks, this uncertainty is negligible. The noise level of the probe pre-amplifiers and telemetry analog to digital conversion system can be measured on the ground. These system noise measurements are, in fact, the basis for the probe voltage error estimates used in the least squares fit. In practice, this approach may be optimistic, because it does not include the effect of ambient high frequency noise of natural geoelectric origin on the data. The fact that the variance is better organized by geographic rather than geomagnetic latitude suggests that ULF fluctuations are not the issue. The relatively low 1 Hz sampling rate of the PPB data may also have contributed to larger uncertainties in this data set than in the high data rate Sprite data. However, the results shown in Fig. 9 indicate that the variance in the PPB data varies with latitude. This would not be expected if the variance were the result of the data rate. The projected PPB latitude variation more or less intersects the Sprite flight data point, indicating that low sampling rate is not contributing significantly to this result. Thus, it does not appear that the spatially structured variance that we observe was the result of experimental uncertainty.

There is no good model that accounts for the day to day fluctuations found in the various campaigns, and in the high precision data of the 1999 flights. Any discussion of site to site and apparent long-term variations must be tempered with an awareness of how large the natural short term fluctuations are at a given site. One aspect of these fluctuations that has emerged from this study is the fact that the natural fluctuation amplitude is latitude dependent. The day-to-day and hour-to-hour variations observed at Hyderabad have an amplitude of about 15%, which is much smaller than the variance observed at Palestine, for example. This latitude gradient of variance is a new observation for which there is, as yet, no proposed model. The fact that the variance is best organized by the absolute value of geographic latitude suggests that its source lies in the properties of the high latitude atmosphere, and not in magnetospheric inputs. Since the basic composition of the stratosphere is not fluctuating, the only parameter that can be changing is the ion mobility. The presence of substantial spatial or temporal structure in ion mobility in turn implies spatial or temporal structure in the fraction of light ions vs. molecular cluster ions. This speculation remains a topic for future research.

4.3. Solar cycle variations

The error bars on the Hyderabad data are estimated to be about 3% of the mean. This level of precision permits an investigation of solar cycle and climatic effects on the data that the noisier higher latitude data do not support (Gupta, 2000). The data indicate that there is a 25% modulation of the stratospheric conductivity during a solar cycle that is positively correlated and in phase with sunspot number, which can be seen by comparing the sunspot number curve in Fig. 4 with the Hyderabad data in the same figure and in Fig. 5. At 32° latitude, the data suggest a similar behavior at the two standard deviation significance level. At higher latitude, 42° and above, the natural short term variance obscures the solar cycle signal, if any is there. However, it is worth noting the largest conductivities observed, at Roberval in 1975, were observed at high latitude near solar minimum (Fig. 4), in agreement with expectation.

Datta et al. (1987) have modeled the latitude variation of the ion production rate in the stratosphere owing to cosmic rays. These results clearly showed that the solar cycle variation due to cosmic ray intensity is negligible at the latitude of Hyderabad. It is, of course, important at high latitude. Our results show that conductivity has positive correlation with solar cycle at low latitude. This correlation can be attributed to a change in ion composition with solar cycle. The solar UV radiation in the 200–300 nm band can increase by 5% from low to high solar activity. This increase can be sufficient to dissociate higher mass ion clusters to lighter ion mass. Hence it can result in increase in conductivity. This conclusion has been explained in an earlier publication (Gupta, 2000).

5. Conclusions

Review of the data presented lead us to realize that very little can be concluded at this time. Unexplained day to day and minute to minute variations dominate the data at high latitude. The data suggest that conductivity is declining in time and that the conductivity is lower in the S. Hemisphere. One might try to explain the former effect as the result of increasing aerosol or water vapor content of anthropogenic origin. However, such an explanation would also predict that the conductivity should be higher rather than lower in the Southern hemisphere. Thus, in terms of possible mechanisms, these suggestions are inconsistent.

An important new observation reported here is the latitude gradient of the variance of the conductivity. There is no proposed model for this phenomenon. The fact that the change of the variance depends on the absolute value of geographic latitude suggests that its source lies in the properties of the high latitude atmosphere, and not in magnetospheric inputs.

References

Benbrook, J.R., Kern, J.W., Sheldon, W.R. Measured electric field in the vicinity of a thunderstorm system at an altitude of 37 km. J. Geophys. Res. 79, 5289–5294, 1974.

Bering, E.A., Rosenberg, T.J., Benbrook, J.R., Detrick, D., Mathews, D.L., Rycroft, M.J., Saunders, M.F., Sheldon, W.R. Electric fields, electron precipitation and VLF radiation during a simultaneous magnetospheric substorm and atmospheric thunderstorm. J. Geophys. Res. 85, 55–72, 1980.

Bering III, E.A., Benbrook, J.R., Holzworth, R.H., Byrne, G.J., Gupta, S.P. Long term changes in the electrical conductivity of the stratosphere. Adv. Space Res. 32, 1725–1735, 2003.

Bering, III. E.A., Benbrook, J.R., Howard, J.M., Oró, D.M., Stansbery, E.G., Theall, J.R., Matthews, D.L., Rosenberg, T.J. The 1985–86 South Pole balloon campaign, in: Proceedings of the Nagata Symposium on Geomagnetically Conjugate Studies and the Workshop on Antarctic Middle and Upper Atmosphere Physics held at SCAR XIX, Memoirs of the National Institute of Polar Research, Japan, Special Issue No. 48, pp. 313–317, 1987.

Bering, III. E.A., Holzworth, R.H., Reddell, B.D., Kokorowski, M.F., Kadokura, A., Yamagishi, H., Sato, N., Ejiri, M., Hirosawa, H., Yamagami, T., Torii, S., Tohyama, F., Nakagawa, M., Okada, T. Balloon observations of temporal and spatial fluctuations in stratospheric conductivity. Adv. Space. Res., this issue, 2005.

Byrne, G.J., Bering, E.A., Benbrook, J.R. Balloon observations of stratospheric electricity above the south pole: vertical electric fields, conductivity, and conduction current. J. Atmos. Terr. Phys. 53, 859–868, 1991.

Byrne, G.J., Benbrook, J.R., Bering, E.A., Oró, D.M. Solar radiation (190–230 nm) in the stratosphere: implications for photoelectric emissions from instrumentation at balloon altitudes. J. Geophys. Res. 95, 5557–5566,, 1990.

Byrne, G.J., Benbrook, J.R., Bering III, E.A., Oró, D.M., Seubert, C.O., Sheldon, W.R. Observations of the stratospheric conductivity and its variation at three latitudes. J. Geophys. Res. 93, 3879–3892, 1988.

Chakravarty, S.C., Gupta, S.P., Chandrasekaran, S. Middle atmospheric electrodynamics at low latitude. Adv. Space Res. 20, 2181–2189,, 1997.

Cole, R.K., Pierce, E.T. Electrification in the Earth's atmosphere for altitudes between 0 and 100 kilometers. J. Geophys. Res. 70, 2735–2749,, 1965.

Datta, J., Chakravarty, S.C. Mitra, A.P., Cosmic ray ion production rates in the middle atmosphere. Scientific Report ISRO-IMAP-SR-16-84, ISRO, Bangalore, 1984.

Datta, J., Chakravarty, S.C., Mitra, A.P. A model for cosmic ray produced ionisation in the middle atmosphere. Indian J. Radio Space Phys. 16, 257–266, 1987.

Ebihara, Y., Kadokura, A., Tonegawa, Y., Tohyama, F., Sato, N., Hirasima, Y., Namiki, M., Bering, E.A., Benbrook, J.R., Ejiri, M. A convection enhancement event observed with the Polar Patrol Balloon #4. Proc. NIPR Symp. Upper Atmos. Phys. 9, 12–24, 1996.

Ejiri, M., Akiyama, H., Bering, E.A., Fujii, R., Hayashi, M., Hirasima, Y., Kadokura, A., Kanzawa, H., Kodama, M., Miyaoka, H., Murakami, H., Nakagawa, M., Namiki, M., Nishimura, J., Ohta, S., Suzuki, H., Tohyama, F., Tonegawa, Y., Yajima, N., Yamagami, T., Yamagishi, H., Yamanaka, M.D. Experimental results of Polar Patrol Balloon project in Antarctica (extended abstract). Proc. NIPR Symp. Upper Atmos. Phys. 8, 60–64, 1995.

Gringel, W., Rosen, J.M., Hofmann, D.J. Electrical structure from 0 to 30 kilometers, in: The Earth's Electrical Environment. National Academy Press, Washington, DC, 1986.

Gupta, S.P. Solar cycle variations of stratospheric conductivity over low latitude. Adv. Space Res. 26, 1225–1229, 2000.

Gupta, S.P. Solar activity and atmospheric tide effect on the polar conductivity and the vertical electric field in the stratosphere at low latitude. Adv. Space Res. 34, 1798–1800, 2004.

Gupta, S., Narayan, A. Balloon borne measurements of ion conductivity over low latitude stratospheric systems. Planet. Space Sci. 35, 439–443, 1987.

Gupta, S.P., Chakravarty, S.C., Chandersekaran, S. (Eds.), Balloon-borne Experiments for Middle Atmosphere Conductivity Campaigns. ISRO-IMAP S.R., 39, ISRO, Bangalore, 1992.

Hays, P.B., Roble, R.G. A quasi-static model of global atmospheric electricity: the lower atmosphere. J. Geophys. Res. 84, 3291–3305, 1979.

Holzworth, R.H. High latitude stratospheric electrical measurements in fair and foul weather under various solar conditions. J. Atmos. Terr. Phys. 43, 1115–1125, 1981.

Holzworth, R.H. Conductivity and electricity field variations with altitude in the stratosphere. J. Geophys. Res. 96 (D7), 12857–12864, 1991.

Holzworth, R.H., Hu, H. Global electrodynamics deduced from long duration balloon-borne measurements, in: Barron, E.J. Fifth Symposium on Global Change Studies and the Symposium on Global Electrical Circuit, Global Change and the Meteorological Applications of Lightning InformationAmerican Meteorological SocietyBoston, MA293–295, 1992.

Holzworth, R.H., Mozer, F.S. Direct evidence of solar flare modification of stratospheric electric fields. J. Geophys. Res. 84, 363–367, 1979.

Holzworth, R.H., Norville, K.W. The global circuit as deduced from balloon-borne measurements, in: Borisenkov, E., Stepanenko, V., Voeikov, A.I. (Eds.), Proceedings 9th International Conference on Atmospheric Electricity, I. Main Geophysical Observatory, St. Petersburg, Russia, pp. 14–17, 1992.

Holzworth, R.H., Norville, K.W., Kintner, P.M., Powell, S.P. Stratospheric conductivity variations over thunderstorms. J. Geophys. Res. 91, 13,263, 1986.

Holzworth, R.H., Onsager, T., Kintner, P., Powell, S. Planetary-scale variability of the fair-weather vertical electric field in the stratosphere. Phys. Rev. Lett. 53, 1398–1401, 1984.

Holzworth, R.H., Norville, K.W., Hu, H., Dowden, R.L., Adams, C.D., Brndell, J., Pinto, O., Pinto, I., Gonzalez, W.D. ELBBO: extended life balloon borne observatories. URSI Radioscientist 4, 33–37, 1992.

Holzworth, R.H., Bering, III. E.A., Kokorowski, M.F., Reddell, B., Kadokura, A., Yamagishi, H., Sato, N., Ejiri, M., Hirosawa, H., Yamagami, T., Torii, S., Tohyama, F., Nakagawa, M., Okada, T. Balloon observations of temporal variation in the global circuit compared to global lightning activity. Adv. Space Res., this issue, 2005.

Hu, H., Global and local electrical phenomena in the stratosphere. Ph.D. Dissertation, University of Washington, 170 p., 1994.

Israel, H. Atmospheric ElectricityNat. Tech Inform. Serv., vol. 1 and 2. U.S. Dept. Commer., Springfield, VA, 1973.

Morita, Y., Ishikawa, H. Simultaneous measurements of electric conductivity and aerosol in the lower stratosphere. J. Geomag. Geoelectr. 28, 309–315, 1976.

Mozer, F.S., Serlin, R. Magnetospheric electric field measurements with balloons. J. Geophys. Res. 74, 4739–4755, 1969.

Norville, K, Holzworth, R. Global circuit variability from multiple stratospheric electrical measurements. J. Geophys. Res. 92, 5685–5695, 1987.

Paltridge, G.W. Measurements of the electrostatic field in the stratosphere. J. Geophys. Res. 69, 1947–1954, 1964.

Paltridge, G.W. Experimental measurements of the small-ion density and electrical conductivity of the stratosphere. J. Geophys. Res. 70, 2751–2761, 1965.

Roble, R.G., Tzur, I. The global atmospheric-electrical circuit. The Earth's Electrical Environment. National Academy Press, Washington, DC, 1986.

Rosen, J.M., Hofmann, D.J. Balloon-borne measurements of electrical conductivity, mobility, and the recombination rate. J. Geophys. Res. 86, 7406–7410, 1981.

Rosen, J.M., Hofmann, D.J., Gringel, W. Measurements of ion mobility to 30 km. J. Geophys. Res. 90, 5876–5884, 1985.

Rosen, J.M., Hofmann, D.J., Kaselau, K.H. Vertical profiles of condensation nuclei. J. Appl. Meteorol. 17, 1737–1740, 1978.

Rosen, J.M., Hofmann, D.J, Gringel, W., Berlinski, J., Michnowski, S., Morita, Y., Ogawa, T., Olson, D. Results of an international workshop on atmospheric electrical measurements. J. Geophys. Res. 87, 1219–1227, 1982.

Udare, R.S., Rajaram, R., Ogawa, T., Yashuhara, M. Height profile of vertical electric field and conductivity over Hyderabad. Indian J. Radio Space Phys. 20, 307–309, 1991.

Widdell, H.U., Rose, G., Borchers, R. Experimental result on the variation of electrical conductivity and ion mobility in the mesosphere. J. Geophys. Res. 81, 6217–6220, 1976.

High-resolution mesospheric layer structures from MST radar backscatter echoes over low latitude

S.C. Chakravarty[a,*], Jayati Datta[a], S. Kamala[b], S.P. Gupta[c]

[a] *Antariksh Bhavan, ISRO Headquarters, New BEL Road, Bangalore 560094, India*
[b] *Physics Department, SV University, Tirupati 517502, India*
[c] *Physical Research Laboratory, Navarangapura, Ahmedabad 380 009, India*

Abstract

The MST radar facility located at the low latitude Indian station Gadanki ($13.5°$N, $79.2°$E) has been used to study the high-resolution spatial structure of the mesospheric return echo power and relate these to the dynamics and electron density irregularities of the region. Special observations carried out using narrow pulse lengths indicate presence of scattering layers down to $\sim$600 m embedded in the broad turbulence field of about 4–5 km thickness around 75 km height region of the mesosphere. Possible cause of generation of such thin layer structure is examined. The percentage amplitudes of the 3 m electron density irregularity profile are reconstructed for 200 m height resolution from the past rocket borne results over SHAR ($13.7°$N, $80.2°$E) close to the radar site. At least two rocket results showed that apart from considerable increase in percentage amplitudes of the 3 m size irregularities in the mesospheric height region of 70–80 km, there is evidence of presence of thinner layers of these irregularities similar to that observed in the radar backscatter intensity. Implications of these results are analysed and directions for further research suggested.
© 2004 Elsevier Ltd. All rights reserved.

Keywords: Mesospheric turbulence; Mesospheric dynamics; Mesospheric scattering; Ionisation irregularities; MST radar; Rocket probes

1. Introduction

The Earth's mesosphere ($\sim$50–85 km) forms the transition region between the meteorological domain of the lower atmosphere and the regime of space plasma, dominated by electrodynamics. In this region, the ionisation produced primarily by cosmic rays, auroral electron flux, solar UV (Lyman-α) and X-rays ($E < 10$ keV) gets mixed with the complex neutral dynamics of winds, waves and turbulence mainly due to high neutral electron collision frequencies. Since mesospheric region is difficult to study by satellite-borne techniques, ground-based radar, lidar and rocket-borne experiments have been extensively used for bridging this gap.

Mesosphere stratosphere and troposphere (MST) radar technique has been used at a number of high, middle and low latitude stations of the world to study the dynamics of the middle atmosphere ($\sim$10–100 km). The unique features of the radar with its high-poweraperture product ($\sim$10^8– 10^9 Wm^2), variable pulse width and coding, coherent detection and integration are well suited to probe mesospheric region of the atmosphere at high spatial and temporal resolutions. Interestingly, these observations are potentially useful to investigate the characteristic variations in turbulent layers of ionisation and associated wave modulations (Harper and Woodman, 1977; Fukao et al., 1979; Datta et al., 2001).

Data collected from the MST radars have been used to derive the broad characteristics of the radar return signals backscattered from the variations in the permittivity of the medium due to spatial and temporal fluctuations in the electron density (δN_e) produced by neutral turbulence (Rastogi and Bowhill, 1976a,b). The basic mechanism of Bragg

scattering is responsible for backscatter from the ionisation irregularity scales of half the radar wavelength. Studies have shown that atmospheric gravity waves, generated by mountain Lee waves, the convective weather systems, etc., propagate upwards and growing in amplitude, may break down/transfer energy to modulate the mean wind leading to shearing flows which may become unstable to produce turbulent motions generating the ionisation irregularities at different scale sizes (Fritts, 1984).

Global data from MST radar observations have revealed the following main characteristics of the MST radar return echoes from the mesosphere (Gage and Balsley, 1980; Kubo et al., 1997; Kamala et al., 2003) (a) at different radar beam directions the backscattered signal is highly variable in time and space, (b) there are certain preferred height regions in the mesosphere, which produce the backscattered echoes more regularly; commonly these are observed as two broad height regions of 65–80 and 80–85 km, (c) over the high latitude region strong echoes are obtained from 82–85 km height range called Polar Mesospheric Summer Echoes (PMSE); during other seasons significant but weak backscatter echoes are generated from lower height regions ($\sim$65–80 km), (d) over the low latitude stations e.g., Jicamarca and Gadanki, the main scattering layer lies around $\sim$75 $\pm$ 5 km with another weak region of radar scattering around 80 $\pm$ 5 km; the 75 $\pm$ 5 km scattering region showing seasonal dependence with strongest echoes seen during June/July months and weakest during winter.

These observations of radar backscatter signals contain information on the structure and thickness of the scattering region which generally correspond to the mesospheic turbulence field (Fukao et al., 1985). Due to poor values of signal-to-noise ratio of back-scattered return echoes, much of the mesospheric observations, particularly over low latitude stations have been carried out at 16 μs pulse lengths equivalent to 2.4 km range resolution. At this resolution, it is possible to resolve the scattering layer thickness of the same order, making it difficult to resolve the possible existence of the fine structure present within the broad layer. Attempt has been made to estimate the fine structure of the mesospheric scattering layer over Jicamarca by operating the radar in FDI mode. While this technique provides a better determination of the location of scattering layer within the broad region, it is not possible to resolve multiple layers, if present within this region (Stitt and Kudeki, 1991). However, the technique has been found useful in computing wind fields with better spatial resolution than normally possible over Jicamarca which is located under the equatorial electrojet. Over the mid-latitude region some preliminary results have been published by Roettger et al. (1979) showing the presence of blobs, sheets and layers by operating the SOUSY radar, Germany at 150 m. However, above 70 km layers of thickness 1–2 km could only be observed.

Sounding rocket experiments have been carried out from many locations for in-situ measurements of the vertical profiles of electron density (N_e) and electron density irregularities ($\Delta_z N_e$) at a higher resolution of $\sim$1 km as compared to the coarser radar resolution. A number of near simultaneous rocket–radar campaigns have been carried out to study the correlation between the presence of ionisation irregularities and that of mesospheric scattering regions derived from the radar data. An important result from these experiments is that on many occasions, the strong layers of ionisation irregularities in the mesosphere as revealed by rocket experiment are associated with the occurrence of significant radar backscattered signal from the same height regions (Royrvik and Smith, 1984; Lehmacher et al., 1997). The basic theoretical understanding that the radar backscatter from mesosphere takes place from δN_e present at the required Bragg wavelength scales and also partial reflection from layers of sharp electron density gradients (Fresnel scatter) have been amply demonstrated by these rocket–radar sets of observations (Roettger, 1994). While these comparisons have broadly demonstrated the presence of ionisation irregularities and corresponding radar backscattered echoes from the same region, a detailed assessment of the layer thickness and structures has not been made particularly over the low latitude region.

In the present work, results of the high-resolution observations using the MST radar at the Indian station Gadanki (13.5°N, 79.2°E) are presented for the first time to study the fine structure of the mesospheric scattering layer. The characteristic features of the mesospheric ionisation layer thickness revealed by rocket observations of ionospheric electron density irregularities over the Indian rocket launching station SHAR (13.7°N, 80.2°E) are examined by reanalysing the data obtained from earlier flights. While one-to-one comparison of radar and rocket results is not possible using past rocket flight data, it is useful to qualitatively demonstrate features of the fine structure of the electron density irregularities, if any, from this new analysis of the earlier rocket data at a location which is only $\sim$100 km away from the radar site.

2. Observations, data and analysis

For this experiment, MST radar at Gadanki was operated at 1.2 km and 600 m range resolutions in addition to the 2.4 km resolution normally used for mesospheric observations, and we succeeded in getting a few days of such high-resolution data with significant SNR values. The radar data are presented in the form of height profiles of the return echo power for selected events (following the criterion of SNR > -10 dB) on different days of observation corresponding to range resolutions of 2.4, 1.2 and 0.6 km. Sample RTI plots are included for the period of near continuous radar backscatter signals at 1.2 km and 600 m resolutions.

High-altitude sounding rocket experiments have been conducted from the Indian station SHAR primarily to study E and F region ionospheric phenomena. These measurements include profiles of ion and electron densities and

electron density irregularities observed over a scale size spectrum. While the rocket measurements are capable to provide statistically significant data at very high resolution (each sample data corresponding to ~50 m height resolution), normally for the E- and F-region studies further averaging is done to get the profile at 1 km height resolution. For the present paper, the rocket probe current data are re-analysed to derive $\Delta_z N_e$ height profiles in the mesosphere containing details of the fine structure. For measuring electron density and electron density irregularities, rocket borne Langmuir probes were flown on two RH-560 rockets from SHAR on May 4, 1987 at 10:10 h LT and on April 19, 1993 at 11:20 h LT, respectively. A fixed bias voltage of +4 V is applied to the sensor and the current collected by the probe is telemetered to the ground. The probe current is converted into electron density using a suitable calibration factor. To measure electron density irregularities an AC amplifier with a frequency bandwidth of 100 Hz–2 kHz is used onboard. The rocket velocity at 75 km is about 2 km/s. The composite amplitude of irregularities is subjected to spectrum analysis using six filters corresponding to different scale sizes. The 3 m size irregularity amplitudes are estimated from these measurements (Prakash et al., 1972; Gupta, 1997, 1999).

3. Results

Fig. 1a shows the vertical beam return echo power of sample mesospheric radar observations for different hours of September 5, 1995, September 7, 1995 and July 21, 1998 at 600 m, 1.2 and 2.4 km range resolutions, respectively. All the three height profiles show considerable enhancement of backscattered power around ~75 km altitude and display the echo layer fine structure of varying degrees. The 600 m resolution data on September 5 shows the presence of two or more scattering layers as compared to one or more at 1.2 and only one broad layer at 2.4 km resolution data. On July 21 the 2.4 km resolution data indicates that the average FWHM value of the thickness of the turbulent layer around ~75 km is ~4–5 km. Different times of occurrence of good return echo power in the same hour slot for different beam directions (not shown in the figure) point to the relatively short horizontal extent (< 10 km) of these turbulent centres as estimated from the off-vertical observations for a radar beam angle of $10°$. The main point to be noted is that the finer details of the layer structure become progressively visible as we go to higher range resolution echoes indicating the presence of thin layers of at least 600 m.

Fig. 1b also shows similar examples of the height profiles of radar return echo power in the vertical radar beam for selected times on two days of radar observation (August 12, 1996 and September 20, 1996). Observations on August 12 were carried out both at 600 m and 1.2 km range resolutions and that of September 20 at 1.2 km. The presence of fine structures in the 600 m resolution data can be clearly seen in the figure. The two panels of August 12 observations indicate how the details of layer fine structure can be lost by switching the radar pulse width from 4 to 8 μs.

Fig. 2 shows a different perspective of the same data given for 600 m range resolution in Fig. 1a. While the first panel shows the observed height profile of the return echo power for the vertical beam at 600 m range resolution the lower panels show the simulation of the same data averaged for 1.2 and 2.4 km range resolutions, respectively. The simulated results mean that had the radar been operated at 1.2 and 2.4 km resolutions on September 5, the height profile of the return echo power would have looked like what is shown in this figure, i.e., smoothing out the higher-order structures. The presence of multiple layers in panel 1 going through intermediate transition is replaced by broader layer structures seen in the lowest panel would virtually correspond to the data at range resolution of 2.4 km. The results shown here in panels for 1.2 and 2.4 km have striking similarities with the second and third panels of Fig. 1a even though the days are different.

The corresponding RTI plots of the data for September 5, 1995 and September 7, 1995 are shown in Fig. 3. The presence of thin layers up to 600 m is discernable from this figure. It may be seen that there is considerable diurnal variability in the occurrence and strength of thin layers within the region of turbulence. Such dynamic situation points to the highly irregular structure of the mesospheric turbulence.

The rocket data over SHAR has been used to examine the possible signatures of the manifestations of neutral density turbulence on the electron density irregularities. The electron density profiles at 1 km resolution and the percentage amplitude of electron density irregularities for 3 m scale size reanalysed for 200 m height resolution are computed from the respective telemetry channel data of rocket flights for May 4, 1987 and April 19, 1993. The values of 200 m resolution data are selected after optimising the minimum height resolution from SNR considerations pertaining to the original time series of rocket data at 50 m height intervals.

The results of the vertical profiles of N_e and the percentage amplitude of 3 m size electron density irregularities are shown in Fig. 4. It can be seen that there is enhanced percentage amplitude of electron density irregularities on both the days in the height region of interest with April 19 showing presence of more irregularities compared to that of May 4 flight data. It may also be noted that the electron density profile shows more gradients during April 19 compared

Fig. 1. (a) Height profiles of radar return echo power (in arbitrary units) as observed on 5 September 1995, 7 September 1995 and 21 July 1998 for three range resolutions of 600 m, 1.2 and 2.4 km, respectively for selected scans every hour in the vertical beam direction. (b) Same as Fig. 1a for 20 September 1996 for 1.2 km range resolution and for 12 August 1996 for 600 m and 1.2 km range resolutions, both for vertical beam directions.

(a)   **Return Echo Power, Arbitrary Units**

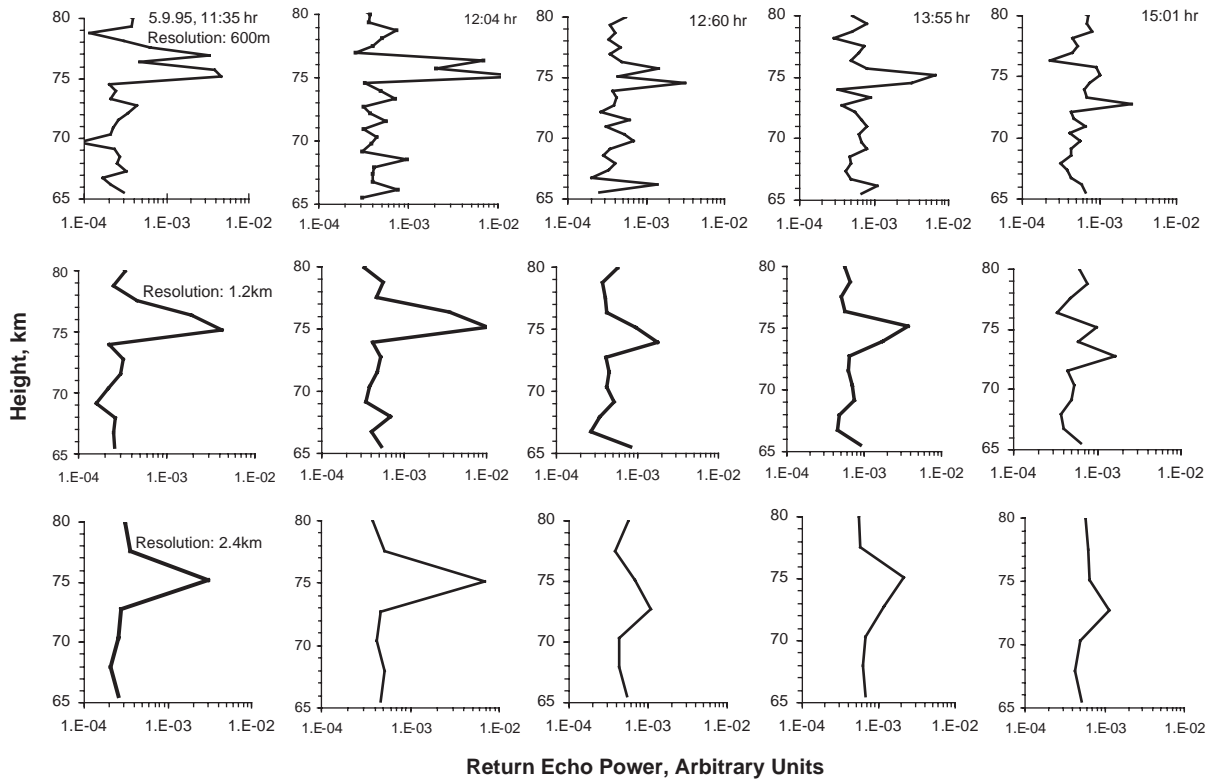(b)   **Return Echo Power, Arbitrary Units**
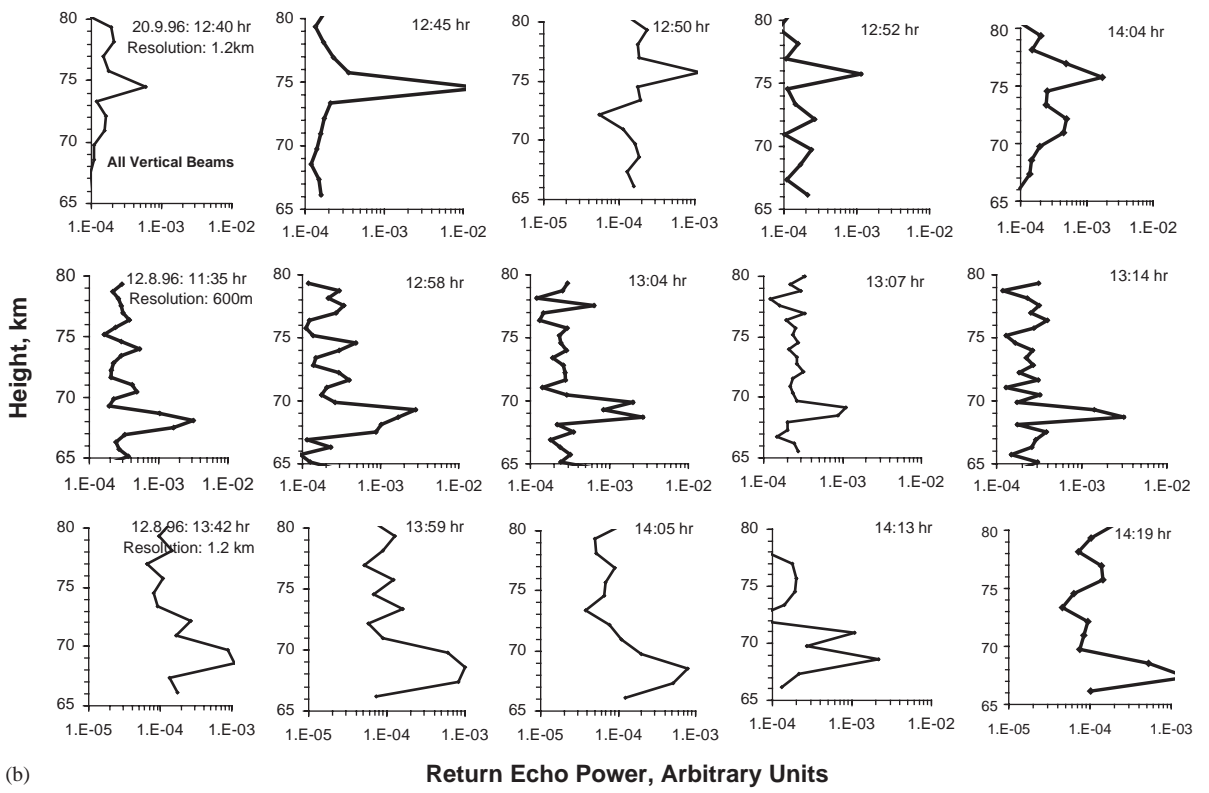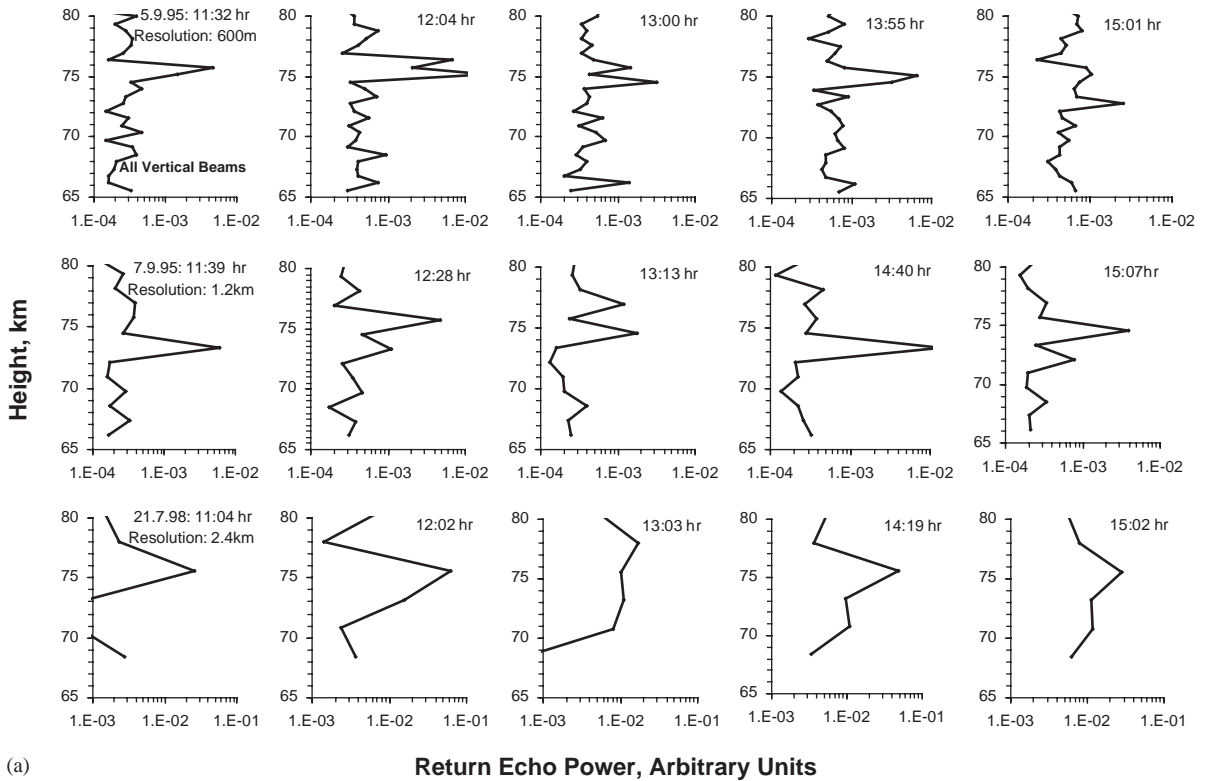
Fig. 2. Height profile of radar return echo power (in arbitrary units) for observations on 5 September 1995 for height resolution of 600 m (top panel). Same data averaged for 1.2 and 2.4 km height resolutions are shown in middle and bottom panels, respectively.
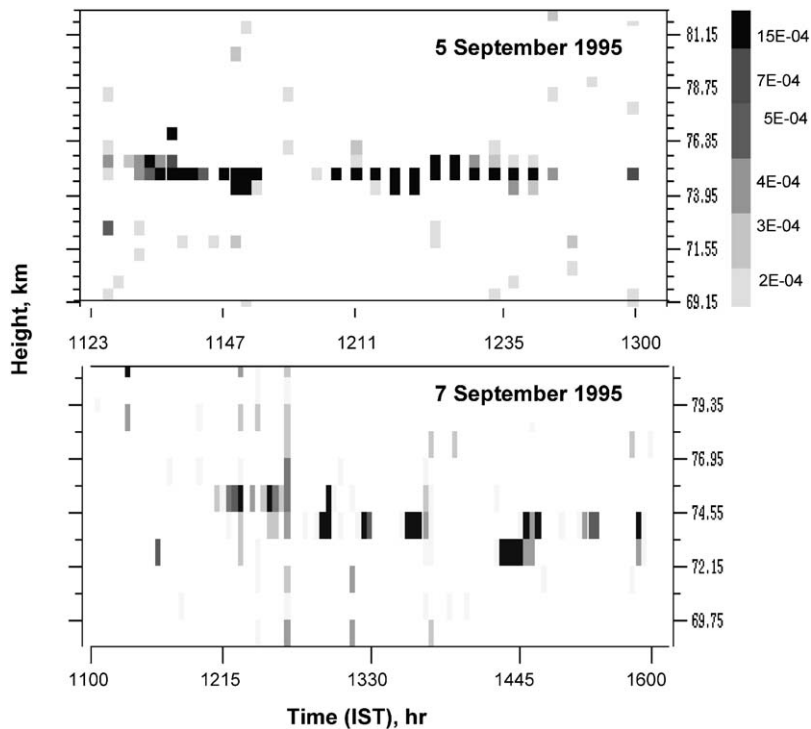

Fig. 3. Range–time–intensity (RTI) plots using return echo power of the radar backscatter signal for vertical beam direction during 5 September and 7 September 1995 at 600 m and 1.2 km height resolutions.
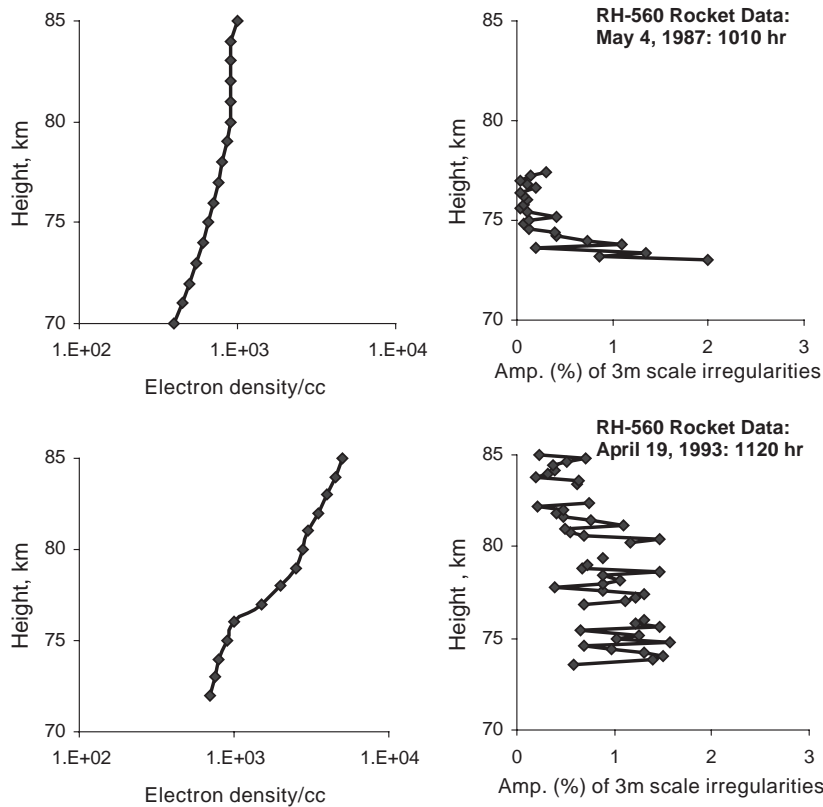
Fig. 4. Electron density profiles obtained using rocket experiments from SHAR on 4 May 1987 (top panel) and 19 April 1993 (lower panel) for 1 km height resolution and the height profiles of the percentage amplitude of electron density irregularities for 3 m-scale size at 200 m resolution for same days.

to that of May 4. Whether the relatively higher percentage (∼1%) of ionisation irregularities at 3 m scale sizes is a very special case can only be determined by more rocket observations over these latitudes. Available results from radar –rocket comparison made from other locations do not indicate presence of such high values of 3 m sizes of ionisation irregularities (Royrvik and Smith, 1984; Pfaff et al., 1985). It is seen from Fig. 4 that the amplitudes of the 3 m size irregularities are enhanced between 73 and 80 km which has been observed at other locations also. The height profile of the percentage amplitude of irregularities indicates presence of thin layers within the broader region of irregularities.

FFT computations are carried out on the rocket electron density data read at 200 m height intervals between 73 and 77 km on May 4, 1987 and between 73 and 85 km (in three separate broad layers) on April 19, 1993 using the channels providing the information on ionisation irregularities. While the spectral power of the fundamental frequency (assumed to correspond to the broad height ranges of occurrence of ionisation irregularities) shows the maximum amplitude, there is above noise level spectral power distribution between the thinner layers. There is clear

indication of presence of thin layers of 400–500 m thickness with above noise-level spectral power fraction within the 3–4 km broad regions of ionisation irregularities. However the analysis between 83.5 and 85 km on April 19, 1993 where the main irregularity region itself is 1.5 km thick did not show clear presence of thin layers. Hence, the thin layer structure would vary with the height range of observed ionospheric irregularities with the region between 70 and 80 km showing presence of finer structures. These rocket results on the fine structure of the layer of the mesospheric ionisation irregularities broadly agree with the thin layer structure inferred from the radar backscatter echoes from the mesosphere in a qualitative sense.

4. Summary and discussion

The paper presents the first results of the fine structure of the mesospheric scattering layers observed by the Indian MST radar facility located at Gadanki. These results are an extension of the already reported work on detailed morphological characteristics of mesospheric backscattered

echoes from the broad region of neutral turbulence between ∼68 and 80 km (Kamala et al., 2003). Over the low latitude region such studies using MST radar technique are very rare. Since the primary cause of the radar backscatter from the lower mesosphere is due to the fluctuations in the electron densities produced by neutral turbulence, past data from the rocket borne measurements of ionisation irregularities ($\Delta_z N_e$) from SHAR station close to the radar site has been reviewed by reanalysing the height profile of $\Delta_z N_e$ for a better than the usual 1 km resolution published earlier.

The results presented here show the following important aspects of the mesospheric turbulent scatter layer and the rocket observed vertical profiles of ionisation irregularities over the low latitude region: (a) the dominant mesospheric scattering layer is located around 68–76 km and it is clear from the average value of FWHM for 2.4 km vertical resolution data of the return echo power that the layer or the region of turbulence field extends between 4 and 5 km in height range, (b) embedded within this broad field of scattering region are thinner layers of at least ∼600 m revealed from the high resolution radar measurements; presently systematic mesospheric observations with better than 600 m range resolution are difficult due to sensitivity limitations of the radar and hence it is not possible to determine if and what could be the lower limit of layer thickness and its morphology, (c) height profiles of the percentage amplitude of electron density irregularities at scale size of 3 m obtained from the reanalysis of data from two days of sounding rocket flights from SHAR, close to the radar site, show considerable enhancement around 70–80 km height range which qualitatively matches with the main region of radar backscatter echoes. The rocket data also indicates presence of fine structure of varied layer thickness between 70 and 80 km height range with substantial spectral power down to 400–500 m height resolutions as demonstrated using FFT analysis.

In the mesosphere, wind shears of 20–40 ms^{-1}/km have been attributed to the gravity wave-mean flow interactions (Fukao et al., 1985; Fritts, 1984). It is known from basic understanding of the phenomenon that such strong wind shears may lead to generation of turbulence if the Richardson number (R_i) reaches a small critical value. By taking the ratio of the potential and kinetic energies of an air parcel R_i is shown to be equal to $(N^2/(du/dz)^2)$, where N is the Brunt–Vaisala frequency and du/dz represents the wind shear. With N being about 5 min in the mesosphere, R_i may reach values between 0.25 and 1.00, while $R_i \leqslant 0.25$ is the condition when the fluid flow becomes unstable generating turbulence. But the instability of the air flow would depend on the whole profile of the flow rather than a value of R_i at a given point.

Another consideration is to check the Reynold's number R_e which is the ratio between the inertial and viscous forces of the flow, given by UL/v, where U and L are the characteristic velocity and length scales, v being the kinematic viscosity. Large R_e values are conducive of generating turbulence as large inertial forces build and viscous forces dampen it. Comparing the two conditions of R_i and R_e it is seen that the presence of strong winds and shears may lead the fluid motion to become turbulent. Due to the decrease in buoyancy or convection, stratification could occur to impart stability to the turbulent flow. The force due to convection which drives the air 'bubble', is given by $\rho v_c^3 H_T/L$, where ρ is density of air, v_c is the convective velocity of air bubble moved by density or temperature perturbations and H_T is C_p/Rg. Hence there may be a combination of related factors, e.g., presence of superadiabatic lapse rate leading to convective forces and presence of strong winds/shears breaking down to become turbulent in the mesosphere.

Hence it can be concluded that the main region or field of turbulence in the low latitude mesosphere, whenever it occurs, contains the 3 m size δN_e and extends to ∼4–5 km in vertical extent. The thin layers of stratification are part of the system restoring the laminar structure of the flow. Both radar and rocket observations indicate that the broad region of shear generated turbulence consists of thinner layers of turbulence that may be partially explained due to the decrease in the value of du/dz with corresponding increase in R_i and increase in R_e within the region of turbulence. Occurrence of strong turbulence may lead to such a situation and hence only few such high-resolution layers have been observed during the period of observation. Further observational data would be required to study if there is any lower limit of the layer thickness, its occurrence characteristics in relation to the energy dissipation rates and other parameters of neutral turbulence. Simultaneous observations of MST radar backscatter signals with better range resolution and mesospheric electron density irregularities using rocket borne probes with higher sensitivity are necessary for further studies in this direction.

References

Datta, J., Chakravarty, S.C., Prasad, B.S.N., 2001. Indian MST radar—mesospheric studies. Current Science 81, 661–666.

Fritts, D.C., 1984. Gravity wave saturation in the middle atmosphere: a review of theory and observations. Review Geophysics and Space Physics 22, 275–308.

Fukao, S., Sato, T., Kato, S., Harper, R.M., Woodman, R.F., Gordon, W.E., 1979. Mesospheric winds and waves over Jicamarca on May 23–24. Journal of Geophysical Research 84, 4379–4386.

Fukao, S., Maekawa, Y., Sato, T., Kato, S., 1985. Fine structure in mesospheric wind fluctuations observed by the Arecibo UHF Doppler radar. Journal of Geophysical Research 90 (A8), 7547–7556.

Gage, K.S., Balsley, B.B., 1980. On the scattering and reflection mechanisms contributing to clear air radar echoes from the troposphere, stratosphere and mesosphere. Radio Science 15, 243–257.

Gupta, S.P., 1997. Features of E-region irregularities at the magnetic equator and its vicinity. Advances in Space Research 20 (11), 2195–2198.

Gupta, S.P., 1999. Diurnal and seasonal variation of D-region electron density at low latitude. Advances in Space Research 21 (6), 875–878.

Harper, R.M., Woodman, R.F., 1977. Preliminary multi-height radar observations of waves and winds in the mesosphere over Jicamarca. Journal of Atmospheric and Terrestrial Physics 39, 959–963.

Kamala, S., Rao, Narayana D., Chakravarty, S.C., Datta, Jayati, Prasad, B.S.N., 2003. Vertical structures of Mesospheric echoes from the Indian MST radar. Journal of Atmospheric and Solar Terrestrial Physics 65, 71–83.

Kubo, K., Sugiyama, T., Nakamura, T., Fukao, S., 1997. Seasonal and inter-annual variability of mesospheric echoes observed with the Middle and Upper Atmosphere Radar during 1986–1995. Geophysical Research Letters 24, 1211–1214.

Lehmacher, G.A., Goldberg, R.A., Schmidlin, F.J., Croskey, C.L., Mitchell, J.D., Swartz, W.E., 1997. Electron density fluctua-tions in the equatorial mesosphere: neutral turbulence or plasma instabilities. Geophysical Research Letters 24, 1715–1718.

Pfaff, R.F., Kelley, M.C., Fejer, B.G., Maynard, N.C., Brace, L.H., Ledley, B.G., Smith, L.G., Woodman, R.F., 1985. Comparative in situ studies of the unstable day-time equatorial electrojet. Journal of Atmospheric and Terrestrial Physics 47, 791–811.

Prakash, S., Subbaraya, B.H., Gupta, S.P., 1972. Rocket measurements of ionisation irregularities in the equatorial ionosphere at Thumba and identification of plasma instabilities. Indian Journal of Radio and Space Physics 1, 72–80.

Rastogi, P.K., Bowhill, S.A., 1976a. Scattering of radio waves from the mesosphere—I theory and observations. Journal of Atmospheric and Terrestrial Physics 38, 399–411.

Rastogi, P.K., Bowhill, S.A., 1976b. Scattering of radio waves from the mesosphere—II evidence for intermittent mesospheric turbulence. Journal of Atmospheric and Terrestrial Physics 38, 449–462.

Roettger, J., 1994. Polar mesospheric summer echoes: dynamics and aeronomy of the mesosphere. Advances in Space Research 14 (9), 123–127.

Roettger, J., Rastogi, P.K., Woodman, R.F., 1979. High resolution VHF radar observations of turbulence structures in the mesosphere. Geophysical Research Letters 6, 617–620.

Royrvik, O., Smith, L.G., 1984. Comparison of mesospheric VHF radar echoes and rocket probe electron concentration measure-ments. Journal of Geophysical Research 89 (A10), 9014–9022.

Stitt, G.R., Kudeki, E., 1991. Interferometric cross-spectral studies of mesospheric scattering layer. Radio Science 26, 783–799.

ELSEVIER

Solar activity and atmospheric tide effect on the polar conductivity and the vertical electric field in the stratosphere at low latitude

S.P. Gupta *

Physical Research Laboratory, P.O. Box 4218, Navrangpura, Ahmedabad 380 009, India

Abstract

Balloonborne measurements of the polar conductivity and the vertical electric field were carried out over a period of 1984–1994 from Hyderabad, Central India. The conductivity values show positive correlation with solar activity between 20 and 35 km. Between 5 and 20 km the conductivity values show an anti-correlation with solar activity. The vertical electric field does not show solar cycle effect. However, the electric field and the conductivity show a semi-diurnal variation at balloon float altitude.
© 2004 COSPAR. Published by Elsevier Ltd. All rights reserved.

Keywords: Vertical electric field; Polar conductivity; Atmospheric tide effect; Solar activity

1. Introduction

The electrical conductivity and vertical electric field in the stratosphere play a very important role in the global electric circuit. The source of ionization in the stratosphere and in the troposphere is cosmic rays. The intensity of cosmic rays varies inversely with solar activity (Neher, 1967; Volland, 1984). The conductivity depends on the ion density and ion composition. Therefore, it should show a solar cycle effect. In fact the results of conductivity measurements in the stratosphere from Hyderabad, India (17.3°N, 78.5°E, Geomagnetic Lat. 8°N) show solar cycle dependence (Gupta, 2000). The vertical electric field in the troposphere and in the stratosphere is mainly due to worldwide lightning activity. This lightning activity keeps the globe at a negative potential with respect to space. So far we do not know whether global lightning activity has a solar cycle effect (Muir, 1979; Stringfellow, 1974). Therefore, measurements of the vertical electric field in the stratosphere

are very important (Gupta et al., 1992). The semi-diurnal variations of the conductivity and the electric field at balloon float altitudes at the stratosphere heights needed to be studied in more detail. Several workers have shown that both of these parameters do show semi-diurnal variations (Croskey et al., 1985; Gupta, 2002; Ogawa and Tanaka, 1976).

2. Results

More than 12 balloon flights were conducted from Hyderabad, India over the period of 1984–1994 to measure electric field and conductivity. For conductivity measurements, different techniques were used, like relaxation probe, Langmuir probe, Ogawa type probe, etc. (Gupta and Narayan, 1987; Gupta et al., 1992; Udare et al., 1991). The electric field was measured by the double probe technique. In some of the flights, measurements were done at float altitude for a longer period ranging from 4 to 10 h. Fig. 1 shows the vertical profile of conductivity for two different days, i.e., 8 April 1987 (IMAP C-2) and 6 December 1989 (TIFR 276). It can be seen that the conductivity values show a solar cycle effect. Fig. 2 shows the conductivity profile for 22

* Tel.: +91-79-6302129; fax: +91-79-6301502.
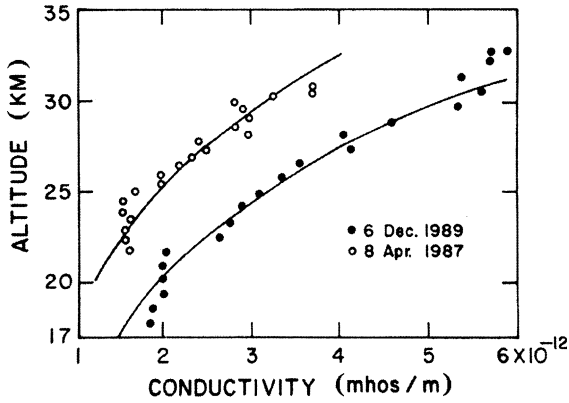 *E-mail address:* spg@prl.ernet.in (S.P. Gupta).

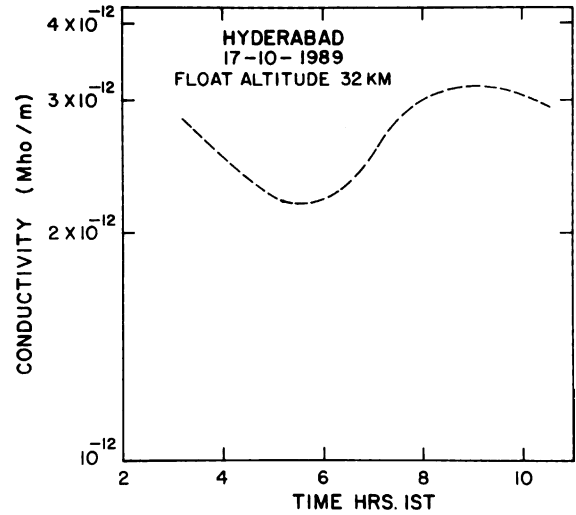Fig. 1. Vertical profile of conductivity for flight IMAP C-2 and TIFR 276.

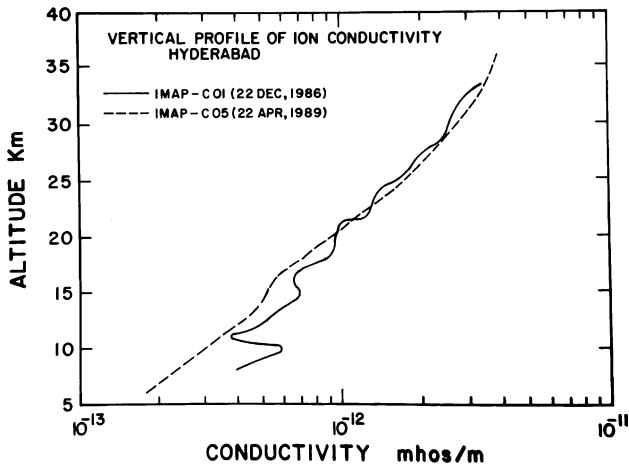Fig. 2. Vertical profile of vertical electric field for same flights as in Fig. 1.

Fig. 3. Conductivity profile for IMAPC-1 and IMAPC-5 from 5 to 35 km altitude.

December 1986 (IMAP C-l) and for 22 April 1989 (IMAP C-5). Here also we can see solar cycle effect. On these two flights we could measure the conductivity from 5 km onwards. Fig. 3 shows the vertical electric

Fig. 4. Semi-diurnal variation of conductivity profile at float altitude for IMAP C-7.

Fig. 5. Semi-diurnal variation of vertical electric field at float altitude for IMAP C-7 and IMAP C-6 flights.

field for same flights as Fig. 1. Fig. 4 shows the diurnal variation of the conductivity for 17 October 1989 (IMAP C-7) at float altitudes (Gupta, 2002). Fig. 5 shows the electric field values at float altitude for two different days: 17 October, 1989 (IMAP C-7) and 11 April, 1988 (IMAP C-6). IMAP C-6 float altitude was 36 km, but we have normalized the values for 32 km altitude since the float altitude of IMAP C-7 was 32 km.

3. Discussion

The polar conductivity of the stratosphere is given by

$$\sigma = -\frac{e2}{v} \sum \left(\frac{n_i}{m_i} \right), \tag{1}$$

where e is the electron charge, v is the collision frequency, n_i is the ion density and m_i is the ion mass. The ionization in stratosphere is mainly due to cosmic rays which has solar cycle dependence. However, the

conductivity also depends on ion mass, which may vary with solar cycle. Therefore, conductivity variation with solar cycle can easily be explained in terms of ion production rate and ion composition. In Fig. 2, we see that in troposphere of 5–20 km, the conductivity is more in low solar activity period compared to high solar activity period because below 20 km only cosmic ray effect will dominate over UV radiation related effect (Lean et al., 1997). Above 20 km, conductivity is high during high solar activity period. This aspect was discussed by Gupta (2000). Also, Byrne et al. (1988) have observed such features. Fig. 1 shows that in 20–35 km the conductivity is high during high solar activity period, compared to low solar activity period.

From Fig. 3, we find that the vertical electric field does not show any clear solar cycle effect. The electric field in the troposphere and stratosphere is mainly due to worldwide lightning activity. Global lightning activity does not show a significant solar cycle effect (Wacker and Orville, 1999). However, we suggest that global lightning activity should be monitored on a long-term basis. Such a study is already undertaken by satellite-borne techniques (Christian and Latham, 1998).

It is important to note that at balloon float altitude both parameters, conductivity and the vertical electric field show a semi-diurnal variation. However, both parameters vary out of phase. Since conductivity has semidiurnal variation, electric field should also show semidiurnal variation, but in opposite phase. So the air earth–current density value can remain constant. This is a necessary condition for global electric circuit. This can be explained that the phenomenon may be due to tidal effect.

4. Conclusion

At low latitude, the stratospheric conductivity shows a solar cycle variations while the electric field does not show such features. Both of these parameters show semidiurnal variations at balloon float altitude.

References

Byrne, G.J., Benbrook, J.R., Bering, E.A., Oro, D., Seubert, C.U., Sheldon, W.R. Observations of the stratospheric conductivity and its variation at three latitudes. J. Geophys. Res. 93, 3879–3891, 1988.

Christian, H.J., Latham, J. Satellite measurements of global lightning. A.J.R. Meteorol. Soc. 124, 1771–1773, 1998.

Croskey, C.L., Hale, L.C., Mitchell, J.D., Muhe, D. A diurnal study of the electrical structure of the equatorial middle atmosphere. J. Atmos. Terr. Phys. 47, 835–844, 1985.

Gupta, S.P. Solar cycle variation of stratospheric conductivity over low latitude. Adv. Space Res. 26, 1225–1229, 2000.

Gupta, S.P. Semi-diurnal variations of stratospheric conductivity at balloon float altitude. Adv. Space Res. 30, 2631–2635, 2002.

Gupta, S.P., Narayan, A. Balloonborne measurements of ion conductivity over low latitude stratosphere. Planet. Space Sci., 439–443, 1987.

Gupta, S.P., Chakravarty, S.C., Chandrasekaran, S. (Eds.), Balloon-borne Experiments Formiddle Atmospheric Conductivity Campaign. ISRO-IMAP S.R., vol. 39, 1992.

Lean, J.L., Rottman, G.J., Kyle, H.L., Woods, T.N., Hickey, J.R., Puga, L.C. Detection and parameterization of variations in solar mid and near ultraviolet radiation (200–400 nm). J. Geophys. Res. 102, 29939–29956, 1997.

Muir, M.S. In: McCormac, B.M., Seliga, T.A. (Eds.), The Role of Atmospheric Electricity in Sun Weather Relationships – Solar Terrestrial Influence on Weather and Climate, pp. 259–262, 1979.

Neher, H.V. Cosmic ray particle that changed from 1954 to 1958 to 1965. J. Geophys. Res. 72, 1527–1539, 1967.

Ogawa, T., Tanaka, Y. Land effect on the stratospheric vertical electric field and current. J. Atmos. Terr. Phys. 38, 599–604, 1976.

Stringfellow, M.F. Lightning incidence in Britain and solar cycle. Nature 249, 332–333, 1974.

Udare, R.S., Rajaram, R., Ogawa, T., Yashuhara, M. Height profile of vertical electric field and conductivity over Hyderabad. Ind. J. Radio Space Phys. 20, 307–309, 1991.

Volland, H. Atmospheric Electrodynamics. Springer Verlag, New York, 1984.

Wacker, R.S., Orville, R.F. Changes in measured lightning flashes count and return stroke peak current after the 1994 US National Lightning Detection Network upgraded. J. Geophys. Res. 104, 2131–2157, 1999.

In situ measurements of sub-meter plasma waves over low-latitude ionosphere during Leonid-99 meteor storm

S. P. Gupta, R. Sekar, and Y. B. Acharya

Physical Research Laboratory, Ahmedabad 380 009, India

Abstract. In situ probe measurements of plasma parameters were carried out on 18 and 20 November 1999 from Sriharikota, India, a low-latitude rocket launching station to investigate the effect of a Leonid meteor storm. Results obtained on plasma waves using a high frequency Langmuir probe are discussed. The characteristics of the sub-meter scale size plasma waves observed for the first time during Leonid meteor storm are presented. Based on the results obtained from both the rocket flights and comparison with the results obtained from previous rocket flights from the same location, it appears these sub-meter waves are associated with intense meteoric activity. A possible mechanism based on the dependence of the meteoric activity and its limitations are discussed.

Key words. Ionosphere (Equatorial ionosphere; Ionospheric irregularities; Plasma waves and instabilities)

1 Introduction

It is known that a typical meteor Zenith Hourly Rate (ZHR) of a Leonid meteor shower associated with Comet Tempel-Tuttle, which occurs every year during 17–18 November, is around 5 (McKinley, 1961). However, the ZHR for a Leonid meteor storm, an event which occurs once in 33 years, is about a few thousands (Aguirre, 2000). The meteor streams enter the Earth's ionosphere with the velocities ranging from 12 km/s to 72 km/s (Hocking, 2000). It is well established that the meteoric species continuously become deposited in the lower thermosphere both in the form of ions due to ablation of the meteorites and also in the form of neutral species. A few in situ measurements (Narcisi, 1968; Shirke et al., 1981) during normal shower activity are available in the literature. The in situ measurement during an intense meteor storm is not available in the literature (McNeil et al., 2001), particularly from a low-latitude region. However, rocket experiments were conducted during a Leonid storm in 1999

from Sriharikota (SHAR), India, with an objective to investigate the effects on plasma parameters and the possible plasma waves in the low-latitude ionosphere induced by intense meteor storm. Based on a single rocket flight, the preliminary result on the existence of a new type of plasma wave over low latitude during a Leonid meteor storm is reported elsewhere (Gupta et al., 2003). The present communication deals with the detailed results obtained from two rocket flights on plasma waves and brings out their association with Leonid meteor storm activity.

The plasma waves in equatorial E region associated with equatorial electrojet have been studied using in situ probes (Prakash et al., 1972; Pfaff et al., 1987) and VHF radars (Balsley and Farley, 1971; Prakash et al., 1974). VHF radars provide temporal behaviour of plasma waves at a particular wavelength, while the in situ probe measurements provide information of various ranges of scale sizes during a limited duration. The earlier studies based on these techniques revealed that there exists two types of plasma waves (conventional two stream and gradient drift waves) over the equatorial ionosphere. As the site (dip lat 6° N) of the observation reported in the present communication is far from the equatorial electrojet effects, the conventional two stream waves are unlikely to become excited. As it can be noticed from the following section that the presence of the observed plasma waves in the present case in a shallow plasma density gradient region and the absence of the same in a steep plasma density gradient region rule out the possibility of gradient drift waves. Further, the scale sizes of the observed plasma waves are considerably lesser than the cut-off wavelength of conventional plasma waves established by the earlier works (Balsley and Farley, 1971; Schmidt and Gary, 1973; Pfaff et al., 1987). Hence the conventional two steam and gradient drift processes cannot account for the new plasma waves. Thus, these conventional processes will not be discussed any further.

In the present communication, the characteristic of a new plasma wave, its association with meteor storm activity and a possible mechanism with its limitation will be discussed.

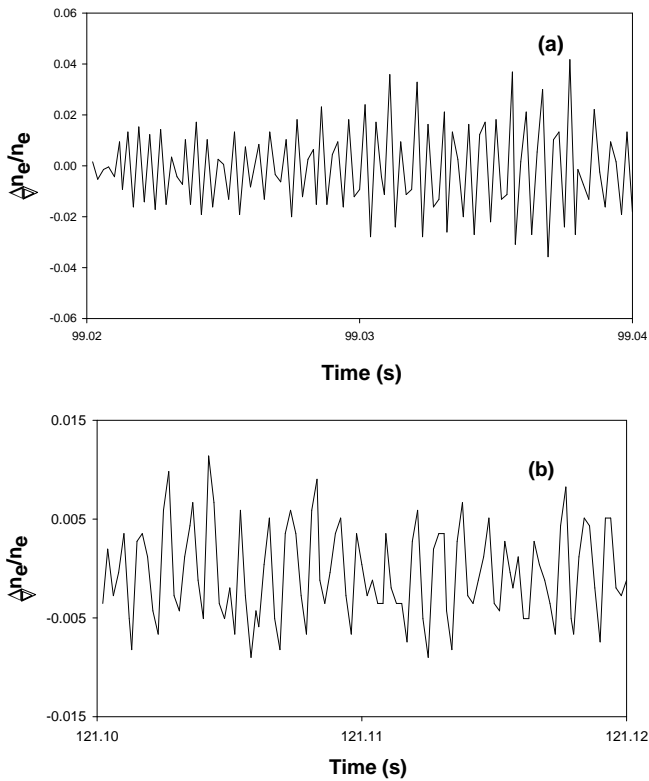*Correspondence to:* R. Sekar
(rsekar@prl.ernet.in)

Fig. 1. Telemetry record of plasma waves obtained on 18 November 1999, **(a)** at an altitude of 105 km and **(b)** at 120 km altitude.
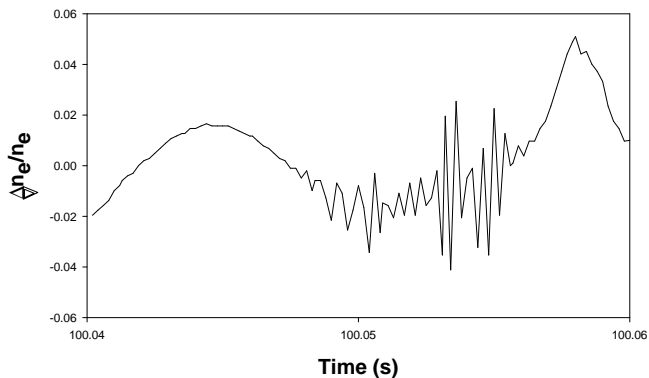

Fig. 2. Telemetry record of the plasma waves obtained at 105 km altitude on 20 November 1999 when the meteor activity level is one-third in comparison to the first flight.

2 Details of the experiments

Two RH-300 Mark II rockets (F01 and F02) with identical instruments were launched from SHAR (13.7° N, 80.2° E, dip lat. 6.0° N), on 18 and 20 November 1999, respectively, at 7:25 and 7:03 IST (Indian standard time). Both the rockets were launched nearly with the same launch azimuth of 90° and a launch elevation of 84°. The rockets attained apogee of 139 and 136 km, respectively. The rocket carried a high frequency Langmuir probe and an electric field probe to mea-

sure plasma wave parameters. The electric field probe did not yield any useful scientific information as the rocket velocity induced electric field could not be eliminated satisfactorily. The uncertainty in the measurement of the plasma wave amplitude is less than 0.4% of the ambient plasma density for the present case.

3 Results

Figure 1a depicts the telemetry record of high frequency (100 Hz to 3 kHz) channel data of the normalized fluctuations in electron densities during 99.02 s to 99.04 s, corresponding to a 105 km altitude. The normalized amplitude of fluctuation (peak to peak) at this altitude corresponds to about 4% of the ambient electron density. During the time interval of 0.02 s, around forty-two peaks are observed which correspond to the frequency of 2.1 kHz in the rocket frame of reference when the rocket velocity is 1 km/s. The amplitude and the wave frequency in the rocket frame of reference of these plasma waves are found to change with altitudes. Thus, in order to ascertain that the observed plasma waves are geophysical in nature, sample data at a different altitude is analyzed. Figure 1b depicts a telemetry record of high frequency oscillations in the same channel (100 Hz to 3 kHz) but at a different altitude region where the vertical component of rocket velocity is only 0.5 km/s. The peak-to-peak amplitude of the wave reduced to nearly 1% of the ambient. During a time of interval of 0.02 s, around 25 peaks are observed which correspond to a 1.25 kHz wave frequency in the rocket frame of reference.

The telemetry record of the high frequency channel obtained from flight F02 between 100.04 to 100.06 s, corresponding to 105 km altitude, is depicted in Fig. 2. High frequency fluctuations are observed at 100.05 s with a normalized amplitude equal to 3.5% of the ambient electron density. During a time interval of 0.008 s, seventeen peaks are seen which correspond to a ∼2.1 kHz wave frequency in the rocket frame of reference when the rocket velocity is 1 km/s. Figure 2 represents a sample of high frequency waves in plasma density observed by the second rocket, which was conducted when the Leonid storm activity level had fallen to one-third of its value corresponding to 18 November.

Figures 3a and b depict the altitude profiles of the amplitudes of the waves, along with electron density profiles obtained on 18 and 20 November, respectively. The plasma waves are observed to confine in the altitude region of 100 to 120 km on 18 November and between 100 and 106 km on 20 November. The plasma wave amplitude attains a maximum at 105 km on 20 November and the wave amplitude is below the detection limit beyond 106 km. The altitude extent varies with the level of Leonid storm activity. The maximum amplitude is found to be nearly at the same altitude (105 km) on both days. The fluctuations observed near the rocket apogee are non-geophysical in nature.

In general, the electron density profile is much more structured on 18 November compared to the profile on

20 November. Further, a small variation in electron density profile is noticed on 18 November and a relatively significant one on 20 November, closer to the altitude region where plasma wave amplitude is significant. A sharp cut-off in the amplitude of the plasma wave is seen on 20 November in Fig 3b when the Leonid storm activity is less.

4   Discussion

Figure 1a and b reveals that the electron density fluctuations are not only different in amplitudes but also different in dominant frequency in the rocket frame of reference. The differences in the frequency at different altitudes suggest that these fluctuations are not associated with a measurement system. Taking into account the measured velocities (V) of the rocket at different altitudes, and the observed dominant frequencies (f), the scale sizes of waves (V/f) are calculated to be 47 cm and 40 cm, respectively, at 105 and 120 km altitudes. Thus, these scale sizes of the plasma wave fall under the sub-meter category. Further, Fourier spectrum analysis of these plasma waves (not shown in the figure) also reveals that the power is centered at the region of sub-meter scale size.

In this context, it is important to study the association between the sub-meter plasma waves and the activity of the Leonid meteor storm. Since the activity on 20 November had fallen to about one-third of its value corresponding to 18 November, the information regarding the presence (or absence) of the plasma waves on a non-meteor storm day could not be obtained by the present set of measurements. However, the earlier flights conducted from the same location on non-meteor storm days with identical probe systems did not reveal the presence of sub-meter category of plasma waves (Thiemann et al., 1995; Gupta, 1997). Further, it is clear from the results (Figs. 3a and b) that the altitude extents of the region wherein the plasma waves are present depend on the activity of the Leonid storm. It is interesting to note that a maximum amplitude of plasma waves exist at an altitude (105 km) where the meteoric deposition is large in general. The recent measurement (Close et al., 2002) on the head echoes from the Leonid meteor shower which occurred during 1998, using UHF ALTAIR radar, supports this view. Further, the maximum amplitude of the sub-meter plasma waves at about 105 km is 4% with an amplitude that is four times more than the usual plasma waves. These experimental evidences indicate that the sub-meter waves are associated with Leonid storm activity.

Regarding the generation of the sub-meter plasma waves, the recent simulation presented by Dyrud et al. (2002) becomes important. In order to explain non-specular VHF and UHF radar echoes from meteor trails observed over the low-latitude region, (Kwajelein Atol, a place having a dip value of the Earth's magnetic field, similar to the present launching station, SHAR) kinetic plasma simulations within a meteor trail have been carried out by Dyrud et al. (2002). These simulations reveal that the meteor trail often develops Farley-Buneman gradient drift waves which become tur-
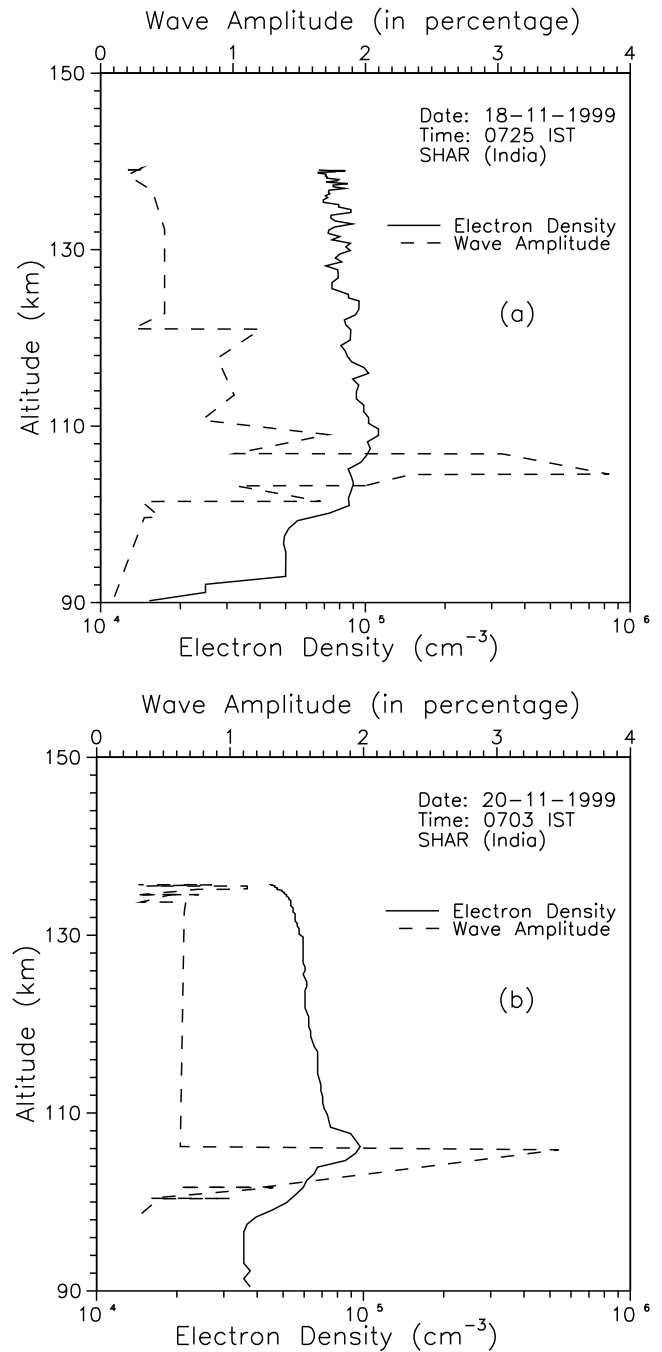

Fig. 3. Altitude profiles of amplitude of plasma waves along with electron densities obtained (**a**) on 18 November 1999, (**b**) on 20 November 1999.

bulent and generate field-aligned irregularities of sub-meter scale sizes in an altitude region 96 km to 106 km. The simulation and earlier computation work by Farley (1963) require that the magnitude of electron drift velocity perpendicular to the magnetic field should be 4 km/s for the generation of sub-meter waves. Such high velocities do exist within the meteor trail. The observations, with changes in the altitude profile of the electron density but to a lesser

extent on 18 November, and a relatively significant change on 20 November at 105 km, where a maximum plasma wave amplitude is observed, support this mechanism of the generation of sub-meter waves. However, their simulation indicates that the actual altitude range for meteor trail instability depends on meteor trail velocity. In the present experimental conditions, the meteor trail velocity is expected to be on the higher side as the Leonid storm activity and the observation took place in the morning sector over the low-latitude region. The actual measurement (Close et al., 2002) of the average meteor trail speed of the Leonid meteor shower which occurred during 1998 when the condition was similar to the present case was 69 km/s. This would not favor the growth of sub-meter plasma waves at a higher altitude (>106 km) region owing to a larger radius of the meteor trail and a corresponding reduction in the electron density gradient within the meteor trail according to the simulation of Dyrud et al. (2002). However, the plasma waves in the present rocket campaign were observed in different parts of the rocket trajectory even at a 120 km altitude (see Fig. 1b). The presence of waves was also recorded during the down leg of the rocket trajectory. In the absence of the spatial distribution of the meteor trails in the ambient ionosphere during a severe Leonid meteor storm, the above mechanism appears to be a viable one. Further investigations are needed to understand the existence of plasma waves at a higher altitude region, particularly on a meteor storm day.

5 Summary

The characteristics of the sub-meter plasma waves over a low-latitude E-region observed for the first time during Leonid meteor storm of November 1999 are presented. Indications for the association of the observed sub-meter waves with the activity of Leonid meteor storm are found. A possible mechanism and its limitations are discussed.

References

Aguirre, E. L.: Leonid storm on schedule, Sky & Telescope, Feb. issue, 120, 2000.

Balsley, B. B. and Farley, D. T.: Radar studies of equatorial electrojet at three frequencies, J. Geophy. Res., 76, 8341–8351, 1971.

Close, S., Hunt, S. M., McKeen, F. M., and Minardi, M. J.: Characterization of Leonid meteor head echo data collected using the VHF-UHF Advanced Research Projects Agency Long-Range Tracking and Instrumentation Radar (ALTAIR), Radio Sci., 37, doi:10.1029/2000RS002602, 2002.

Dyrud, L. P., Oppenheim, M. M., Close, S., and Hunt, S.: Interpretation of non-specular radar meteor trails, Geophys. Res. Lett. 29 (21), 2012, doi:10.1029/2002GL015953, 2002.

Farley, D. T.: A plasma instability resulting in field aligned irregularities in the ionosphere, J. Geophy. Res., 68, 6083–6097, 1963.

Gupta, S. P.: Features of E region irregularities at the magnetic equator and in its vicinity, Adv. Space Res., 20, No. 11, 2195–2198, 1997.

Gupta, S. P., Sekar, R., and Acharya, Y. B.: A new plasma wave over low-latitude ionosphere during Leonid meteor storm, Current Science, 84, 1340–1342, 2003.

Hocking, W. K.: Real time meteor entrance speed determinations made with interferometric meteor radars, Radio Sci., 35, 1205–1220, 2000.

McKinley, D. W. R.: Meteor science and engineering, McGraw-Hill Book Co., New York, 146–147, 1961.

McNeil, W. J., Dressler, R. A., and Murad, E.: Impact of major meteor storm on Earth's ionosphere : A modeling study, J. Geophy. Res., 106, 10 447–10 465, 2001.

Narcisi, R. S.: Process associated with metal ion layers in the E region of ionosphere, Space Res., VIII, 360–369, 1968.

Pfaff, R. T., Kelley, M. C., Kudeki, E., Fejer, B. G., and Baker, K. D.: Electric field and plasma density measurements in the strongly driven day time equatorial electrojet, 2. two stream waves, J. Geophy. Res., 92, 13 597–13 612, 1987.

Prakash S., Subbaraya, B. H., and Gupta, S. P.: Rocket measurements of ionization irregularities in the equatorial ionosphere at Thumba and identification of plasma irregularities, Indian J. Radio space Phy., 1, 72–80, 1972.

Prakash S., Jain, C. L., Balsley, B. B., and Greenwald, R. W.: Evidence of two types of electron density irregularities in the electrojet over Thumba, India, J. Geophs. Res., 79, 4334–4336, 1974.

Schmidt, M. J. and Gary, S. P.: Density gradients and Farley-Buneman instability, J. Geophy. Res., 78, 8261–8265, 1973.

Shirke, J. S., Sridharan, R., Gupta, S. P., Danilov, A. D., Pokhunkov, A. A., Semenov, V. K. and Verfolomeev, V. A.: On the formation of sharp layer of metallic constituents at sun rise in the lower thermosphere, Proc. Indian Acad. Sci., 91, 141–146, 1981.

Thiemann-Rhode, H. V., Piel, A., Steigies, C., and Gupta, S. P.: Gradient drift waves at the edge of equatorial electrojet over SHAR, Proc. 12th ESA Symp. On rockets and balloon programme, Lillehammer, Norway, 291–294, 1995.

A new plasma wave over low latitude ionosphere during Leonid meteor storm

Now

$$\begin{pmatrix} tr\ x^{n-1} \\ tr\ x^{n-2} \\ \vdots \\ tr\ 1 \end{pmatrix} = M^{-1} \begin{pmatrix} a_1 \\ 2a_2 \\ \vdots \\ na_n \end{pmatrix}$$

and hence we have, for $1 \le i \le n$,

$$tr\ x^{n-i} = ia_i + (i+1)a_{i+1}c_{n-1} + (i+2)a_{i+2}c_{n-2}$$
$$+ \cdots + (n-1)a_{n-1}c_{n-i+1} + nc_{n-i}.$$

It can also be verified that c_{n-i} is a polynomial in a_{n-1} of degree i with leading coefficient $(-1)^i$, so that $tr\ x^i$ is a polynomial in a_{n-1} of degree i, with the same property. This yields a fairly explicit formula for the traces of powers of a linear transformation in terms of the entries of the companion matrix.

1. Serre, J. P., *Local Fields*, GTM 67, Springer Verlag, New York, 1979.
2. Weber, H., *Lehr Buch Der Algebra*, Erster Band, Chelsea Publishing Co.

A new plasma wave over low latitude ionosphere during Leonid meteor storm

S. P. Gupta, R. Sekar* and Y. B. Acharya

Physical Research Laboratory, Navrangpura, Ahmedabad 380 009, India

Leonid meteor storm is a unique astronomical event that occurs once in 33 years. In order to investigate the effect of Leonid meteor storm over low latitude ionosphere, rocket measurements of plasma parameters were carried out on 18 and 20 November 1999 from Sriharikota, India. The meteoric activity was at its peak on 18 November 1999. Results obtained on plasma waves using a high frequency Langmuir probe revealed for the first time, an experimental evidence for the presence of sub-meter scale size plasma wave over low latitude E-region. The peak amplitude of the plasma wave occurs at 105 km with a magnitude of ~ 4% of ambient electron density. The ambient plasma conditions during these measurements imply that the causative mechanism for the generation of this plasma wave is different from well known gradient drift waves.

LEONID meteor shower associated with comet Tempel-Tuttle occurs every year during 17–18 November with a

*For correspondence. (e-mail: rsekar@prl.ernet.in)

typical meteor zenith hourly rate (ZHR) of around five[1]. However, Leonid meteor storm occurs once in about 33 years with intense ZHR of a few thousands[2,3] when the above comet approaches inner solar system. In the literature[3,4], *in situ* measurements during an intense meteor storm is not available from a low latitude region prior to the present rocket measurements during Leonid storm 1999. Two RH-300 Mark-II rockets (F.1 and F.2) carrying high frequency Langmuir probe sensor mounted on booms perpendicular to spin axes of the rockets were launched from Sriharikota (13.7°N, 80.2°E, dip lat. 6.0°N) on 18 and 20 November 1999 respectively at 7.25 and 7.03 IST (Indian Standard Time = UT + 5.30). The launch of F.1 coincided with the peak activity of Leonid meteor storm, while the launch of F.2 happens to be when the activity reduced to one-third. The ambient electron densities (n_e) and fluctuations (Δn_e) in them which represent the plasma waves were measured along the trajectories of the rockets. Earlier studies[5-7] on plasma waves during normal days revealed only gradient drift waves over a low latitude station like Sriharikota. However, over magnetic equator, other plasma waves known as type I waves[5,8,9] associated with equatorial electrojet have also been observed. The above two types of plasma waves have a cut-off scale size of a few meters[5,9].

Figure 1 depicts the telemetry raw data from a high frequency (100 Hz to 3 kHz) channel representing the fluctuations in the electron densities corresponding to about 105 km altitude obtained on 18 November 1999. The expanded portion of the diagram corresponding to the time interval when high frequency fluctuations are observed in Figure 1 *a*, is given in the bottom panel of the diagram as Figure 1 *b*. During a time interval of 0.02 s, forty peaks are seen in Figure 1 *b* which correspond to ~ 2 kHz wave frequency in the rocket frame of reference. Similar features were observed on 20 November 1999. It can be noticed from Figure 1 *a* that these high frequency fluctuations are found only on certain durations revealing that these fluctuations are geophysical and anisotropic in nature. Taking into consideration measured vertical velocity of the rocket (~ 1 km/s) at 105 km altitude, the observed 2 kHz plasma waves (in Figure 1 *b*) correspond to a scale size of about 50 cm. Thus, an evidence for the presence of sub-meter scale size of the plasma waves is reported here for the first time from a low latitude E-region of the ionosphere.

Figure 2 depicts the altitude profiles of electron density along with the average values of the amplitudes of the plasma waves observed on 18 November 1999. Considering the errors in the measurements, wave amplitudes greater than ~ 0.5% have physical significance. The plasma waves are observed to confine in the altitude region of 100 to 120 km with a maximum amplitude at an altitude of 105 km. From Figure 2 it is clear that the absence of plasma waves in a steep electron density gradient region (90–94 km) and a presence of maximum
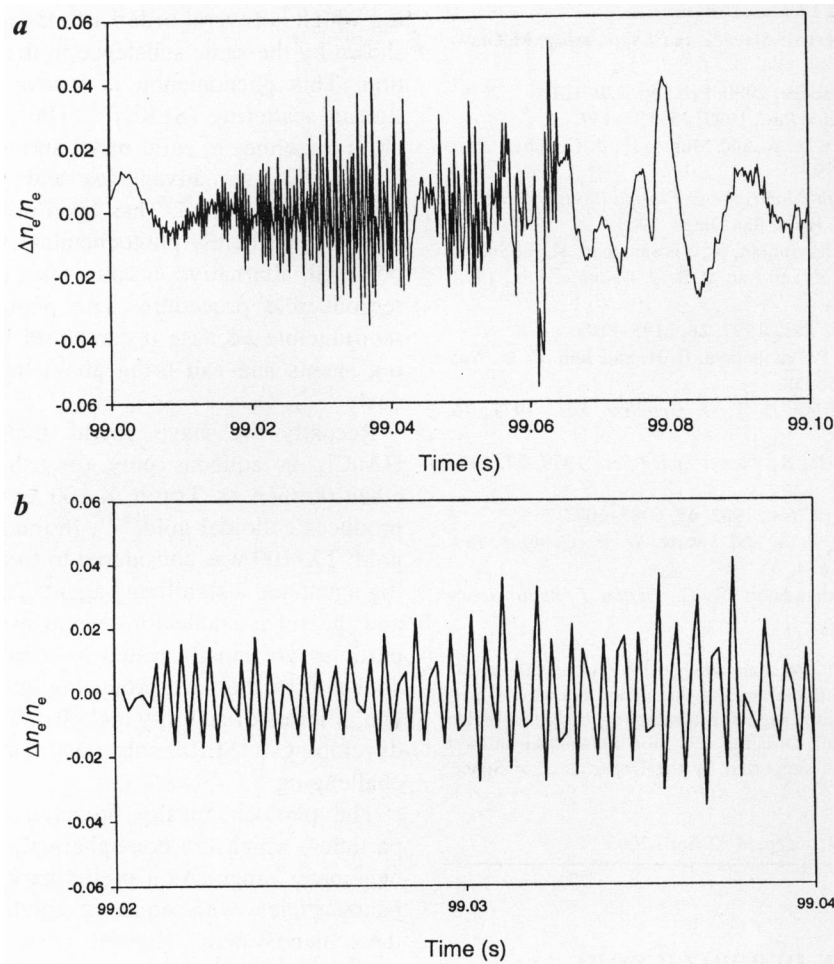
Figure 1. *a*, Telemetry record of plasma waves at around 105 km observed on 18 November 1999; *b*, Expanded portion of figure corresponding to the time interval of 99.02 to 99.04 s.
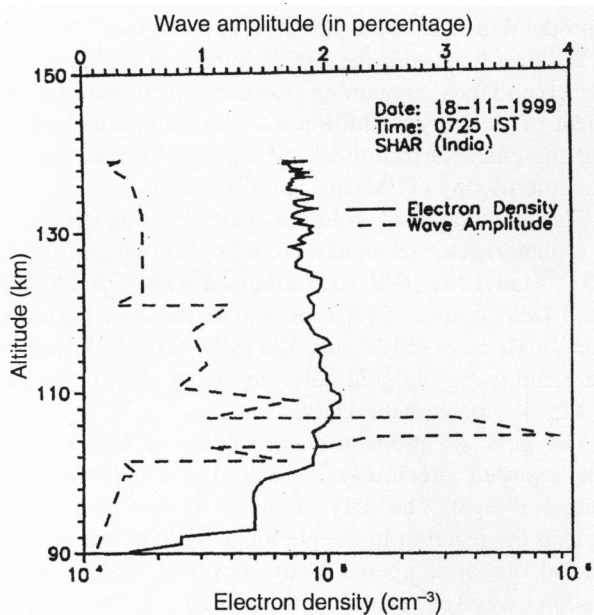

Figure 2. Altitude profiles of amplitude of plasma waves along with electron densities observed on 18 November 1999.

amplitude of plasma waves at 105 km where electron density gradient is negligibly small reveal that the causative mechanism for the generation of these plasma waves is different from well known gradient drift waves[5–7] observed over low latitudes. The fluctuations observed near the rocket apogee are non-geophysical in nature[5] and are associated with subsonic motion of the rocket[10].

The plasma waves of a few meter scale sizes over magnetic equator are known to exist as type I waves[8,11,12] when the electron drift velocity driven by Hall polarization field associated with equatorial electrojet exceeds ion thermal velocity (350 m/s). As the polarization field associated with equatorial electrojet reduces by an order of magnitude over Sriharikota[13], the type I waves are unlikely to exist over low latitude. Several rocket flight experiments[7] conducted earlier from Sriharikota and the radar experiments[6] from nearby site located 100 km west of this station also support the non-existence of type I wave over such location. Thus, an experimental evidence for a new kind of plasma wave over low latitude during Leonid 99 meteor storm is reported in this communication.

1. McKinley, D. W. R., *Meteor Science and Engineering*, McGraw-Hill, New York, 1961.
2. Aguirre, E. L., *Sky Telescope*, 2000, Feb., pp. 120–121.
3. Jenniskens, P., *Adv. Space Res.*, 1999, **23**, 137–147.
4. McNeil, W. J., Dressier, R. A. and Murad, E., *J. Geophys. Res.*, 2001, **106**, 10447–10465.
5. Kelley, M. C., *The Earth's Ionosphere: Plasma Physics and Electrodynamics*, Academic Press, San Diego, 1989.
6. Krishnamurthy, B. V., Ravindran, S., Viswanathan, K. S., Subbarao, K. S. V., Patra, A. K. and Rao, P. B., *J. Geophys. Res.*, 1998, **103**, 20761–20772.
7. Gupta, S. P., *Adv. Space Res.*, 1997, **20**, 2195–2198.
8. Prakash, S., Gupta, S. P., Subbaraya, B. H. and Jain, C. L., *Nat. Phys. Sci.*, 1971, **233**, 56–58.
9. Balsley, B. B. and Farley, D. T., *J. Geophys. Res.*, 1971, **76**, 8341–8351.
10. Gupta, S. P. and Prakash, S., *Planet Space Sci.*, 1979, **27**, 145–150.
11. Farley, D. T., *J. Geophys. Res.*, 1963, **68**, 6083–6097.
12. Pfaff, R. F., Marionni, P. A. and Swartz, W. E., *Geophys. Res. Lett.*, 1997, **24**, 1671–1674.
13. Raghavarao, R. and Anandarao, B. G., *Indian J. Radio Space Phys.*, 1987, **16**, 54–75.

Photochemically prepared gold nanoparticles: A substrate for surface enhanced Raman scattering

Anjali Pal[*,#], Tarasankar Pal[†], David L. Stokes[§] and Tuan Vo-Dinh[§]

[#]Department of Civil Engineering, [†]Department of Chemistry, Indian Institute of Technology, Kharagpur 721 302, India
[§]Advanced Monitoring and Development Group, Life Sciences Division, Oak Ridge National Laboratory, Oak Ridge, TN 37830-6101, USA

Gold nanoparticles have been prepared in aqueous Triton X-100 medium using a new photochemical procedure. The characterization of the particle is made using transmission electron microscopy studies. The effects of analyte molecules such as pyridine and salt such as sodium chloride on the sol are studied. The photochemically prepared gold nanoparticles has been used successfully for surface enhanced Raman scattering studies with various types of compounds.

MOLECULES that are adsorbed or are at least in close proximity to a particular surface, exhibit Raman scatter-

*For correspondence. (e-mail: anjalipal@civil.iitkgp.ernet.in)

ing which is several orders of magnitude greater than that shown by the same substance in the pure state or in solution. This phenomenon is known as surface enhanced Raman scattering (SERS)[1,2]. The phenomenon has been observed either in solid metal surface[3–5] or in sol[6,7], each having its own advantages and limitations. Although chemical reduction[8–10] has been used for the preparation of metal particles, photochemical reduction could be a potential alternative because it can afford simple and reproducible procedure. The photochemical process is reproducible because it can avoid local excess of reducing agents and can bring about the reaction homogeneously[11–15].

Recently we have found that photoirradiation of $HAuCl_4$ in aqueous poly (oxyethylene) isooctylphenyl ether (known as Triton X-100 or as TX-100) medium produces colloidal gold[16–19]. In the formation of colloidal gold, TX-100 was considered to function both as a reducing agent and a stabilizing agent. The procedure is simple and the sol is stable for several months. Although silver particles are mostly tested as a substrate for SERS and shown to be the most promising, gold has its own advantage in terms of stability and chemical inactivity[20,21]. Thus developing a SERS substrate made of gold is always challenging.

The photochemically prepared colloid contains gold particles, which are non-spherical, and the size is in the nanometer range. As a preliminary study we tested gold nanoparticles with aqueous solution of pyridine and, these nanosystems showed great promise as a SERS active substrate[17]. But more elaborative studies with various other compounds are warranted to really show its potential to be a good SERS substrate. The advantage of this particular sol is that it is extremely stable and has a reproducible and simple preparation procedure[18].

We deal here with the SERS studies of different organic compounds containing various functionalities. The effect of electrolyte addition into the sol and its stability, and the characterization of the sol by transmission electron microscopy (TEM) are also discussed.

The preparation of gold nanoparticles was carried out in a photoreactor (Southern New England Ultraviolet Co. USA, Model No. RPR 100) equipped with RPR 2537 UV lamp (8W) source. SERS measurements were performed using a Kr laser (647.1 nm, 180 mW). The SERS spectra were run using the gold sol with added electrolyte NaCl or $MgCl_2$ (concentration 0.004 M).

The gold sol preparation procedure is similar to the one reported previously[16,17] with the exception of the source of light. The only exception is that here we performed the reaction in the photoreactor. The reaction was carried out in stoppered quartz cuvettes. The photoirradiation was performed for 20 min. 1.7 ml TX-100 (10^{-2} M) containing 0.3 ml $HAuCl_4$ (final concentration 200 ppm) was irradiated for 20 min to obtain the gold sol which exhibits a ruby red colour.

LONG TERM CHANGES IN THE ELECTRICAL CONDUCTIVITY OF THE STRATOSPHERE

E. A. Bering III[1], J. R. Benbrook[1], G. J. Byrne[2] , R. Holzworth[3], and S. P. Gupta[4]

[1]*Physics Department, University of Houston, 617 Science and Research I, Houston, TX 77204-5005, USA*
[2]*NASA Johnson Space Center, 2101 Nasa Rd. 1, Houston, TX 77058, USA*
[3]*Department of Earth and Space Sciences, University of Washington, Room 346A Johnson Hall, Box 351310, Seattle, WA 98195-1310, USA*
[4]*Physical Research Laboratory, Navarangpura, Ahmedabad 380 009, Gujarat, India*

ABSTRACT

Stratospheric electrical conductivity measurements have been made from high altitude research balloons at various locations around the world for more than 30 years. In the stratosphere, conductivity is affected by a number of things, including changes in aerosol or water vapor content. In this paper, we compare data taken in the last five years at mid latitude locations with data taken in the previous three decades at both mid and high latitude from a total of more than 40 balloon flights. Existing models for the effects of geomagnetic latitude, temperature, and other factors have been used to normalize the conductivity data for comparison. Low noise background has permitted the observation of a solar cycle dependence in the equatorial data. Otherwise, this limited statistical sample exhibits short term variations that completely obscure any long term climatic trends that may have occurred during the past three decades. © 2003 COSPAR. Published by Elsevier Ltd. All rights reserved.

INTRODUCTION

Balloon-borne measurements in the past have consistently shown that the atmospheric electrical conductivity generally increases exponentially with altitude through the troposphere and stratosphere. However, there are considerable uncertainties in the nature of the conductivity because of spatial and temporal variations that are not well understood. In this paper we report measurements of the stratospheric conductivity by more than 40 high-altitude balloons, launched from eight locations widely separated in latitude over a period of 30 years. The measurements provide the opportunity to investigate long-term variations in conductivity profiles on local and global scales. This research was motivated by the lack of global measurements of the atmospheric conductivity and its variations, which are crucial to our understanding of the global electrical environment (Hays and Roble, 1979; Roble and Tzur, 1986).

The atmospheric conductivity is proportional to the product of the ion concentration and the ion mobility. Variations in conductivity may be caused by a variety of factors that alter either of these two basic quantities. These factors include latitudinal and temporal variations in the ionizing cosmic ray flux, global or local variations in the ion mobility due to ion attachment to aerosols (Gringel et al., 1986), and changes in the ion mobility and ion recombination rate as functions of temperature (Israel, 1973). In previous publication (Byrne et al., 1988, 1991), we investigated these and other effects extensively with regard to their effects on our conductivity data from the earlier flights (prior to 1987).

The balloon flights were conducted during many separate balloon campaigns, some by our groups and others taken from the literature: 1973, 1976, and 1999 at Palestine, Texas; 1975 at Roberval, Quebec; 1980-81 at Siple Station, Antarctica, 1985-86 at South Pole, 1999 at Ottumwa, Iowa, 1983-84 and 1992-93 from Christchurch, New Zealand, 6 flights from 1986 to 1994 from Hyderabad, India, and several flights from 1978, 1979, and 1983 from Laramie, Wyoming (Benbrook et al., 1974; Rosen et al., 1978, 1982, 1985; Bering et al., 1980, 1987; Holzworth, 1981, 1991; Rosen and Hoffman, 1981; Holzworth et al., 1984, 1986, 1992; Norville and Holzworth. 1987: Byrne et al.. 1991: Holzworth and Hu. 1992: Holzworth and Norville. 1992:

Table 1. Summary of the Balloon Flights

Campaign	Location	Month	Year(s)	Latitude	Number
Palestine	Texas	July	1973	32° N	1
Roberval	Quebec	July	1975	48° N	3
Palestine	Texas	September	1976	32° N	1
Laramie	Wyoming	May-Aug.	1978	41° N	4
Laramie	Wyoming	May	1979	41° N	1
Laramie	Wyoming	March	1983	41° N	2
Siple Station	Antarctica	Dec.-Jan.	1980-81	80° S	5
EMA	S. Ocean	Dec-Jan.	1985-86	< 45° S	8
South Pole	Antarctica	Dec.-Jan.	1985-86	90° S	8
Hyderabad	India	Dec.,Jan., Apr.,Oct.	1986,87, 1989,94	17° N	6
PPB	Antarctica	Dec.-Jan.	1990,92	78° S	3
ELBBO	S. Ocean	Nov.-Feb.	1992-93	< 45° S	5
Sprites 99					
Palestine	Texas,	July	1999	32° N	1
Ottumwa	Iowa	August	1999	41° N	1

Gupta et al., 1992, Ejiri et al., 1995; Ebihara et al., 1996; Gupta, 2000). The locations of the launch sites, dates and times of the balloon flights, and maximum altitudes attained by the balloons are summarized in Table 1.

INSTRUMENTATION

On most of the flights the conductivity measurements were obtained by the relaxation time method (Mozer and Serlin, 1969; Benbrook et al., 1974; Bering et al., 1980; Holzworth, 1981; Rosen et al., 1982; Holzworth et al., 1986; Norville and Holzworth, 1987). Four of the Hyderabad flights and all of the Laramie flights used other methods (Rosen et al., 1982, 1985; Gupta et al., 1992; Gupta, 2000). Various types of probes were used on theflights. Both flat plates 30 cm square and spherical probes of various diameters (15 to 30 cm) were used in various University of Houston (UH) and University of Washington (UW) campaigns. The UH and UW probes were coated with a colloidal suspension of carbon (aquadag) to increase the surface work function, thereby suppressing the emission of photoelectrons which contaminate the positive ion conductivity measurements. The payload ground consisted of four similarly coated aluminum plates, typically 30 cm × 60 cm, mounted on the payload body. The probes were configured on the payload to enable the measurement of the electrical potential difference in the atmosphere between two points on three orthogonal axes. For this purpose each of five (Siple, Roberval) or six (Palestine, Iowa, southern ocean) probes was mounted on 2-m-long phenolic insulating booms, two probe pairs horizontally and one probe-pair (probe) vertically (downward). All of the flat plate probes lay in a vertical plane. The payloads were rotated about the vertical axis at a period of typically 20 s in order to permit removal of DC offsets from the horizontal probe data. This type of double-probe system has been used frequently during the past 40 or so years to measure stratospheric electric fields (Paltridge, 1964, 1965; Mozer and Serlin, 1969; Benbrook et al., 1974; Holzworth and Mozer, 1979; Bering et al., 1980, 1986; Holzworth, 1981; Holzworth et al., 1984, 1986). The electric field was passively measured, so that the conductivity in the vicinity of the probes was not disturbed.

In the relaxation time technique, one or more probes are driven to a potential different from the "ground" potential of the payload for a short period of time and then released and allowed to lose their excess charge by conduction through the atmospheric medium. In order for the technique to work, the voltmeter that senses the potential difference between the driven probe and the payload ground must draw significantly less current than the current that flows from the probe to the medium. This is achieved by using MOSFET preamplifiers with input impedances $>10^{13}$ ohms. The resistance to infinity from the probe through the
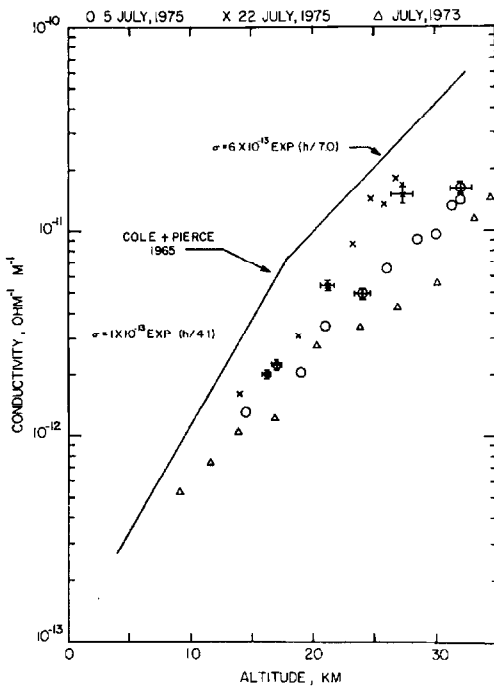
Fig. 1. Total conductivity versus altitude measured by two balloon flights during the 1975 Roberval, Quebec, campaign. The solid and open circles represent data points obtained during ascent and descent, respectively, on July 22. For comparison, the Cole and Pierce (1965) model profile and the 10 July 1973 Palestine data are also shown. (Byrne et al., 1988; ©1988 AGU.)
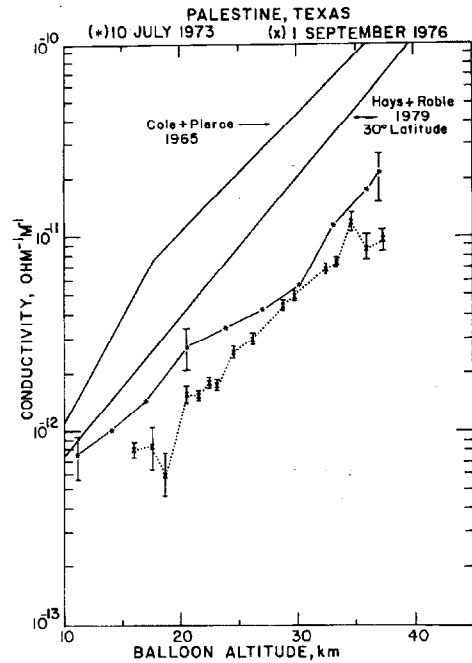
Fig. 2. Total conductivity versus altitude measured at Palestine, Texas, by two balloon flights in 1973 and 1976, respectively. The measured profiles are compared with two model profiles.(Byrne et al., 1988; ©1988 AGU, Figures 1 and 2 reproduced with permission.)

medium is of order 10^{11} ohms at float altitude, but it increases roughly exponentially with decreasing altitude, with an e-folding distance of order 6 km. Thus this technique is useful only for altitudes above 10 km. An extensive discussion of the expected response of the probes and the methods used to obtain the conductivity data can be found in Byrne, et al. (1988).

OBSERVATIONS

The conductivity measurements during the ascent or descent of many of the balloon flights are presented as a function of altitude in Figures 1–4. Each conductivity measurement was individually plotted and examined to see how well the fitted exponential matches the data. Those measurements that did not fit well were omitted from the data base.

All measurements in this paper were obtained in fair-weather conditions, i.e., there were no direct effects of thunderstorms on the local electrical conditions of the atmosphere. Bering et al. (1980) have reported stratospheric conductivity measurements obtained in the vicinity of a thunderstorm during the 1975 balloon campaign. In each of Figures 1–4, the measured conductivity profiles are compared with two model profiles. One model was derived by Cole and Pierce (1965) from microphysical considerations. The other, by Hays and Roble (1979), is an empirical model which includes a correction for latitudinal variations of cosmic ray ionization. Both model profiles are of the functional form $\sigma(z) = \sigma_o \exp(z/h)$, where σ_o is a reference conductivity, z is the altitude above mean sea level, and h is the conductivity scale height. In the Cole and Pierce model these parameters have the values

$$\sigma_o = 1 \times 10^{-13}; \qquad h = 4.1 \qquad 3.6 < z < 17.7$$
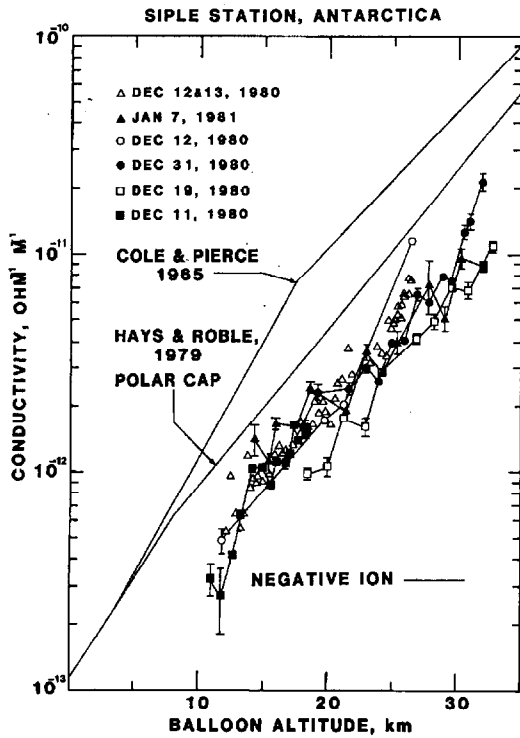$$\sigma_o = 6 \times 10^{-13}; \qquad h = 7 \qquad 17.7 < z < 40$$

(1)

Fig. 3. Negative polar conductivity versus altitude measured by five balloon flights during the 1980–1981 campaign at Siple Station, Antarctica. The measured profiles are compared with two model profiles of the negative conductivity. Data points without error bars have error estimates smaller than the size of the symbol. (Byrne et al., 1988; ©1988 AGU.)
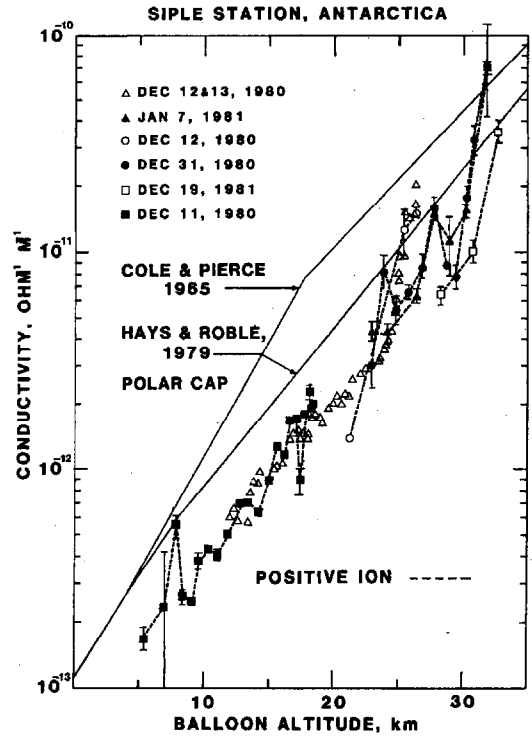
Fig. 4. Positive polar conductivity versus altitude measured by five balloon flights during the 1980–1981 campaign at Siple Station, Antarctica. The measured profiles are compared with two model profiles, as in Figure 3. (Byrne et al., 1988; ©1988 AGU, Figures 3 and 4 reproduced with permission.)

where the units for σ_o are ohm^{-1} m^{-1}, and the units for h and z are km. In the Hays and Roble model

$$\sigma_o = 1.14 \times 10^{-14}; \qquad h = 3.5 \qquad 0 < z < 8$$
$$\sigma_o = 1.14 \times 10^{-13}; \qquad h = 6 \qquad 8 < z < 60 \tag{2}$$

The variation with latitude in the Hays and Roble model enters as a multiplying factor to (2). For Palestine, Roberval, and Siple Station latitudes, these factors are 1.2, 1.34, and 1.4, respectively, during solar quiet conditions.

For simplicity the model assumes coincident geographic and geomagnetic latitudes. The model profiles are included here as references for comparison with our data; however, neither model supposes to be a complete representation of the actual conductivity. For example, the Cole and Pierce model does not consider latitudinal variations, while the Hays and Roble model is oversimplified for mathematical expediency in their global model of atmospheric electricity (R. G. Roble, personal communication, 1987). A more complete representation of the atmospheric conductivity is lacking at this time.

Figure 1 presents the total conductivity profiles measured during two flights of the July 1975 Roberval balloon campaign, as well as the 10 July 1973 Palestine flight for comparison. The July 5 flight attained a maximum altitude of 32 km. This conductivity profile agrees well with the Hays and Roble model up to 17 km and between 22 km and 24 km. Above 24 km the conductivity remained below the Hays and Roble profile. The July 22 flight attained a maximum altitude of 27 km before slowly descending as a result of a helium leak. Both the ascent and descent data of this flight are shown and are in good agreement. The conductivity profile measured in this flight is in good agreement with the Hays and Roble model for
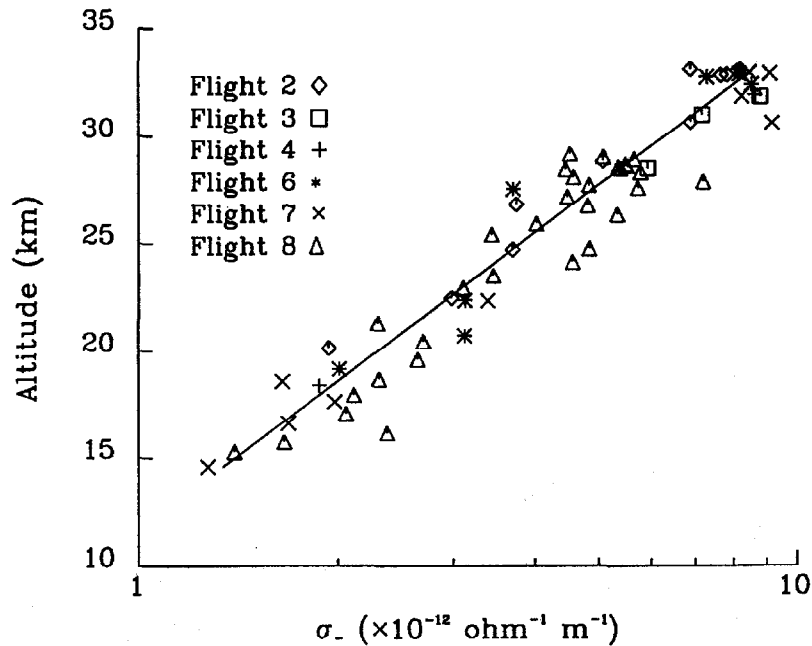
Fig. 5. Negative polar conductivity versus altitude measured by six balloon flights during the 1985–1986 campaign at Amundsen-Scott South Pole Station, Antarctica. The measured profiles are compared to a least squares fit to all six of the profiles. (Byrne et al., 1991)

this latitude and is substantially different from the July 5 profile. Most notable is the lack of significant departures from an exponential increase in conductivity with altitude. The measured conductivities from both flights are below the Cole and Pierce model values by more than a factor of 2 and are above the lower latitude Palestine data, as expected.

Figure 2 shows the total conductivity profiles measured in two flights over Palestine in 1973 and 1976, respectively. Both flights attained an altitude of 36 km. The 1973 data exhibit a fairly smooth exponential increase with altitude. The data are in good agreement with the Hays and Roble model near 11 km but diverge from the model with increasing altitude. The 1976 data are slightly lower but in good agreement with the 1973 data, except for a sharp decrease in the conductivity near 19 km, which may indicate the presence of an aerosol layer. The measured values disagree with the Cole and Pierce model by a factor of 5 or more.

Figures 3 and 4 present the negative and positive conductivity data, respectively, from five balloon flights over a 4-week period during the 1980–1981 Siple Station campaign. The December 11 and 12 balloon flights attained altitudes of only 20 and 28 km, respectively, as a result of helium leaks. Both balloons descended slowly, providing conductivity measurements with much greater spatial resolution than the ascent measurements. Excellent positive and negative data were received above 10 km in these two flights. In the other three flights the negative data were of good quality above approximately 15 km, while usable positive data were returned only above 20–25 km. For easier comparison with our data, we have drawn the curves representing the model profiles as one-half the total conductivity values predicted by each model (both models assume $\sigma_- = \sigma_+$).

Below 25 km the measured positive and negative conductivities were approximately equal. Above 25 km the positive values were 2–3 times larger than the corresponding negative values during midday hours. We attribute this effect to photoelectric emissions from the probe surfaces at high altitudes as discussed below. Therefore above 25 km, meaningful comparisons of the profiles from the various flights can only be made from the negative data. Except for the positive conductivities above 25 km, the profiles agree well with the Hays and Roble model for this latitude. The Cole and Pierce model values are again 2–3 times larger than the observed data. Except for minor fluctuations in the profiles, the data from the flights of December 11,
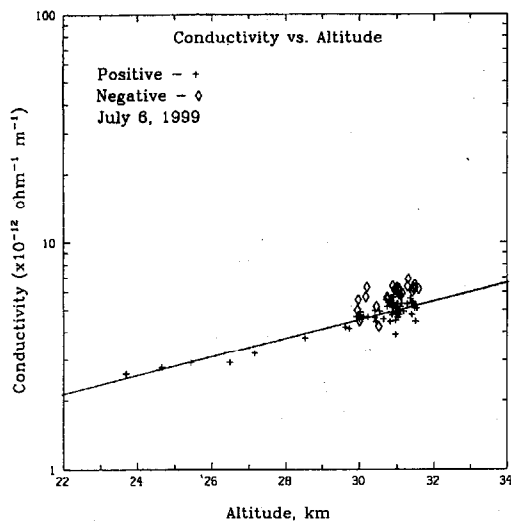
Fig. 6. Negative and positive polar conductivity versus altitude measured at night during a flight in 1999 from Palestine, Texas. The cluster of points above 30 km is the float data accumulated throughout the flight. Fits to the negative data during ascent were not successful.
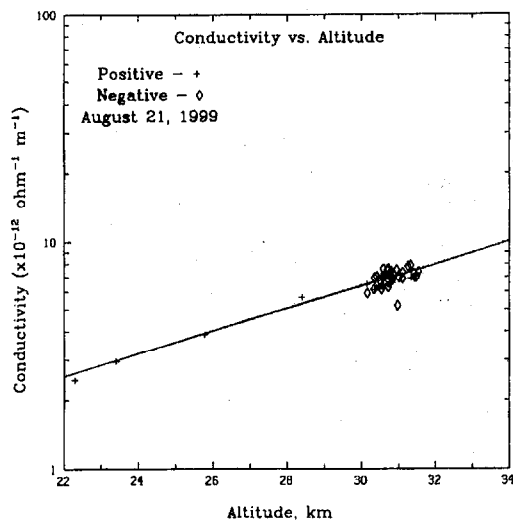
Fig. 7. Same as Figure 6 for a flight in 1999 from Ottumwa, Iowa.

12, and 31 agree well with each other. The December 19 conductivity was observed to be the lowest of the 5 flight days in this campaign over the range of altitudes in which good data were received. The January 7 flight recorded the highest values of the 5 flight days below about 20 km and values in good agreement with those on December 12 and 31 above 20 km. There do not appear to be significant departures from a general exponential increase with altitude in these profiles.

We now turn our attention to the data from the 1985-86 South Pole balloon campaign (Byrne et al., 1991). We have observed over the years that our probe voltages are at times noisy and rapidly time varying during the high-velocity ascent stage of a balloon flight. There are probably very good reasons for this, such as passage through wind-shears, aerosol layers, swinging of the payload, etc. It has been the case that much of the electric field data during the ascent portion of a given flight is simply too noisy to be useful, and few or none of the conductivity cycles (relaxation of the probe potential) could be adequately fitted to an exponential. The latter is because one has to be a bit lucky to have the infrequent conductivity measurement cycle occur during a period of reasonable stability (a time which is long compared to the relaxation time of a few seconds) of the electric field in order to get a reliable conductivity data point at low altitudes during ascent. This situation is one that varies from flight to flight. On the other hand, during times of float or slow descents, these types of noise signals (rapid, large excursions in potential) are not introduced, so that the electric field signal is stable and time constants can be unambiguously determined. We have taken the position that a conductivity data point is presented only if the exponential relaxation of the probe potential during a measurement cycle meets stringent goodness-of-fit criteria. Each of the conductivity measurement cycles during ascent or descent have been visually examined to see how well the fitted exponential of the probe potential during relaxation matches the data and how the basic data look. Those cycles that are too variable are simply omitted from the data base. During the 1985-86 South Pole campaign, the entire ascent data of flights 1 and 5 were noisy, and the probe potentials stabilized only after the balloons reached float. All of the ascent data from flights 1 and 5 were thereby removed from the data base. In the ascent portions of flights 2, 3, 4, 6, and 7, approximately one third of the total number of conductivity measurements were omitted. The ascent rate of flight 8 was much slower than the other flights. As a result, flight 8 provided more ascent conductivity data points than the other flights, and the overall quality of the ascent data was better than the other flights (only two conductivity data points were omitted). Flights 1 and 2 provided
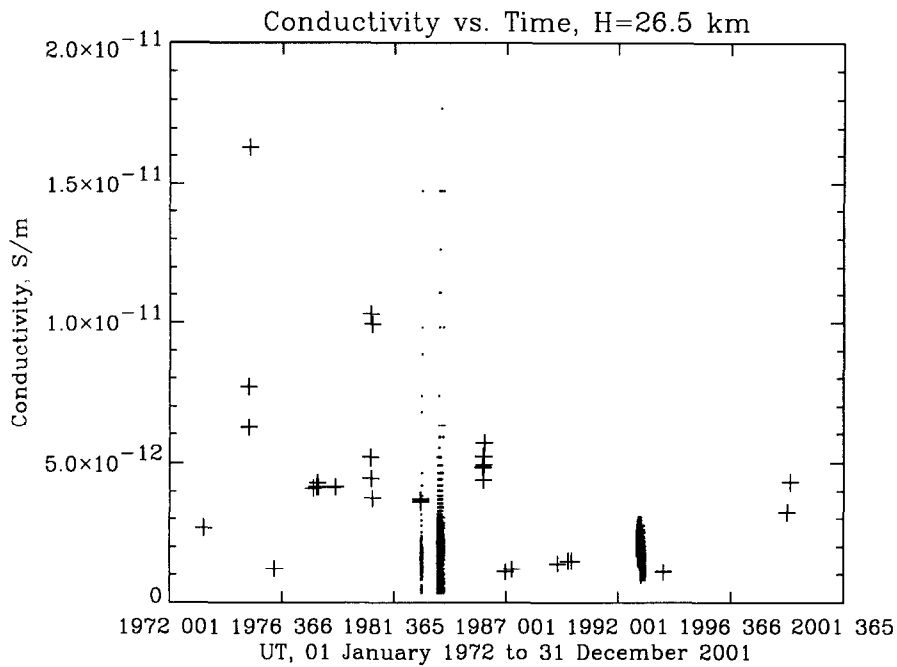
Conductivity vs. Time, H=26.5 km

Fig. 8. Conductivity at 26 km altitude is plotted vs. time from all flights considered in this study. Negative polar conductivity is plotted for all flights except the Laramie, Wyoming results (41°N, 1978-1983). All float altitude points from EMA and ELBBO have been plotted, using smaller dots.

stable vertical profiles during descent. The vertical profiles of σ_- measured during the 1985-86 balloon ascents are shown in Figure 5. On average, σ_- increased exponentially with increasing altitude, and over the range from 15 km to 32 km can be expressed by

$$\sigma_- = \sigma_0 \, exp(z/h) \tag{1}$$

where $\sigma_0 = 3.17 \times 10^{-13} \mathrm{ohm}^{-1}\mathrm{m}^{-1}$, z is the altitude in km, and the scale height $h = 10.0$ km.

Space does not permit us to show the ascent profiles from all of the flights that we have included in this study. The data from the most recent two flights are shown in Figures 6 (Palestine, Texas) and 7 (Ottumwa, Iowa). Two improvements in the precision of conductivity determination were incorporated in these results. The PCM telemetry system used on these flights was a 16 bit 1 kHz system, which provided a two order of magnitude increase in the resolution of the time constant measurements. Second, precise, high resolution altimetry was provided by GPS tracking, which is very much more accurate than barometric altimetry at these altitudes. In addition to the ascent profiles, the float interval data have also been included in the figures. These two figures show, first, that the conductivity over Palestine has not changed significantly in nearly 30 years. Second, the fluctuations in the conductivity that occurred at a fixed altitude during the night were nearly a factor of two. Owing to the technical refinements just mentioned, these fluctuations must be the result of actual ambient variations, rather than random measurement errors. During ascent, only the positive conductivity data yielded acceptable fits, as discussed above. After float was reached, the + and - data agreed.

In order to compare data from different times and places, the data must be normalized to a chosen altitude. Since the two largest data sets used in this study, EMA and ELBBO, were super-pressure balloons that floated at an altitude of 26 km, this height has been selected as the common reference height. This choice has the added advantage that the positive conductivity data are only slightly affected by photo-emission effects. In order to display the entire data base in as comprehensible a way as possible, data from all of the flights in Table I have been plotted as a function of time (Figure 8) and as functions of both time and geographic latitude using a projected trimetric plot (Figure 9). In both of these figures, a single point has been plotted for each zero-pressure balloon flight. Since the super-pressure flights covered a period of months, every data
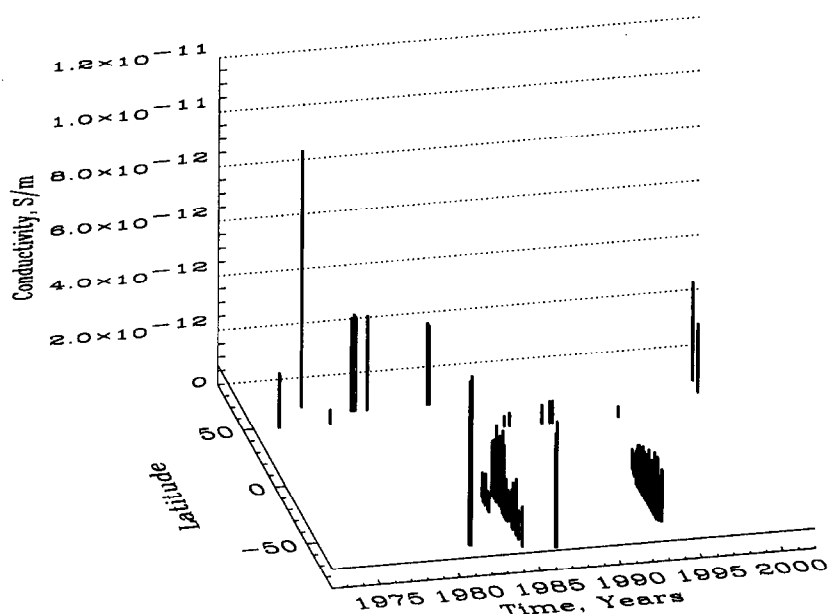
Fig. 9. Conductivity at 26 km altitude is plotted as a function of latitude and time using a projected trimetric view from all flights considered in this study. Negative polar conductivity is plotted for all flights except the Laramie, Wyoming results (41°N, 1978-1983).

point from these flights was plotted using smaller symbols in Figure 8.

DISCUSSION

Early Palestine, Roberval and Siple Flights

In our earlier papers that focused on flights prior to 1985, electrical conductivity profiles in the stratosphere were obtained from nine high-altitude balloons launched from three locations, widely separated in latitude (Byrne et al., 1988). Variations in the conductivity profiles were examined on local and global scales. The major conclusions of this work that are germane to this paper are as follows:

1. The average profile at high latitude (76°S) is in good agreement with the Hays and Roble (1979) model profile. The disagreement between their model and the measured profiles increases with decreasing latitude. The Cole and Pierce (1965) model appears to significantly overestimate the conductivity for all latitudes.

2. The conductivity profiles at each latitude exhibited a significant day-to-day scatter. The measurements over Palestine and Roberval were made during quiet solar and geomagnetic conditions. Therefore the major differences in these profiles do not appear to be explained by this type of activity. The measurements over Siple Station were made during periods of variable geomagnetic conditions, which may partly account for the observed scatter in the conductivity profiles. However, the scatter cannot be explained simply on the basis of changes in the ionizing cosmic ray flux, which did not vary significantly from flight to flight. The day-to-day variations in conductivity were apparently dominated by local effects.

3. The effect of cosmic ray ionization on the latitudinal variation of the conductivity was examined. The observed latitudinal variation in conductivity is not explained by a latitudinal distribution of cosmic ray ionization alone.

4. The effects of aerosols and temperature on the latitudinal variation of the conductivity were examined. A background distribution of aerosol concentrations as a function of altitude and latitude was estimated and parameterized. By including the effects of aerosols, the agreement between the observed and calculated variation of the conductivity with latitude was improved although, the effect is too small to account for the observed variation. At high latitudes the conductivity may be maintained by a balance of ion recombination and cosmic ray ionization, while ion-aerosol attachment is insignificant. The role of aerosols becomes more

important with decreasing latitude. The large variation in stratospheric temperatures with latitude was found to be a more important factor than the background aerosols. Overall, the addition of both aerosol and temperature effects results in a significant improvement in the agreement between the calculated and observed variation in conductivity. The implication of this work is that although the conductivity is quite variable due to many meteorological factors (Roble and Tzur, 1986), global models of conductivity may be improved by including the effects of a latitudinal distribution of aerosols and temperature.

Later Flights

Most of the recent discussion of the results used in this paper have focused on issues such as the effect of thunderstorms on stratospheric conductivity, which are not germane to the results of this study. One interesting result is that geomagnetic latitude is the dominant organizer of the ELLBO data (Holzworth et al., 1992; Holzworth and Hu, 1992; Hu, 1994). Ionization rate variations associated with cosmic ray cut-off rigidity variations appear to be sufficient to account for the latitude variations encountered by ELBBO, without the necessity of considering latitude gradients of temperature and aerosol content.

There is no good model that accounts for the day to day fluctuations found in the various campaigns, and in the high precision data of the 1999 flights. Any discussion of site to site and apparent long term variations must be tempered with an awareness of how large the natural short term fluctuations are at a given site. One aspect of these fluctuations that has emerged from this study is the fact that the fluctuation amplitude appears to be latitude dependent. The day-to-day and hour-to-hour variations observed at Hyderabad have an amplitude of about 5%, which is much smaller than the variance observed at Palestine, for example. This latitude gradient of variance is a new observation for which there is, as yet, no proposed model.

Solar Cycle Variations

The error bars on the Hyderabad data are estimated to be about 3% of the mean. This level of precision permits an investigation of solar cycle and climatic effects on the data that the noisier higher latitude data do not support (Gupta, 2000). The data indicate that there is a 25% modulation of the stratospheric conductivity during a solar cycle that is positively correlated and in phase with sunspot number. At 32° latitude, the data suggest a similar behaviour at the two standard deviation significance level. At higher latitude, 42° and above, the natural short term variance obscures the solar cycle signal, if any is there.

CONCLUSIONS

Review of the data presented lead us to realize that very little can be concluded at this time. Unexplained day to day variations dominate the data at high latitude. The data suggest that conductivity is declining in time and that the conductivity is lower in the S. Hemisphere. One might try to explain the former effect as the result of increasing aerosol or water vapor content of anthropogenic origin. However, such an explanation would also predict that the conductivity should be higher rather than lower in the Southern hemisphere. Thus, in terms of possible mechanisms, these suggestions are inconsistent.

REFERENCES

Benbrook, J. R., J. W. Kern, and W. R. Sheldon, Measured electric field in the vicinity of a thunderstorm system at an altitude of 37 km, *J. Geophys. Res., 79*, 5289–5294, 1974.

Bering, E. A., T. J. Rosenberg, J. R. Benbrook, D. Detrick, D. L. Mathews, M. J. Rycroft, M. F. Saunders, and W. R. Sheldon, Electric fields, electron precipitation and VLF radiation during a simultaneous magnetospheric substorm and atmospheric thunderstorm, *J. Geophys. Res., 85*, 55–72, 1980.

Bering, III, E. A., J. R. Benbrook, J. M. Howard, D. M. Oró, E. G. Stansbery, J. R. Theall, D. L. Matthews, and T. J. Rosenberg, The 1985-86 South Pole balloon campaign *Proceedings of the Nagata Symposium on Geomagnetically Conjugate Studies and the Workshop on Antarctic Middle and Upper Atmosphere Physics held at SCAR XIX, Memoirs of the National Institute of Polar Research, Japan, Special Issue No. 48* 313-317, 1987.

Byrne, G. J., J. R. Benbrook, E. A. Bering III, D. M. Oro, C. O. Seubert, and W. R. Sheldon, Observations of the stratospheric conductivity and its variation at three latitudes, *J. Geophys. Res., 93*, 3879-3892, 1988.

Byrne, G. J., E. A. Bering, and J. R. Benbrook, Balloon observations of stratospheric electricity above the south pole: Vertical electric fields, conductivity, and conduction current, *J. Atmos. Terr. Phys., 53* , 859-868, 1991.

Chemical Rubber Company, *CRC Handbook of Chemistry and Physics*, 50th ed., edited by R. C. Weast, CRC Press, Boca Raton, Fla., 1970.

Cole, R. K., and E. T. Pierce, Electrification in the Earth's atmosphere for altitudes between 0 and 100 kilometers, *J. Geophys. Res., 70*, 2735–2749, 1965.

Ebihara, Y., A. Kadokura, Y. Tonegawa, F. Tohyama, N. Sato, Y. Hirasima, M. Namiki, E. A. Bering III, J. R. Benbrook, and M. Ejiri, A convection enhancement event observed with the Polar Patrol Balloon #4, *Proc. NIPR Symp. Upper Atmos. Phys., 9*, 12-24, 1996.

Ejiri, M., A. Akiyama, E. A. Bering III, R. Fujii, M. Hayashi, Y. Hirasima, A. Kadokura, H. Kanzawa, M. Kodama, H. Miyaoka, H. Murakami, M. Nakagawa, M. Namiki, J. Nishimura, S. Ohta, H. Suzuki, F. Tohyama, Y. Tonegawa, N. Yajima, T. Yamagami, H. Yamagishi, and M. D. Yamanaka, Experimental results of Polar Patrol Balloon project in Antarctica, *Proc. NIPR Symp. Upper Atmos. Phys. , 8*, 60-64, 1995.

Gringel, W., J. M. Rosen, and D. J. Hofmann, Electrical structure from 0 to 30 kilometers, in *The Earth's Electrical Environment*, National Academy Press, Washington, D. C., 1986.

Gupta, S. P., Solar cycle variations of stratospheric conductivity over low latitude, *Adv. Space Res., 26*, 1225-1229. 2000.

Gupta, S. P.,S. C. Chakravarty, S. Chandersekaran, (Eds.), Balloon-borne experiments for middle atmosphere conductivity campaigns, ISRO-IMAP S.R. Vol. 39, 1992.

Hays, P. B., and R. G. Roble, A quasi-static model of global atmospheric electricity: The lower atmosphere, *J. Geophys. Res., 84*, 3291–3305, 1979.

Holzworth, R. H., High latitude stratospheric electrical measurements in fair and foul weather under various solar conditions, *J. Atmos. Terr. Phys., 43*, 1115–1125, 1981.

Holzworth, R. H., Conductivity and electricity field variations with altitude in the stratosphere, *J. Geophys. Res. 96*(D7), 12857-12864, 1991

Holzworth, R. H., H. Hu, Global electrodynamics deduced from long duration balloon-borne measurements, in *Fifth Symposium on Global Change Studies and the Symposium on Global Electrical Circuit, Global Change and the Meteorological Applications of Lightning Information*, Ed., Barron, E. J. , American Meteorological Society, Boston, MA, 293-295, 1992.

Holzworth, R. H., K. W. Norville, The global circuit as deduced from balloon-borne measurements, *Proceedings 9th International Conference on Atmospheric Electricity, I*, Ed's., E. Borisenkov, and V. Stepanenko, A.I. Voeikov Main Geophysical Observatory, St. Petersburg, Russia, pp. 14-17, 1992.

Holzworth, R. H., K. W. Norville, H. Hu, R. L. Dowden, C. D. Adams, J. Brndell, O. Pinto, I. Pinto, W. D. Gonzalez, ELBBO: Extended Life Balloon Borne Observatories, *URSI Radioscientist, 4*, 33-37, 1992.

Holzworth, R. H., and F. S. Mozer, Direct evidence of solar flare modification of stratospheric electric fields,

J. Geophys. Res., 84, 363–367, 1979.

Holzworth, R. H., T. Onsager, P. Kintner, and S. Powell, Planetary-scale variability of the fair-weather vertical electric field in the stratosphere, *Phys. Rev. Lett., 53,* 1398–1401, 1984.

Holzworth, R. H., K. W. Norville, P. M. Kintner, and S. P. Powell, Stratospheric conductivity variations over thunderstorms, *J. Geophys. Res., 91,* 13,263–13,263, 1986.

Hu, H., Global and local electrical phenomena in the stratosphere, Ph.D. dissertation, University of Washington, 170 p., 1994.

Israel, H., Atmospheric Electricity, Vol. 1 and 2, Nat. Tech Inform. Serv., U. S. Dept. Commer., Springfield, VA., 1973.

Mozer, F. S., and R. Serlin, Magnetospheric electric field measurements with balloons, *J. Geophys. Res., 74,* 4739–4755, 1969.

Norville, K, and R. Holzworth, Global circuit variability from multiple stratospheric electrical measurements, *J. Geophys. Res., 92,* 5685–5695, 1987.

Paltridge, G. W., Measurements of the electrostatic field in the stratosphere, *J. Geophys. Res., 69,* 1947–1954, 1964.

Paltridge, G. W., Experimental measurements of the small-ion density and electrical conductivity of the stratosphere, *J. Geophys. Res., 70,* 2751–2761, 1965.

Roble, R. G., and I. Tzur, The global atmospheric-electrical circuit, in *The Earth's Electrical Environment,* National Academy Press, Washington, D.C., 1986.

Rosen, J. M., and D. J. Hofmann, Balloon-borne measurements of electrical conductivity, mobility, and the recombination rate, *J. Geophys. Res., 86,* 7406–7410, 1981.

Rosen, J. M., D. J. Hofmann, and K. H. Kaselau, Vertical profiles of condensation nuclei, *J. Appl. Meteorol., 17,* 1737–1740, 1978.

Rosen, J. M., D. J., Hofmann, W. Gringel, J. Berlinski, S. Michnowski, Y. Morita, T. Ogawa, and D. Olson, Results of an international workshop on atmospheric electrical measurements, *J. Geophys. Res., 87,* 1219–1227, 1982.

item Rosen, J. M., D. J. Hofmann, and W. Gringel, Measurements of ion mobility to 30 km, *J. Geophys. Res., 90,* 5876–5884, 1985.

PREFACE

The Scientific Symposium 2.6
LIGHTNING MIDDLE ATMOSPHERE INTERACTION
held on 20 July, 2000

Session Chairperson : Dr. R. Goldberg

It is well known that several types of signatures of upward propagating lightning activity have been observed in the middle atmosphere and upper atmosphere. These aspects were discussed in the Symposium ``Lightning Middle Atmosphere Interaction". This Symposium comprised of one invited paper and eight contributed papers. The invited paper was presented by E.A. Bering III on balloon borne results on sprites. A.N. Lyakhov discussed the atmospheric response to electromagnetic pulse to trigger sprites. M.J. Rycroft presented a model calculation for the generation of elves. R.H. Holzworth discussed rocket-borne measurements over a thunderstorm. L.C. Hale discussed the mesospheric electric field measured by rocket-borne probes. G.A. Mikhailova presented satellite observations of A.C. electric field in different frequency bands over powerful typhoons in the Pacific ocean. P.I.Y. Velinov discussed a model on ionospheric effects of thunder clouds. The balloon-borne measurements of stratospheric conductivity at float altitudes over low latitude were presented by S.P. Gupta. The credit for the success of the Symposium goes to many persons. Prof. R.H. Holzworth and Dr. R. Goldberg were scientific organisers of the Symposium. I am very thankful to them. I would like to thank referees Professors M.J. Rycroft, B.H. Subbaraya and Harish Chandra.

S.P. Gupta

Ahmedabad, India

2583

SEMIDIURNAL VARIATIONS OF STRATOSPHERIC CONDUCTIVITY AT BALLOON FLOAT ALTITUDE

S.P. Gupta

Physical Research Laboratory, Ahmedabad 380 009, India

ABSTRACT

Ten balloon flights were conducted from Hyderabad, India to measure polar conductivity. Measurements were carried out during balloon ascent as well as at float altitude. At float altitude, i.e. 32-36 km, the measurements were carried out for a period ranging from 5 hrs to 10 hrs. At sunrise the conductivity always decreases. At around 1000 hrs local time the conductivity is maximum and again decreases at around 1400 hrs. This variation shows that at float altitude, 32-36 km the conductivity shows semi-diurnal variations. We suggest that this is due to semidiurnal tide. © 2002 COSPAR. Published by Elsevier Science Ltd. All rights reserved.

INTRODUCTION

The electrical conductivity of middle atmosphere is an important parameter, which plays a significant role in global electric circuit. The stratospheric conductivity has a solar cycle variation, which is latitudinal dependent (Neher 1967). However, over a low latitude site like Hyderabad (17.3°N, 78.5°E, Geomag. Lat. 8°N) the solar cycle effect should be negligible (Neher 1967). The conductivity in troposphere and stratosphere is dependent on cosmic rays intensity. The cosmic ray flux varies inversely with solar cycle. The production of ionization due to cosmic rays is maximum at 15 km altitude (Volland 1984).

Existence of a solar cycle variation in stratospheric conductivity over Hyderabad was shown by Gupta (2000). For the first time Gupta (2000) showed the results of four flights conducted from Hyderabad during low and high solar activity period, two flights each on low solar activity period and high solar activity periods. Between 20 km and 35 km region the polar conductivity is found to be larger during high solar activity period compared to low solar activity period. This was explained by Gupta (2000) to be due to changes in ion composition from low solar activity period to high solar activity period. The UV radiation intensity is higher during high solar activity period as compared to lower solar activity period (Lean et al., 1997) and hence heavier cluster ions can break to lighter mass ions more easily which in turn can give higher conductivity.

Diurnal variation of conductivity is believed to be very small since the cosmic ray flux does not vary over a period of a day. But Gupta et al. (1992) have shown that conductivity at float altitude has diurnal variation also. Norville and Holzworth's observations (1987) show that at 26 km float altitude conductivity increases at noon, but they neglected the effect. Croskey et al. (1985) have shown pre-sunrise effect on conductivity at low latitudes at 18 km altitude. Ogawa and Tanaka (1976) had also reported conductivity values at float altitude at

25 km. They also have observed semidiurnal variation in conductivity. But they did not explain the results according to semi diurnal tidal effect.

RESULTS

We present here the results of polar conductivity. These measurements were carried out from Hyderabad. We consider only float altitude measurements. All the measurements, except one flight, are made with a relaxation time probe (Gupta and Narayanan, 1987).

Figure 1 shows the results of the flight conducted on 17 October, 1989. The balloon was launched around mid-night and it reached float altitude around 02.00 hrs. It was kept at float altitude till 1000 hrs. It can be seen that conductivity decreases at sunrise (around 06.00 hrs) and recovers to normal value at 10.00 hrs which is same as night time value. Figure 2 shows the results of the flight conducted on 29 December, 1985. The float altitude in this flight was 34 km. Here also we see a decrease after sunrise, but the magnitude is smaller. We could float the balloon only upto 08.30 hrs IST and therefore cannot see the recovery. Figure 3 shows the conductivity results of two balloon flights conducted on 11 April, 1988 and 22 April, 1989 which also demonstrates the sunrise effect, i.e. a decrease after sunrise and becoming maximum around noon and again decreasing around 1400 hrs. The float altitude in this case was 36 km. The extrapolated values were taken from our earlier flight conducted on 18 April 1984 (Gupta and Narayanan, 1987). Figure 4 shows the results of flight conducted on 5 January, 1994 which also shows the sunrise effect.

DISCUSSION

The polar conductivity measurements carried out from Hyderabad at float altitude show that the conductivity decrease at sunrise, is maximum around 1000 hrs and again at around 1400 hrs there is a minimum. So we see a semidiurnal variation of conductivity. The time interval between two minimum values of two maximum values is about 10 hrs to 12 hrs. (Gupta et al., 1992).

We suggest that this is not a solar zenith angle dependence effect, but related with semi-diurnal tide. The semidiurnal tide is dominant over low latitude. Our conductivity values exactly follow semidiurnal tide pattern. Sarabhai et al. (1953) have studied at ground level the daily variation of cosmic ray intensity. The cosmic ray intensity at ground level was found to be inversely proportional to the ground level pressure.

The production rate of ions by cosmic rays is given by

$$dn/dt = q-\alpha n^2 \qquad (1)$$

where q is production rate, α is recombination coefficient and n is ion density.

The cosmic ray produced ionization, is neutral density dependent. Perkeris (1937) has shown that the semidiurnal variation of pressure at 30 km altitude is 180 degree out of phase with the observed pressure oscillations at the ground. That the pressure at ground level over
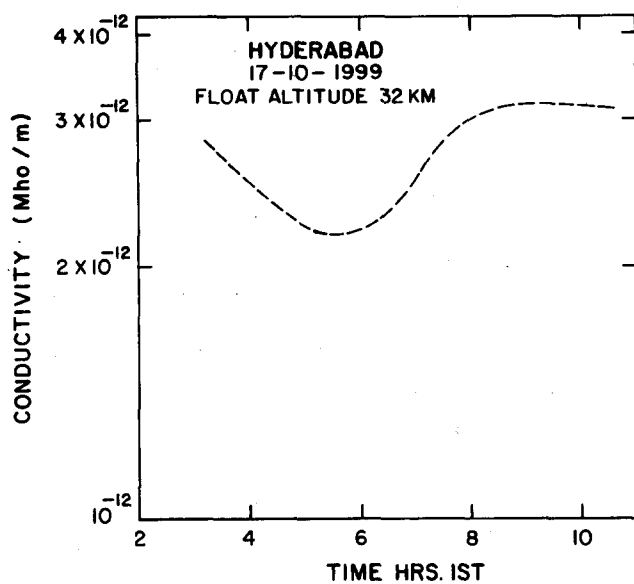
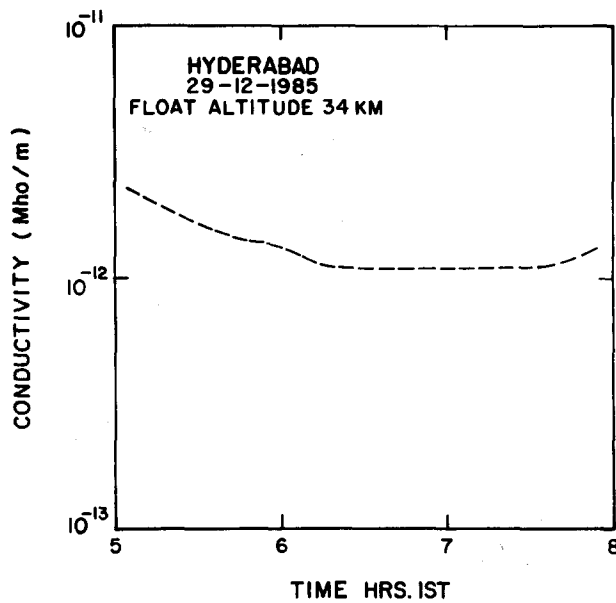**Fig. 1. Negative ion conductivity at float altitude on 17 October, 1989**

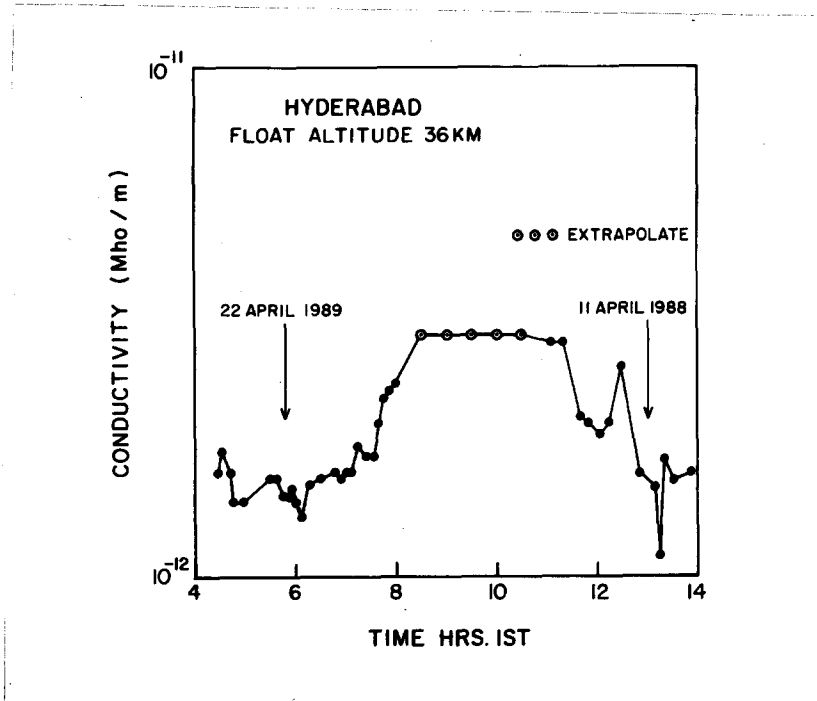**Fig. 2. Negative ion conductivity at float altitude measured on 29 December, 1985**

Fig. 3. Negative ion conductivity values at float altitude measured on 22 April, 1989 and 11 April, 1988.
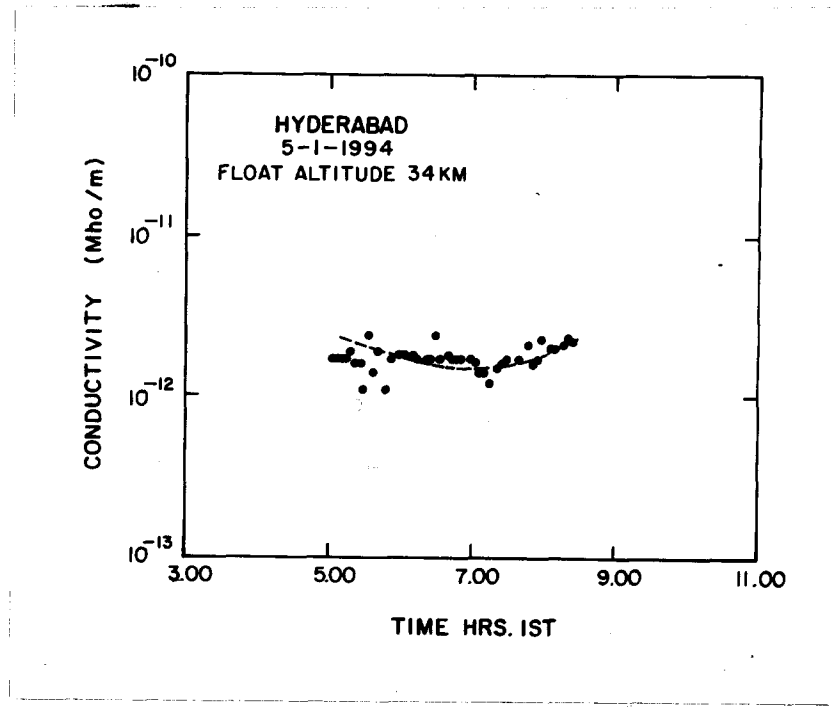

Fig. 4. Negative ion conductivity at float altitude measured on 5 January, 1994

low latitude decreases at sunrise as is well known. Therefore according to Perkeris (1937) the pressure at 30 km altitude should increase at sunrise. Since the conductivity is a function of pressure, higher the pressure, lower the conductivity. We conclude that the decrease in conductivity at sunrise and again at afternoon hours is due to semidiurnal pressure oscillations at these altitudes.

ACKNOWLEDGEMENTS

REFERENCES

Croskey, C.L., L.C. Hale, J.D. Mitchell and D. Muhe, A diurnal study of the electrical structure of the equatorial middle atmosphere, J. Atmos. Terr. Phys., 47, 835-844, 1985.

Gupta, S.P. and A. Narayan, Balloonborne measurements of ion conductivity over low latitude stratosphere, Plan. & Space Sci., 439-443, 1987.

Gupta, S.P., S.C. Chakravarty and S. Chandrasekaran (Editor), Balloonborne experiments for middle atmospheric conductivity campaign, ISRO-IMAP S.R. 39, 1992.

Gupta, S.P., Solar cycle variation of stratospheric conductivity over low latitude, Adv. Space Res., 26, 1225-1229, 2000.

Perkeris, C.L. Atmospheric Oscillation, Proc. Roy. Soc., A158, 650-671, 1937.

Lean, J.L., G.J. Rottman, H.L. Kyle, T.N. Woods, J.R. Hickey and L.C. Puga, Detection and parameterization of variations in solar mid and near ultraviolet radiation (200-400 nm), J. Geophy. Res., 102, 29939-29956, 1997.

Neher, H.V., Cosmic ray particle that changed from 1954 to 1958 to 1965, J. Geophys. Res., 72, 1527-1539, 1967.

Norville, K. and R. Holzworth, Global circuit variability from multiple stratospheric electric measurements, J. Geophys. Res., 92, 5685-5695, 1987.

Ogawa, T. and Y. Tanaka, Land effect on the stratospheric vertical electric field and current, J. Atmos. Terr. Phys., 38, 599-604, 1976.

Sarabhai, V., U.D. Desai and R.P.Kane, Meteorological and extraterrestrial causes of the daily variation of cosmic ray intensity, Proceed. Ind. Acad. Sci., A37, 287-303, 1953.

Volland, H., Atmospheric electrodynamics, Springer Verlag, N.Y., 1984.

Phd Thesis Abstract

THE STUDY OF THE LOWER IONOSPHERE AT LOW LATITUDE

Thesis

Presented by

S.P.GUPTA

to the

Gujarat University Ahmedabad

for the Ph.D. degree.

Physical Research Laboratory

Ahmedabad - 9.

January 1970

<u>STATEMENT</u>

The work presented in this thesis is based on the results obtained from the rocket borne Langmuir probe and plasma noise probe studies over Thumba near geomagnetic equator. Working under the guidance of Prof.V.A.Sarabhai and Prof.Satya Prakash at the Physical Research Laboratory, the author was responsible for the design and development of the plasma noise probe that was employed to study the fluctuations in Langmuir probe current which is termed as plasma noise in the thesis. The necessary telemetry system which includes subcarrier oscillators and band pass filters as per I.R.I.G. specifications was developed by the author. A spectrum analyser was also developed to study the spectrum of the observed plasma noise. The author also made improvements in the Langmuir probe system.
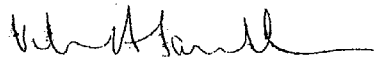
The author took active part in extensive testing and checking of the Langmuir probe and plasma noise probe system prior to launching. He was also responsible for analysing the data and interpreting the experimental results.

The Langmuir probe was employed to determine the electron density and electron temperature while the plasma noise probe was used to study the Langmuir probe current fluctuations with amplitudes as low as 0.05% in the frequency range 70 Hz to 1 KHz. Fluctuations with frequencies less than 70 Hz can be studied directly from the telemetry record of the Langmuir probe current. These measurements of ionospheric irregularities have been inter- preted in terms of processes taking place in the equatorial

ionosphere. Many conclusive results have come out from the present study.

The results presented in the thesis contain probably the first in situ measurements of equatorial E region irregularities with scale sizes of the order of a few meters. They also contain probably the first systematic in-situ measurements of disturbances created in the medium by a moving rocket. It is believed that ion acoustic waves are generated in the wake of a vehicle moving through the ionosphere, but so far no in-situ measurements were available. The present results therefore provide fresh insights into plasma instabilities in the equatorial ionosphere and the disturbances produced by the rocket.

Prof.V.A.Sarabhai
Director
Physical Research Laboratory
Navrangpura
Ahmedabad-9

S.P.Gupta
Author

January 24, 1970

Epilogue

Dr. Kuldeep Pandey

PRL PhD 2018

My interaction with Prof. S. P. Gupta began in 2014 when I started my doctoral research under Prof. R. Sekar and Dr. D. Chakrabarty of the Space & Atmospheric Sciences Division at PRL. At that time, Prof. Gupta was one of the senior-most persons who regularly visited the division to continue his research works. In PRL, he was famous as "Gupta-ji". Gupta-ji and my supervisors shared a relationship of trust and friendship. They were active scientific collaborators for more than a decade and had many scientific publications to their name. Gupta-ji offered positive comments suggestions in my research works and was a co-author in many of my publications. Therefore, our interactions increased during my doctoral and post-doctoral tenures at PRL. Our work on the altitude of equatorial electrojet is probably his last publication (year 2020).

Gupta-ji was wholly engaged in the sounding rocket experiments since the early years of such campaigns in India. He had more than 40 successful-sounding rocket experiments from Thumba Rocket Launch Station. He cherished this tremendous experience and the time spent in Germany during his early research career. Our tea-table discussions reflected this when he would narrate the time spent at Thumba and occasionally speak in German. Gupta-ji had an amazing memory! He would narrate in detail his experiences dating back to even the 1970s.

For me, he was a walking encyclopedia of the facts on rocket flights and related observations. He immensely helped me to work with those datasets and revisit the old telemetry records whenever required. He always applauded my scientific approach and encouraged me to look for great opportunities in life. He would share his father's advice, "Try to be in the company of great people; even if you acquire a glimpse of their qualities, you will grow faster."

I always admired his positive approach towards life. He would try to be active, keep life simple, crack jokes and laugh loudly. He was this way until our last telephonic conversation when he got COVID (a few days before his sad demise). He will forever remain in our hearts.